Marine Anoxia During Past Warm Climates

by

Leila Behrooz

School of Chemistry
September 2018

A dissertation submitted to the University of Bristol
in accordance with the requirements for award of the degree of
Doctor of Philosophy in the Faculty of Science

Word count: 52500

Abstract

Sedimentological and geochemical evidence indicate that during particular periods of Earth history, oceanic anoxia expanded and became widespread. These time intervals are associated with expansion of organic-rich black shale in the ocean. The extent, intensity and ecological effects of oceanic deoxygenation, however, differed amongst these events, and what caused those differences is still under debate. The strong association of anoxia with past warm periods, provides an appropriate platform to explore past anoxic systems and the formation of hydrocarbon source rocks, as well as a unique opportunity to investigate the interaction between the two major components, i.e. ocean oxygenation and a greenhouse climate. This thesis explores the processes that led to the spread of marine anoxia during the Cretaceous and across the Palaeocene Eocene Thermal Maximum (PETM), using organic biomarkers and a bulk geochemical approach. Reconstruction of the intensity and persistence of redox conditions and associated biomarker proxies for ecological change, in the proto South Atlantic during the Early Cretaceous suggests that during the initial stages of basin development, when the basin was restricted, anoxic and euxinic conditions were prevalent and occasionally extended into the upper water column. However, strong cyclicity in organic geochemical parameters imply that the anoxia/euxinia was not a persistent state. High amplitude fluctuations in redox conditions accompany fluctuations in marine productivity, likely resulted from the astronomically-controlled variations in the delivery of biolimiting nutrients from terrestrial runoff. This indicates that basin restriction, *per se*, did not cause anoxia but instead preconditioned the basin for oxygen depletion during episodes of enhanced organic matter production and export. Following a detailed characterisation of the Cretaceous anoxic system and black shales in the South Atlantic, the extent and persistence of PETM anoxia and photic zone euxinia were investigated within the Peri-Tethys margins. Organic biomarker proxies indicate an expansion of anoxia and photic zone euxinia during the PETM, but only in restricted marginal and epicontinental basins that amplified nutrient trapping and not in open marginal settings.

This thesis is dedicated to science,
In the hope of a better world for the generations to come…

Acknowledgments

I would like to thank my supervisors, Prof. Rich Pancost and Dr. David Naafs– I am truly grateful to them for their expertise, guidance, and support of my research, and their mentorship and friendship over the years. I would like to thank the University of Bristol, School of Chemistry, and the organic geochemistry group (OGU) for their world-class and friendly academic environment, and the generous support that they provided to me during my studies. I wish to thank the following people from University of Bristol for their kind supports over the years; Prof. Richard Evershed and Dr. Fanny Monterio for the constructive feedbacks at my annual progress monitoring sessions, Dr. Ian Bull and Mrs. Alison Kuhl for the technical supports, and Dr. Jens Holtvoeth for the helpful discussions.

I would like to acknowledge specific people with whom I had the pleasure to collaborate during this research project. In chapter 3, Prof. Gordon Love, Dr. Alex Dickson, Dr. Sietske Batenburg, Dr. Sabine Lengger, Dr. Gordon Inglis, Dr. Megan Rohrssen helped with discussion and performing some of the experiments and analysis; Prof. Philip A. Meyers and an anonymous reviewer for their constructive feedbacks and valuable suggestions on the published paper. In chapters 5 and 6, Dr. Alex Dickson, Dr. Stephen Grimes, Dr. Hayley Manners, Dr. Hassan Khozyem, Dr. Kyle Taylor for samples contribution; Prof. Ann Pearson and Dr. Jenan Kharbush for performing some of the analysis and helpful discussion. I wish to thank my viva examiners Dr. Stuart Robinson form University of Oxford and Prof. Paul Valdes from University of Bristol, for accepting to review my thesis.

I enjoyed every moment of the past four years by sharing the office and lab with my kind and supportive friends; Megan, Matt, Felipe, JP, Gordon, David, Sabine, Claudia, Vittoria and Jerome. My special thanks go to my lovely, caring and supportive friends beyond the school of Chemistry: Mehdi, Morti, Ida, Omid, Golnaz, Maryam, Ehsan, Mahsa, Yalda, Vida, Elham, Bahar, Shirin and many others who I could not have made this journey without.

Finally, and most importantly I would like to truly thank my amazing parents, Mehri & Ali, for their endless love, incredible supports and all the encouragements over the whole years of my studies, especially during my PhD. I never can thank enough to my brilliant family, and I cannot begin to describe how blessed I am to have Ali, Mehri, Mehdi & Morteza in my life.

Author’s declaration

I declare that the work in this dissertation was carried out in accordance with the requirements of the University's Regulations and Code of Practice for Research Degree Programmes and that it has not been submitted for any other academic award. Except where indicated by specific reference in the text, the work is the candidate's own work. Work done in collaboration with, or with the assistance of, others, is indicated as such. Any views expressed in the dissertation are those of the author.

SIGNED: ..... DATE: .....

Table of Contents

List of Figures

List of Tables

Abbreviation

°C	Degrees Celsius
‰	Permil
AOM	Anaerobic oxidation of methane
BIT	Branched vs Isoprenoidal Tetraether (index)
CCD	Calcium carbonate compensation depth
cm	Centimeters
CPI	Carbon preference index
Cren.′	Crenarchaeol
DCM	Dichloromethane
DSDP	Deep Sea Drilling Project
GC-FID	Gas Chromatography-Flame ionization detector
GC-C-IRMS	Gas Chromatography combustion isotope ratio mass spectrometry
GDGT	Glycerol dialkyl glycerol tetraether
hrs	Hours
HEX	Hexane
HI	Hydrogen Index
HPLC	High performance liquid chromatography
IC	Inorganic carbon
IPA	Isopropanol
IS	Internal Standards
ITCZ	Intertropical Convergence Zone
IODP	Integrated Ocean Drilling Program
m	Meters
m/*z*	Mass to charge ratio
Ma	Mega-Annum (million years)
mbsf	Meters below sea floor
MeOH	Methanol
MRM-GC-MS	Metastable Reaction Monitoring-gas chromatography-mass spectrometry
OAE	Oceanic Anoxic Events
OI	Oxygen Index
OM	Organic Matter
OSC	Organic sulphur compounds

PZE	Photic Zone Euxinia
PETM	Paleocene Eocene Thermal Maximum
Ph	Phytane
PMI	2,6,10,15,19-pentamethylicosane
PPM	Parts per million
Pr	Pristane
SA	South Atlantic
SIM	Single ion monitoring
SST	Sea surface temperature
TAR	Terrestrial_Aquatic Ratio
TC	Total Carbon
TEX_{86}	Tetraether index of tetraethers containing 86 carbon atoms
TLE	Total Lipid Extract
T_{max}	Temperature at which the maximum release of hydrocarbon occurs during Rock-Eval pyrolysis
TOC	Total Organic Carbon
TS	Total Sulfur
µl	Microlitre
VPDB	Vienna Pee Dee Belemnite
Wt.%	Weight percent carbon
$\delta^{13}C$	Ratio of carbon-13 to carbon-12 relative to VPDB
$\delta^{15}N$	Ratio of nitrogen-15 to nitrogen-14 relative to atmospheric standard
ρCO2	Partial pressure of atmospheric carbon dioxide

Chapter 1

Introduction

Preface

This chapter presents a brief overview of the mechanisms thought to cause anoxia in modern and past marine environments, as well as their biogeochemical implications. It also provides more focused reviews of marine anoxia and photic zone euxinia during, the PETM and the Early–Late Cretaceous, the specific time intervals of relevance to my thesis. From this discussion, I develop the main hypothesis and aims of my thesis and summarise the subsequent chapters. The primary approaches that I used during this research, especially biomarker proxies for past environmental conditions, are introduced and reviewed in Chapter 2.

1.1. Introduction

The modern ocean is largely oxygenated. Development of persistent anoxia in the modern marine realm is confined to isolated basins and area of high primary productivity, e.g. silled basins, meromictic lakes, coastal upwelling zones and fjords (reviewed in Meyer and Kump, 2008). Numerous studies, however, show that oceanic deoxygenation is expanding due to the largely agriculture-related increase in nutrient runoff (e.g. Conley et al., 2011; Diaz and Rosenberg, 2008; Slomp, 2009), causing physiological stress on marine life (Diaz, 2001). Additionally, anthropogenically-induced warming of the atmosphere-ocean system is expected to cause a general deoxygenation in the marine environment. Nevertheless, many details regarding this future expansion of marine deoxygenation remain uncertain.

Sedimentological and geochemical evidence indicate that during particular periods of Earth history, oceanic anoxia expanded and became widespread (e.g. Dickson et al., 2014b; Jenkyns, 2010; Pancost et al., 2004; Schlanger and Jenkyns, 1976; Sluijs et al., 2014). In fact, some of the most significant climate changes in the Earth history are accompanied with oceanic deoxygenation. The extent, intensity and ecological effects, however, differed amongst these

events, and what caused those differences is still under debate, indicating that a more complex response to current (anthropogenic-) climate change might be anticipated. This thesis explores the processes that lead to the spread of marine anoxia during the Cretaceous and across the Palaeocene Eocene Thermal Maximum (PETM).

1.2. Scientific Background

1.2.1 Terminology

Dissolved oxygen (largely essential to marine life) refers to the level of non-bonded or free oxygen molecules in the marine environment. Marine dissolved oxygen is sourced from atmospheric contact (equilibrium) and photosynthesis. The level of marine dissolved oxygen is generally influenced by physical (temperature, pressure, salinity) and biological (photosynthesis, aerobic respiration and decomposition of organic matter (OM)) processes. Depending on how all of these factors interact, oxygenation varies in different basins and at different depths and locations. The best example of this interaction is the development of oxygen minimum zones (OMZs), occurring at the chemocline (typically at the depths of <1000m) in the ocean water column. The OMZ is defined as the most O_2-deficient zone in the water column and is formed as a result of the downward flux of OM from above and its associated respiration (e.g. Cline and Richards, 1972; Devol, 1981; Wishner et al., 2000). The term "anoxia" refers to the total depletion of dissolved oxygen. Under anoxic conditions, much marine life is largely extinct (i.e. so called "dead zone"). Anaerobic microorganisms, however, thrive under anoxic conditions, largely by reducing alternative electron acceptors (subsequently: NO_2^-, NO_3^-, MnO_2, $FeHO_2$, SO_4^{2-}, $CH_3O_2^-$) (Canfield et al., 1995; Canfield et al., 1993a,b; Canfield and Thamdrup, 2009; Christensen et al., 1989; Murray and İzdar, 1989). Typically, sulfate (SO_4^{2-}) reduction leads to the production and accumulation of dissolved sulfide (H_2S) to toxic levels in the water column, and the presence of sulfide in the water column is termed as "Euxinia". The occurrence of euxinic (sulfidic) waters into the photic zone, i.e. the surface water layer (to the depth of about 100 m) that is exposed to a sufficient intensity of sunlight for photosynthesis, is termed "photic zone euxinia (PZE)".

1.2.2 What cause(s) anoxia/euxinia?

Persistent anoxic conditions in the modern ocean occur when certain physical and biogeochemical conditions are combined; i.e. elevated nutrient concentration and restricted water circulations (reviewed in Meyer and Kump, 2008); for examples in the Black Sea (Arthur and Sageman, 1994). However, anoxic conditions can also develop in non-stratified basins, e.g. in the upwelling coastal margins of Peru (Dugdale et al., 1977) and Arabian Sea (Ivanenkov and Rozanov, 1961). Thus, basin stratification likely contributes to development of anoxia (via decreasing oxygen supply to the deep ocean) but alone it is not a sufficient and necessary condition. The common feature between both stratified and non-stratified anoxic basins is an elevated nutrient supply which is required to maintain elevated productivity and is therefore the critical factor (Hotinski et al., 2001; Shen et al., 2002). There are also other factors occasionally invoked as important in causing local or more widespread anoxia, including restricted basin geography (Fischer and Arthur, 1977; Stanley, 1978), transgression (Arthur and Sageman, 2004) and warm climates (Fischer and Arthur, 1977).

Restricted basin geography and the development of estuarine circulation (e.g. Mediterranean Sea and Black Sea), especially where it amplifies the nutrient trap efficiency of the basin (Demaison and Moore, 1980; Stanley, 1978) are thought to be important controls. However, its significance in ancient events is contested. The GENIE Modelling (Ridgwell et al., 2007) of nutrient trapping efficiency in different continental configurations at different geological time intervals, i.e. Permian, Cretaceous, Paleocene-Eocene and Modern, exhibit a similar range of oxygen concentrations for a given nutrient input regime (Meyer and Kump, 2008). Similarly, changing the morphology of the basin via transgression (Arthur and Sageman, 2004) can also influence the nutrient trap efficiency and cause anoxia, but the relative importance of this mechanism has also been contested (Nielsen and Shen, 2004). For instance, the spread of severe anoxia during the late Permian occurs simultaneously with the marine regression (Hotinski et al., 2001). Similarly warm climates appear to be associated with marine anoxia, especially in those basins that are preconditioned by efficient nutrient trapping (Fischer and Arthur, 1977; Schlanger and Jenkyns, 1976), but the mechanism(s) are debated. During warm periods the solubility of oxygen in water is decreased (Hotinski et al., 2001), but the hydrological cycle is also intensified, resulting in enhanced continental weathering and nutrient supply to the ocean (Jenkyns, 2010).

The development of water column anoxia has a range of other biogeochemical impacts, some of which maintain the anoxic conditions. For instance, one of the biogeochemical feedbacks resulting from development of marine anoxia (expansion of photic zone euxinia), is

the process of denitrification, associated with nutrient (N) deficiency (Schubert and Calvert, 2001), which favours nitrogen fixing photoautotrophs. The establishment of nitrogen fixing photoautotrophs is followed by the export of the biologically fixed nitrogen through the anoxic water column (without oxidation) and provides enhanced nutrient to the deep ocean (Meyer and Kump, 2008), and enhances deoxygenation. Following the establishment of anoxia and the subsequent Fe reduction, iron-sorbed phosphate liberates into the water column (Ingall et al., 1993; Canfield et al., 1995; Canfield et al., 1993a,b; Canfield and Thamdrup, 2009), creating a highly eutrophic condition (positive feedback). The subsequent production of sulfide (by sulfate reducing bacteria) combining with the stimulated phosphate concentration, amplifies anoxia to the more sever state of euxinic condition.

Overall, there appears to be an emerging consensus that the dominant control on regional and more globally widespread anoxia is the delivery to and partitioning of nutrients in the ocean (Jenkyns, 2010). This is modulated by regional (basin geomorphology), creating localised areas or basins of extreme anoxia, and global (climate) factors that impact oxygen solubility, ocean circulation and the weathering of the terrestrial environment (Carmichael et al., 2017).

1.2.3 Development of anoxia during past warm climates

The strong association of anoxia with past warm periods (e.g. Dickson et al., 2014b; Forster et al., 2008; Naafs et al., 2013; Pancost et al., 2004; Sluijs et al., 2014; Fischer and Arthur, 1977; Seymour O Schlanger and Jenkyns, 1976), provides an appropriate platform to explore past anoxic systems as well as a unique opportunity to investigate the interaction between the two major components, i.e. ocean oxygenation and a greenhouse climate.

1.2.3.1 Development and intensity of anoxia during the Cretaceous

During the Cretaceous (~145-66 million years ago), the Earth was characterised by a greenhouse climate (e.g. Francis & Frake 1993; Wilson & Norris 2001; Hay 2008) with elevated atmospheric CO_2 levels (typically > 500 ppm, e.g. Beerling et al. 2002; Wang et al. 2014; Naafs et al. 2016), high sea surface temperatures (SSTs) (Schouten et al. 2003; Bice et al. 2006; Sinninghe Damsté et al. 2010; Littler et al. 2011; Naafs and Pancost, 2016; O'Brien et al. 2017), high terrestrial mean annual temperature (MAT; Amiot et al., 2004; Herman and Spicer, 1996), warm deep oceans (Cramer et al., 2009; Friedrich et al., 2012), little or no

continental ice sheets (Huber et al., 2002), and a weak latitudinal temperature gradient (Barron, 1983; Huber et al., 1995, 2002). The Cretaceous greenhouse, however, was interrupted by some short intervals of global cooling (e.g. Frakes and Francis, 1988; Hong and Lee, 2012; Jenkyns et al., 2012; McAnena et al., 2013; Mutterlose et al., 2009; Dumitrescu and Brassell, 2006; Kim et al., 2010; Kuhnt et al., 2011; Pucéat et al., 2003). The Cretaceous is also characterised by a series of oceanic anoxic events (OAEs) that are associated with the expansion of anoxia and deposition of organic rich black shales in the ocean (e.g. Schlanger & Jenkyns 1976; Jenkyns 2010), *Figure 1.1*. OAEs are associated with profound perturbations in global climate (e.g. thermal maxima), ocean chemistry and global biogeochemical cycles (reviewed by Jenkyns, 2010), reflected, for example, in the variety of pronounced isotopic events. Most significantly, the enhanced burial of ^{13}C-depleted organic matter means that many OAEs are defined by the presence of negative carbon isotope excursions (CIEs).

It is generally thought that OAEs were triggered by CO_2-induced global warming (reviewed by Jenkyns, 2010), although the source and magnitude of the injected carbon is still under debate. In many cases, the source of carbon appears to be from a reduced reservoir (hydrates or organic matter) and therefore depleted in ^{13}C. Thus, the $\delta^{13}C$ record is characterised by a negative CIE associated with this injection of 'light' carbon, followed by a positive CIE due to the burial of ^{13}C-depleted organic matter, although the relative duration and magnitude of these features vary. The global imprint of OAEs have been identified even in some lake sediments (Xu et al., 2017), which is consistent with a global driver i.e. warming induced changes in chemical weathering and nutrient inputs as discussed above. However, development of anoxia during these events is not spatially ubiquitous. What controls the expansion and intensity of anoxia during different OAEs is still debated, but it is likely is modulated by geography and ocean circulation as it is today (Jenkyns, 2010; Weissert, 2000).

There are six OAEs proposed for the mid-Cretaceous (Arthur et al., 1990) and one for the Jurassic (Jenkyns, 1988). Mesozoic OAEs that are associated with major changes in marine chemistry are T-OAE (Posidonienschiefer event), OAE1a (early Aptian), OAE1b (early Albian), and OAE2 (Cenomanian/Turonian, ~93.5 Ma) (Jenkyns, 2010), Figure 1.1. The most expanded of these episodes, is the OAE2 (Cenomanian/Turonian) which is largely evidenced and studied (e.g. Beil et al., 2018; Forster et al., 2008; Sinninghe Damsté et al., 2010).

There are numerous evidences of redox changes during the OAE2, for instance the relatively low bulk carbonate I/Ca values as the robust suboxic proxy during the OAE 2 (Zhou et al., 2015), enrichment of redox-sensitive trace metals such as Fe and Mo (Owens et al., 2012), laminated black shales and high TOC values (e.g. Forster et al., 2008; Kuypers et al., 2002), presence of isorenieratane as the biomarker of photic zone euxinia (e.g. Kuypers et al., 2004,

2002). Monteiro et al. (2012) represent an intermediate-complexity Earth system model GENIE (Ridgwell et al., 2007) of development of anoxia and photic zone euxinia during the OAE2. This model-data comparison indicates that ocean anoxia expands from 5% to at least 50% during the OAE2, and this expansion was mainly (85%) caused by higher nutrient content and enhanced primary production (Monteiro et al., 2012).

The occurrence of anoxia during the Cretaceous is not exclusive to OAEs, and organic rich black shales are often deposited during other time intervals (e.g. Huang et al., 2010). The regional development of anoxia is controlled by local factors, e.g. changes in nutrient availability, continental hydrology, and basin morphology. However, these have not been as thoroughly studied. Identifying the factors involved in the formation of Cretaceous black shales could provide a better understanding of Cretaceous biogeochemical cycles and climate feedbacks, in general, as well as the development of anoxia in a greenhouse system.

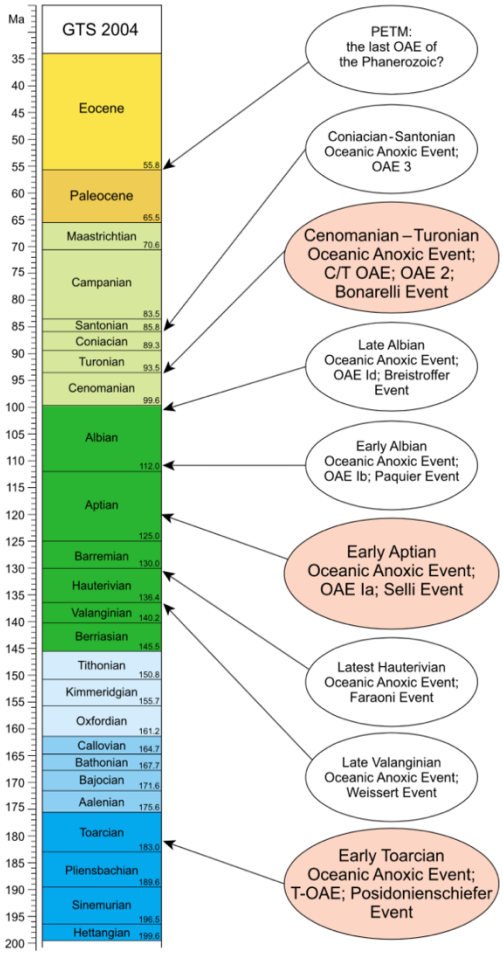

Figure 1.1. The stratigraphic position of the major Mesozoic OAEs, and the Paleocene-Eocene Thermal Maximum (PETM) (Jenkyns, 2010).

1.2.3.2 Development and intensity of anoxia during the PETM

The Paleocene-Eocene Thermal Maximum (PETM; 56 Ma) (Kennett and Stott, 1991) is the most pronounced hyperthermal event (e.g. Frieling et al., 2014; A. Sluijs et al., 2006; Sluijs et al., 2011, 2014) of the Cenozoic. Although classically not considered an OAE, the PETM shares many features with Mesozoic OAEs (e.g. Jenkyns, 2010), in particular a strong negative carbon isotope excursion indicative of a rapid injection of isotopically light carbon into the ocean-atmosphere system (Kennett and Stott, 1991). The PETM negative excursion, however, is not followed by a positive excursion, likely indicating that global burial of ^{13}C-depleted organic matter was not as significant as during the Mesozoic OAEs.

Nonetheless, the PETM still experienced a similar pCO_2 and warming driver as those associated with Mesozoic OAEs. The PETM was also characterised by increased sedimentation rates, nutrient inputs and increased algal productivity that are invoked as causes of widespread anoxia during the OAEs (Sluijs et al., 2014). As such, some similarities are expected with Mesozoic OAEs. The deep ocean during the PETM experienced a minor deoxygenation (e.g. Chun et al., 2010; Plike et al., 2014; Colosimo et al., 2006; Palike et al., 2014; Zhou et al., 2014). Shelf and marginal marine settings and restricted basins experienced suboxic/anoxic conditions (e.g. Sluijs et al., 2008; Nicolo et al., 2010; Egger et al., 2005; Bolle et al., 2000; Dickson et al., 2014a, 2014b; Gavrilov et al., 2003, 1997), and on a few continental shelves photic zone euxinia occurred (e.g. Sluijs et al., 2006; Schoon et al., 2013; Frieling et al., 2014; Sluijs et al., 2014; Frieling et al., 2017), *Figure 1.2*. Nonetheless, widespread black shale deposition did not occur, either because greenhouse forcing was insufficient, climate-weathering feedbacks were different and/or paleogeography was not conductive to water column stratification and development of extensive euxinic conditions (Jenkyns, 2010; Sluijs et al., 2008). Mapping the extent of PETM anoxia/euxinia, therefore, is crucial to better understanding the underlying mechanisms and relationships between warming and anoxia.

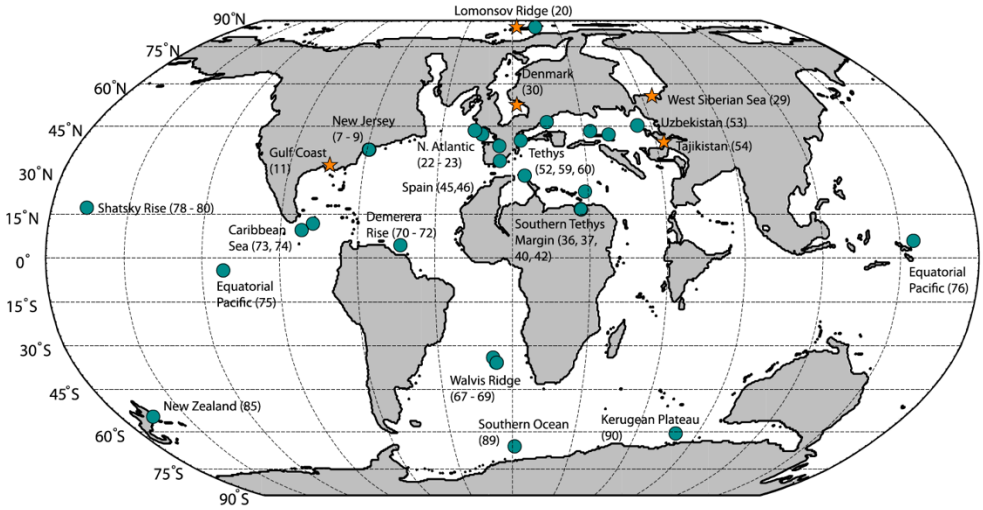

Figure 1.2. Paleogeographic map during the PETM. Highlighting the locations where deoxygenation is observed. Locations with the evidence of deoxygenation (suboxic) are shown with green circles, and locations with the evidence of photic zone euxinia are shown with the red star (Carmichael et al., 2017).

1.2.3.3. Perturbations to the biogeochemical cycles during the OAEs and PETM

OAEs and PETM were associated with major disturbance in the chemistry of oceans, this is featured in the perturbations in geochemical cycles e.g. carbon cycle (Jenkyns, 2010) and nitrogen cycle (Higgins et al., 2012; Junium et al., 2018) during these events.

The dynamic of the carbon cycle in paleo-environments can be traced by analysing boron isotope (Pearson and Palmer, 2000), plant fossils indices (Berner, 1997), and $\delta^{13}C$ in marine sediments, marine phytoplanktons and paleosols (Foster et al., 2017). The latter is used more frequently and is also used in this thesis. Naturally, there are two stable carbon isotopes (^{12}C, ^{13}C) and an unstable carbon isotope (^{14}C) with a half-life of 5730±40 years (Godwin, 1962), with ^{12}C be the most abundant (98.9%). Therefore, the carbon cycle is dominated by ^{12}C and contribution of only minor amounts of stable ^{13}C (1.1%) and unstable ^{14}C (10^{-10} %). Isotope records can be representative of perturbations in carbon cycle either in global or regional scales. $\delta^{13}C$, is the measure of the ratio of stable isotopes ^{12}C and ^{13}C which is reported in per mil (‰). The negative excursion in $\delta^{13}C$ during OAEs and PETM, is interpreted as a

massive and rapid injection of isotopically light carbon into the ocean-atmospheric system (Jenkyns, 2010; Mcinerney and Wing, 2011), as the cause or perhaps a positive feedback of the hyperthermal event. Nevertheless, the several hypothesis for the possible source of ^{13}C-depleted carbon at the onset or during these events (e.g. Deconto et al., 2012; Dickens et al., 1995; Hesselbo et al., 2000; Higgins and Schrag, 2006; Jahren et al., 2001; Jenkyns et al., 2003; Svensen et al., 2004; Westerhold et al., 2009); the source, magnitude and mechanism of this carbon release during or at the onset of the OAEs (reviewed by Jenkyns, 2010) and PETM (reviewed by McInerney & Wing, 2011) is an ongoing debate.

The dynamics of the marine N-cycle in paleo-environments can be reconstructed by analysing the $\delta^{15}N$ of biomass ($\delta^{15}N_{bulk}$) (Galbraith et al., 2008). Depleted $\delta^{15}N_{bulk}$ record in black shales, have been explained by enhanced ammonium (NH_4) assimilation, rather than nitrification, under anoxic/euxinic condition (Higgins et al., 2012; Junium et al., 2018; Kuypers et al., 2004; Meyer and Kump, 2008). Such depleted $\delta^{15}N_{bulk}$ record is reported from recent sediments (Holocene sapropels) of the Eastern Mediterranean Sea (Möbius et al., 2010), the Cretaceous OAEs (Rau et al., 1987), and during the PETM in the Peri-Tethys (Junium et al., 2018) and Arctic Ocean (Knies et al., 2008). $\delta^{15}N_{bulk}$, however, are subject to diagenetic alternations (Robinson et al., 2005; Sachs et al., 1999). Therefore measuring the isolated organic nitrogen is a more robust proxy to reconstruct nitrogen cycles (Chicarelli et al., 1993; Higgins et al., 2009; Pearson et al., 2010), for instance porphyrins, derived from chlrophylls, that contain N in their structure (Gibbison et al., 1995). $\delta^{15}N_{porphyrin}$ is a suitable proxy to measure the composition of nutrient utilised by phytoplanktons(Higgins et al., 2011). The difference (ε_{por}) between $\delta^{15}N_{porphyrin}$ and $\delta^{15}N_{bulk}$ provides insights into the relative contribution of N_2 fixing eukaryotes and cyanobacteria (Higgins et al., 2011), and ultimately enables to constrain the paleoceanography of the basin (Higgins et al., 2012, 2011).

1.3. Research objectives and aims

The overall objective of my PhD is to explore and develop a more robust insight into the climatic processes and mechanisms that lead to the spread of marine anoxia during past warm climates. My thesis explores a range of related but distinct questions related to the spread and intensity of anoxia in the Mesozoic and Cenozoic, and it explores a variety of different contexts and therefore different predominant tectonic and climatic controls on marine anoxia. The specific aims (1.3.1–1.3.4) of this thesis are as follows:

1.3.1. To assess the derivers of anoxia and redox variability in the proto-South Atlantic basin during the Aptian

Early Aptian OAE 1a (Bralower et al., 1994) is one of the most widely studied of the Mesozoic OAEs (Jenkyns, 2010); however, our understanding of it is largely based on Northern Hemisphere (N Atlantic and Tethyan) records, with the extent and persistence of anoxia in the Southern hemisphere being poorly constrained. In order to develop a better understanding of the extent, nature and controls on South Atlantic anoxia, I investigated Aptian age bulk geochemical and sedimentary organic matter obtained from DSDP Site 364 in the proto-South Atlantic. I used high resolution geochemical records (TOC, HI and T_{max}) and geochemical biomarkers (lycopane, isorenieratane, chlorobactane, isoprenoid thiophenes) to reconstruct the variations in redox climate and chemocline depth. Furthermore, other geochemical biomarkers (e.g. steranes and hopanes) were used to reconstruct the variations in marine productivity and marine ecosystem.

1.3.2. To reconstruct sea surface temperature in the proto-South Atlantic basin during the Aptian–late Albian, and the perturbations in the carbon cycle

Although the Albian sedimentary record indicates intense periods of anoxia, a complete record of SSTs through the Albian is not reconstructed yet (*Figure 1.3*). In this chapter, I reconstruct a long-term record (Aptian–late Albian) of SSTs from the low latitude South Atlantic (DSDP Site 364). I used the distribution of GDGTs and the established calibrations; i.e. TEX_{86}^{H}-SST and $TEX_{86-linear}$-SST to reconstruct the sea surface temperature. I also used bulk TOC stable carbon isotope ($\delta^{13}C_{org}$) analysis to reconstruct the perturbations of carbon cycle which are preserved in the basin.

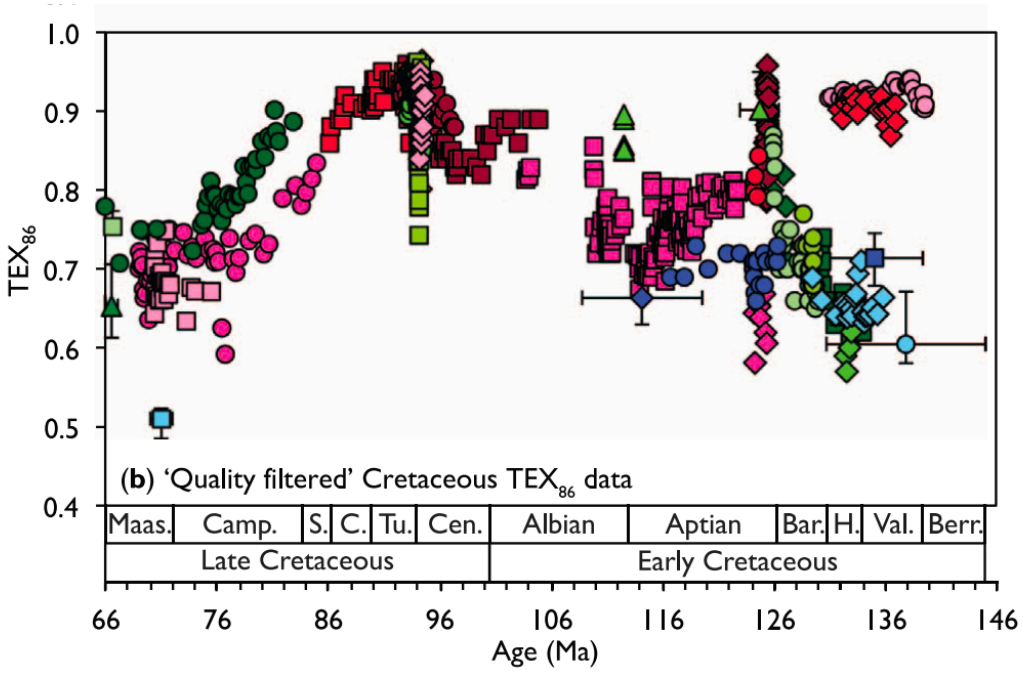

Figure 1.3. Compiled TEX_{86} values during the Cretaceous (146–66 Ma). Low- latitude (0–±30°) Sites are shown in red shades, mid-latitude (–±30°–48°) sites in green shades, and high latitudes (>±48°) blue shades (O'Brien et al., 2017).

1.3.3. To reconstruct the spread of photic zone euxinia during the Paleocene-Eocene Thermal Maximum (PETM)

The Paleocene-Eocene Thermal Maximum (PETM) is the most dramatic hyperthermal event of the Cenozoic, and has been argued to be the best analog for current climate change (e.g. Dickson et al., 2012). However, the intensity of anoxia; i.e. the extent and persistence of photic zone euxinia (PZE), during the PETM is still not well constrained. The occurrence of the PETM throughout the northern Peri-Tethys realm, is associated with the deposition of organic-rich sediments (Gavrilov et al., 2003) and extent of anoxia (Dickson et al., 2014b). I compile sediments from the margins of northern Peri-Tethys (Guru-Fatima, Kheu River, and Dzhengutay), southern Peri-Tethys (Dababiya) and western Peri-Tethys (North Atlantic; Zumaia) PETM sections. I analysed geochemical biomarkers (lycopane and isorenieratane) to reconstruct the development of anoxia and PZE during the PETM. One of the consequences of marine anoxia is an increase in denitrification, which causes perturbations in the nitrogen cycle. $\delta^{15}N_{Porphyrin}$ and $\delta^{15}N_{bulk}$ were also analysed at Dzhengutay and Guru Fatima sections (this analysis was performed in collaboration with Harvard University), the results assist in reconstructing the source of nitrogen fixing that was dominated during the PETM.

1.3.4. To reconstruct the PETM record of sea surface temperature in the Peri-Tethys

The key feature of PETM is an abrupt increase in global temperature, inferred by geochemical proxies. However, there are only few records of SST from the mid latitudes, and there is no record of SST from the Peri-Tethys region where some of the most intense anoxia and record of black shales has been recorded during the PETM (Dickson et al., 2014b). Assuming that enhanced marine productivity in the Peri-Tethys during the PETM played an important role in consuming the excessive atmospheric CO_2, and decrease of temperature, I determined the distribution of GDGTs and applied the TEX_{86} proxy at Kheu River, to reconstruct the magnitude of SST warming during the PETM.

1.4. Thesis structure

The objectives and specific aims of this thesis are explored in Chapters 3–7, whereas Chapter 2 includes a review of the methods that are used to approach these objectives.

In **chapter 3**, I reconstruct the intensity and persistence of redox conditions, as well as associated biomarker proxies for ecological change, in the proto South Atlantic during the Aptian–late Aptian. High organic burial is restricted to deepest studied interval (Unit 7b), likely associated with the basin restriction prior to more complete opening of the South Atlantic. However, high amplitude fluctuations in redox conditions accompany fluctuations in marine productivity, likely resulting from eccentricity-modulated precession changes in the delivery of biolimiting nutrients from terrestrial runoff. This indicates that basin restriction, *per se*, did not cause anoxia but instead preconditioned the basin for oxygen depletion during episodes of enhanced organic matter production and export.

To explore the longer term history of the proto South Atlantic, **chapter 4** examines the long term (Aptian–Coniancian; ~20 Myr) changes in the carbon cycle as expressed in $\delta^{13}C_{org}$ values and TOC contents. This suggests that OAE 1a and OAE 1d have been recorded in this sequence, both of which are associated with enhanced OM burial. This also provides a framework for determining SST change in the S Atlantic through the Aptian–late Albian using TEX_{86} proxy. Aside from being an important new low latitude record, this is a more complete, single-site record of SST through the Albian.

Following a detailed characterisation of Cretaceous paleoclimate, **chapter 5** investigates the extent and persistence of PETM anoxia and photic zone euxinia within the Peri-Tethys margins. Collectively, these data suggest that photic zone euxinia during the PETM only developed in restricted continental shelf basins and not in open marginal settings. Moreover,

the nitrogen cycle is studied by measuring the $\delta^{15}N_{Porphyrin}$ and $\delta^{15}N_{Total}$ values in Dzhengutay sediments. Bulk nitrogen isotope values are consistently more depleted when the basin experienced photic zone euxinia; further insight is provided by the offset between $\delta^{15}N_{Porphyrin}$ and $\delta^{15}N_{bulk}$, reflective of the dominant cyanobacteria contributor to buried OM (Higgins et al., 2011). This chapter demonstrates that during the PETM, anaerobic oxidation of organic matter precedes from denitrification to sulfate reduction in the sediments. Consequently euxinic (H_2S) and stratified waters expanded (episodically) toward the photic zone where green sulfur bacteria thrived. This chapter is of importance because it reveals a significant expansion of marine water column anoxia and persistent PZE during the PETM, which heretofore had been largely limited to the enclosed Arctic Ocean.

In **chapter 6,** I investigate the carbon isotope profiles through the Tethyan PETM using marine biomarkers; i.e. pristane ($\delta^{13}C_{Pr}$) and phytane $\delta^{13}C_{Ph}$), and associated TEX_{86}-derived SST change. These results demonstrate that during the PETM isotopic fractionation by marine algae increased, as expected with an increase in *p*CO2. The GDGT-based sea surface record is the first record of PETM SST in the northern Peri-Tethys and reveals a strong PETM warming but one that is broadly consistent with other PETM sites.

Finally, **chapter 7** provides a synthesis of the results and a conclusion to this research work. It also provides a context for future investigations.

Chapter 2

Materials and methodology

This chapter comprises three components. First, it reviews the literature related to the biomarkers central to achieving the aims and objectives of this thesis, i.e. the methodological approach for examining past redox changes, stratification, SST, etc. Second, it summarises the samples including sampling sites and ages (further details are provided in individual chapters). Third, it describes the specific analytical methods by which biomarker abundances, distributions and isotopic compositions (and other non-biomarker data) are determined.

2.1. Biomarkers and associated environmental proxies

This section provides a brief literature review related to the biomarkers and proxies which are frequently used in the thesis. More details are provided in their attributed chapters (chapters 3–6).

2.1.1 Biomarker proxies used to identify the source of OM

2.1.1.1 *n*-Alkanes

n-Alkanes (*m/z* 71) are too widespread and general to be considered as diagnostic biomarkers, especially once biologically-specific distribution patterns have been lost during diagenesis. However, a range of parameters and ratios involving *n*-alkanes have been proposed and widely used to assess source of organic matter. For instance, long-chain odd numbered *n*-alkanes (i.e. C_{25}-C_{33}) are abundant in epicutular waxes of higher plants, i.e. to prevent water loss, minimize mechanical damage and prevent fungal and insect attack (e.g. Rieley et al., 1991). Therefore, the Carbon Preference Index (CPI) has been developed as a proxy for estimating the potential contribution of *n*-alkanes from higher land plants to sediments. The CPI is calculated as the ratio of odd to even *n*-alkanes (in the long-chain range of C_{24} to C_{34} centred on C_{29}), usually calculated as the following equation (Bray and Evans, 1961):

$$CPI = \frac{1}{2}\left(\frac{C25+C27+C29+C31+C33}{C24+C26+C28+C30+C32} + \frac{C25+C27+C29+C31+C33}{C26+C28+C30+C32+C34}\right)$$

CPI>>1, then the terrestrial component of the organic matter has been minimally degraded (Bray and Evans, 1961). However, CPI is also influenced by thermal maturity (Hatch et al., 1987), especially in sediments and rocks of ages similar to those studied here. The *n*-alkane ratio of $\frac{C17}{C17+C31}$ is another classic proxy used to assess the relative contribution of marine and terrestrial organic matter (González-Vila et al., 2003; Meyers, 2003; Ratnayake et al., 2006; Wenchuan et al., 1999). This proxy is based on the fact that marine organisms predominantly produce short-chain *n*-alkanes (<C_{21}), i.e. for the purpose of food storage, insulation and buoyancy in water. On the other hand, the C_{27}, C_{29} and C_{31} *n*-alkane are dominant in terrestrial higher plants, with the dominant homologue depending on the plant types (Cranwell, 1973; Ficken et al., 2000). Similarly, the more inclusive ratio of long vs short chain odd number n-alkanes is also used to assess the proportion of terrestrial and marine (Jaffé et al., 2001) sources of organic matter, the Terrestrial-Aquatic Ratio (TAR):

$$TAR\ (HC) = \frac{C27+C29+C31}{C15+C17+C19}$$ (Bourbonniere and Meyers, 1996);

Where, the proportion of terrestrial *n*-alkanes increases with TAR. However, both of these ratios are strongly impacted by catagenesis (Bray and Evans, 1961; Gonzalez-Vila, 1995; González-Vila et al., 2003)

2.1.1.2 Steranes

Steranes (*m/z* 217) are derived from sterols, widespread and important components in the cell membranes of eukaryotes (de Leeuw et al., 1989; Mackenzie et al., 1982). Some sterols (C_{27}-C_{30}) are specific to certain photosynthetic organisms and their diagenetic derivatives are considered as biomarkers (i.e. C_{27}-C_{30} regular steranes and methylsteranes, *Figure 2.1)*. However, there are some limitations regarding the connection between regular C_{27}-C_{29} steranes and their precursors, largely arising from the fact that few are entirely diagnostic with all deriving from a range of sources (e.g. Huang and Meinschein, 1979, Kodner et al., 2008; Volkman et al., 1994, 1993). Therefore, it is not recommended to interpret the biological source of organic matter based solely on the dominance of the sterane carbon number distribution (e.g. Kodner et al., 2008). For instance, C_{27} and C_{29} sterols are preferentially synthesized by red algae and green algae, respectively. However in both of these groups, in some species, either C_{28} and/or low-high quantities of C_{29} and C_{27} sterols can occur (Kodner et al., 2008). Therefore,

although the variations in C_{27}-C_{29} sterane distribution provide evidence for ecological and/or OM source change, the specific meaning of these changes is difficult to detangle. It is generally thought that the C_{30} steranes and methylsteranes are somewhat more diagnostic, and especially for inputs of marine organic matter (Moldowan, 1984), e.g. the C_{30} regular sterane (24-npc) is a biomarker for predominantly marine pelaogophyte algae in Devonian and younger sedimentary rocks (e.g. Cao et al., 2009); 4-methylstigmastane and dinosteranes are indicators for marine (Goodwin et al., 1988; Moldowan et al., 1985; Summons et al., 1987) and non-marine (Jiamo et al., 1990) dinoflagellates.

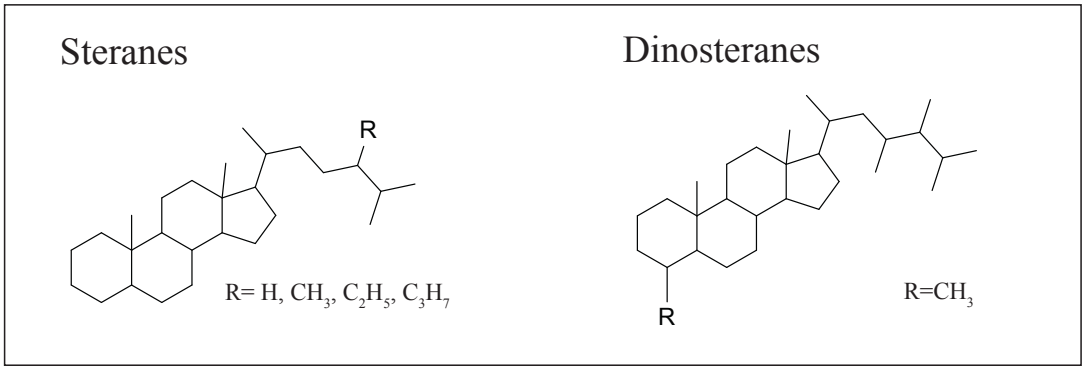

Figure 2.1 . Schematic structure of steranes and dinosteranes

2.1.2. Biomarker proxies for paleo redox conditions

2.1.2.2 Isorenieratene, Chlorobactene and their derivatives

Isorenieratane (*m/z* 134+133 and *m/z* 546 as the molecular ion, *Figure 2.2*) is derived from the carotenoid isorenieratene, which occurs in the brown coloured strains of photosynthetic green sulfur bacteria (chlorobiacae) (Gloe et al., 1975; Imhoff, 1995; Koopmans et al., 1996; Schmidt, 1978). These GSB require both sunlight and hydrogen sulphide, typically where the chemocline occurs in the photic zone (i.e. depths < 150 m, where the light levels 1% of sea surface irradiance) (Imhoff, 1995; Van Gemerden and Mas, 1995). Therefore, the biomarker isorenieratane, is a robust proxy for photic zone euxinia (e.g. Koopmans et al., 1996) with its abundance reflecting either the depth of penetration by euxinic waters into the photic zone, or their persistence. The nine conjugated double bonds of isorenieratene make it highly susceptible to reactions with reduced inorganic sulphur species (i.e. HS-) that occur in euxinic waters and sediments, and incorporation of sulphur into isorenieratene results in the early

diagenetic formation of multiple S-linked isorenieratene moieties in high molecular weight (HMW) fractions and kerogen (Sinninghe Damste et al., 1989, Schouten et al., 1994).

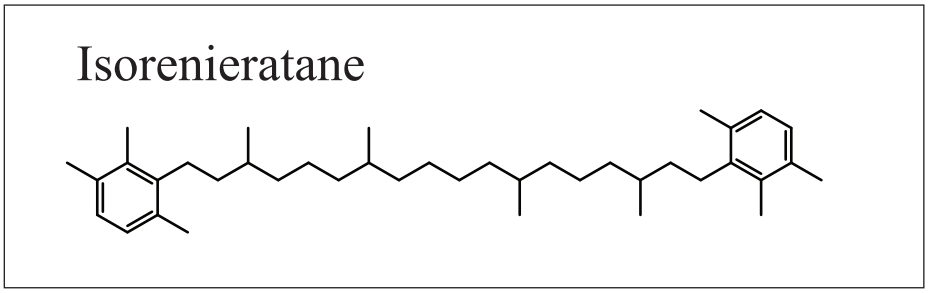

Figure 2.2 Schematic of isorenieratane molecule.

Chlorobactane (*m/z* 134+133 and *m/z* 554 as the molecular ion, Figure *2.3*) is derived from chlorobactene, a carotenoid similar to isorenieratane but is exclusively produced by the green strain of green sulfur bacteria (Brocks and Schaeffer, 2008; Gloe et al., 1975; Imhoff, 1995; Sousa Júnior et al., 2013), which thrive at shallow depths (<15 m) (Van Gemerden and Mas, 1995). As such, it is generally considered to be a biomarker for more pronounced euxinic conditions, at shallower depths, than isorenieratane.

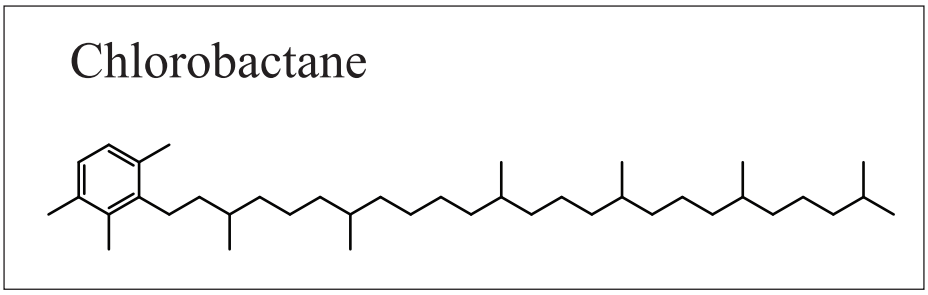

Figure 2.3 The schematic of chlorobactane molecule.

2.1.2.4 Lycopane

Lycopane (2,6,10,14,19,23,27,31-octamethyl dotriacontane, Figure *2.4*) is a C_{40} isoprenoid and a biomarker often invoked as an indicator of water column anoxia (Sinninghe Damsté et al., 2003); however the biological source of lycopane has not yet been identified (Sinninghe Damsté et al., 2003). Lycopane co-elutes with C_{35} *n*-alkane (on most GC stationary phases).

Therefore, the proportion of "C_{35}+lycopane" relative to the series of other long-chain *n*-alkanes is typically determined. Such lycopane ratios are generally higher in sediments underlying oxygen minimum zones (OMZ) (Farrington et al., 1988; Schulte et al., 1999; Sinninghe Damsté et al., 2003). In particular, the ratio of C_{35}+lycopane/C_{31} (lycopane ratio) has been proposed to be a proxy for anoxic conditions in the water column (Sinninghe Damsté et al., 2003). This anoxic proxy is generally interpreted as local relative changes within a sedimentary sequence rather than as an absolute values for degree of anoxia (Sinninghe Damsté et al., 2003). For example, the maximum value of the lycopane ratio in the OMZ sediments of the Arabia Sea is ~0.8 (Schulte et al. 1999, Sinninghe Damsté et al. 2003) and across the Peruvian Shelf it is ~2.5 (Farrington et al. 1988; Sinninghe Damsté et al. 2003), but this cannot simply interpret as more intensity of anoxia in Peruvian Shelf than Arabia Sea.

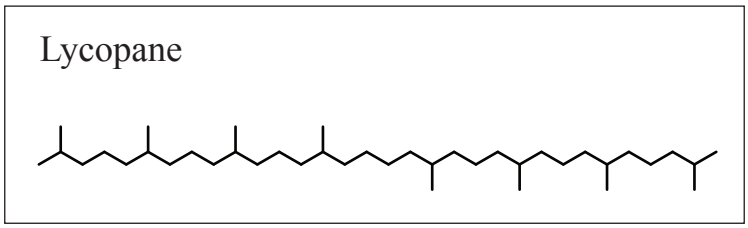

Figure 2.4. The schematic of lycopane molecule.

2.1.3 Biomarker proxies for paleosalinity

2.1.3.1 C_{20} isoprenoid thiophene

Organic sulphur compounds (OSC) are formed by incorporation of inorganic sulfur into organic matter during diagenesis (Sinninghe Damste et al., 1990; Sinninghe Damsté et al., 1988). Their formation requires presence of free H_2S (other polysulphides), which requires specific sedimentary conditions (sulphate reduction, low availability of iron) (Sinninghe Damst'e et al., 1990), especially euxinic conditions (Sinninghe Damsté et al., 1989). OSC are more stable than the original compounds against microbial attack, and they can provide insights into environmental conditions that could have been lost during degradation of their characteristic labile precursors (Brassell et al., 1986). Distributions of OSC vary considerably and are considered as paleoenvironment proxies (Sinninghe Damsté et al. 1989), for example the distribution of C_{20} isoprenoid (mid-chain) thiophenes (*m/z 308*, Figure *2.5.*) varies in hypersaline and non-hypersaline environments and is used as an indicator of hypersalinity

(Sinninghe Damsté et al. 1989; de Leeuw et al., 1990; Sinninghe Damsté and de Leeuw, 1990). The isoprenoid ratio to determine hypersalinity is described by the equation below;

$$\frac{\text{VII+VI}}{\text{I+II+III+IV+V}}$$ (*the numbers are described in figure* 2.5., Sinninghe Damsté and de Leeuw, 1990)

This ratio is recommended as a hypersalinity proxy for paleoenvironments, i.e. the ratio of <0.5 reflects hypersaline environment (Sinninghe Damsté and de Leeuw, 1990).

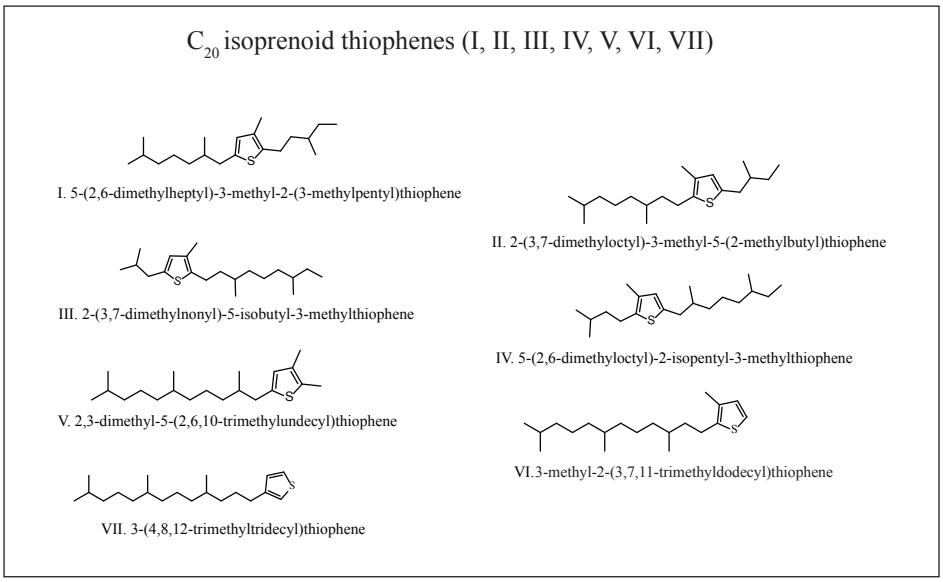

Figure 2.5. The schematic of mid chain C20 isoprenoid thiophene molecules.

2.1.4. Biomarker proxies used to constrain thermal maturity

2.1.4.1 Hopane group

During thermal maturation, bonds can crack – with C-S and C-O bonds typically doing so before C-C bonds – and compounds will rearrange into more stereochemically stable configurations (e.g. Mackenzie et al., 1980). This can negatively impact some proxies, i.e. the cracking of n-alkanes undermines their use as source indicators as discussed above. Similarly, the fidelity of GDGT-based temperature proxies (see below) is sensitive to thermal degradation (Schouten et al., 2004). Therefore, assessing the thermal maturity of sediments is important for

the evaluation of biomarker proxies and devising an analytical strategy. Stereochemical rearrangement, especially of hopanes and steranes, can be determined and used to assess thermal maturity. Hopanes (*m/z* 191) are ubiquitous biomarkers derived from bacteriohopanepolyols (BHPs; Quirk et al., 1984; Sinninghe Damsté et al., 1995). BHPs are an essential part of some bacterial membranes and are thought to contribute to their stability – analogous to sterols in eukaryotic membranes (Ourisson and Albrecht, 1992; Sinninghe Damsté et al., 1995). The carbon skeletons of BHPs and hopanes contain several chiral centres, mainly at C-17 and C-21 (but also at C-22 in $>C_{31}$ hopanoids) and resulting in hopanoids with three stereoisomeric series, i.e. 17α,21β(H)-, 17β,21β(H)-, and 17β,21α(H)-hopanes (Seifert and Moldowan, 1980). The ββ series is almost ubiquitously the biological form (Ensminger, 1977) but it is also the most thermally unstable. Therefore, during ongoing thermal maturation, the biological configuration of hopanes (ββ) converts to the βα and then the most stable αβ configurations. Therefore, the proportion of ββ over the other hopane configurations, i.e. ββ /(ββ+βα+ αβ) is used as a proxy for the thermal maturity of sediments (Seifert and Moldowan, 1980; Mackenzie et al., 1980), Figure *2.6*

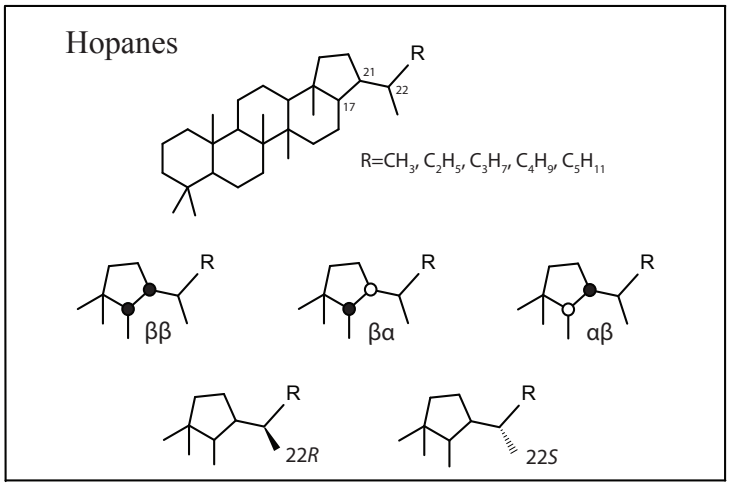

Figure 2.6. The schematic of molecules with the stereochemistry configurations of hopanes (ββ, βα, αβ, R, S).

2.1.5. Biomarker proxies used to identify paleo sea surface temperature (SST)

2.1.5.1 Isoprenoid GDGTs

Isoprenoidal glycerol dialkyl tetraethers (isoGDGTs) are characteristic membrane lipids of the Archaea (Gambacorta et al., 1995; Uda et al., 2001). The Thaumarcharota belong to the domain

Archaea (Woese et al., 1990) and are widespread in marine and terrestrial environments (Karner et al., 2001). The particular isoGDGTs synthesised by Thaumarchaeota are diverse but typically contain 0–3 cyclopantane moieties (GDGT 0–3) or contain four cyclopantane and one cyclohexane moiety (crenarchaeol (Cren.) and crenarchaeol regioisomer (Cren.′). Experiments have shown that the relative distribution of cyclopentane and cyclohexane rings in the GDGTs strongly depends on the temperatures (Schouten et al., 2002), with cyclopentane ring number increasing with growth temperature. This was initially observed in sediment core-tops, with ring numbers being positively correlated to the temperature of overlying sea surface temperatures (Schouten et al., 2002). Hence, the distribution of GDGTs was proposed to be a SST proxy, most commonly via the TEX_{86} (TetraEther indeX of GDGTs with 86 carbons) ratio. TEX_{86} values in marine sediments (and lacustrine sediments) have been used to reconstruct SSTs from all around the world e.g. (Naafs and Pancost, 2016; O'Brien et al., 2017). The calibrations used in this thesis to reconstruct SST are TEX_{86}^{H} (Kim et al., 2010) and $TEX_{86\text{-}linear}$ (O'Brien et al., 2017). TEX_{86}^{H}-SST has been recommended for reconstruction of SST>15°C (e.g. Cretaceous) and involves a combination of GDGT-1, GDGT-2, GDGT-3 and Cren.′ *Figure 2.7*. GDGT index-2 is defined as below:

$$\text{GDGT index-2 } (TEX_{86}^{H}) = \log\frac{(GDGT-2)+(GDGT-3)+(Cren.')}{(GDGT-1)+(GDGT-2)+(GDGT-3)+(Cren.')}$$

TEX_{86}^{H}-SST= 68.4 × (GDGT index-2) + 38.6 (calibration error: ± 2.5 °C)

$TEX_{86-linear}$-SST is recommended by O'Brien et al. (2017) and is defined as below:

$$TEX_{86} = \frac{(GDGT-2)+(GDGT-3)+(Cren.')}{(GDGT-1)+(GDGT-2)+(GDGT-3)+(Cren.')}$$ (Schouten et al., 2002)

$TEX_{86-linear}$-SST= (TEX_{86}−0.19)/0.017 (calibration error: ± 2.0°C)

Some evidences indicate that TEX_{86} calibrations have geographical dependency and vary at different oceans and environments (Ho et al., 2014; Trommer et al., 2009). Therefore the calculated TEX_{86}-SST might be biased by local effects (Tierney and Tingley, 2014). Tierney and Tingley (2015 and 2014) have developed a new GDGT-SST calibration, i.e. BAYSPAR model. BAYSPAR model SST calibration is not geographically dependant and is derived from linear-regression parameters. The MATLAB code used in BAYSPAR model SST calibrations is explained by Tierney and Tingley (2014, 2015).

It is noteworthy to mention that GDGT distribution can be influenced by various diagenetic factors. GDGTs are sensitive to thermal maturity (Schouten et al., 2004). If GDGTs are thermally alternated, then the GDGTs distribution is dominated by GDGT0 (Schouten et al., 2013, 2004). Distribution of GDGTs is also influenced by sedimentary methanogenic (Koga et al., 1993; Weijers et al., 2006), evaluated by %GDGT-0 index (Sinninghe Damsté et al., 2012):

$$\%\text{GDGT-0} = \left(\frac{\text{GDGT}-0}{\text{GDGT}-0+\text{Cren}}\right)\times 100$$

%GDGT-0 is not yet calibrated for marine sediments. However in lacustrine sediments, if the %GDGT-0 index is >67 then GDGT distribution is considered to be biased by large contribution of methanogenesis derived GDGTs (Blaga et al., 2009; Sinninghe Damsté et al., 2012). Distribution of GDGTs can be also influenced by methanotrophic archaea (Pancost et al., 2001; Wakeham et al., 2003). To evaluate the input of methanotrophic archaea, the Methane Index (MI) is applied (Zhang et al., 2011):

$$\text{MI} = \frac{\text{GDGT}-1 + \text{GDGT}-2 + \text{GDGT}-3}{\text{GDGT}-1 + \text{GDGT}-2 + \text{GDGT}-3+\text{Cren}'}$$

In normal sedimentary conditions, MI values are <0.3 (the threshold of being influenced by methanotrophic GDGTs derived).

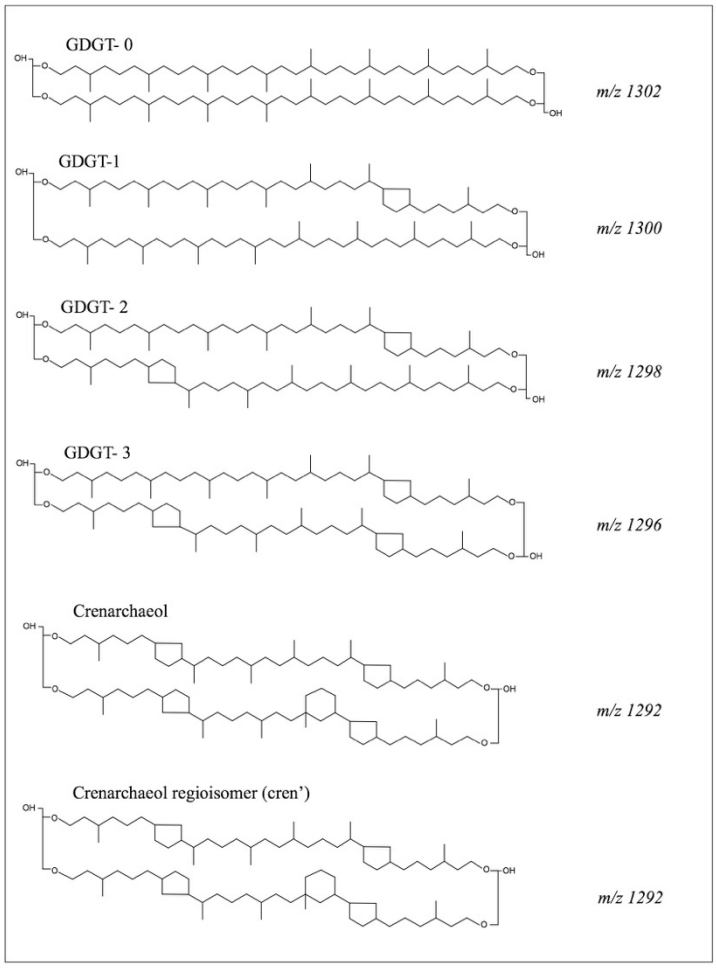

Figure 2.7. Schematic molecule structures of isoprenoidal glycerol dialkyl glycerol tetraethers (GDGTs) used to calculate TEX_{86} and related indices and their $[M+H^+]$ ion.

2.2. Semple information

Sediments and rocks analysed and discussed in this thesis are from two different time intervals:

1. The Cretaceous, i.e. Aptian–Coniancian ~120–90 Ma (chapters 3 and 4)
2. The Paleocene–Eocene ~56 Ma (chapters 5 and 6)

A brief summary of the sampling locations is provided in this chapter. More information such as site descriptions, lithology and sampling strategies are particularly explained in the appropriate chapters (Chapters 3, 4, 5 and 6).

2.2.1. Samples from the Cretaceous (Aptian–Coniancian)

These sediments, obtained from the International Ocean Discovery Program (IODP), are from Deep Sea Drilling Project (DSDP) Site 364 (modern latitude: 11°34.32'S, 11°58.30'E, 2450 m water depth). Site 364 is located in the South Atlantic, and was drilled on the seaward edge of the salt plateau at the transition from the outer Kwanza Basin to the Benguela Basin (Leg 40 Shipboard Scientific Party, 1978). Site 364 covers a 427 m cored section (46 cores) to a bottom depth of 1086 meter below sea floor (mbsf) (top of the Aptian evaporite and salt formations), and consists of Pleistocene to Lower Cretaceous sediments (Kochhann et al., 2014; Leg 40 Shipboard Scientific Party, 1978). Site 364 is divided into seven lithological units (e.g. Leg 40 Shipboard Scientific Party, 1978; Matsumoto et al., 1978). Sediments from Unit 7 (cores 45–39; Aptian) and Unit 6 (cores 38–26; Aptian–Late Aptian) (Kochhann et al., 2013; Kochhann et al., 2014; Leg 40 Shipboard Scientific Party, 1978) were obtained to investigate the development of anoxia in the South Atlantic (chapter 3). Additionally, sediments from Unit 7–Unit 5 (Aptian–Coniancian; Kochhann et al., 2014, 2013; Leg 40 Shipboard Scientific Party, 1978) are used to reconstruct sea surface temperature (SST) and carbon cycle perturbations (chapter 4).

2.2.2. Samples from Paleocene–Eocene

Peri-Tethyan Paleocene to Eocene sediments were collected prior to this study and are provided by collaborators, i.e. A.J. Dickson, H. Khozyem, H.R. Manners and S.T. Grimes. In particular, the sediments analysed span one of the most pronounced hyperthermal events, the Paleocene–Eocene thermal maxima (PETM; Chapter 1), and the changes in temperature and redox changes across this event are described and explored in Chapters 5 and 6.

These specific sediments originate from the northern-, southern- and western margins of the Peri-Tethys, and in some cases are represented by organic-rich black shales. The PETM black shales of the northern Peri-Tethys extend from Central Asia to Caucasus (e.g. Gavrilov et al., 2009, 2003), including the Guru-Fatima section located in the eastern (Central Asia) region and the Dzhengutay and Kheu River sections located in the western (Caucasus) regions, all three of which are discussed in Chapters 5 and 6. Sediments from Dababiya section located on the southern continental shelf (Khozyem et al., 2015) of the Peri-Tethys realm were also analyzed and are discussed in chapter 5. The Dababiya section is the Global Stratotype Standard Section and Point (GSSP) (Aubry et al., 2007), and one of the most expanded PETM sections. Sediments from Zumaia section, located in the western Peri-Tethys (North Atlantic) were also analyzed and are discussed in chapter 5. These sediments were deposited in lower to mid bathyal settings, at about 1km depth (Rodríguez-Tovar et al., 2011). The Zumaia section

is the most complete and representative section of the early Paleogene of the Pyrenees and a key reference for the Paleocene-Eocene boundary (Pujalte et al., 1998).

2.3. Analytical Methods

This section describes the analytical methods and the specific research techniques (protocols) by which samples were analyzed.

2.3.1 Sample preparation

Bulk samples were freeze-dried at -40°C, in order to remove excess water, and were powdered and homogenized using either a ball-mill (Retsch PM100 Ball Mill) device or a mortar and pestle. Sample powders were stored in furnaced glass jars. Between samples, the appliances were washed using double distilled water (DDS) and lab-grade acetone.

2.3.2. Bulk Geochemistry

To obtain total organic carbon (TOC) contents, total carbon (C) and inorganic carbon (IC) contents were determined using a CHN elemental analyzer Eurovector EA 3000 and Strohlein Coulomat 702, respectively. These elemental analyses were performed in duplicate, and the presented values are the mean of these duplicates. TOC was then determined by differences between total carbon and IC.

To determine bulk organic stable carbon isotopic ratios ($\delta^{13}C_{org}$), IC was removed from total carbon (TC) using acidification (2M HCl acid). About 10 ml of hydrochloric acid (HCL) was added to ~5 g of sediments. Sample tubes were placed in a water bath and heated at ~60°C to 80°C for ~5 hrs to aid the reaction (also ensuring the removal of pyrite). Sample tubes were centrifuged, and hydrochloric acid was removed from the sediments. This procedure was repeated by adding fresh acid to sediments until there was no visible reaction. When decarbonated, sediments were washed with DDW until neutrality. Samples were then re-powdered and dried in an oven at ~50°C for 24 hrs. ~10–25 µg of each sediment (depending on TOC content) were used to measure $\delta^{13}C_{org}$. These analyses were performed at the Open University, UK., using a Thermo Flash HT Elemental Analyser coupled to a Thermo Finnegan MAT 253 mass spectrometer (with the 1 σ uncertainty of 0.03 ‰ and 0.09 ‰ for IAEA CH-6 and NIST 8573 standards, respectively).

Rock-Eval analyses were performed using a Rock-Eval 6 instrument. Rock-Eval is a pyrolysis method using programmed heating under inert atmosphere (He) and is used to

identify the type and maturity of organic matter (Barker, 1974). To obtain hydrogen index (HI), oxygen index (OI) and T_{max} values (the temperature at which the maximum release of hydrocarbons occurs during Rock-Eval pyrolysis and is an indication of thermal maturity), approximately 30–50 mg of dried sample powders were weighed for each measurement. These analyses were performed at Oxford University, UK.

Bulk $\delta^{15}N$ analysis was performed on a Thermo Scientific Flash IRMS Elemental Analyzer, coupled to a Delta V Advantage IRMS through a Conflo IV universal interface. $\delta^{15}N$ values were calculated using the standards USGS40 and USGS41a (both are glutamic acid, purchased from USGS), along with several in-house laboratory standards (glutamic acid and tyrosine). These analyses were performed in Harvard University, US.

2.3.3. Biomarker Extraction

To obtain total lipid extracts (TLEs), 7 g of each sample were placed into microwave glass insert tubes. 10 ml of dichloromethane (DCM): methanol (MeOH) (9:1, vol) and a stirrer magnet were added to each tube. Extraction was performed using a microwave-assisted method (MILESTONIE Ethos Ex Microwave solvent extraction). The microwave program was set to a 10 min ramp to 70°C (max. 1000 W), followed by a 10 min hold at 70°C (max. 1000 W) and a 20 min cooling period. In order to monitor the temperature program, a fiber optic sensor was placed into the control sample. Following extraction, samples were centrifuged at 1500 rpm for 5 minutes in order to separate lipid extracts from sediments. To collect all the lipid extracts, the latter process was repeated (×4) by adding 10 ml DCM:MeOH (9:1, vol) to sediments. Lipid extracts were collected into round-bottom flasks (RB flasks).

To obtain TLEs from organic lean sediments, larger masses (~30g) were extracted with 220ml of a more polar mixture of dichloromethane (DCM): methanol (MeOH) (1:1, vol) using a Soxhlet apparatus for 24 hrs.

After extraction and remove of elemental sulfur (2.3.4), the TLE was then concentrated using rotatory evaporation.

2.3.4 Removal of sulfur

Activated copper cuttings ware added to the TLEs and left for 24 hrs to react with elemental sulfur. If the copper turns black (CuS), the black cuttings are replaced with the new activated Cu cuttings. In cases, copper color does not change after 24 hrs, the reaction is completed and this is an indication that the sample is sulfur free.

2.3.5 TLE fractionation

The TLE was then separated into three fractions (aliphatic, aromatic and polar) using short (4 cm) silica gel open column chromatography. Firstly, the column was cleaned by hexane (x2), and then the TLE was introduced to the columns using approximately 1ml of hexane. Aliphatic, aromatic, and polar fractions were eluted using 3 ml of hexane, 4 ml of hexane:DCM (3:1) and 4 ml of DCM:MeOH (1:2), respectively. All fractions were then dried under a gentle stream of N_2.

2.3.6 Filtration prior to LCMS

Prior to the analysis of glycerol dialkyl glycerol tetraether lipids (GDGTs) on LCMS (2.1.6.4), polar fractions were filtered to remove particulate matter. To achieve that, the polar fractions (or TLEs) were dissolved in hexane:IPA (99:1) and passed through a 0.45 μm PTFE filter by a syringe with a bayonette adaptor. Then, the samples were dried under a gentle stream of N_2 and were dissolved in 60 μl hexane:IPA (99:1), prior to the injection into LCMS.

2.3.7 Raney-Nickel desulfurization

To desulfurize the polar fraction (Sinninghe Damsté et al., 1989), the polar fraction was dissolved in absolute ethanol (~2 ml) and refluxed at 120 °C under a nitrogen atmosphere. A 1.5 ml suspension of Raney Ni (0.5 mg/ml) was added and refluxed for 1.5 hours under nitrogen. An additional 0.5 ml Raney Ni suspension was added to the sample after 30 and 60 min. The desulfurization products were then centrifuged and extracted using DCM. The supernatant was transferred into a separation funnel and washed with saturated aqueous NaCl solution (30 ml). The DCM-layer was extracted and excess water removed using an anhydrous $MgSO_4$ column. The desulfurized sample was separated into two fractions (apolar and polar) using a short flash column (4 cm) packed with alumina oxide. The apolar and polar fractions were eluted using 4ml of hexane:DCM (9:1) and 4 ml of DCM:MeOH (2:1), respectively. The apolar fraction was hydrogenated with platinum oxide (PtO_2, one spatula tip) in ethyl acetate (3 ml) at room temperature. Excess ethyl acetate was removed using a $MgSO_4$ (2 cm, bottom) and Na_2CO_3 (2 cm, top) column. G.N. Inglis and S.K. Lengger helped LB with this procedure.

2.3.8 (Semi-) quantification

To quantify the abundance of biomarkers, an appropriate internal standard should be added to the sediments prior to extraction. However, the exact response factors (RF) for the biomarkers and internal standards were not determined here, therefore quantifications should be considered as semi-quantitative. Moreover, to quantify isorenieratane in the aromatic fraction, an aromatic standard was required which was not done here. Instead, C_{36} *n*-alkane (1.25 µg) was added as an internal standard to the aromatic fractions, following TLE fractionation. This was used to calculate the concentrations shown in this thesis in ng of compound per g of sediment, but we note the semi-quantitative nature of these determinations.

2.3.9 Biomarker Analyses

2.3.9.1 GC-FID

Prior to the analysis of the samples on GS-MS (2.1.7.2), they were screened via Gas Chromatography-Flame Ionisation Detector (GC-FID), to adjust the injection concentrations for subsequent analyses. The sample was introduced and rapidly heated and vaporised at the injection port. Separation of organic compounds in gas chromatography (GC) is achieved via their interaction with a carrier inert gas (e.g. He) as the mobile phase and the solid film on the capillary column serving as the stationary phase. The separated organic compounds then combust (under H_2 flame), and the resultant ions are detected by the flame detector (FID). GC-FID analysis was performed on a Thermo Scientific Trace 1300 with a (50 m × 0.32 mm i.d.) Restek fused silica capillary column coated with 0.17 µm film thickness (Rtx-1). The injection volume was 1 µl. The GC programme was injection at 70 °C (1 min hold), heating to 130°C at a rate of 20°C/min, then to 300 °C at 4 °C/min, followed by a 24 min hold.

2.3.9.2 GC-MS

Biomarker distributions in the aliphatic, aromatic and desulfurized polar fractions were analysed by a gas chromatograph coupled with a mass spectrometer (GS-MS). In GC-MS, the mass spectrometer is a selective detector for identification of known analytes in complex mixtures. It measures the relative molecular masses (molecular weight) and molecular fragmentation patterns (mass spectra) of compounds eluted from the GC, making it possible to

deduce the molecular formulae and structures of compounds. Identification of molecules is achieved via a library of known compounds. Here, we have used electron impact mass spectrometry, in which the separated organic compounds (via GC; 2.1.7.1) experience electron impact in the source, bringing about ionisation and subsequent fragmentation. The resultant molecular ions and fragment ions are separated based on their mass (*m*) to charge (*z*) ratio and via a variable electromagnetic field applied by quadrupole rods at the detector. The power of voltage and therefore the applied electromagnetic field varies constantly, and at each power stage ions of specific *m*/*z* will be in resonance and move to the detector.

GC-MS analysis was performed on a Thermo Scientific™ ISQ Series Single Quadrupole gas chromatography mass spectrometry (GC-MS) system. Separation of compounds was performed on a Zebron non-polar column (50 m × 0.32 mm, 0.10 µm film thickness). The injection volume and GC temperature programme were the same as for GC-FID. The mass spectrometer continuously scanned between *m/z* 50 and 650. Identification of biomarkers was carried out based on published retention times and spectra as well as comparison with standard samples.

2.3.9.3. MRM-GC-MS (GC-MS-MS)

Metastable Reaction Monitoring-gas chromatography-mass spectrometry (MRM-GC-MS) or GC-MS-MS is used to probe molecular structures via more detailed fragmentation, thereby achieving more robust identification compared to GC-MS. Generally, following GC-MS fragmentation, target (or precursor) ions are selected based on their specific *m/z* (for example, their molecular ions) and these are then induced to further fragmentation via collision with He yielding (product ions). Therefore, there are two mass analysis detectors, with a precursor ion selected in the first stage and the product ions being detected in the second stage. Therefore, even if the analyte contains two compounds with the same mass, it is very unlikely that the they would yield the same daughter ion spectra.

The MRM GC-MS analyses were conducted at UC Riverside, US, and that system comprises a Waters AutoSpec Premier mass spectrometer interfaced to a HP 6890 gas chromatograph. For GC, splitless injection at 320°C and a DB-1MS coated capillary column (60 m × 0.25 mm, 0.25 µm film thickness) were used, with He as carrier gas; the GC temperature program consisted of an initial hold at 60°C for 2 min, heat ng to 150°C at 10 °C/min followed by heating to 320°C at 3°C/min and a final hold for 22 min; analyses were performed in electron impact mode, with an ionization energy of 70 eV and an accelerating voltage of 8 kV. Polycyclic biomarker alkanes (tricyclic terpanes, hopanes, steranes, etc.) were quantified by

addition of a deuterated C_{29} sterane standard [d4-ααα-24-ethylcholestane (20R)] to aliphatic hydrocarbon fractions and comparison of relative peak areas.

2.3.9.4. GC-IRMS

Gas Chromatography - Isotope Ratio Mass Spectrometry (GC-IRMS) is used to measure the atomic isotopic ratios (e.g. $\delta^{13}C$) of GC-separated compounds. To achieve this, compounds eluting from the GC pass through a combustion reactor where they are oxidatively combusted to CO_2 and H_2O. Following this H_2O is removed in a water separator, and CO_2 enter into a reduction reactor to reduce to carbon. Following the reduction, the analytes are ionized in the mass spectrometry ion source. Similar to GC-MS, the ionized gasses are separated in a magnetic sector analyzer. The *m/z* 44, 45 and 46 ions (i.e. the molecular masses for $^{12}CO_2$, $^{13}CO_2$ and $C^{18}O^{16}O$, respectively) are continuously detected at high sensitivity. The output from the detector is used to calculate the final stable isotope ratio.

GCIRMS was conducted using an Agilent Industries 7890A gas chromatograph coupled to an IsoPrime 100 MS via a continuous flow combustion interface (GC-C-IRMS). Samples were introduced onto a capillary column (50 m x 0.32 m, 0.17 μm) using He for carrier gas. The GC oven temperature programme was the same as for GC-MS. Samples were measured in duplicate and the presented value is the mean of duplicates. $\delta^{13}C$ values were are reported against the Vienna Pee Dee Belemnite (VPDB) standard, determined by bracketing with an in-house gas (CO_2) of known $\delta^{13}C$ value. Instrument stability was monitored by regular analysis of an in-house fatty acid methyl ester standard mixture and the instrument's long-term precision is ± 0.3‰.

2.3.9.5. LC-MS

The distribution of large, non-GC amenable organic molecules (~850 Daltons), i.e. GDGTs, can be determined by High Pressure Liquid Chromatography-Mass Spectrometry (HPLC-MS). The fractionation of the sample is performed by the interaction of the analyte with the liquid and stationary phase of the column. Unlike gas chromatography, the temperature is constant during the analysis, while the polarity of the liquid phase changes throughout. Following that, eluting components are detected and identified mass spectrometry in a manner analogous to GC-MS.

For GDGT analyses, atmospheric pressure chemical ionization (APCI) is used, which generates both GDGT specific ions (i.e. loss of hydroxyl groups or glycerol moieties) and,

most importantly for identification, protonated molecular ions $(M+H)^+$ ions. Here, HPLC-APCI-MS was conducted with a ThermoFisher Scientific Accela Quantum Access triple quadrupole MS in selected ion monitoring mode. Normal phase separation was achieved with two HPLC BEH HILIC columns (2.1 mm x 150 mm, 1.7 µm i.d) at a flow rate of 0.2 ml/min. The initial solvent hexane:iso-propanol (IPA) (98.2:1.8) eluted isocratically for 25 min, followed by an increase in solvent polarity to 3.5% IPA in 25 min, and then by a sharp increase to 10% IPA in 30 min (Hopmans et al., 2016). After separation, to analyse isoprenoid and branched GDGTs, Selection Ion Monitoring (SIM) was performed at *m*/*z*: 1302, 1300, 1298, 1296, 1294, 1292, 1050, 1048, 1046, 1036, 1034, 1032, 1022, 1020, 1018, 744, 659 (Schoon et al., 2013) to increase the sensitivity; during data processing GDGTs were analyzed and quantified using their respective molecular ion $(M+H)^+$ chromatograms.

2.3.9.6. Analysis of $\delta^{15}N_{porphyrin}$

Prior to the $\delta^{15}N_{porphyrin}$ analysis, porphyrin purification was conducted using silica gel open column chromatography. TLEs were separated into four fractions: F1, F2, F3, F4 were eluted with hexane (4ml), hexane:DCM (1:1, 4 ml), DCM (5 ml), MeOH (4ml). Porphyrins (Ni- and VO-chelated porphyrins) eluted in the middle two fractions, i.e. hexane/DCM (1:1) and DCM. Subsequently, the porphyrin fractions were purified by HPLC (Agilent 1200 series) equipped with a multi-wavelength UV/Vis detector, using a method modified from Higgins et al. (2009). Porphyrin-containing fractions were injected onto two ZORBAX SIL columns (4.6 x 250 mm, 5 µm) connected in series and eluted at 1 mL min^{-1} using the solvent gradient described in table 1. Porphyrin peaks were detected by absorbance at 393 and 405 nm.

Time (min)	% Hexane	% Ethyl acetate	% Methanol
0	100	0	0
3	80	15	5
18	70	23	8
22	60	30	10
25	0	50	50
30.5	0	25	75
40.5	0	25	75
45.5	60	30	10
50	100	0	0
90	100	0	0

Table 1. HPLC solvent gradient for chlorophyll purification, with elution at 1mL/min.

$\delta^{15}N_{porphyrin}$ of the mixed porphyrins was analyzed according to the methods in Higgins et al., (2009). Briefly, HPLC-purified porphyrins were placed in quartz tubes and oxidized under UV light in a biosafety cabinet for six hours, then dried and chemically oxidized using re-crystallized 0.05 M $K_2S_2O_8$ dissolved in fresh 0.15 M NaOH. Nitrate concentration was measured using a chemiluminescent NO_x analyzer (Teledyne NO/NOx Analyzer 200E), and $\delta^{15}N_{porphyrin}$ values were measured using the denitrifier method (Sigman et al., 2001), on a Delta V Advantage isotope ratio mass spectrometer with a custom built purge and trap system. Isotopic measurements were standardized to the N_2 reference scale using standard reference materials IAEA N3 and USGS 34. Purification of porphyrin and $\delta^{15}N_{porphyrin}$ measurements were conducted at Harvard University, US.

2.3.10. Data Processing (Peak integration)

Chromatogram peak areas were integrated manually using the manufacturer-supplied software, i.e. Thermo X-Caliber for GC-MS and LC-MS, and MassLynx V4.1 for GC-MS-MS, and Ion Vantage (version 1.5.6.0) for GC-IRMS.

2.3.11. Time Series Analyses

Time series analyses were performed in chapter 3 by S.J. **Batenburg**. Power spectra was generated with Redfit 3.8 (Schulz and Mudelsee, 2002), using a Welch window. A Matlab script was applied to generate wavelet power spectra (Grinsted et al., 2004). Band-pass filtering was performed with AnalySeries (Paillard et al., 1996), centered at the dominant periodicities, with bandwidths at ¼ of the center frequency.

Chapter 3

Astronomically driven variations in depositional environments in the South Atlantic during the Early Cretaceous

Preface

This chapter is based on a manuscript published as an article in the journal *Paleoceanography and Paleoclimatology, 33*, http://doi.org/10.1029/2018PA003338. The lead author of the paper is LB. Co-authors of the paper are David Naafs (University of Bristol), Alex Dickson (Royal Holloway University of London), Gordon Love (University of California Riverside), Sietske Bathenburg (University of Oxford) and Rich Pancost (University of Bristol). LB carried out analysis, interpreted the organic geochemical data set and wrote the chapter. AD helped with Rock-Eval and stable carbon isotope analyses. GL helped with MRM analyses. SB helped with time series analyses. DN and RP made comments and suggestions on the initial draft made by LB. All co-authors made comments and suggestions before final submission.

Abstract

The extent and persistence of anoxia in the South Atlantic Ocean during its early opening phase in the Early Cretaceous is not well constrained, hindering a holistic understanding of the processes and mechanisms that drive past changes in water column redox conditions, as well as the impacts of such changes on marine ecosystems. Here we provide high-resolution geochemical records from Deep Sea Drilling Project (DSDP) Site 364 that document variations in redox conditions, chemocline depth, marine productivity and marine ecosystem dynamics in the northern South Atlantic during the Aptian. We show that many of these parameters varied across discrete sedimentary cycles expressed in the DSDP 364 succession. Our data indicate that during the initial stages of basin development, anoxic and euxinic conditions were prevalent, and occasionally extended into the upper water column. However, strong cyclicity in sedimentological and geochemical parameters imply that the anoxia/euxinia was not a

persistent state. We argue that the water column redox conditions during the Aptian were driven by changes in the hydrological cycle, induced by variations in astronomical forcing. We suggest that the episodically amplified hydrological cycle not only enhanced nutrient availability and marine productivity, but might also have caused density-driven upper ocean stratification. The presence of black shales of similar age in other ocean basins suggest that this mechanism is broadly important for the formation of Early Cretaceous organic-rich successions.

3.1 Introduction

The Cretaceous Period (~145–66 million years ago) was characterized by a greenhouse climate (Hay, 2008 and references therein), with elevated atmospheric CO_2 levels (e.g. Foster et al., 2017; Naafs et al., 2016), high sea surface temperatures (SSTs) (e.g. Bice et al., 2006; Naafs and Pancost, 2016; O'Brien et al., 2017; Schouten et al., 2003), and little or no continental ice (Huber et al., 2002; MacLeod et al., 2013). Superimposed on this general greenhouse climate are the Oceanic Anoxic Events (OAEs). Classically, OAEs are time intervals associated with expansion of anoxia and deposition of organic rich black shales in the ocean (Jenkyns, 2010 and references therein), although some OAEs have also been identified in lake sediments (Xu et al., 2017). OAEs are associated with intense perturbations in global climate, ocean chemistry and global biogeochemical cycles (Jenkyns, 2010), reflected, for example, in the carbon isotope excursions (CIEs) that accompany the major OAEs. Some OAEs have been associated with a positive CIE (e.g. OAE 2), others with a negative CIE (Toarcian OAE) and some, like OAE 1a, contain both (see review by Jenkyns, 2010).

The occurrence of anoxia during the Cretaceous, however, was not exclusive to OAEs, as black shales formed at more limited regional scales at other times (e.g. Huang et al., 2010). The regional formation of black shales is dominated by local factors, e.g. changes in nutrient availability, hydrology and water column stratification, and basin morphology. Preservation of organic rich sediments is frequently linked to the development of anoxia, induced by either increased primary productivity and organic matter export overwhelming the rate of organic matter (OM) remineralization, and/or decreased oxygen flux resulting in decreased OM remineralization. Black shales can occur as both singular sedimentary units or as repetitive units interbedded with organic lean facies (Beckmann et al., 2005; Hofmann & Wagner, 2011; Huang et al., 2010; Kuypers et al., 2004; Malinverno et al., 2010; Meyers et al., 2006; Wagner et al., 2004), the latter which is often attributed to climate variability driven by astronomical

forcing during the Cretaceous. Identifying the factors involved in the formation of Cretaceous black shales can provide a better understanding of Cretaceous biogeochemical cycles and climate feedbacks, as well as the formation of hydrocarbon source rocks.

Within the Cretaceous, the Aptian Stage is of particular interest as the opening of the S. Atlantic started during this time period, leading to the development of a series of local rift basins in the Southern and Equatorial South Atlantic that were potentially prone to the development of black shales (e.g. Pérez-Díaz and Eagles, 2017). In addition, one of the major OAEs occurred during the Aptian: OAE 1a (T J Bralower et al., 1994). Therefore, there is much interest in the Aptian carbon cycle on both short (e.g. Huang et al., 2010) and long timescales (T J Bralower et al., 1994; Jenkyns et al., 2012). However, to the best of our knowledge there are remarkably few studies on Aptian organic carbon production and preservation from the South Atlantic (Simoneit, 1978; Raynaud & Robert, 1978; Foresman, 1984; Stein et al., 1986; Zimmerman et al., 1987; Bralower et al., 1994; Jenkyns et al., 2012; Naafs & Pancost, 2014) or even the Southern Hemisphere (van Breugel et al., 2007) and most of these are of low stratigraphic resolution. Almost all orbitally resolved records (i.e. with sampling steps at <~10–20 kyr intervals) from this period are from Europe (e.g. Huang et al., 2010). Early ocean drilling expeditions (e.g. Leg 40 Shipboard Scientific Party, 1978) recovered Aptian black shales in the northern South Atlantic and described the organic rich to organic lean interchanging nature of these successions. However, the triggering factors involved in the formation of these organic rich layers and their alternating nature are not fully constrained. Here, we provide high-resolution records of total organic carbon (TOC), total sulfur (TS) and carbonate (%$CaCO_3$) contents to trace astronomically-paced variations in the depositional environment of the northern South Atlantic (Site 364, at ~25 °S paleolatitude) during the Aptian. In addition, high-resolution molecular organic geochemical analyses are provided from selected intervals to test whether apparently astronomically-forced variations in sedimentary facies are related to primary marine productivity, chemocline expansion or marine anoxia.

3.2 Samples and Methods

3.2.1 Sampling location and lithology

Deep Sea Drilling Project (DSDP) Leg 40, Site 364 (modern latitude: 11°34.32’S, 11°58.30’E, 2450 m water depth), is located in the Kwanza Basin of the South Atlantic (Leg 40 Shipboard Scientific Party, 1978) and was drilled on the seaward edge of the salt plateau at the transition from the outer Kwanza Basin to the Benguela Basin (Leg 40 Shipboard Scientific Party, 1978).

Site 364 covers a 427 m cored section (46 cores) to a bottom depth of 1086 meter below sea floor (mbsf) (top of the Aptian evaporite and salt formations), and consists of sediments that are Pleistocene to Early Cretaceous in age (Kochhann et al., 2014; Leg 40 Shipboard Scientific Party, 1978).

Site 364 is divided into seven lithological units (e.g. Leg 40 Shipboard Scientific Party, 1978; Matsumoto et al., 1978), with Units 6 and 7 investigated here. Unit 6 is predominantly composed of calcium carbonate (limestone), with a TOC content < 3 wt.%. The underlying Unit 7, the deepest lithological section of Site 364, comprises dolomitic limestones and thin black shales, with TOC contents as high as 40 wt.% (Leg 40 Shipboard Scientific Party, 1978; Matsumoto, 1978; Raynaud & Robert, 1978; Simoneit, 1978). On the basis of the proportion of black shales, Unit 7 is divided into two subunits: 7a (Cores 39 to 41) with fewer and 7b (Cores 42 to 46) with more abundant and more intense black shale horizons (Leg 40 Shipboard Scientific Party, 1978). Guided by previous work (Leg 40 Shipboard Scientific Party, 1978; Naafs & Pancost 2014), we mainly focus on subunit 7b (1020–1086 mbsf), characterized by the highest TOC contents and apparent pronounced cyclic variation in lithology. The timing of deposition of Unit 7 (Aptian) and Unit 6 (Aptian–Late Aptian) coincided with the initial opening of the South Atlantic and deepening of the basin (Zimmerman et al., 1987). During this time DSDP Site 364 was located at approximately 25°S, 10°W paleolatitude. Biostratigraphic evidence indicates that sediments at Site 364 were deposited on a continental shelf setting (Kochhann, et al. 2014). The paleodepth of Site 364 during the Early Cretaceous (Unit 7) is estimated to be ~300–400 m (Zimmerman, 1987).

3.2.2 Analytical methods

A total of 288 samples were obtained from the International Ocean Discovery Programme (IODP) Bremen Core Repository, Germany. Unit 7b was sampled with a resolution of ca. 10 cm (250 samples). 34 samples were taken from Unit 7a and Unit 6 at a lower resolution. Bulk samples were freeze-dried to remove excess water and were powdered using either a ball-mill device or a mortar and pestle.

3.2.2.1 Bulk geochemistry

Total carbon (C) and inorganic carbon (IC) contents were determined using a CHN elemental analyzer Eurovector EA 3000 and Strohlein Coulomat 702, respectively. All elemental analyses were performed in duplicate and the presented data reflect the mean of these duplicates. Total Organic Carbon (TOC) was determined by C and IC differences. To analyze

bulk organic stable carbon isotopic ratios ($\delta^{13}C_{org}$), inorganic carbon was removed using 2M HCl acid. Sample tubes were placed in a water bath and heated at ~60°C to 80°C for 5 hours to aid the reaction (also ensuring the removal of pyrite). Samples were then re-powdered and dried in an oven at 50°C for 24 hours. Between 10 and 25 µg of each sample (depending on TOC content) were used to measure $\delta^{13}C_{org}$ at the Open University, UK. $\delta^{13}C_{org}$ was measured using a Thermo Flash HT Elemental Analyser coupled to a Thermo Finnegan MAT 253 mass spectrometer (with the 1 σ uncertainty of 0.03 ‰, 0.09 ‰ and 0.01‰ for IAEA CH-6, NIST 8573 and IR-R041 standards, respectively; n=20).

A selection of 68 samples from Unit 7b with an average resolution of ~50 cm were selected for Rock Eval analyses. Rock-Eval analyses were performed using a Rock-Eval 6 instrument to obtain estimates of the hydrogen index (HI) and the temperature of maximum hydrocarbon generation (T_{max}). Respective 2σ uncertainties were estimated with repeated measurements of an in-house shale standard (St. Audries Bay Shale), and were 3 mg HC/g TOC and 19ºC. Approximately 30–50 mg of dried sample powders was weighed for each measurement.

3.2.2.2 Biomarker extraction

The same 68 samples used to obtain Rock Eval data from Unit 7b, alongside 14 samples from Unit 7a and 20 samples from Unit 6, were selected for detailed biomarker analysis. To obtain total lipid extracts (TLEs), 14 g of each sample was extracted with 20 ml of dichloromethane (DCM): methanol (MeOH) (9:1, vol) by microwave-assisted method (MILESTONIE Ethos Ex Microwave solvent extraction). The microwave program consisted of a 10 min ramp to 70°C (max. 1000 W), followed by a 10 min hold at 70°C (max. 1000 W) and a 20 min cooling period. Activated copper turnings were added to the TLEs for 24 hrs to remove elemental sulfur. The TLE was then concentrated using rotatory evaporator and separated into three fractions (aliphatic, aromatic and polar) using short (4 cm) silica gel open column chromatography. Aliphatic, aromatic, and polar fractions were eluted using 3 ml of hexane, 4 ml of hexane:DCM (3:1) and 4 ml of DCM:MeOH (1:2), respectively. All fractions were then dried under a gentle stream of N_2. To quantify the abundance of aromatic biomarkers, 1.25 µg of C_{36} *n*-alkane was added as an internal standard to the aromatic fractions. We did not determine exact response factors for the aromatic biomarkers and the quantifications should thus be considered as semi-quantitative.

Incorporation of inorganic sulfur into unsaturated bonds of hydrocarbons within the water column or sediment results in the formation of sulfurized hydrocarbon moieties in the

polar fraction (Sinninghe Damsté & de Leeuw, 1990), potentially biasing the biomarker results if only the aliphatic and aromatic fractions are analyzed. To explore some aspects of the sulfurized biomarker assemblage, the polar fraction of one black shale sample from Unit 7b was desulfurized using Raney Nickel desulfurization and subsequent hydrogenation (Sinninghe Damsté et al., 1989).

3.2.2.3 Biomarker analysis

Biomarker distributions in the aliphatic, aromatic and desulfurized polar fractions were analyzed using a Thermo Scientific^{TM} ISQ Series Single Quadruple gas chromatography mass spectrometry (GC-MS) system. Separation of compounds was performed on a Zebron non-polar column (50 m x 0.32 mm, 0.10 µm film thickness). The injection volume was 1 µl. The GC programme was injection at 70 °C (1 min hold), heating to 130°C at a rate of 20°C/min, then to 300 °C at 4 °C/min, followed by a 24 min hold. The mass spectrometer continuously scanned between *m/z* 50 and 650. Identification of biomarkers was carried out based on published retention times and spectra as well as comparison with standard samples.

In addition to the classical GC-MS system, 27 samples from Core 43 were analyzed using Metastable Reaction Monitoring-gas chromatography-mass spectrometry (MRM-GC-MS) conducted at UC Riverside, US to identify and quantify isomers of methylsteranes and methylhopanes. The MRM GC-MS system operates on a Waters AutoSpec Premier mass spectrometer equipped with a HP 6890 gas chromatograph and DB-1MS coated capillary column (60 m × 0.25 mm, 0.25 µm film thickness) using He as carrier gas. The GC temperature program consisted of an initial hold at 60°C for 2 min, heating to 150°C at 10 °C/min followed by heating to 320°C at 3°C/min and a final hold for 22 min. Analyses were performed via splitless injection at 320°C in electron impact mode, with an ionization energy of 70 eV and an accelerating voltage of 8 kV. MRM transitions for C_{27}–C_{35} hopanes, C_{31}–C_{36} methylhopanes, C_{21}–C_{22} and C_{26}–C_{30} regular (4-desmethyl) steranes, C_{30} methylsteranes and C_{19}–C_{26} tricyclics were monitored. Polycyclic biomarker alkanes (tricyclic terpanes, hopanes, steranes, etc.) were quantified by addition of a deuterated C_{29} sterane standard [d4-ααα-24-ethylcholestane (20R)] to aliphatic hydrocarbon fractions and comparison of relative peak areas.

Compound specific $\delta^{13}C$ of the saturated hydrocarbon fraction was determined for two samples (one carbonate and one black shale) to explore the source of the biomarker 2,6,10,15,19-pentamethylicosane (PMI; e.g. Pancost et al., 2000). For this purpose, we used an

Agilent Industries 7890A gas chromatograph coupled to an IsoPrime 100 GC-combustion-isotope ratio MS (GC-C-IRMS) system. Samples were introduced onto a capillary column (50 m x 0.32 m, 0.17 µm film thickness) using He for carrier gas. The GC oven temperature programme was the same as for GC-MS analyses. Samples were measured in duplicate and the presented value reflects the mean of duplicates. $\delta^{13}C$ values were converted to Vienna Peedee Belemnite (VPDB) by bracketing with an in-house gas (CO_2) of known $\delta^{13}C$ value. Instrument stability was monitored by regular analysis of an in-house fatty acid methyl ester standard mixture; long-term precision is ± 0.3‰.

3.2.3 Time series analyses

Time series analyses were performed on the whole TOC dataset of Unit 7b (Cores 42-45) and on the upper interval from 1024.62 to 1037.92 mbsf (Cores 42 and 43). Power spectra were generated with Redfit 3.8 (Schulz and Mudelsee, 2002), using a Welch window. A Matlab script was applied to generate wavelet power spectra (Grinsted et al., 2004), and band-pass filtering was performed with AnalySeries (Paillard et al., 1996), centered at the dominant periodicities, with bandwidths at ¼ of the center frequency (details in the caption for Figure *3.3*).

3.3 Results

3.3.1 Elemental analyses

TOC contents at Site 364 vary significantly (Figure *3.1*), from less than 1 wt.% up to 40 wt.%. Highest TOC contents occur in Unit 7b, which displays regularly paced variations between organic lean carbonates with around 1 wt.% TOC (typically ranging from 0.5 % to 2 wt.%) and sapropelic black shales with up to 40 wt.% TOC (typically ranging from 10 to 25 wt.%). Unit 7a is characterized by similar cyclic variations, but with a lower maximum TOC content up to 11 wt.%. Unit 6 consists predominately of carbonates with maximum TOC contents of 1-3 wt.%. Elemental sulfur contents exhibit similar variations as TOC contents, with the maximum values of 11 wt.% occurring in black shale horizons of Unit 7b and lower values in Unit 7a and 6.

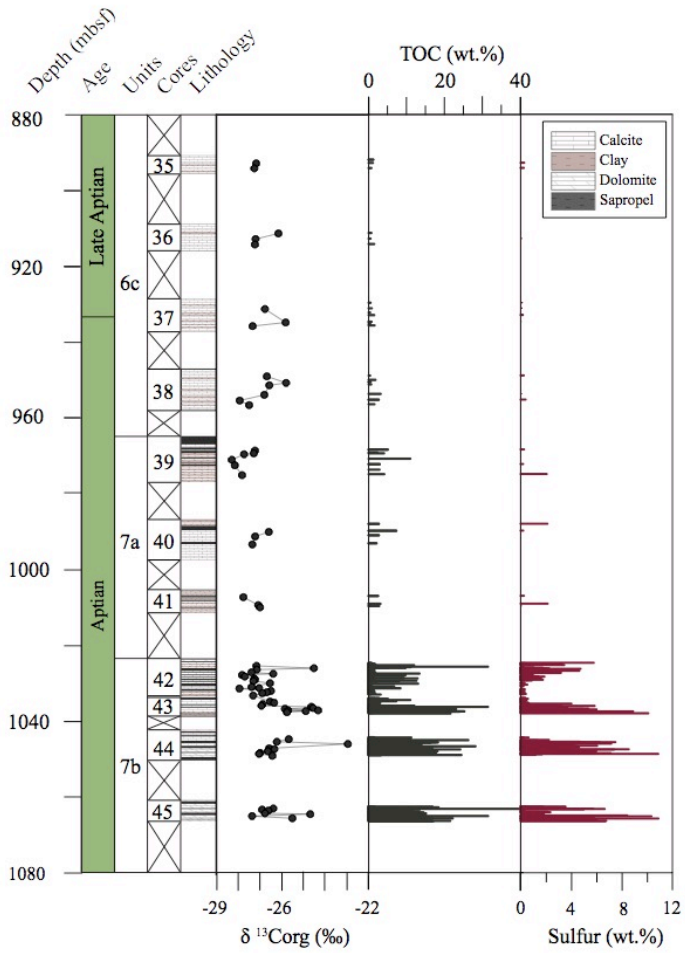

Figure 3.1. Lithology (Leg 40 Shipboard Scientific Party, 1978), bulk $\delta^{13}C_{org}$, total organic carbon (TOC) content, and sulfur content across Units 7b, 7a, and Unit 6 (1070-890 mbsf) for DSDP Site 364. Note the presence of multiple core gaps.

3.3.2 Time series analysis

The dominant periodicities in the depth domain over the whole Unit 7b TOC dataset (Cores 42–45) are 46 cm and 73 cm (above the 99% confidence level) (Figure *3.2*, left panel). When analysing only the upper part of the record from 1024.62 to 1037.92 mbsf (Cores 42 and 43), the dominant periodicity is again 46 cm (above the 99% confidence level) (Figure *3.2*, right panel), but a periodicity of 2.4 m can also be detected with more than 80% confidence. The differences between the power spectra of the entire record (revealing 46 and 73 cm periodicities) and that of only Cores 42 and 43 (46 cm and 2.4 m periodicity) is likely caused by the core gaps in the longer record. The wavelet spectrum of TOC (Figure *3.3*) confirms

these findings, revealing the presence of 46 cm and 2.4 m periodicities from 1024.62 to 1037.92 mbsf (Cores 42 and 43) (Figure *3.3*, right panel) and the persistent presence of the 46 cm periodicity through all of Unit 7b TOC dataset (Cores 42-45), where data are available (Figure *3.3*, left panel).

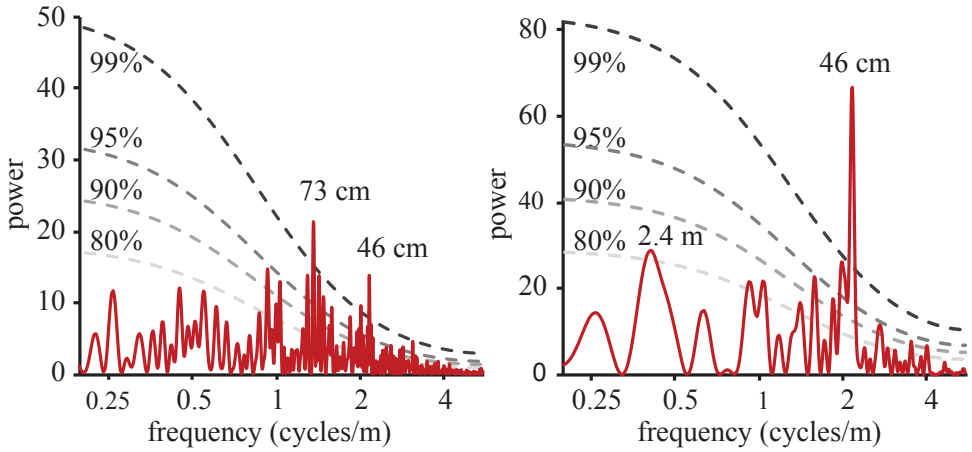

Figure 3.2. Redfit 3.8 power spectra of the TOC record for the entirety of Unit 7b between 1066 and 1024 mbsf (left) and of the upper interval of Unit 7b only from 1024 to 1038 mbsf (right). Confidence levels are given in dashed lines and dominant periodicities are labelled.

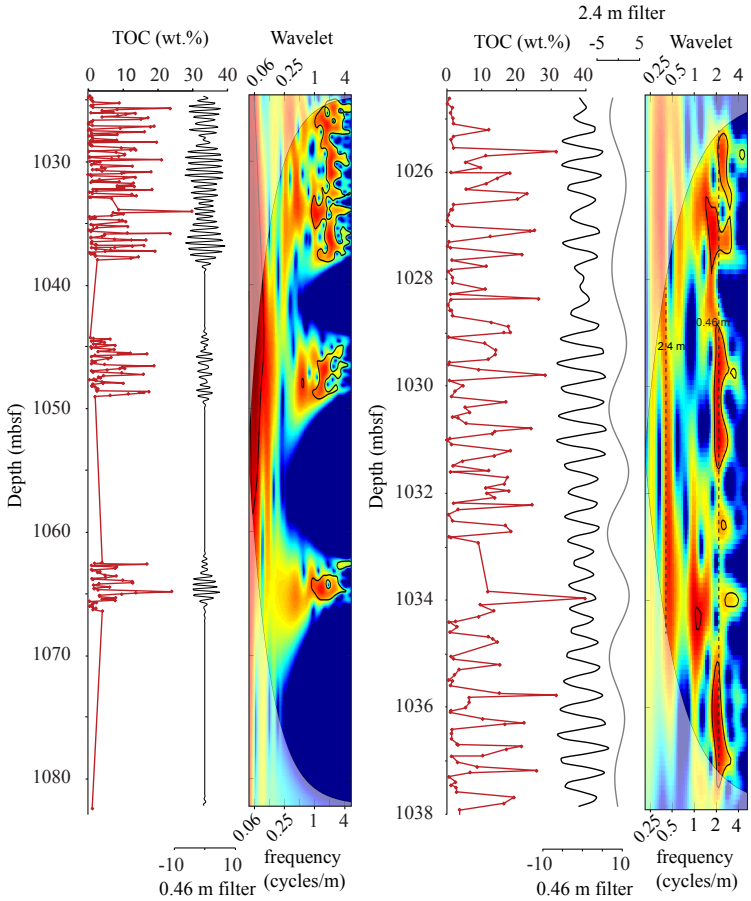

Figure 3.3. TOC content and evolutionary spectra of the TOC record in the depth domain. The left figure shows the spectrum for the entirety of Unit 7b and depicts the band-pass filters centered at 0.46 m (bandwidth 0.37 – 0.60 m). The figure on the right spans only the upper part of Unit 7b and depicts the band-pass filters centered at 46 cm (bandwidth 0.37 – 0.61 m) and 2.4 m (bandwidth 1.9 – 3.2 m).

3.3.3 Rock-Eval

Hydrogen indices (HIs) for Unit 7b range from undetectable in some organic lean carbonates to 740 mg HC/g TOC in black shales (Figure *3.4*). In the organic rich black shales, bulk OM is hydrogen-rich (HI on average ~440) type I/II kerogen, whereas in carbonates with low TOC, OM is dominated by oxygen-enriched but hydrogen depleted (mean HI ~110) type III kerogen. T_{max} values range from 387 to 440 °C, and are generally lower in black shales (mean ~395) than carbonates (mean ~420).

3.3.4 TOC stable carbon isotopes ($\delta^{13}C_{org}$)

Bulk $\delta^{13}C_{org}$ values vary between -28 and -24 ‰ across Unit 7b (Cores 45–42) (Figure *3.1*). There is no variation with lithology, but the $\delta^{13}C_{org}$ record does exhibit a 2 ‰ positive excursion in Sections 2 and 3 of Core 43 at around 1035 mbsf (Figure *3.1*). $\delta^{13}C_{org}$ values in the upper parts of the section (Unit 7a and 6) are again stable, but lower than those of Unit 7b with values between -26 and -24‰.

3.3.5 Aliphatic compounds

As shown previously (Hartwig et al., 2012; Naafs and Pancost, 2014; Simoneit, 1978), the aliphatic hydrocarbon fractions contain a mixture of *n*-alkanes, isoprenoids (pristane and phytane), steranes and hopanes. The organic rich black shale aliphatic fraction comprises mainly short chain *n*-alkanes (C_{14}–C_{21}) with no obvious odd-over-even predominance, long chain (C_{25}–C_{37}) *n*-alkanes with a slight odd-over-even carbon number predominance (CPI~1.6), C_{27}–C_{35} hopanes, C_{27}– C_{29} regular steranes and acyclic isoprenoids such as pristane (Pr) and phytane (Ph). The organic lean carbonates are also dominated by short chain *n*-alkanes (C_{16}–C_{21}) with no obvious carbon number preference and pristane (Pr) and phytane (Ph); also present are long chain *n*-alkanes (C_{25}–C_{29}), C_{27}–C_{31} hopanes and C_{27}–C_{29} regular steranes. The ratio of the short to long chain *n*-alkanes [$C_{17}/(C_{17}+C_{31})$] in both organic rich and organic lean intervals is ~0.9. The ratio of steranes (only the regular steranes, see below) to hopanes, expressed here as $\frac{\sum \text{Steranes } (C_{27}-C_{29})}{\sum \text{hopanes } (C_{27}-C_{31})}$, is higher in black shales (0.86, with a typical range between 0.6 and 1.5) than carbonates (0.76, with a typical range between 0.4 and 1) (Figure *3.6*). The C_{31} hopane maturity index (C_{31} $\frac{\beta\beta}{\beta\beta+\beta\alpha+\alpha\beta}$) in both

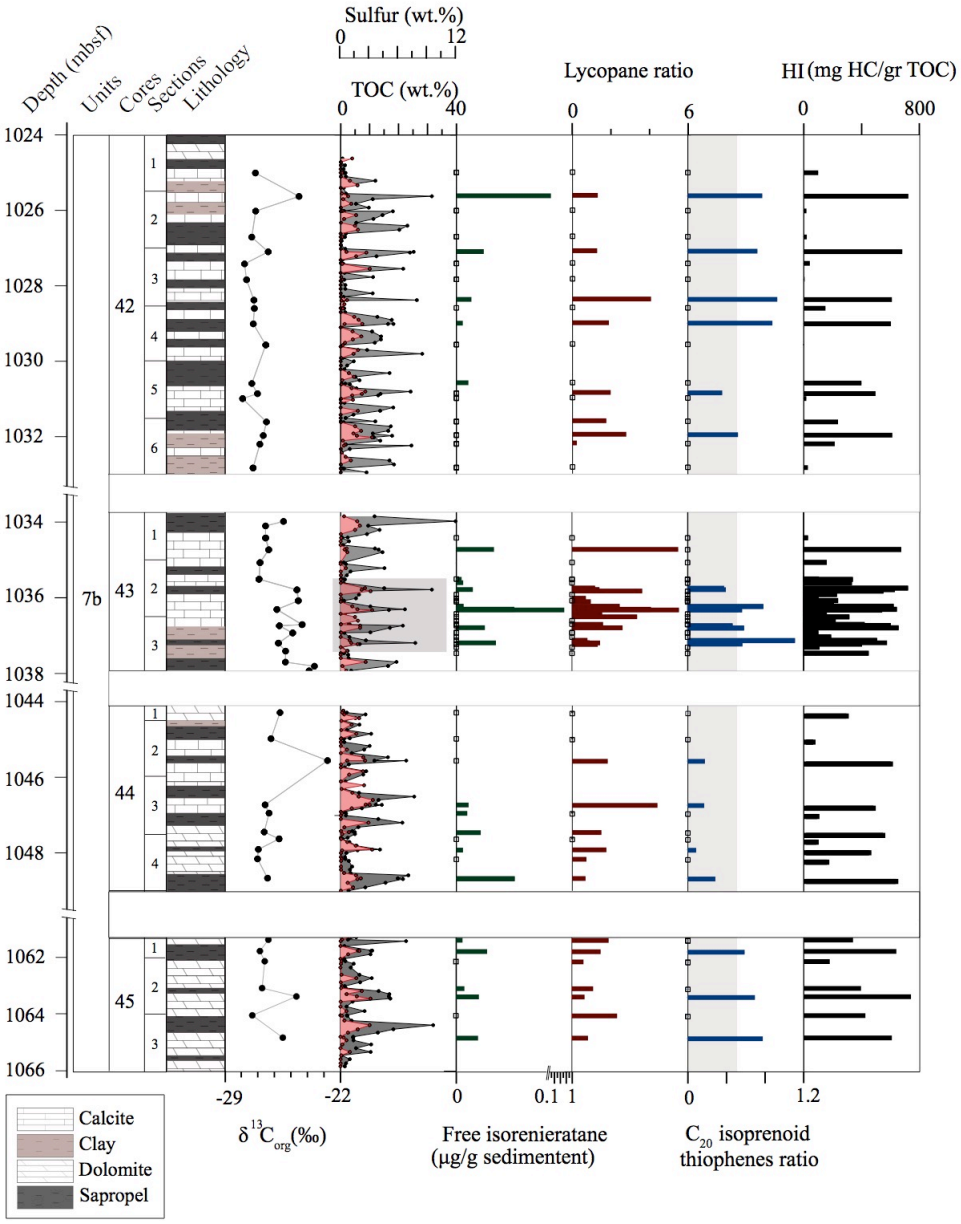

Figure 3.4. Lithology (Shipboard Scientific Party, 1984), bulk $\delta^{13}C_{org}$, total organic carbon (TOC) content (grey), sulfur content (red), free isorenieratane, lycopane ratio, C20 isoprenoid and hydrogen index (HI) across Units 7b (1066–1024 mbsf) for DSDP Site 364. The presence of high amplitude-short term cyclic variations in both TOC and sulfur content. The mechanisms are studied with a higher resolution (10 cm^{-1}) in four representative cycles (1037.5-1035.5 mbsf) from Core 43, highlighted by a grey band.

organic rich and organic lean intervals is approximately 0.15; expressing the alternation in the biologically stereochemistry in a significant portion of the hopane stereoisomers, consistent

with the thermal maturity of the host strata. The acyclic isoprenoid, 2,6,10,15,19-pentamethylicosane, PMI; derived from both methanotrophic (e.g. Pancost et al., 2000) and methanogenic (Schouten et al., 1997) Archaea, occurs in both lithologies. TOC-normalized concentrations of PMI in Cores 42–45 are higher in the carbonate intervals than the black shales (Figure *3.7*). The $\delta^{13}C$ values of PMI in a black shale and carbonate samples from Unit 7b are -28 ‰ and -29 ‰, respectively. Lycopane is rarely present in carbonates, and occasionally abundant in black shales of Unit 7b. The lycopane/C_{31} *n*-alkane ratio can be applied as a proxy for anoxic conditions in the water column (Sinninghe Damsté et al., 2003). Lycopane ratios are around 2 in black shales of Unit 7b but reach values as high as 5.5 in some horizons (Figure *3.4* and Figure *3.5*). Lycopane is largely absent in the Units 7a and 6.

3.3.5.1 MRM (GC-MS-MS)

In addition to the aliphatic biomarkers, both organic rich and organic lean samples contain methylsteranes. However, due to low abundances and co-elution, their identification required the use of MRM-GC-MS. As such, MRM-GC-MS was used to discriminate and confirm the presence of a full range of 4(α,β),23,24-trimethylcholestane isomers (dinosteranes, *m/z* 414 → 231 transition), 4(α,β)-methylstigmastanes (*m/z* 414 → 231 transition), as well as 24-*n*-propylcholestane ($C_{30,}$ *m/z* 414 → 217 transition) and the commonly observed C_{27}–C_{29} regular steranes. Both regular and 4-methylsteranes occur in abundance in both organic-lean and organic-rich stratigraphic intervals and dominate 2-methylsterane and 3-methylsterane. However, the relative abundance of 24-*n*-propylcholestane (24-*n*pc) to C_{27}–C_{30} regular steranes varies between 2–3.5%, with the highest values in black shales (Figure *3.6*). Similarly, the proportion of dinosteranes and 4-methylstigmastanes relative to total regular steranes and C_{30} 4-methylsteranes is generally higher in black shales (0.11–0.4) than in the carbonates (0.1–0.17, Figure *3.6*). The proportion of 4-methylstigmastanes relative to dinosteranes is higher in black shales (mean ~0.9) than in carbonates (mean ~0.7) (Figure *3.6*). MRM analysis also revealed trace abundances of 3β-methylhopanes (*m/z* 205) in both carbonates and black shales. The abundance of C_{31} 3β- methylhopane relative to C_{30} hopane and C_{31} 3β- methylhopane (3β-methylhopane index; $\left(\frac{C_{31}\ 3\beta-\text{methylhopanes}}{C_{31}\ 3\beta-\text{methylhopanes}+\ C_{30}\ \text{hopane}}\right)$) is generally higher in carbonates (2–4%) than black shales (<1–2%) (Figure *3.7*).

3.3.5.2 Thiophenes

The aliphatic hydrocarbon fractions also contain a series of *n*-alkyl and isoprenoidal thiophenes, organic sulfur compounds (Sinninghe Damsté and de Leeuw, 1990 and refrences therein). Both classes of thiophenes are largely absent in the organic lean intervals. The C_{20} isoprenoid thiophene (*m/z 308*) is the most abundant isoprenoidal homologue. The C_{20} isoprenoid thiophene ratio ($\frac{VII+VI}{I+II+III+IV+V}$; for details see Figure *3.8*) ranges between 0.2 and 1 (Figure *3.4*).

3.3.6 Aromatic compounds

The aromatic fraction from organic rich intervals in Unit 7b comprises, among other compounds, isorenieratene, C_{35} hopane stereoisomers with thiophene rings, isoprenoid thiophenes and isoprenoid thiolane. Of particular significance for this study is the presence of isorenieratane (*m/z* 546 and characteristic fragments of *m/z* 131+133), derived from isorenieratene, a carotenoid predominantly produced by phototrophic brown-pigmented green sulfur bacteria (*Chlorobiaceae*, Imhoff, 1995). Isorenieratane concentrations vary from 0 to 900 ng/g with highest values in organic rich intervals (Figure *3.4* and Figure *3.5*). Although largely absent, isorenieratane also occurs in some of the organic lean carbonates of Unit 7b (<6 ng/g) (Figure *3.4* and Figure *3.5*). Isorenieratane was not detected in Units 7a and 6, including the black shales in those core sections.

3.3.7 Desulfurized polar compounds

Similar to the aliphatic fraction of organic rich rocks, the apolar fraction of the desulfurized samples are dominated by short chain *n*-alkanes (C_{16}-C_{21}) with no clear odd-over-even predominance, pristane (Pr) and phytane (Ph), PMI, lycopane (lycopane ratio~1.4), and regular steranes (C_{27}-C_{29}, *S* and *R* isomers, base peak at *m/z* 217). Unlike the aliphatic fractions, long chain (C_{25}-C_{40}) *n*-alkanes in desulfurized fractions do not exhibit any odd-over-even carbon number predominance (CPI~1). Moreover, the hopanes are dominated by the C_{35} homohopane, as is often the case for desulfurized polar fractions (e.g. de Leeuw and Sinninghe Damsté, 1990). Consistent with the composition of the aromatic fractions, the desulfurized polar fractions contain isorenieratane. Desulfurization also yielded chlorobactane (base peak at *m/z* 133, molecular ion *m/z* 554), a derivative of chlorobactene, derived from green-pigmented green sulfur bacteria, Chlorobiaceae (Imhoff, 1995).

3.4 Discussion

To explore the processes governing palaeoceanographic and carbon burial processes across multiple timescales, we first discuss the long-term decrease in TOC content from Unit 7b to Unit 6 (1080–880 mbsf), considering it in the context of the opening phase of the South Atlantic Ocean (section 4.1). This is followed by a discussion that focuses on the short term-high amplitude cyclic variations observed in the bulk records (TOC and S) and a high-resolution biomarker study of Unit 7b (1080–1025 mbsf), providing detailed insights in the depositional environment (section 4.2), the intensity of anoxia (section 4.3), and variations in the ecology (section 4.4) of the basin during the Aptian, methane cycling (4.5) and ultimately the processes behind these variations (section 4.6).

3.4.1 Long term redox changes during the opening of the South Atlantic

Units 7b to Unit 6, spanning ~200 meters of sediment of Aptian to late Aptian age, are characterized by relatively stable $\delta^{13}C_{org}$ values between -28 to -26 ‰ (Figure *3.1*). However, sediments in Core 44 and 43 (Unit 7b) demonstrate a ~2‰ shift to more positive values (Figure *3.1* and Figure *3.4*). This positive carbon isotope excursion could be interpreted as a reflection of enhanced carbon burial, and considering the age of these sediments (Aptian), it could potentially be attributed to the later stages of OAE 1a at around 120 Myr. OAE 1a is characterized by a brief negative and subsequent prolonged positive carbon isotope excursion (Menegatti et al., 1998) related to the input of isotopically light carbon into the ocean-atmospheric system and subsequent increased burial of ^{12}C-enriched organic matter. At Site 364 the positive carbon isotope excursion occurs directly above a ~13 m long coring gap, which might explain the lack of a negative carbon isotope excursion that is characteristic for the onset of OAE 1a. As such, the sediments recovered in Core 44 and 43 likely only represent the later stages of OAE 1a. Evidence of (the later part of) OAE 1a is also recorded in the evaporites of the Brazilian margin of the S. Atlantic (Tedeschi et al., 2017).

The most significant characteristic of the Aptian–late Aptian sediments at Site 364 is the long-term decrease in (maximum) TOC content from Unit 7b (max. 40 wt.%) to Unit 7a (max. 11 wt.%) and Unit 6 (max. 3 wt.%). This change is accompanied by a parallel decrease in sulfur content (Figure *3.1*). Although present in Unit 7b, the biomarker isorenieratane, indicative of photic zone euxinia (e.g. Koopmans et al., 1996) is absent in Units 7a and 6. The absence of lycopane, a biomarker predominantly produced in anoxic zones (Sinninghe Damsté

et al., 2003 and references therein) in Unit 6 is also consistent with an overall decrease in the intensity of anoxia/euxinia in the basin throughout the Aptian.

Although the rifting process initiated in the Late Jurassic (e.g. Sibuet et al., 1984 and references therein), recent studies suggest that the northern South Atlantic basins remained isolated from significant oceanic water influx from the south until the Late Cretaceous (Pérez-Diaz and Eagles, 2014; Pérez-Díaz and Eagles, 2017). The South Atlantic basins also remained restricted to the north until sometime between the Aptian and Campanian stages, when a north-south Atlantic connection became established (Kochhann et al., 2013) and gradually intensified (Friedrich and Erbacher, 2006; Voigt et al., 2013). We therefore attribute the long-term decrease in TOC content, intensity of anoxia, and disappearance of photic zone euxinia to the gradual opening of the South Atlantic, deepening of the basin, and an associated decrease in basin restriction, which changed the sensitivity of the basin to climatic and depositional perturbations.

Although restricted, the basin was not uniformly anoxic/euxinic during the deposition of Unit 7b, as revealed by the cyclicity in TOC contents and the rhythmic occurrence of biomarker evidence of anoxia/euxinia (discussed below). Evidently, the basin geometry, with limited connectivity to the open ocean, pre-conditioned it for climatically induced changes in productivity and anoxia, similar to the Mediterranean during the Quaternary (Menzel et al., 2003; Meyers, 2006; Rohling, 1994) or as seen in the Deep Ivorian Basin to the north (ODP Site 959) during the Coniacian to Santonian (Beckmann et al., 2005; Hofmann et al., 2003; Wagner & Pletsch, 1999). This paleodepositional model is discussed further in section 4.2.

3.4.2 High amplitude, short term cyclic variations in TOC contents and Rock Eval hydrogen indices

Superimposed on the long-term changes in TOC and sulfur content and shifts in biomarker distribution, are high amplitude, short-term cyclic variations that are especially pronounced in Unit 7b (Figure *3.4*). These cycles are most prominent in the high-resolution TOC record, but are also visible in biomarker records (Figure *3.5*, 3.6 and 3.7). The power spectrum of the high-resolution TOC record from Unit 7b highlights the strong periodicity of organic rich black shales with a regular spacing of 46 cm (Figure *3.2* and Figure *3.3*). The difference between the power spectra of the entirety of Unit 7b (Cores 42–45) and only Cores 42 and 43 likely stems from the large coring gaps in Unit 7b. Nonetheless, both records highlight the dominance of a 46 cm periodicity. This observation suggests that rhythmically paced changes in the depositional environment occurred in the basin during the Early Cretaceous. This cyclicity

bears a strong resemblance to the astronomically paced formation of organic rich sapropels at Deep Ivorian Basin (ODP Site 959) during the Coniacian (Beckmann et al., 2005); at Demerara Rise (Leg 207) during the Cenomanian–Turonian (Flögel et al., 2008; Hofmann & Wagner, 2011; Meyers et al., 2006); at Site 530 during the Cenomanian–
Turonian (Arthur et al., 1984; Deroo et al., 1984; Forster et al., 2008; Stow and Dean, 1984); and at Site 1138 during the Cenomanian–Turonian (Dickson et al., 2017).

To constrain these cycles to specific astronomical frequencies requires rigorous age constraints. Unfortunately, these are not available for Site 364 because Unit 7b does not have a precisely defined chronology and is characterized by coring gaps. However, the black shale layers appear to cluster in groups of five in the upper part of the section (Cores 42-45), bundled within the longer 2.4 m cycles (Figure *3.2* and Figure *3.3*). Based on this cycle hierarchy, and considering the subtropical location of Site 364 (~25°S), we suggest that changes in depositional environment are related to eccentricity-modulated precession, where the primary periodicity of 46 cm likely reflects the influence of precession (~21 kyr), and the 2.4 m periodicity may reflect the short eccentricity modulation of precession (~100 kyr). Below, we use detailed biomarker data to probe changes in the depositional environmental of the northern South Atlantic basin during the Aptian and across individual cycles.

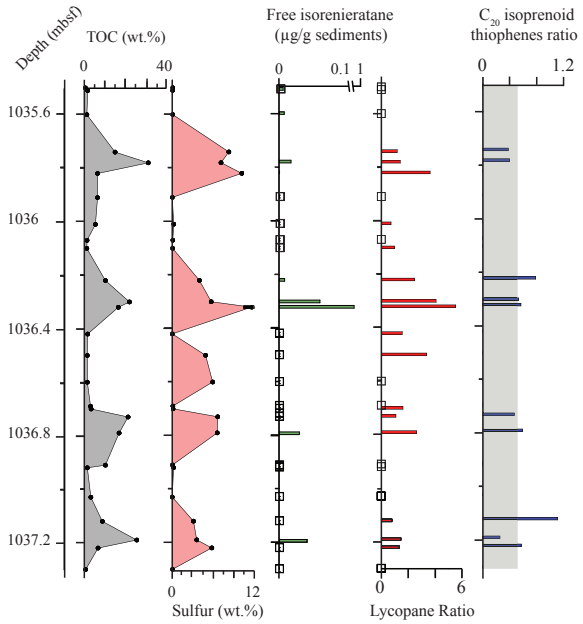

Figure 3.5. Total organic carbon (TOC) content (grey), sulfur content (red), free isorenieratane, lycopane ratio, C_{20} isoprenoid for the four representative cycles of Unit 7b, with a high-

resolution sampling (10 cm^{-1}). The peak in TOC cycles correspond to the maximum abundance of isorenieratane and lycopane (photic zone euxinia and water column anoxia) and the minimum of C_{20} isoprenoid thiophene ratio (hypersalinity).

3.4.3 Redox changes associated with cyclicity in Unit 7b

Multiple lines of evidence indicate that significant redox changes accompany the black shale–carbonate cyclicity at Site 364; these include the laminations and high sulfur contents in the black shales (Figure *3.1* and Figure *3.4*) as well as observations that they are devoid of or contain poorly preserved benthic foraminifera specimens (Leg 40 Shipboard Scientific Party 1978; Kochhann et al. 2014). In addition, the pattern of lower HI index and higher T_{max} in the carbonates strongly suggest development of more oxic diagenetic conditions when organic lean sediments deposited (Landais et al., 1991; Stein, 1991). Here, we explore evidence for the intensity of redox changes and their impact on OM character using biomarkers for sedimentary and water column redox conditions. These biomarkers provide evidence that low oxygen or even euxinic conditions extended into the water column (and photic zone) during intervals of black shale deposition. First, lycopane mainly occurs in black shales, with particularly high lycopane ratios (up to 5.5) in some horizons indicating low oxygen condition or anoxia in the water column (Sinninghe Damsté et al., 2003). Lycopane is not detected in most carbonate intervals, indicative of an oxygenated water column during periods of carbonate formation.

The interpretation of a lower water column oxygenation during black shale deposition is further supported by the presence of thiophene compounds such as C_{20} isoprenoid (mid-chain) thiophenes. Organic sulfur compounds (OSC) are thought to be formed under euxinic conditions (Sinninghe Damsté et al., 1989). Their distribution ($(\frac{VII+VI}{I+II+III+IV+V})$, for details see Figure *3.8*) has been proposed as an indicator of changes in salinity (Sinninghe Damsté et al., 1989; Sinninghe Damsté & de Leeuw, 1990). The C_{20} isoprenoid thiophenes ratio, although variable across the record, suggests episodes of hypersalinity and stratification in some, but not all, euxinic periods (Figure *3.4* and Figure *3.5*).

Euxinia likely extended into the photic zone, as indicated by the presence of isorenieratane, a derivative of carotenoids of green sulfur bacteria (Imhoff, 1995; Koopmans et al., 1996a). Isorenieratene originates from brown colored strains of photosynthetic green sulfur bacteria (chlorobiacae) (Imhoff, 1995 and references therein) that thrive near the chemocline at depths of up to 150 m, where the light levels are less than 1% of sea surface

irradiance (Imhoff, 1995). In addition, the one desulfurized black shale sample contained chlorobactane. Chlorobactene is exclusively produced by the green strain of green sulfur bacteria (Imhoff, 1995 and references therein), which requires higher light intensity and thrives at shallower depths (<15 m) (Imhoff, 1995 and references therein). Assuming a similar light dependence for these phototrophic sulfur bacteria during the Early Cretaceous, the presence of chlorobactane indicates that the chemocline occasionally extended to very shallow depths during black shale deposition, although the limited number of samples we desulfurized precludes us from concluding that these conditions occurred during the deposition of all black shales. Altogether, the biomarker assemblage provides compelling evidence that during deposition of Unit 7b, the northern S. Atlantic water column periodically became profoundly depleted in oxygen, with anoxia and euxinia extending from the sediments to the (shallow) photic zone. Moreover, the basin was anoxic before, during and after the potential OAE 1a positive CIE, resembling conditions that have been reported from other basins during the Cretaceous (e.g. Site 959) (Beckmann et al., 2005; Hofmann et al., 2003; Wagner & Pletsch, 1999).

3.4.4 Biomarker evidence of cyclical changes in ecology

The high OM preservation and reducing conditions during the deposition of black shales could have resulted from increased marine productivity which would have dynamically maintained a redox-stratified water column. This mechanism is consistent with the cyclic variations in the absence/presence and/or changes in the distribution of marine plankton community markers (Figure *3.6*). For example, the abundance of (mainly algal-derived) steranes relative to bacterially derived hopanes, expressed as a sterane/hopane ratio (Summons et al., 2006 and references therein), as calculated for the most abundant sterane and hopane compounds, are slightly elevated in the black shales (mean ~ 0.86) compared to carbonates (mean ~ 0.76) (Figure *3.6*). Consistent with this ecological change is the higher concentration of C_{30} steranes (24-*n*pc) and particularly high (max ~0.4) dinoflagellate C_{30} methylsterane signal (dinosteranes and 4-methylstigmastanes) in the organic rich black shales (Figure *3.6*). The C_{30} regular sterane (24-npc) is biomarker for predominantly marine pelaogophyte algae in Devonian and younger sedimentary rocks (e.g. Cao et al., 2009), whereas as dinosteranes are mainly derived from marine dinoflagellates in Mesozoic and younger rocks and oils (e.g. Summons et al., 1992). Cyclic changes in water column ecology are also indicated by the predominance of C_{27} over all regular steranes (C_{27}–C_{30} (24-*n*pc)) in black shales, a distribution that changes to a predominance of C_{29} regular sterane in carbonates (Figure *3.6*). Numerous studies of regular

sterane (C_{27}–C_{29}) distributions and their specific precursors (Huang & Meinschein, 1979; Kodner et al., 2008; Volkman et al., 1994) have led to various suggestions regarding their utility in inferring changes in organic matter source (although such approaches must be done cautiously, e.g. Kodner et al., 2008). For instance, the C_{27} and C_{29} sterols are preferentially synthesized by red algae and green algae, respectively (e.g. Huang and Meinschein, 1979; Volkman et al., 1994; but see Kodner et al., 2008 for exceptions). Classically, higher relative abundances of C_{29} regular steranes have been interpreted as evidence of proportionally greater terrigenous inputs. Therefore, the observed variations in sterane distribution provide further evidence for ecological and/or OM source change, but the specific meaning of these changes is difficult to detangle. A shift to C_{27} sterane predominance is, however, consistent with a pulse of dinoflagellate activity during black shale deposition as dinoflagellates are from a derived red algal clade and C_{27} steranes are their major regular sterane marker (Volkman et al., 1994). Proportion of 4-methylstigmastane over dinosteranes as a signal of lacustrine fresh water (Goodwin et al., 1988; Hou et al., 2000; Summons et al., 1992, 1987) is higher in black shales (mean ~0.9) than carbonates (mean ~0.78), (Figure *3.6*). 4-methylstigmastane and dinosteranes are indicators for marine (Goodwin et al., 1988; Moldowan et al., 1985; Summons et al., 1987) and non-marine dinoflagellates (Jiamo et al., 1990). The dominance of 4-methylstigmastane over dinosteranes in our samples strongly suggests a lacustrine fresh water origin (Goodwin et al., 1988; Hou et al., 2000; Summons et al., 1992, 1987). 4-methylstigmastane are not selective biomarkers of dinoflagellates (Volkman et al., 1990), however considering the higher proportion of C_{27} regular sterane in black shales, dinoflagellates are the likely source of 4-methylstigmastane (Fowler and McAlpine, 1995) in black shales. The dominance of 4-methylstigmastane in black shales (Figure *3.6*) indicates the establishment of fresh (lower salinity) surface water layer and stratification in the basin particularly during the periods of enhanced terrestrial input and during the deposition of black shales, although the system remained marine (C_{30} regular steranes). Altogether, the biomarker evidence, alongside the high HIs in black shales indicates that high marine algal productivity drove the water column anoxic/euxinic in a restricted basin, likely aided by elevated nutrient inputs and stratification.

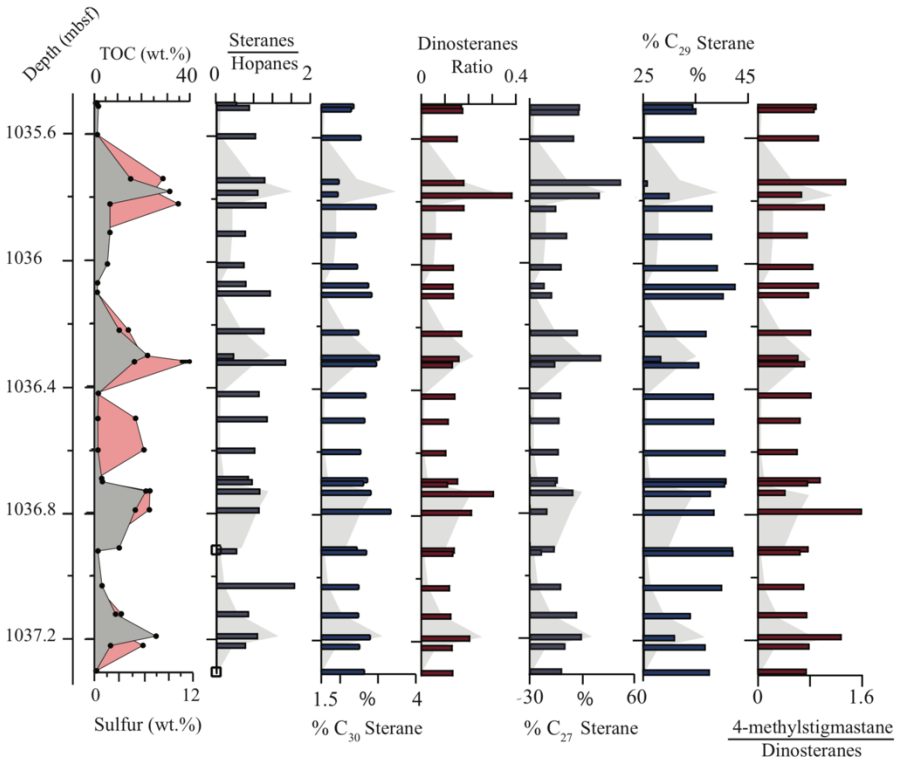

Figure 3.6. Total organic carbon (TOC) content (grey), sulfur content (red), C_{27}-C_{30} (24-npc) steranes/ C_{27}+C_{35} hopanes ratio, % C_{30} (24-npc) sterane, dinoflagellate C_{30} methylsterane signal, % C_{27} and % C_{29} regular steranes, 4-methylstigmastames/dinosteranes, for the four representative cycles of Unit 7b, with a high-resolution sampling (10 cm^{-1}). Biomarkers distribution show that marine algal productivity was favored under photic zone euxinia condition, and stratification was established in the basin particularly during when black shales deposited.

3.4.5 Methane cycling in Aptian South Atlantic

Other changes in basin ecology are documented by the abundances of microbial biomarkers, providing insights into the Aptian methane cycle in the northern South Atlantic. Compound specific $\delta^{13}C$ of the archaeal lipid PMI ($\delta^{13}C_{PMI}$) (see section 3.5) suggests a methanogenic rather than methanotrophic archaeal origin in this setting (e.g. Schouten et al. 1997). Concentrations of PMI are higher in the organic lean carbonates than in the black shales (Figure *3.7*). However, the desulfurized polar fraction of the black shale sample is also dominated by PMI and the lower concentration of PMI in the aliphatic fraction of black shales is likely due to rapid sulfurization of PMI's highly unsaturated precursor during the early stages of

diagenesis (sulfur incorporation reactions (Sinninghe Damsté and de Leeuw, 1990 and references therein)), rather than ecological changes. Our data suggest that methanogenesis as the final step of OM biodegradation was occuring consistently in both carbonates and black shales.

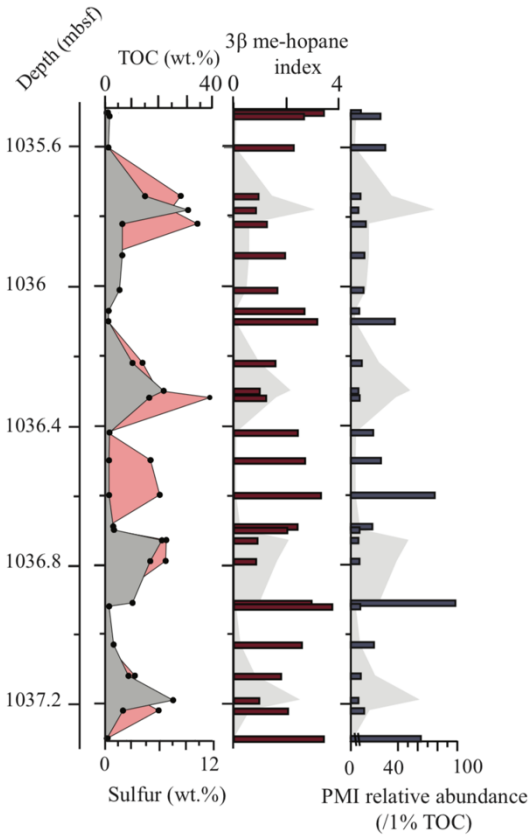

Figure 3.7. Total organic carbon (TOC) content (grey), sulfur content (red), 3β methylhopane index and PMI relative abundance, for the four representative cycles of Unit 7b. The lower concentration of PMI in the aliphatic fractions of black shales than carbonates could be more attributed to the sulfur incorporation reactions rather than ecological changes.

Another aspect to consider is the concentration of 3β-methylhopanes in both carbonates and black shales (Figure *3.7*). The most likely source of 3β-methylhopanes in marine environments is Type I methanotrophs (reviewed by Farrimond et al., 2004). This assumption can be supported by depleted carbon isotope compositions (Ruble et al., 1994), but that was not possible here due to overall low concentrations of this biomarker. Methanotrophs are methane oxidizing bacteria that tend to live under microaerophilic conditions, such as the

chemocline in stratified environments (Hanson and Hanson, 1996). Because the 3β-methylhopane ratios are low (1%–4%) throughout the entire studied section and in the typical range for Phanerozoic sediments (1%–3%; Cao et al., 2009), (i.e. there is no evidence for particularly enhanced abundances of aerobic methanotrophic bacteria), we suggest that the primary mode of methane oxidation was likely via anaerobic oxidation of methane (AOM) (e.g. Orphan et al., 2002), similar to what has been previously reported for the Black Sea water column (Wakeham et al., 2003). However, the elevation of the 3β-methylhopanes ratio $\left(\frac{C_{31}\ 3\beta\text{-methylhopanes}}{C_{31}\ 3\beta\text{-methylhopanes} + C_{30}\ \text{hopane}}\right)$ by ~2% in carbonates, when the water column was more oxygenated, suggests that different bacterial communities (potentially type I methanotrophic bacteria; reviewed by Farrimond et al., 2004) prevailed during carbonate deposition. We suggest that aerobic methanotrophy dominated during these times, whereas anaerobic oxidation of methane was more important when the water column was largely anoxic.

3.4.6 Causes of sedimentary cycles

As discussed above, during the initial opening stages of the northern South Atlantic, sedimentary deposition was characterized by putatively cyclic burial of OM, reflecting a regular alternation between oxic and anoxic/euxinic conditions. Crucially, the cyclic changes in the concentrations of lycopane and isorenieratane confirm that these variations were not restricted to sediments or bottom waters but extended into the water column and even photic zone. We attribute these cyclical (precession-driven) changes primarily to increased stratification but also increased productivity during black shale deposition, the latter inferred from changes in algal biomarker assemblages that document ecological change. Enhanced productivity was likely driven by an increased input of biolimiting nutrients.

Wagner et al. (2013) presented a conceptual framework for the formation of proto Atlantic black shales in the (sub)tropics during the Cretaceous (Albian, Cenomanian–Turonian), linking the richness and quality of OM to changes in upwelling in the proto-Atlantic and continental runoff into the basin. However, in modern upwelling regions such as off the coast of Peru (Dugdale et al., 1977) and those in the Indian ocean (Ivanenkov and Rozanov, 1961) photic zone euxinia does not occur; furthermore, isoreniaretane (or its biological precursor isoreniaratene) is only found in the sediments and water column of stratified basins such as the Black Sea (Repeta et al., 1989). We therefore argue that the occurrence of anoxic/euxinic conditions during deposition of the Aptian black shale horizons at Site 364 was probably related to water column stratification combined with enhanced primary productivity driven by

terrestrial nutrient delivery. This situation is similar to what has been invoked for the formation of Coniacian-Santonian black shales (ODP Site 959) in the tropics (Beckmann et al., 2005; Flögel & Wagner, 2006; Wagner et al., 2013) and Albian black shale deposits of DSDP Site 367 in the eastern North Atlantic (Hofmann et al., 1999; Wagner et al., 2013). This hypothesis is further supported by the dominance of 4-methylsteranes in C_{30} methylsteranes as an evidence for salinity stratification (Goodwin et al., 1988) in both carbonates and black shales. Additionally, the higher proportion of 4-methylstigmastane over dinosteranes in black shales (Figure *3.6*) as a signal of lacustrine fresh water layer (Goodwin et al., 1988; Hou et al., 2000; Summons et al., 1987, 1992), and establishment of stratification in the basin, particularly during the periods black shale deposited. In addition, overall low (<0.5) C_{20} isoprenoid thiophene ratio in black shale horizons at Site 364, suggests episodes of hypersalinity and stratification during (some) of the euxinic periods (Figure *3.4* and Figure *3.5*). Moreover, the pattern of HI and Tmax values in carbonates and black shales, propose a significant background composition of transported terrestrial organic matter (kerogen type III) in the organic lean carbonates. This is consistent with the pulses of high marine productivity dynamically maintaining reducing conditions within the water column during the deposition of black shales (kerogen type II).

We argue that Aptian organic rich black shales (with high HI values) in Site 364 represent the strong influence of continental runoff from tropical South Africa, whereas carbonate horizons with low organic content (and low HI values) formed when the basin was influenced from the SW trade winds and more oxic conditions developed (when the Inter-tropical Convergence Zone (ITCZ) was located in a relatively northern position). Climate model simulations support our hypothesis, demonstrating that the appearance of the Atlantic Ocean led to significant changes in the hydrological cycle and modulated the monsoonal influenced regions (Ohba and UEDA, 2010).

Crucially, the impact of these climatic factors was modulated by the evolution of the South Atlantic, which resulted in the formation of series of rift basins in the (sub)tropics which gradually became connected to the open ocean through the (Early) Cretaceous (e.g. Friedrich and Erbacher, 2006; Pérez-Diaz and Eagles, 2014). These rift basins and the early restricted South Atlantic were particularly sensitive to orbitally-controlled changes in monsoonal runoff and episodic formation of organic rich black shales. To the best of our knowledge, there is no other Aptian-age black shale or modelling study in the South Atlantic to help us build a wider concept regarding the formation of black shales in the region. However, our findings shed some light on the sedimentary pattern of Aptian black shales deposition, and in particular, they support the hypothesis that changes in organic carbon richness is controlled by orbitally-paced

variations in the hydrological cycle, as has been inferred for the Cretaceous (Hofmann and Wagner, 2011; Wagner et al., 2013) and Jurassic (Armstrong et al., 2016). Based on our results from Site 364 we argue that the southward development of the ITCZ (~25°S) during the Aptian alongside with the paleogeography of the region, made the South Atlantic sensitive to the orbitally forced variations in hydrology, and likely led to a widespread occurrence of Aptian black shales in the South Atlantic. A strength of the hydrologically-modulated mechanism is that it would have not only enhanced nutrient inputs but could have contributed to density-driven water column stratification. This combination of enhanced productivity and stratification-limited oxygenation of deep waters could have combined to generate the particularly dramatic changes in TOC content and character, as has been invoked for Site 959 (ODP Leg 159; the deep Ivorian Basin), (e.g. Wagner and Pletsch, 1999). Previous work (Słowakiewicz et al., 2015) has cautioned against interpreting basin-scale stratification on the basis of a single site, but the particularly high TOC contents observed here do suggest changes in productivity and ocean circulation. Crucially, the cyclic burial of such organic-rich sediments appears to have stimulated a particularly strong methane cycle. The very high concentration of PMI in desulfurized black shale extracts suggests intense methanogenesis in those horizons, whereas the 3ß-methylhopanes provide evidence for aerobic methanotrophy, perhaps in the water column. Altogether, the carbon cycle in the northern South Atlantic during the Aptian seems to have been controlled by astronomical forcing (precession), driving changes in the hydrological cycle that subsequently regulated the methane cycle via biodegradation of OM.

Although our results are specific to Site 364 and the margins of northern South Atlantic, periodic black shales of similar age (Early Cretaceous) have been reported elsewhere in the proto-Atlantic, for example at Site 530 in the Angola basin (e.g. Deroo et al., 1984; Katz, 1984; Meyers et al., 1984; Rullkötter et al., 1984; Stow and Dean, 1984); Site 511 in the Falkland Plateau (e.g. Deroo et al., 1983), and Site 367 in Gambia Abyssal Plain (e.g. Hofmann et al., 1999; Wagner et al., 2013). There are also numerous publications on the astronomically controlled formation of black shales in the Late Cretaceous, for example from Site 959 in the Ivorian Basin (Beckmann et al., 2005; Holbourn et al., 1999), Leg 207 (Sites 1257-1261) at Demerara Rise (Hofmann & Wagner, 2011; Meyers et al., 2006), Site 530 in the Angola basin (e.g. Arthur et al., 1984; Deroo et al., 1984; Forster et al., 2008; Stow and Dean, 1984), the Western Interior Seaway (Eldrett et al., 2015) and ODP Site 1138 in the Indian Ocean (Dickson et al., 2017). These results suggest that the proposed depositional mechanism for Site 364 of a hydrographically restricted basin that was pre-conditioned to astronomically-controlled variations in terrestrial runoff was probably a common feature of the proto-Atlantic region

during the Cretaceous. These observations highlight the strong links between climate, the hydrological cycle, terrestrial weathering and nutrient availability, primary production and deoxygenation in the marine system.

3.5 Conclusions

High-resolution geochemical data from DSDP Site 364 (Units 7b to 6) allows reconstruction of the intensity and persistence of redox conditions in the northern South Atlantic Ocean during its early opening phase in the Aptian. The opening history of the northern South Atlantic is documented by the accumulation of organic carbon, with the relatively high preservation of organic matter in the restricted basin (Unit 7b and to a less extent in unit 7a), terminated by continued rifting, basin deepening and increased connectivity with the open ocean by the late Aptian (Unit 6). High amplitude fluctuations in TOC and TS contents and HIs indicate that basin restriction alone did not cause anoxic conditions to develop, but instead preconditioned the basin for oxygen depletion during episodes of enhanced organic matter production and export. Productivity fluctuations most likely resulted from eccentricity-modulated precession changes in the delivery of biolimiting nutrients from weathering and terrestrial runoff. Enhanced terrestrial runoff, perhaps associated with a strengthened hydrological cycle, might also have caused salinity stratification in the upper ocean, as evidenced by elevated proportion of 4(αβ)-methylstigmastane over dinosteranes during the periods of increased terrestrial input, also cyclic variations in C_{20} isoprenoid thiophene abundances. Regardless of the forcing mechanism(s), the impact of cyclical changes in climate on the South Atlantic was pronounced, evidenced by increased primary production and changes in algal assemblages; anoxic conditions in the water column, including photic zone euxinia and sometimes extending to very shallow water depths (<15 m); and a pronounced methane cycle.

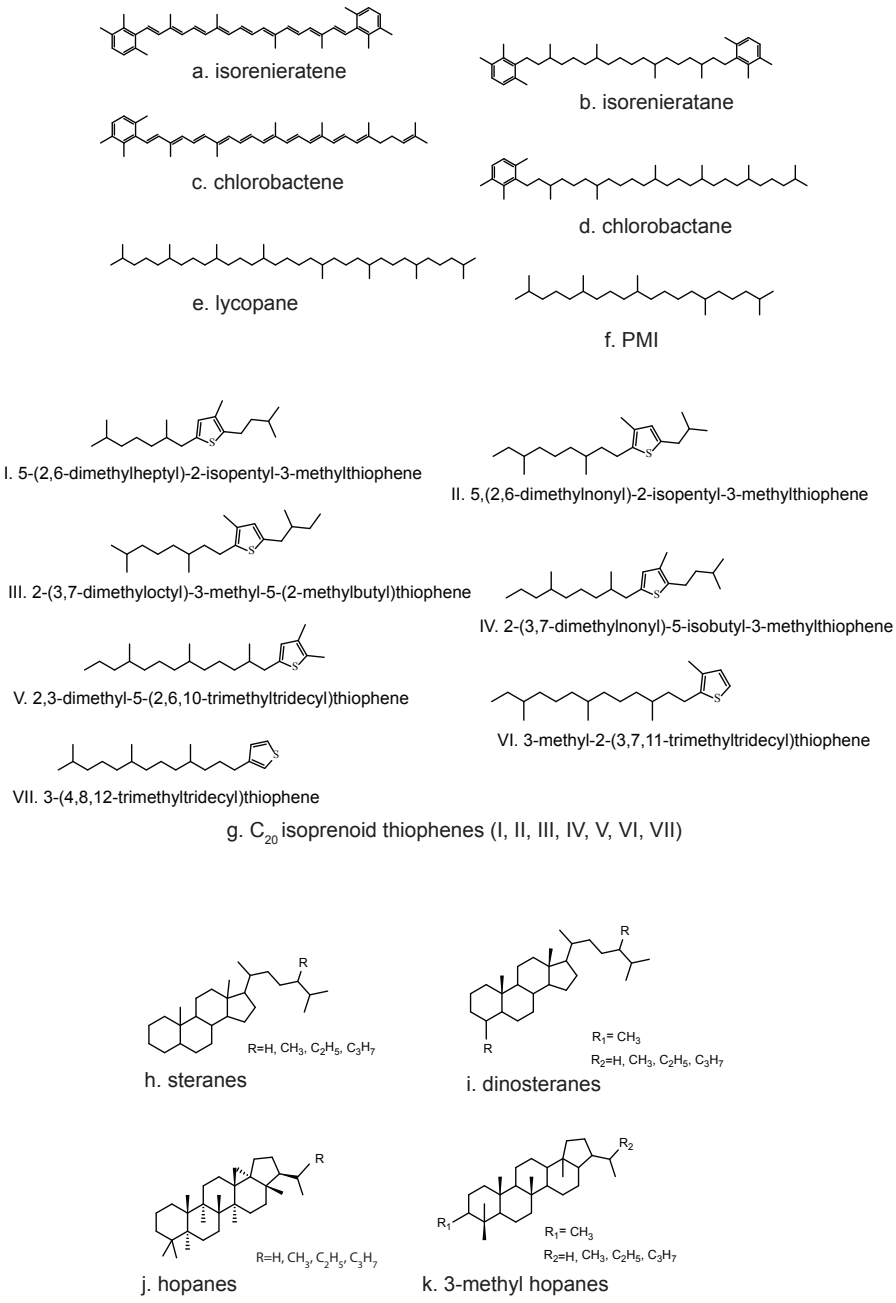

Figure 3.8. The schematic molecular structure of lipid biomarkers analyzed in this paper.

Chapter 4

Early Cretaceous record of tropical sea surface temperature (DSDP 364)

Preface

This chapter is based on a manuscript which is under modification and preparation for submission as an article to the journal *Earth and Planetary Science Letters (EPSL)*. LB carried out analysis (unless stated), interpreted the organic geochemical data set and wrote the chapter. RP and DN made comments and suggestions on the initial draft made by LB. A. Dickson (Royal Holloway University of London) supported this project by analyzing carbon isotope measurements.

Abstract

While reconstruction of Cretaceous temperature is vital to understand the dynamics of a greenhouse Earth system, a complete record of sea surface temperature (SST) from the Albian is not yet available. Here, we provide a ~20 Myr long (late Aptian–late Albian) record of TEX_{86}-based SSTs from the low latitude South Atlantic (DSDP Site 364). The record of TEX_{86} during the Aptian (~0.95) indicate a rather steady SST for almost ~10 Myr (TEX_{86}^{H}-SST ~37±2.5°C, $TEX_{86-linear}$-SST ~45±2.0°C). The cooler TEX_{86}-SST values of the late Albian–Cenomanian (TEX_{86}~0.85, TEX86H-SST was at ~33.7 ±2.5°C and $TEX_{86-linear}$-SST at ~38.7±2.0°C) associated with OAE 1d, could be as a result of local changes in the geomorphology or hydrography of the basin or a cooling episode during OAE 1d as previously observed during OAE 1a and OAE 2. Additionally, the Aptian–Coniacian records of $\delta^{13}C_{org}$ provides evidence for the Cretaceous oceanic anoxic events in the South Atlantic. OAE 1a and OAE 1d, are recognized as the driving factors for the recorded carbon cycle perturbations in the basin.

4.1. Introduction

The Cretaceous period (~145-66 Ma) was characterized by a greenhouse climate (e.g. Clarke and Jenkyns, 1999; Friedrich et al., 2012; Hay, 2008; Huber et al., 2002; Littler et al., 2011), with elevated atmospheric CO_2 levels (typically > 500 ppm, Freeman and Hayes, 1992; Naafs et al., 2016; Sinninghe Damsté et al., 2008; Wang et al., 2014), high terrestrial mean annual temperatures (MAT; Amiot et al., 2004; Herman and Spicer, 1996), warm deep oceans (Cramer et al., 2009; Friedrich et al., 2012), high sea surface temperatures (SSTs; e.g. Bice et al., 2006; Forster et al., 2007; Naafs and Pancost, 2016; O'Brien et al., 2017; Schouten et al., 2003), little or no polar ice (Huber et al., 2002; MacLeod et al., 2013; Miller et al., 2005), and a reduced latitudinal temperature gradient (Barron, 1983; Huber et al., 1995, 2002). The most pronounced sea surface warming is recorded during the Cenomanian–Turonian (e.g. Clarke and Jenkyns, 1999; Huber et al., 1995; Jarvis et al., 2011; Jenkyns et al., 1994; Macleod et al., 2011; Schouten et al., 2003; Wilson et al., 2002) followed by a significant cooling trend towards the end of Cretaceous, likely caused by a combination of ocean gateways rifting and atmospheric pCO_2 decline (Clarke and Jenkyns, 1999; Friedrich et al., 2012; Li and Keller, 1998; Miller et al., 2005; Thibault and Gardin, 2006). The Cretaceous greenhouse climate was interrupted by intervals of global cooling (e.g. Hong and Lee, 2012; Jenkyns et al., 2012; McAnena et al., 2013; Mutterlose et al., 2009), i.e. the two cooling episodes; recorded during the Aptian (Dumitrescu and Brassell, 2006; Kim et al., 2010; Kuhnt et al., 2011; Pucéat et al., 2003).

Superimposed on this general greenhouse climate were the Oceanic Anoxic Events (OAEs) (Jenkyns, 1980). OAEs record profound perturbations in global climate (e.g. OAEs are associated with thermal maxima), ocean chemistry and global biogeochemical cycles (reviewed by Jenkyns, 2010), reflected, for example, in the carbon isotope excursions (CIEs) that accompanied the main OAEs. The major forcing function behind OAEs is not well understood. However, since OAEs are classically associated with a negative carbon excursion, it is suggested that OAEs are accompany and triggered by a rapid injection of ^{13}C depleted carbon to the ocean-atmospheric system (reviewed by Jenkyns, 2010). This influx of isotopically light carbon is associated with a record of negative carbon isotope excursion (CIE) in the OAEs organic carbon profile. Following the enhanced organic carbon burial, the sea water remains enriched in ^{13}C, expressed as positive CIE. The early Aptian OAE (OAE 1a; e.g. Menegatti et al., 1998), early Albian OAE (OAE 1b; e.g. Kuypers et al., 2002; Tsikos et al., 2004) and late Albian OAE (OAE 1d; Scott et al., 2013) have experienced both negative and

positive excursions (see review by Jenkyns, 2010). However, some OAEs are only associated with a positive CIE, e.g. Cenomanian–Turonian OAE (OAE 2; Forster et al., 2007b; Kuypers et al., 2002) and Coniancian–Santonian OAE (OAE 3; Jarvis et al., 2006; Wagreich, 2012).

Reconstruction of past greenhouse climates is necessary in order to understand the performance of Earth climate system under a greenhouse condition. Therefore, there is much interest in the reconstruction of Cretaceous SST and the associated phenomena, particularly pCO_2 and carbon cycle perturbations, as direct interactions. In spite of the large number of SST records from the Cretaceous (reviewed by O'Brien et al., 2017), an Albian record of SST, except for the Early Albian record of SST at Site 545 (McAnena et al., 2013), is not yet available. In addition, during the Albian Site 545 was located in the upwelling West African coast (Handoh et al., 2003; Hofmann et al., 2008; McAnena et al., 2013; Poulsen et al., 1999), and therefore the Early Albian record of TEX_{86}-based SSTs might not be representative for the subtropical regions during the Early Cretaceous.

This study fills the early Albian–mid Albian gap, and provides a ~20 Myr records of TEX_{86} to trace variations in sea surface temperatures (SST) during Aptian-late Albian. In addition, we present an Aptian–Coniancian record of $\delta^{13}C_{org}$ to reconstruct carbon cycle perturbations.

4.2. Samples and Methods

4.2.1. Sampling location and lithology

Deep Sea Drilling Project (DSDP) Site 364 (modern latitude: 11°34.32'S, 11°58.30'E, 2450 m water depth), is located in the Kwanza Basin of the South Atlantic, and was drilled on the seaward edge of the salt plateau at the transition from the outer Kwanza Basin to the Benguela Basin (Leg 40 Shipboard Scientific Party, 1978). Site 364 covers a 427 m cored section (46 cores) to a bottom depth of 1086 meter below sea floor (mbsf) (top of the Aptian evaporite and salt formations), and consists of Pleistocene to Early Cretaceous sediments (Kochhann et al., 2014; Leg 40 Shipboard Scientific Party, 1978). Site 364 is divided into seven lithological units (e.g. Leg 40 Shipboard Scientific Party, 1978; Matsumoto et al., 1978), with Units 7 to 5 investigated here. During this time DSDP Site 364 was located at approximately 25°S. Sediments at Site 364 were deposited on a continental shelf setting (Kochhann, et al. 2014). Unit 5 (Late Albian–Santonian) is composed of marly chalk and black shale. On the basis of the proportion of black shales, Unit 5 (Leg 40 Shipboard Scientific Party, 1978) is divided into two subunits 5a (Cores 20-22) and 5b (Cores 23-25) with respectively less and more abundant black shales (Leg 40 Shipboard Scientific Party, 1978). Unit 6 (Late Aptian-Albian) (

Kochhann et al., 2013; Kochhann et al., 2014; Leg 40 Shipboard Scientific Party, 1978) predominantly consist of calcium carbonate (limestone) (Leg 40 Shipboard Scientific Party, 1978). The underlying Unit 7 (Aptian; Kochhann et al., 2014, 2013; Leg 40 Shipboard Scientific Party, 1978), the deepest lithological section of Site 364, comprises dolomitic limestones and thin black shales (Behrooz et al., 2018; Leg 40 Shipboard Scientific Party, 1978; Matsumoto, 1978; Raynaud and Robert, 1978; Simoneit, 1978). On the basis of the proportion of black shales, Unit 7 is divided into two subunits: 7a (Cores 39 to 41) with fewer and 7b (Cores 42 to 46) with more abundant and more intense black shale horizons (Leg 40 Shipboard Scientific Party, 1978).

4.2.2. Dating of the studied sediments

Coring gaps and calcium carbonate dissolution in some sections of Site 364 hinders precise age determination in some sections. Overall, the studied sections here, spanning ~400 meters of sediment, span the Aptian (Kochhann et al., 2013; Kochhann et al., 2014; Leg 40 Shipboard Scientific Party, 1978) to Coniancian, i.e. ~35 Myr based on the Geological Time Scale 2012 (GTS 2012; Gradstein et al., 2012).

Studied sediments of Unit 7 here are cores 39-41 (Unit 7a) and cores 42-45 (Unit 7b), Fig. 4.1. Sediments from Cores 43-45, although being devoid of planktonic foraminifera and suffering from very poor preservation of benthic foraminifera (Leg 40 Shipboard Scientific Party, 1978), have been assigned to lower-upper Aptian (Bralower et al., 1994). In addition, the later stage of OAE 1a (positive carbon isotope excursion) assigned to Aptian (Menegatti et al., 1998) is observed in Cores 44 and 43 (discussed in chapter 3, Fig 4.1). Based on both planktonic (Kochhann et al., 2013) and benthic (Kochhann et al., 2014) foraminifera, Cores 39-42 are also assigned to the Aptian, Figure *4.2*. Sediments of Unit 6 (Cores 38-26) span from Late Aptian-Late Albian. Both planktonic (Kochhann et al., 2013) and benthic (Kochhann et al., 2014) foraminifera concur with Core 38 (Aptian), Cores 37-33 (late Aptian), 32 (early Albian), 31-26 (late Albian), Fig. 4.1. Studied sediments of Unit 5 here are from cores 22-25 (Figure *4.2*). On the basis of benthic foraminifera, cores 24 and 25 are late Albian-early Cenomanian in age (Leg 40 Shipboard Scientific Party, 1978), however planktonic foraminifera are dispersed due to poor preservation or carbonate dissolution and age determination is not possible based on planktonic foraminifera. Dissolution is less pronounced in cores 22 and 23. Both planktonic and benthic foraminifera confirm aging in core 23 to be Upper Touronian–Lower Coniancian and core 22 to be upper Coniancian (Leg 40 Shipboard

Scientific Party, 1978). Likely a disconformity is present in Unit 5 where Cenomanian and Touronian are missing (Leg 40 Shipboard Scientific Party, 1978).

4.2.2.1. Strengths and Weaknesses of the used age model at Site 364

Overall, there is a general agreement on ageing at Unit 7 (cores 45–39) being assigned to Aptian (Bralower et al., 1994; Kochhann et al., 2014, 2013; Leg 40 Shipboard Scientific Party, 1978; Menegatti et al., 1998). Similarly, based on the high-resolution studies on both planktonic and benthic foraminifera (Kochhann et al., 2014, 2013), Unit 6 (Cores 38–26) is assigned to Late Aptian-Late Albian.

However age definition at Unit 5 (cores 25–20), specially at the lower sections (cores 25–23) is still under debate (Leg 40 Shipboard Scientific Party, 1978). While nanoplanktons, planktonic and benthic foraminifera assemblage indicate that the upper section at Unit 5 (cores 22–20) is Upper Coniacian–Santonian; age determination is not possible at the lower section (cores 25–23), (Leg 40 Shipboard Scientific Party, 1978). Therefore, the part of this study which is related to cores 25–23 (Unit 5, Figure 4.1), suffers from age certainty (expanding from Upper Albian–Coniacian) raised from poor preservation of foraminifera, carbonate dissolution and the Cenomanian–Early Turonian hiatus (Leg 40 Shipboard Scientific Party, 1978).

4.2.3. Opening of the equatorial Atlantic gateway

The opening of the Atlantic, as the equatorial gateway connecting major ocean currents, is thought to be a controlling climate factor during the Cretaceous (Pérez-Díaz and Eagles, 2017; Tedeschi et al., 2017). Atlantic rifting process initiated in the Late Jurassic (e.g. Sibuet et al., 1984; Dean et al. 1984; Zimmerman et al. 1987; Hartwig et al. 2012) . Furthermore, the recent models of South Atlantic indicate that the onset of spreading start at the latest by the Early Cretaceous (138Ma) (Pérez-Diaz et al., 2014).

Recent plate kinematic models of the South Atlantic (Pérez-Diaz et al., 2014; Pérez-Díaz and Eagles, 2017) indicate that equatorial shallow and intermediate water connection commenced at Cenomanian (100 Ma) via the Agulhas Gap (Pérez-Díaz and Eagles, 2017), followed by the deep water exchange. Although according to the planktonic foraminifera, the connection between the South and North Atlantic commenced during the late Aptian (Kochhann et al., 2013).

However, the connection between the isolated basins of the northern South Atlantic and the South Atlantic has developed earlier than the connection to the North Atlantic, i.e. in the mid-Aptian (e.g. Sibuet et al., 1984).

4.2.4. Analytical Method

A total of 422 samples were obtained from the International Ocean Discovery Programme (IODP) Bremen Core Repository, Germany. Unit 7b was sampled with a resolution of ca. 10 cm (253 samples; discussed in chapter 3 in more details). 14 samples from Unit 7a, 39 samples from Unit 6 and 116 samples from 5 were taken at a lower resolution. Bulk samples were freeze-dried to remove excess water and were powdered using either a ball-mill device or a mortar and pestle.

4.2.4.1. Bulk Geochemistry

Total carbon (C) and inorganic carbon (IC) contents were determined using a CHN elemental analyzer Eurovector EA 3000 and Strohlein Coulomat 702, respectively. All elemental analyses were performed in duplicate and the presented data reflect the mean of these duplicates. Total Organic Carbon (TOC) is determined by taking the difference between total carbon and inorganic carbon. To analyze bulk organic stable carbon isotopic ratios ($\delta^{13}C_{org}$), inorganic carbon was removed using 2M HCl acid. Sample tubes were placed in a water bath and heated at ~60°C to 80°C for 5 hours to aid the reaction (also ensuring the removal of pyrite). Samples were then re-powdered and dried in an oven at 50°C for 24 hours. Between 10 and 25 µg of each sample (depending on TOC content) were used to measure $\delta^{13}C_{org}$ at the Open University, UK. $\delta^{13}C_{org}$ was measured using a Thermo Flash HT Elemental Analyser coupled to a Thermo Finnegan MAT 253 mass spectrometer (with the 1 σ uncertainty of 0.03 ‰, 0.09 ‰ and 0.01‰ for IAEA CH-6, NIST 8573 and IR-R041 standards, respectively; n=20).

Rock-Eval analyses were performed on 126 sediments from Units 7b to 5 using a Rock-Eval 6 instrument to obtain estimates of the hydrogen index (HI) and the temperature of maximum hydrocarbon generation (T_{max}). Respective 2σ uncertainties were estimated with repeated measurements of an in-house shale standard (St. Audries Bay Shale) and were 3 mg HC/g TOC and 19 °C. Approximately 30–50 mg of dried sample powders was weighed for each measurement.

4.2.4.2. Biomarker Extraction

124 samples were selected for detailed biomarker analysis. To obtain total lipid extracts (TLEs), 14 g of each sample was extracted with 20 ml of dichloromethane (DCM): methanol (MeOH) (9:1, vol) by microwave-assisted method (MILESTONIE Ethos Ex Microwave solvent extraction). The microwave program consisted of a 10 min ramp to 70°C (max. 1000 W), followed by a 10 min hold at 70°C (max. 1000 W) and a 20 min cooling period. Activated copper turnings were added to the TLEs for 24 hrs to remove elemental sulfur. The TLE was then concentrated using rotatory evaporator and separated into three fractions (aliphatic, aromatic and polar) using short (4 cm) silica gel open column chromatography. Aliphatic, aromatic, and polar fractions were eluted using 3 ml of hexane, 4 ml of hexane:DCM (3:1) and 4 ml of DCM:MeOH (1:2), respectively. All fractions were then dried under a gentle stream of N_2.

4.2.4.3. Biomarker Analysis

Biomarker distributions in the aliphatic, aromatic and polar fractions were analysed using a Thermo Scientific^{TM} ISQ Series Single Quadruple gas chromatography mass spectrometry (GC-MS) system. Separation of compounds was performed on a Zebron non-polar column (50 m x 0.32 mm, 0.10 µm film thickness). The injection volume was 1 µl. The GC programme was injection at 70 °C (1 min hold), heating to 130°C at a rate of 20°C/min, then to 300 °C at 4 °C/min, followed by a 24 min hold. The mass spectrometer continuously scanned between *m/z* 50 and 650. Identification of biomarkers was carried out based on published retention times and spectra as well as comparison with standard samples.

The distribution GDGTs (Glycerol Dialkyl Glycerol Tetraethers) in the polar fraction was determined using a High Pressure Liquid Chromatography-atmospheric pressure chemical ionisation-Mass Spectrometry (HPLC-APCI-MS) with a ThermoFisher Scientific Accela Quantum Access triple quadrupole MS in selected ion monitoring mode. Normal phase separation achieved with two HPLC BEH HILIC columns (2.1 mm x 150 mm, 1.7 µm i.d) at a flow rate of 0.2 ml/min. The initial solvent hexane:iso-propanol (IPA) (98.2:1.8) eluted isocratically for 25 min, followed by an increase in solvent polarity to 3.5% IPA in 25 min, and then by a sharp increase to 10% IPA in 30 min (Hopmans et al., 2016). After separation,

isoprenoid and branched GDGTs were analysed using Selection Ion Monitoring (SIM) at *m*/*z*: 1302, 1300, 1298, 1296, 1294, 1292, 1050, 1048, 1046, 1036, 1034, 1032, 1022, 1020, 1018, 744, 653 to increase the sensitivity and reproducibility. Distribution of GDGTs was analysed in the respective molecular ion (M^+) chromatograms.

4.3. Results

4.3.1. Elemental Analysis

TOC contents at Site 364 vary significantly (Fig. 4.1), from less than 1 wt.% up to 40 wt.%. Highest TOC contents occur in Unit 7b, which displays regularly paced variations between organic lean carbonates with around 1 wt.% TOC and sapropelic black shales with up to 40 wt.% TOC (discussed in chapter 3). Unit 7a is characterized by similar cyclic variations, but with a lower maximum TOC content up to 11 wt.%. Unit 6 consists predominately of carbonates with maximum TOC contents of 1-3 wt.%. TOC in Unit 5 varies from less than 1 wt.% in carbonates to 32 wt.% occurring in sapropelic black shales. Elemental sulfur contents show similar variations as TOC contents, with the maximum values of 11 wt.% and 5 wt.% occurring in black shale horizons of Unit 7b and 5, respectively; and lowest values (<1 wt.%) in Units 7a and 6. Although T_{max} values vary depending of their host rock (carbonates and black shales; Behrooz et al., 2018), generally remain < 420 °C at Site 364 and does not show any changes between the studied Units.

4.3.2. TOC Stable Carbon Isotopes

Bulk $\delta^{13}C_{org}$ values vary between -28 and -24 ‰ across Unit 7b (Cores 45–42) (Fig. 4.1). There is no variation with lithology, but the $\delta^{13}C_{org}$ record does exhibit a 2 ‰ positive excursion in Sections 2 and 3 of Core 43 at around 1035 mbsf (Fig. 4.1). $\delta^{13}C_{org}$ values in the upper parts of the section (Unit 7a, 6 and 5) are stable, but values are lower than those of Unit 7b with values between -26 and -24‰. In Unit 5 $\delta^{13}C_{org}$ record exhibits a 2 ‰ negative excursion in Cores 23 to 25 with the most depleted $\delta^{13}C_{org}$ values (-28 ‰) in Core 24.

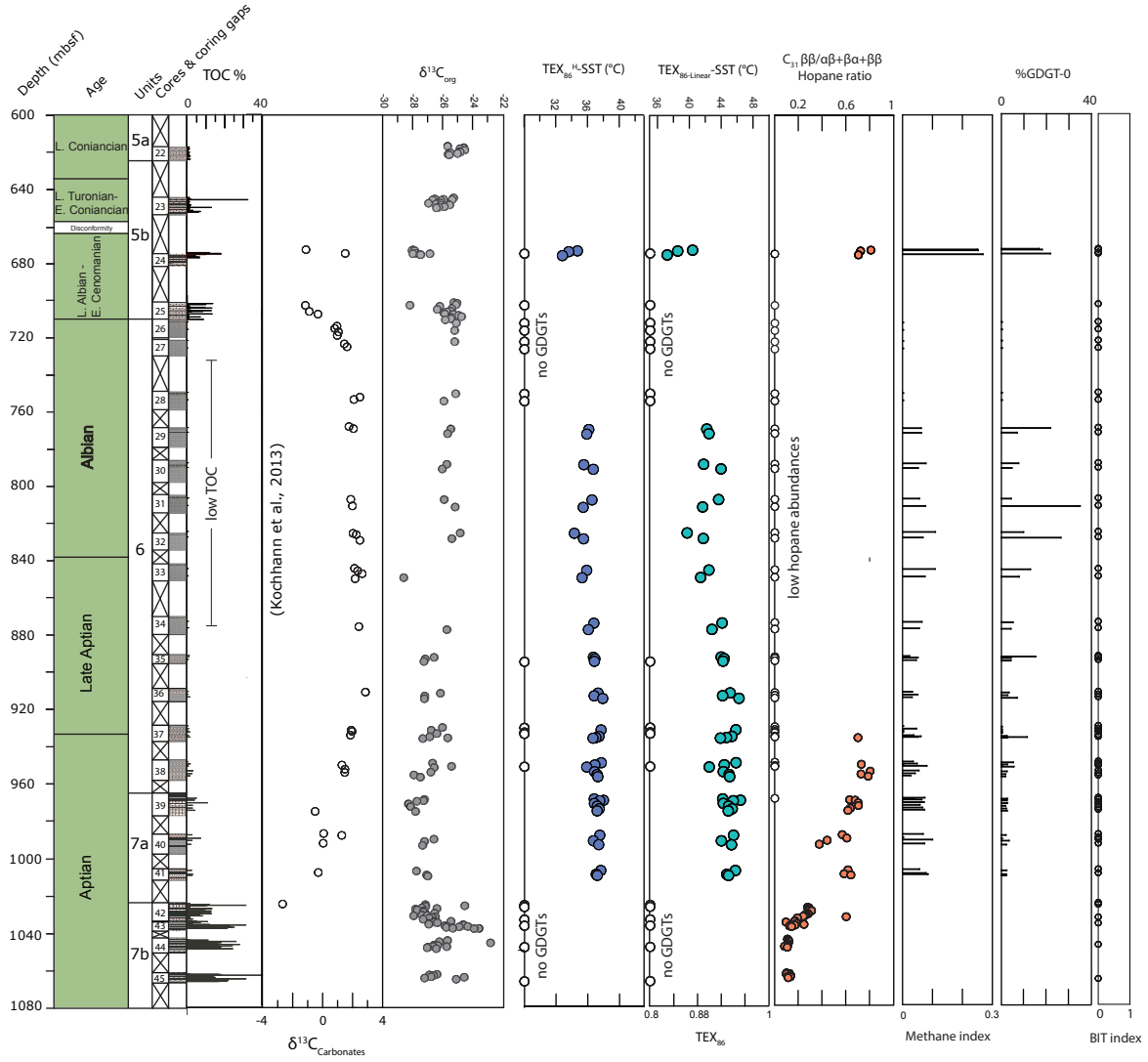

Figure 4.1. Lithology (Leg 40 Shipboard Scientific Party, 1978), total organic carbon (TOC) content, bulk δ^{13}_{org}, sea surface temperature, hopane maturity ratio across Units 7b, 7a, 6, and Unit 5 (1070-610 mbsf) for DSDP Site 364. Note the presence of multiple core gaps.

4.3.3. Distribution of Hopane

The aliphatic hydrocarbon fractions of Unit 7b (broadly discussed in chapter 3), 7a, 6 and 5 contain a wide range of *n*-alkanes, isoprenoids (pristane and phytane), steranes and hopanes.

Of interest of this project is the hopanes distribution. The C_{31} hopane maturity index (C_{31} $\frac{\beta\beta}{\beta\beta+\beta\alpha+\alpha\beta}$) in Units 5,6 and 7a is approximately 0.6, but values are much lower (~0.2) in Unit 7b (Figure *4.2*). Most samples from Unit 6, characterized by low TOC content, do not contain measurable amounts of hopanes. The low abundance of hopanes prevented us from measuring the hopane distribution in this part of the section.

4.3.4. Distribution of GDGTs

The polar fractions of Units 7a, 6 and 5 contain marine isoprenoid GDGTs, but branched GDGTs are not measurable. Isoprenoid GDGTs are dominated by crenarchaeol and crenarchaeol regioisomer. Unit 7b samples did not show any measurable signals of GDGTs. The GDGT distribution can also be influenced by sedimentary methanogenic (Koga et al., 1993; Weijers et al., 2006) and methanotrophic archaea (Pancost et al., 2001; Wakeham et al., 2003). To evaluate these aspects, the following GDGT indices were used %GDGT-0 (Sinninghe Damsté et al., 2012) and the Methane Index (MI) (Zhang et al., 2011):

$$\%\text{GDGT-0} = \left(\frac{\text{GDGT}-0}{\text{GDGT}-0+\text{Cren}}\right)\times 100$$

$$\text{MI} = \frac{\text{GDGT}-1 + \text{GDGT}-2 + \text{GDGT}-3}{\text{GDGT}-1 + \text{GDGT}-2 + \text{GDGT}-3+\text{Cren}'}$$

%GDGT-0 varies between 2-20, with the mean value of 7. MI values are generally about 0.07, ranging between 0.02-0.25.

To reconstruct SST, the TEX_{86} and the TEX_{86}^{H} (Kim et al., 2010) and $TEX_{86\text{-linear}}$ calibrations (O'Brien et al., 2017) are used.

$$TEX_{86} = \frac{(\text{GDGT}-2)+(\text{GDGT}-3)+(\text{Cren.}')}{(\text{GDGT}-1)+(\text{GDGT}-2)+(\text{GDGT}-3)+(\text{Cren.}')}$$

TEX_{86} values are ~0.95 in Unit 7a, ~0.93 in Unit 6, and ~0.85 in Unit 5. TEX_{86}^{H}-SST vary between 37-32 ± 2.5°C, expressing a decreasing trend towards younger sediments (Fig. 4.1). $TEX_{86\text{–linear}}$-SST values are higher; ranging from 45-38 ± 2.0 °C and the degree of cooling is amplified compared to that using TEX_{86}^{H}.

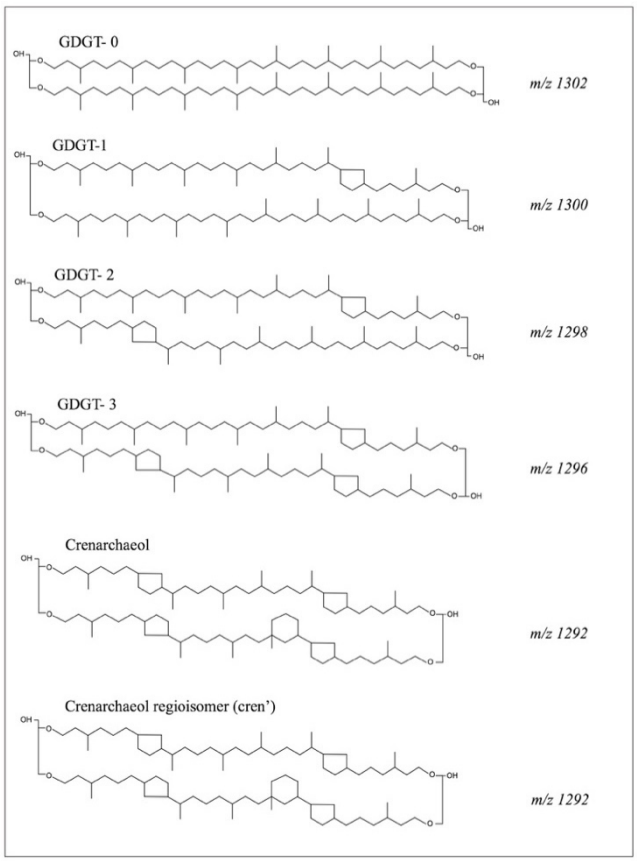

Figure 4.2. Schematic molecule structures of isoprenoidal glycerol dialkyl glycerol tetraethers (GDGTs) used to calculate TEX_{86} and related indices and their $[M+H^+]$ ion.

4.4. Discussion

4.4.1. Is the GDGT distribution reliable?

Although T_{max} values are in the same range in all the studied Units, the C_{31} hopane ratio varies. Particularly, the C_{31} hopane ratio is lower (~0.2) in Unit 7b and indicates thermal alternation of the biological stereochemistry of the hopane stereoisomers. The mechanism causing the rapid decline in C_{31} hopane ratio in Unit 7b is currently not known. However, as GDGTs are sensitive to thermal maturity, and degrade when biomarker parameters indicate high levels of thermal maturities (Schouten et al., 2004), the absence of GDGTs in Unit 7b could be due to thermal alternation. However, if distribution of GDGTs is thermally altered, then the domination of GDGT0 is expected (Schouten et al., 2013, 2004). As discussed in Naafs and Pancost, (2014), the low abundance (or absence in the samples discussed in this paper) of

GDGT0 in Unit 7b does not support the domination of thermal maturity as the controlling factor on GDGTs distribution.

The higher values (~0.6) of the C_{31} hopane ratio in Units 5, 6 and 7a, express the biologically inherited stereochemistry in a significant portion of the hopanes stereoisomers, indicating a lower thermal maturity. The presence of isoprenoid GDGTs in these units allow us to calculate TEX_{86}. Considerable work suggests that distribution of GDGTs is influenced by non-thermal sedimentary factors, e.g. input of soil derived GDGTs (Weijers et al., 2006), sedimentary methanogenesis (Koga et al., 1993; Weijers et al., 2006) and methanotrophic archaea (Pancost et al., 2001; Wakeham et al., 2003). The absence of branched GDGTs in Units 7a, 6 and 5, i.e. BIT=0; suggest a low input of soil derived GDGTs. Methanogenic archaea can syntheses isoprenoid GDGTs, i.e. GDGT-0 and smaller quantities of GDGT-1 and GDGT-2 and GDGT-3 (Koga et al., 1993; Weijers et al., 2006). The %GDGT-0 index (4.3.4; Sinninghe Damsté et al., 2012), is used to evaluate the contribution of methanogenesis derived GDGT-0. In our samples the %GDGT-0 index stays <20. If the %GDGT-0 index is >67 then lacustrine TEX_{86} values are considered to be biased by large contribution of methanogenesis derived GDGTs (Blaga et al., 2009; Sinninghe Damsté et al., 2012). Although a specific threshold is not yet available for marine sediments, considering the low %GDGT-0 index (<20) in the entire studied section, it seems unlikely that the GDGT distribution is biased by input from methanogenic archaea. To elucidate the input of methanotrophic archaea, the Methane Index (MI) is applied (Zhang et al., 2011). MI values stay below the threshold (<0.3) in the entire sedimentary section, suggesting normal sedimentary conditions. Ecological difference is another potential factor to bias TEX_{86}, e.g. a systematic offset in TEX_{86} values between interbedded lithologies (Littler et al., 2014). However, we do not observe such regularity between carbonates and black shales of Unit 7a. Altogether, we therefore consider the distribution of GDGTs reliable for calculation of TEX_{86} and SST in the entire studied section.

4.4.2. Calibration of TEX_{86} to sea surface temperature (SST)

The TEX_{86} values observed at Site 364 are significantly higher than observed in recent marine sediments (Kim et al., 2010), confirming that SST during the Early Cretaceous was notably higher than modern. The TEX_{86} values of ~0.9 from Aptian to late Albian are consistent with the previously reported high TEX_{86} values of a similar age (reviewed by O'Brien et al., 2017) in the low latitudes (30°N–30°S), i.e. Aptian records of TEX_{86} ~0.82 at DSDP 463 (17.2°S; Schouten et al., 2003), TEX_{86} ~0.8 at DSDP 545 (25.8°N; McAnena et al., 2013), TEX_{86} ~0.9

in ODP 1207 (2.6°S, Dumitrescu and Brassell, 2006) and the Albian record of TEX_{86} ~0.88 at Demerara Rise (8.2°N; Forster, 2007), all supporting the high (sub)tropical sea surface temperatures, Figure *4.3*. Although the Aptian records of TEX_{86} at Cismon core (24.7°N; Bottini et al., 2015) shows lower values of ~0.65, these sediments are likely biased by thermal degradation of GDGTs.

Regardless of the choice of calibration method, application of TEX_{86}-SST calibration to high TEX_{86} values (>0.8, as here) requires extrapolations above the upper limit of modern core top data set, i.e. TEX_{86} <0.72 (Kim et al., 2010; Tierney and Tingley, 2015). The difference between these two calibrations (TEX_{86}^{H} and $TEX_{86\text{-linear}}$) emerges from the logarithmic versus the linear approach differences. When TEX_{86} >0.7, the logarithmic SST calibration (TEX_{86}^{H}-SST) yields smaller differences as TEX_{86} increases, causing lower SSTs compared to $TEX_{86\text{–linear}}$.

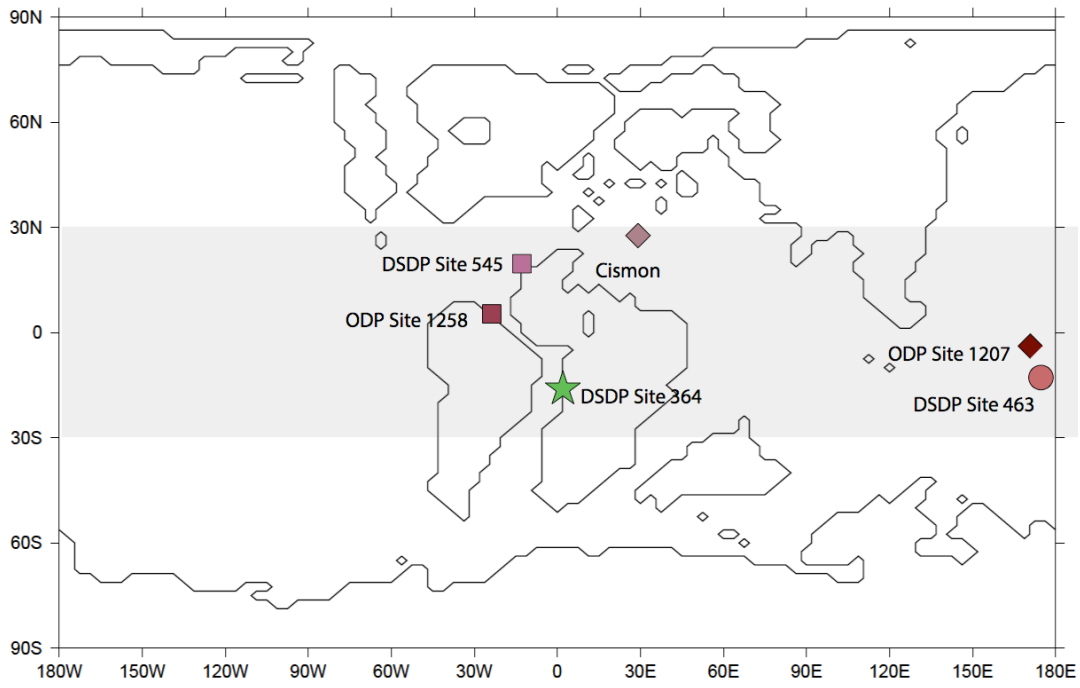

Figure 4.3. The Early Cretaceous (Albian) map (Lunt et al., 2016) highlighting the schematic paleo-location of the DSDP and ODP Sites (<±30°) discussed in this chapter. i.e. DSDP 364 (~25°S), ODP Site 1207 (~2.6°S, Dumitrescu and Brassell, 2006), DSDP Site 463 (~17.2°S, Forster et al., 2007b; Schouten et al., 2003), Cismon (~24°N, Bottini et al., 2015), DSDP Site 545 (~25.8°N, Hofmann et al., 2008; McAnena et al., 2013; Wagner et al., 2008), ODP Site 1258 (~8.2°N, Forster et al., 2007a).

4.4.3. Evolution of SST during the Aptian-upper Albian

Irrespective of the calibration method, SSTs in Unit 7 (TEX_{86}^{H}-SST ~37±2.5°C, $TEX_{86-linear}$-SST ~45±2.0°C) and in Unit 6 (TEX_{86}^{H}-SST ~36.5±2.5°C and $TEX_{86-linear}$-SST ~44.7±2.0°C) are significantly higher than modern (max. 30°C). Extremely high SSTs of >35°C have also been recorded elsewhere at low latitudes (<±30°) during the early Aptian (Schouten et al., 2003; Forster et al., 2007a). On the contrary, the Aptian–Albian (~20 Myr) record of TEX from Site 545 at Mazagan Plateau, ~25 °N (McAnena et al., 2013) indicate lower SSTs in the subtropics during the Aptian (TEX_{86}^{H}-SST ~30±2.5°C, $TEX_{86-linear}$-SST ~32.8±2.0°C) and Albian (TEX_{86}^{H}-SST ~30.7±2.5°C, $TEX_{86-linear}$-SST ~34±2.0°C) (Figure *4.4*). However TEX_{86} values at Site 545 might have been influenced by local factors, i.e. upwelling (e.g. Hofmann et al., 2008; Wagner et al., 2008). Evidences such as the abundance of steryl alkyl ethers (Schouten et al., 2005; Wagner et al., 2008), distribution of HI and type of kerogen (Wagner et al., 2013), alongside with the enhanced accumulation of siliceous skeletons and a sharp increase in the abundance of benthic foraminifera simultaneously with a decrease in planktonic foraminifera diversity (Leckie, 1984), all acknowledge the existence of an upwelling system at Site 545 during the latest Aptian to middle Albian. Therefore, TEX_{86} values from Site 545 might not be well representative for the sea surface temperature of the subtropical regions during the Early Cretaceous.

The TEX_{86}-SST values at Site 364 during the Aptian in the South Atlantic suggest quite stable subtropical SSTs for almost ~10 Myr (Figure *4.2*). This bears a resemblance to the ~13 Myr steady record of subtropical SST during the Valanginian–Hauterivian at Site 534, proto-North Atlantic (Littler et al., 2011), and may indicates the resistance of the (sub)tropical climate to transient changes. These stable SSTs were interrupted by a decrease (~2 °C) from late Aptian (Core 34) to Albian (Core 30), occurring simultaneously with a positive carbon isotope excursion (CIE ~+1.5 ‰) as $\delta^{13}C_{org}$ values increase from ~–27 ‰ in the late Aptian to ~–25.5 ‰ during the Albian. This might be related to the late Aptian cold snap that has been also reported elsewhere (Clarke and Jenkyns, 1999; Fassell and Bralower, 1999; Herrle, 2006; Kemper, 1987; Mutterlose et al., 2009; Pirrie et al., 2004), e.g. TEX_{86}-based SST and $\delta^{18}O$ records from the North Atlantic Site 545 (McAnena et al., 2013; Mutterlose et al., 2009), and $\delta^{18}O$ records at the Tethyan Ocean (ODP Sites 766, 511 and 693A, Vocontian Basin, Vöhrum section in North Germany, BGS Borehole 81/40 in the North Sea Basin) (Mutterlose et al., 2009). McAnena et al. (2013) argued that the development and termination of the late Aptian

cold snap were caused by a combination of volcanism and tectonically induced changes in the rate of carbon burial. Taking the TOC values prior (~1%) and after (~0.1%) the Core 34 (Figure *4.2*) into account, the cooling event and the positive carbon isotope excursion, are likely promoted as the consequence of CO_2 sequestration following the pronounced burial of organic matter during the Aptian to late Aptian. Following the carbon burial, and the consequent atmospheric *p*CO2 reduction, promoting SST cooling.

GDGTs are absent in Cores 28 to 25 and this causes a disconnectivity in the TEX_{86} record, however TEX_{86}-SST records from Aptian (Unit 7a) to the late Albian–Cenomanian (Unit 5) express a cooling trend towards late Albian–Cenomanian (Figure *4.2*). This implies that the South Atlantic experienced a colder climate during the late Albian–Cenomanian relative to the Aptian–mid Albian. During the late Albian–Cenomanian (Core 24, Unit 5), TEX_{86}^{H}-SST was at ~33.5 ± 2.5°C and $TEX_{86-linear}$-SST at ~38.5 ± 2.0°C. This is comparable to the late Albian–Cenomanian records of SST in Demerara Rise (ODP 1258, 8.2°N), i.e. TEX_{86}^{H}-SST was at ~34.6 ±2.5°C and $TEX_{86-linear}$-SST at ~40.2±2.0°C (Forster et al., 2007a). The absence of TEX data from before and after the low SST values in Core 24, makes it problematic for an accurate interpretation in Site 364. However, assuming that a cooling trend is recorded during the mid–late Albian, it bears a resemblance to the cooling trend at the late Albian recorded at Demerara Rise (Site 1258) (Forster et al., 2007).

We suggest a few scenarios that could explain the colder SSTs from Unit 5. A) the cooling at Unit 5 might be derived from changes in local factors, which cause the late Albian–Cenomanian SST to be colder comparing to mid Albian, e.g. local changes in the geomorphology of the basin, causes changes in the local oceanography condition. In line with that is the opening history of the northern South Atlantic basin where Site 364 is located. The South Atlantic rifting process initiated in late Jurassic (Dean et al., 1984). Although the deep ocean connectivity did not developed until late Cretaceous (Pérez-Díaz and Eagles, 2017), surface water connectivity with the open ocean developed earlier in the late Aptian to the North Atlantic (Kochhann et al., 2013) and in the late Albian through the Walvis Ridge (Kennedy and Cooper, 1975; Reyment and Tait, 1972). Although this scenario might be unlikely, the cooccurrence of sea surface connection to the high latitudes of the South Atlantic and the low SST values at Site 5 are considerable. B) The next scenario is based on the fact that the record of low SST at Unit 5 is associated with an organic carbon isotope negative excursion (

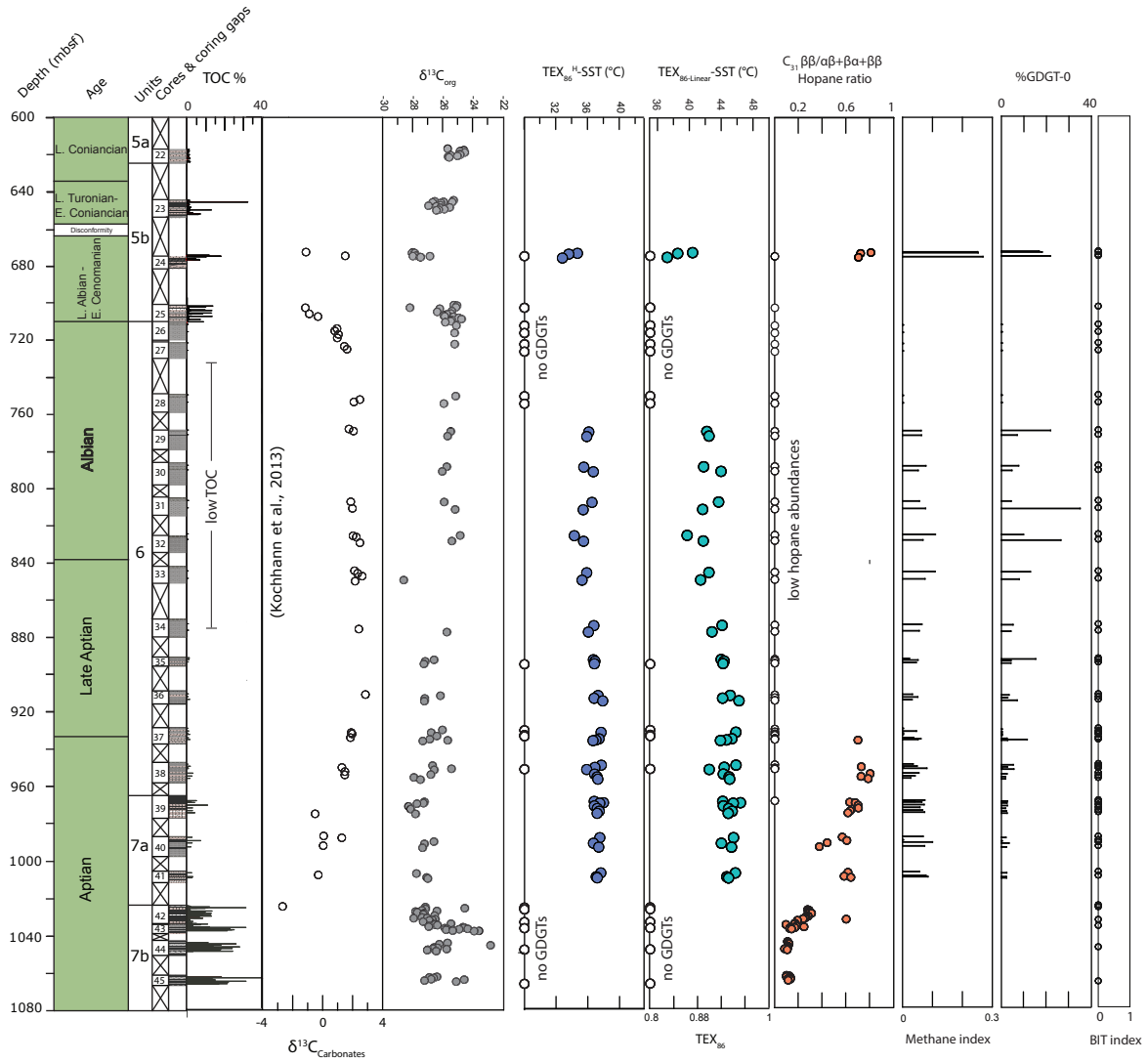

Figure 4.1) and high preservation of OM (TOC> ~20 wt.%;

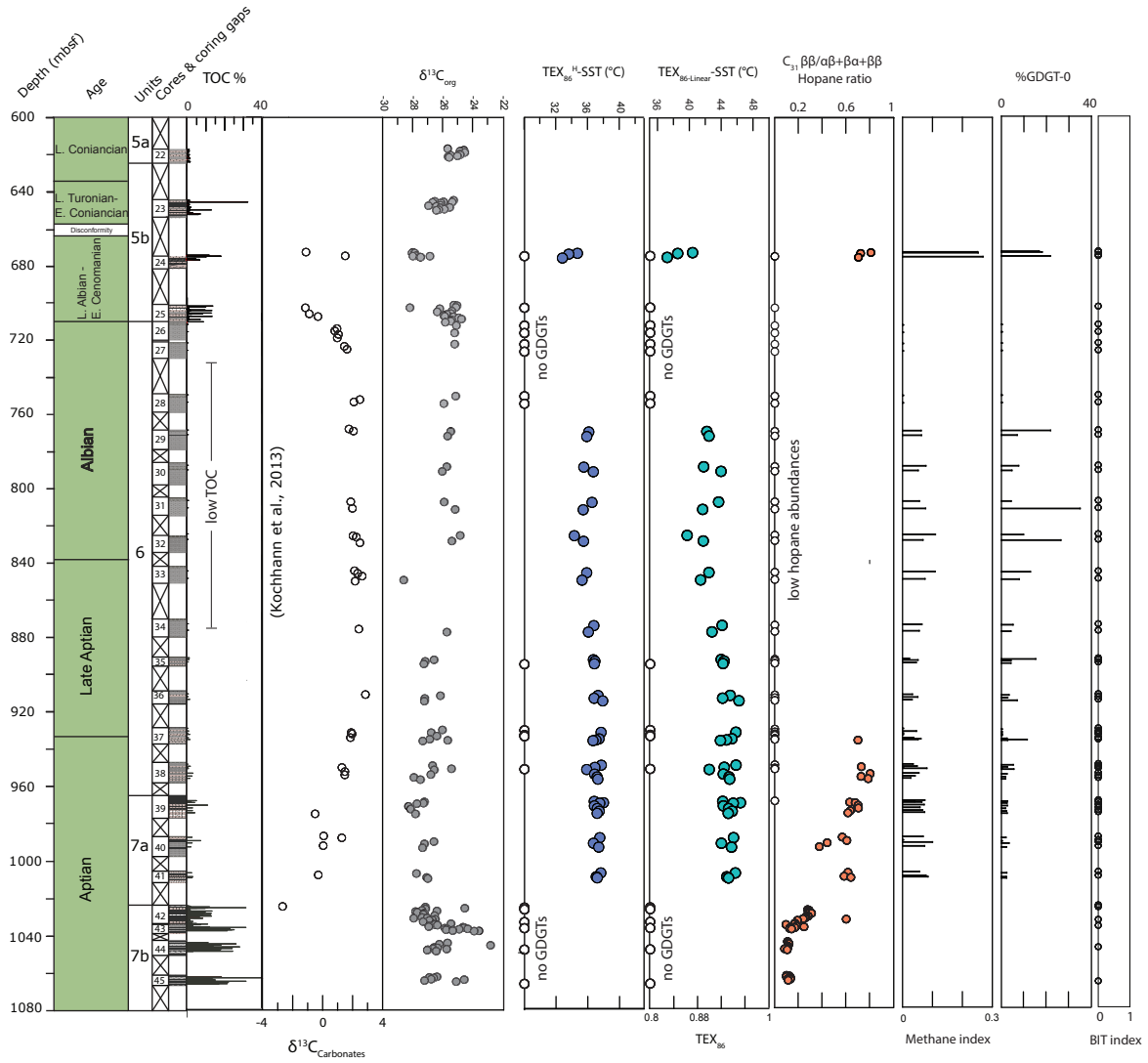

Figure 4.1). This negative CIE is recorded simultaneously in the carbon isotope records of carbonates at DSDP 364 (Kochhann et al., 2013). Considering the age of sediments, the recorded CIE could be attributed to the short negative excursion prior to the OAE 1d positive excursion (e.g. Bornemann et al., 2005; Wilson and Norris, 2001; discussed below in 4.4.4). However, if we consider this scenario, then the low SST record would be in conflict with the occurrence of the negative excursion. Similarly, Wilson and Norris, (2001) report a decrease of sea surface temperature associated with the OAE 1d negative excursion prior to the development of black shale at Site 1052 (western N Atlantic). Since the decrease of sea surface temperature at Site 1052 is associated with an increase in thermocline temperature, the low record of SST is suggested to be related to hydrography and reduced stratification in the basin (Wilson and Norris, 2001). However, there is no evidence of thermocline temperature or hydrography changes at Site 364. Alternatively, the low SST values at Unit 5 might be caused

by a potential cooling episode during the OAE 1d. The transient cooling episodes have been recorded during the OAE 1a and OAE 2 (Jenkyns, 2018) and might be a potential explanation for the record low SST values during OAE 1d.

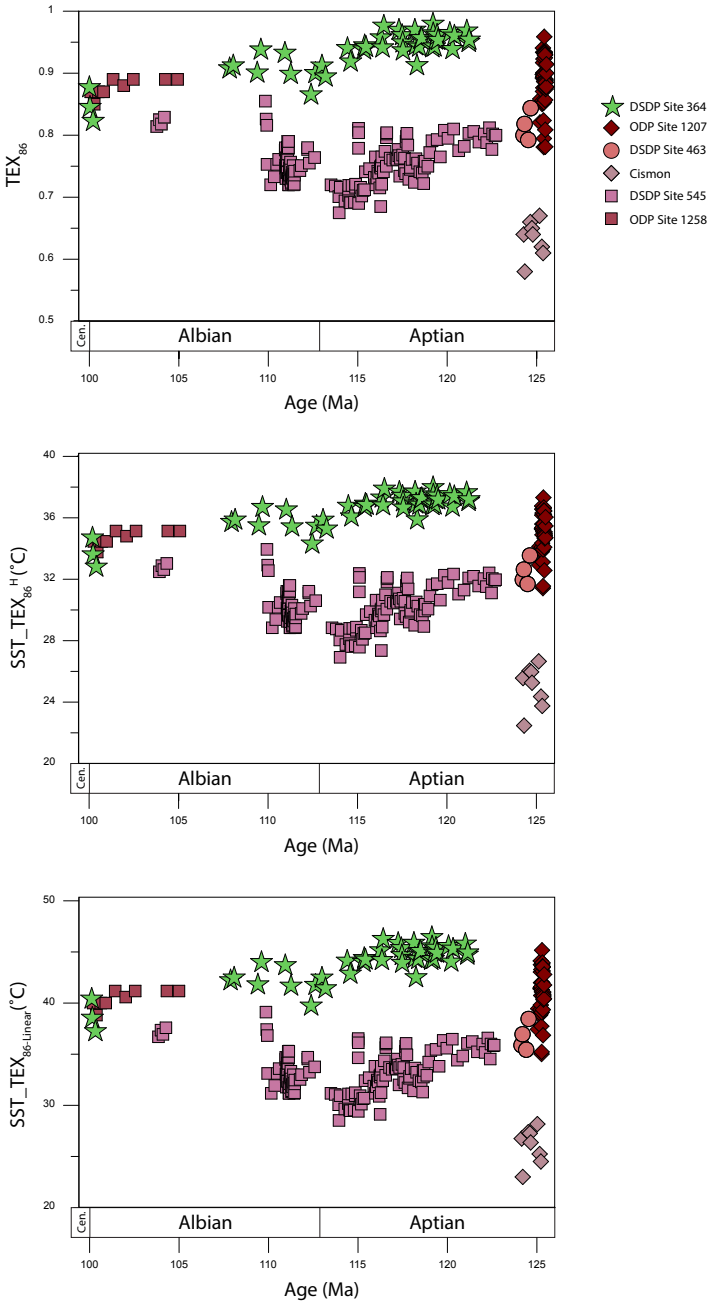

Figure 4.4. TEX_{86}-SST reconstruction during Aptian-Albian, in Site 364 and compiled data from low latitudes (>± 30°, reviewed in (O'Brien et al., 2017), i.e. ODP Site 1207 (Dumitrescu and Brassell, 2006), DSDP Site 463 (Forster et al., 2007b; Schouten et al., 2003), Cismon

(Bottini et al., 2015), DSDP Site 545 (Hofmann et al., 2008; McAnena et al., 2013; Wagner et al., 2008), ODP Site 1258 (Forster et al., 2007a).

4.4.4. Perturbations in the carbon cycle during Aptian-Coniancian

As discussed in Behrooz et al (2018) (chapter 3) the positive excursion of OAE 1a ~120 Myr (~+2‰,

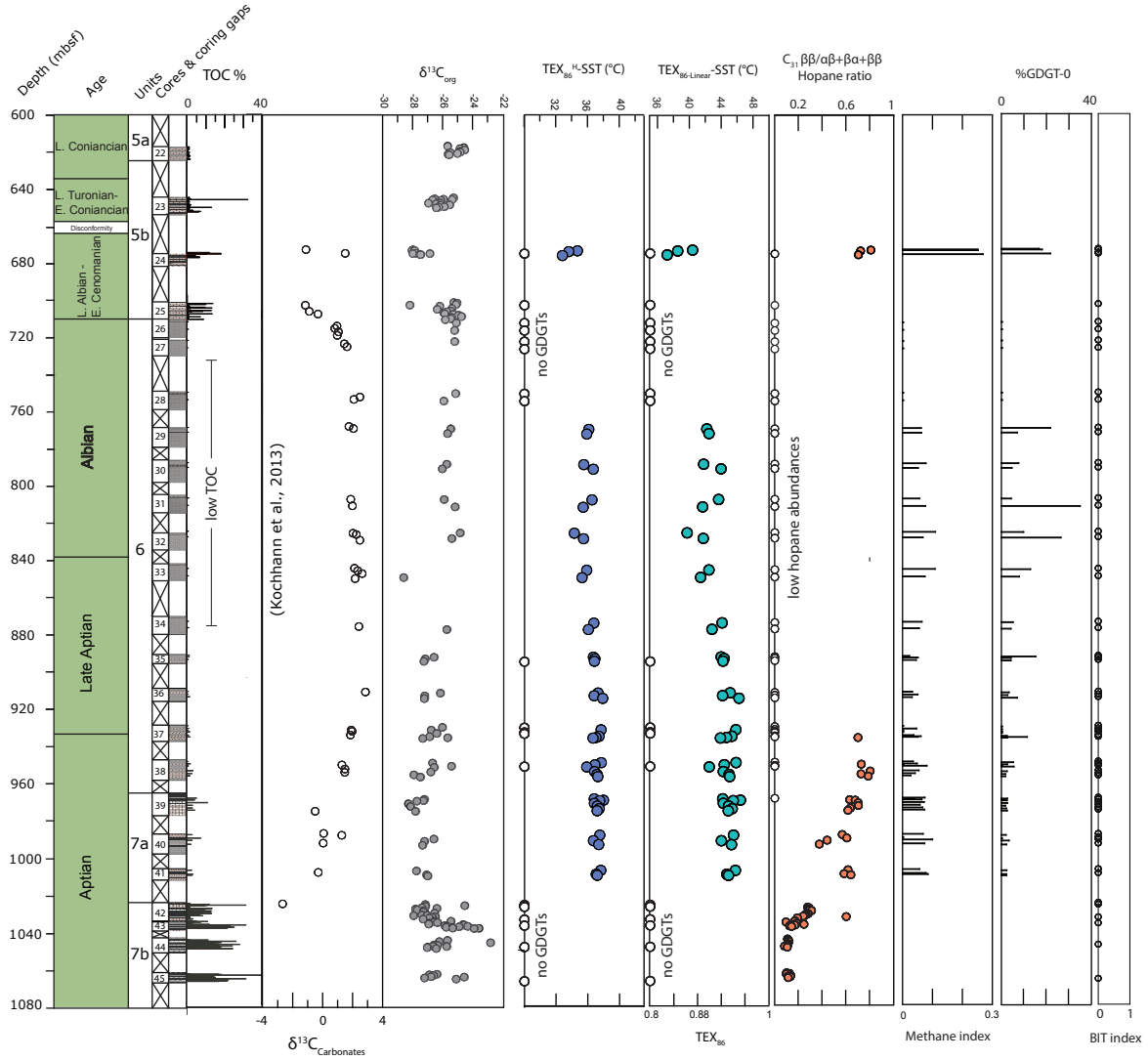

Figure 4.1, Menegatti et al., 1998) was recognised in Unit 7b (Cores 44 and 43). OAE 1a is characterized by a brief negative and subsequent prolonged positive carbon isotope excursion (Menegatti et al., 1998). The positive carbon isotope excursion at Site 364 occurs directly

above a ~13 m long coring gap, and therefore the negative carbon isotope excursion that is characteristic for the onset of OAE 1a is not recovered here. As such, the sediments recovered in Cores 44 and 43 only represent the later stages of OAE 1a.

At the beginning of Unit 5 (late Albian-Early Cenomanian, i.e. Cores 25 and 24), $\delta^{13}C_{org}$ (also $\delta^{13}C_{carbonate}$ in Kochhann et al., 2013) indicate a major negative carbon isotope excursion (~ –3‰) in the basin. Considering the age of Unit 5, this excursion could be caused by latest Albian "Breistroffer event", i.e. OAE 1d (e.g. Robinson et al., 2008; Wilson and Norris, 2001). OAE 1d is associated with the positive carbon excursion which is succeeding a short-term negative excursion (e.g. Bornemann et al., 2005; Wilson and Norris, 2001). Although the positive OAE 1d excursion here is not recovered at Site 364, due to the coring gap between the Cores 23 and 24 (~13 m,

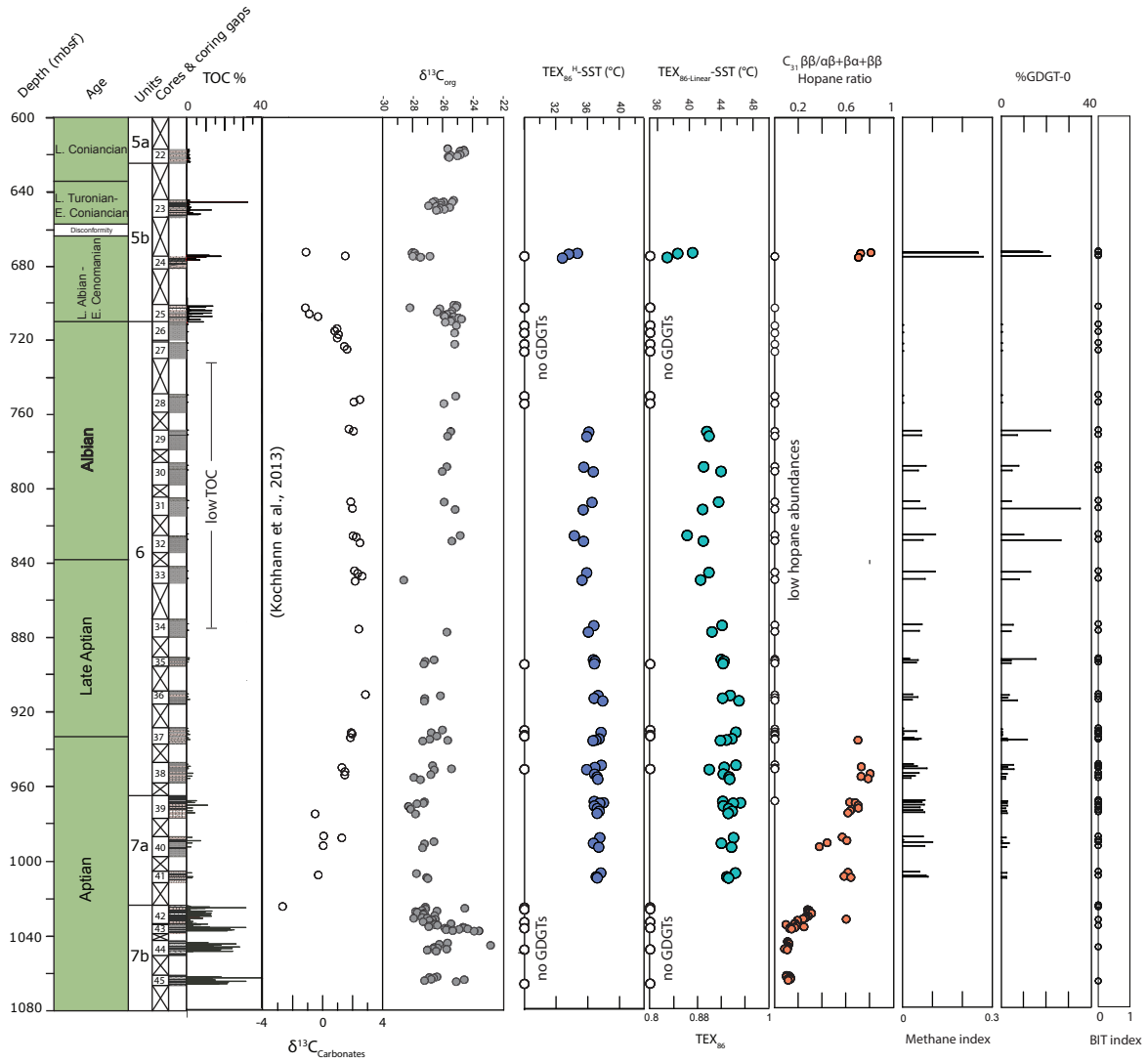

Figure 4.1). The occurrence of OAE 1d in the Atlantic Ocean has been previously reported, e.g. at ODP Site 1052 in the North Atlantic (Wilson and Norris, 2001). The OAE 1d negative excursion in Unit 5 is also associated with an increase in the preserved organic carbon (TOC <~20 wt.%). The high OM burial accompanied OAE 1d is usually represented by several black shale horizons, e.g. in the Niveau Breistroffer (SE France; Bornemann et al., 2005) and in the Monte Petrano (Italy, Giorgioni et al., 2015), such as appear in the cyclic nature of black shales at Cores 23 and 24. Wilson and Norris, (2001) have also attributed the occurance of Unit 5 black shales at Site 364 to OAE 1d.

However, in the general model for the development of anoxia during the OAEs a combination of warming, increased sedimentation rates, nutrient inputs and increased algal productivity, are invoked as the causes of anoxia and its consequent OM preservation (black shales) in the preconditioned basins. This model suggests an increase of pCO_2 and tempratue in atmosphere-ocean system (SST), as triggering factors to the accelerated hydrological cycle, increased flux of nutrient to the ocean, intensified of upwelling and enhanced marine productivity (Jenkyns, 2010). Nevertheles there is no evidence of increased sea surface temprature during the presumed OAE 1d at Site 364, this contradict is explained in the previous section (4.4.3). The low SST at Unit 5 might be derived from a prospective long-term cooling trend at Unit 5, (

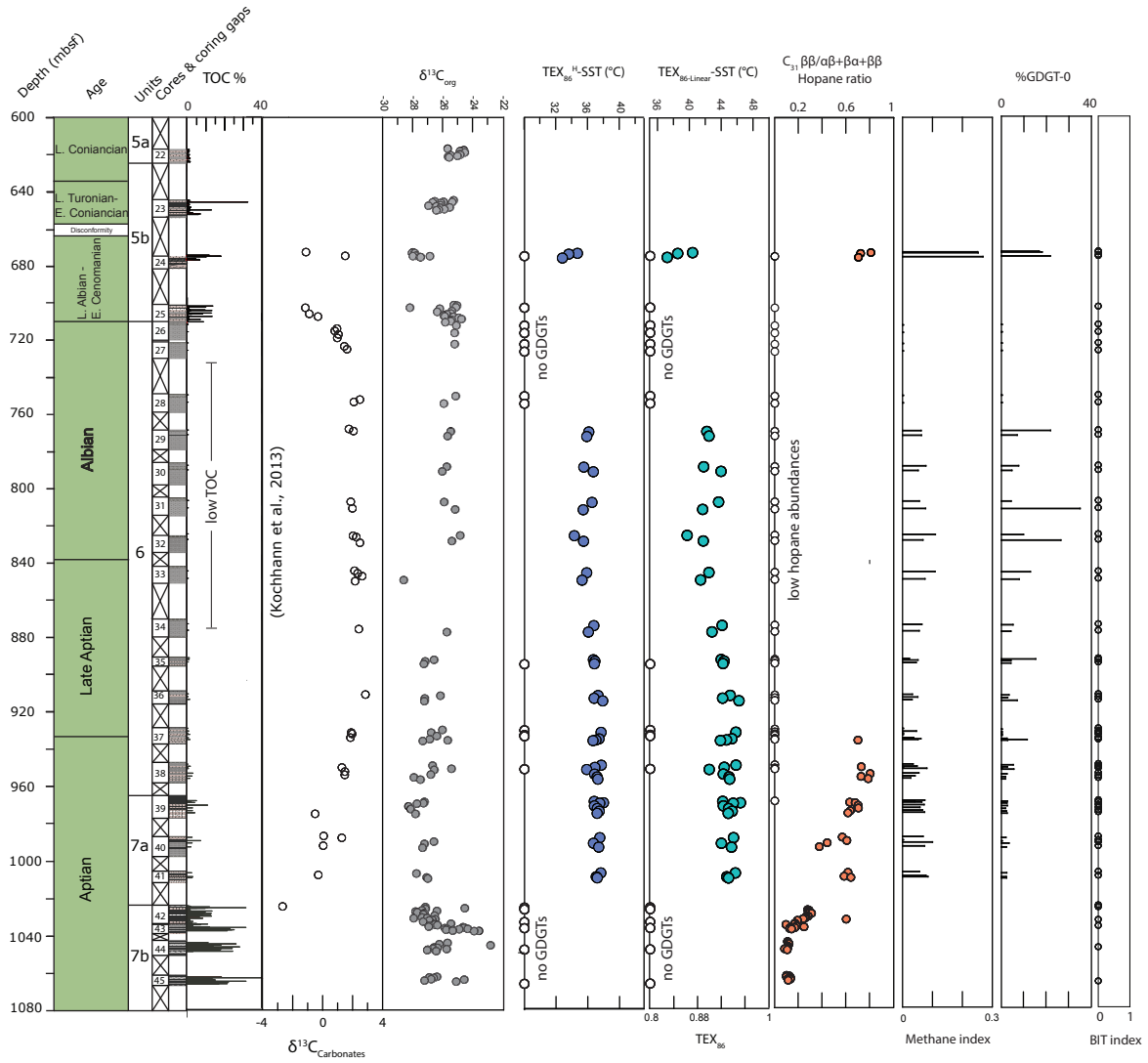

Figure 4.1), although the disconnectivity in SST record from mid–late Albian at Site 364 is problematic and does not allow to reconstruct it.

4.4.5. Comparison to climate models

The GDGT record at Site 364 is mainly covering Aptian–Albian intervals (To the best of our knowledge, the current published SST models do not cover Aptian–Albian sections). However according to the published records and models, a decreasing SST trend towards the late Cenomanian (before OAE2) is expected (Barral et al., 2017; Bice et al., 2006; Forster et al., 2007; Martin et al., 2014; O'Brien et al., 2017). For instance, TEX_{86} records (Forster et al., 2007) from ODP Sites 1258 and 1259 and Mg/Ca and $\delta^{18}O$ proxies from Site 1257 (Bice et al., 2006) at Demerara Rise (North Atlantic) demonstrate a decreasing temperature trend before

OAE2, with the minimum temperature occurring in the mid to late Cenomanian. OAE 2 and so that the maximum temperature during the Cenomanian–Turonian is not recorded at Site 364 (Leg 40 Shipboard Scientific Party, 1978). However the Earth system multi-proxy model zonal mean SSTs (Tabor et al., 2016) demonstrates the cooling trend after the Cenomanian-Turonian OAE towards the Late Cretaceous, as also recorded in TEX_{86} values at the tropical Atlantic (Demerara Rise, Forster et al., 2007) and Southern Tethyan (Alsenz et al., 2013).

4.5. Conclusions

The long-term records of TEX_{86} from DSDP Site 364 (Units 7a to 5) allow reconstruction of SST in the northern South Atlantic during the Aptian–Albian, alongside with the long term (Aptian–Coniancian) records of carbon cycle expressed by $\delta^{13}C_{org}$. The presented SST record once again confirms that the Early Cretaceous SST was significantly higher than modern ocean. The stability of SST values during the Aptian indicates the resistance of tropical climate to transient changes for about ~10 Myr. The cooler SST values at late Albian–Cenomanian (although associated with OAE 1d) could be as a result of either local changes in the geomorphology of the basin, a potential cooling episode during OAE 1d as invoked for OAE 1a and OAE 2 (Jenkyns, 2018) or reduced stratification as invoked for the OAE 1d at Site 1052 (Wilson and Norris, 2001). Evidence of Cretaceous oceanic anoxic events, i.e. OAE 1a and OAE 1d are recognised in the South Atlantic.

Chapter 5

Photic zone euxinia and N cycle during the PETM

Preface

This chapter is under preparation and modification for submission as a research article to *Nature Geoscience.* The lead author of the paper is LB. LB carried out analysis (unless stated), interpreted the organic geochemical data set and wrote the chapter. RP and DN made comments and suggestions on the initial draft made by LB. Total lipid extraction, GC-MS and LC-MS analyses of Kheu River PETM sediments were performed by K. Taylor and R. Rees-Owen (as published in (Dickson et al., 2014b)), although the identification and integration of anoxia biomarkers were performed by LB. Total lipid extraction and GC-MS analysis of Zumaia were mainly performed by A. Ralph (project student, supervised by LB). Sediment samples are provided by collaborators; i.e. northern Peri-Tethys sediments by A. Dickson (Royal Holloway University of London), Dababiya samples by H. Khozyem (Aswan University, Egypt), Zumaia samples by H.R. Manners (National Oceanography Centre, UK) and S.T. Grimes (University of Plymouth, UK). $\delta^{15}N_{bulk}$ and $\delta^{15}N_{Porphyrin}$ analyses were carried on lipid fractions prepared by LB by Prof. A. Pearson's lab (Harvard University).

Abstract

Despite some similarities that the Paleocene–Eocene Thermal Maximum (PETM) shares with the Oceanic Anoxic Events (OAEs) of the Mesozoic, the extent and persistence of anoxia, and especially photic zone euxinia, during the PETM is still not well constrained. Moreover, although a negative bulk stable nitrogen isotope ($\delta^{15}N_{bulk}$) excursion has been reported for the PETM, the dynamics of the PETM nitrogen cycle are still poorly understood. Here, we analyse a range of biomarkers in sediments from the margins of the northern Peri-Tethys (Central Asia: Guru-Fatima, Kheu River, and Dzhengutay) and North Atlantic (northern Spain: Zumaia section) that span the PETM. We focus on biomarkers that are indicators of past redox change and especially the presence/absence of green sulfur bacterial biomarkers. Collectively, these data, combined with previously published records, indicate an expansion of anoxia and photic

zone euxinia during the PETM, but only in restricted marginal and epicontinental basins that amplified nutrient trapping and not in open marginal settings. One of the consequences of an expansion of marine anoxia is an increase in denitrification, perturbating the marine nitrogen cycle. To explore this further, we measured $\delta^{15}N_{Porphyrin}$ and $\delta^{15}N_{bulk}$ values in the Dzhengutay sediments and $\delta^{15}N_{Porphyrin}$ at Guru-Fatima. $\delta^{15}N_{bulk}$ values are consistently more depleted (by –4‰) when the basin experienced photic zone euxinia during the PETM. However, the offset (ε_{por}‰) between $\delta^{15}N_{Porphyrin}$ and $\delta^{15}N_{bulk}$, suggests that cyanobacteria dominated marine export production during the PETM, which is different from that previously observed for the Mesozoic OAEs, suggesting that the marine N-cycle during the PETM might have operated different than during the OAEs.

5.1. Introduction

The Paleocene–Eocene Thermal Maximum (PETM; (Kennett and Stott, 1991) ~56 million years ago (Ma) was the largest hyperthermal event of the Cenozoic, and lasted for ~120-220 ka (reviewed by McInerney & Wing, 2011). The PETM is defined by an abrupt increase in global temperature (5-8˚C in <10 ka; e.g. Frieling et al., 2014; Sluijs et al., 2006; Sluijs et al., 2014, 2011; Zachos et al., 2006) and an associated negative stable carbon isotope ($\delta^{13}C$) excursion (CIE) of 4.7 ± 1.5 ‰ for terrestrial and 2.8 ± 1.3 ‰ for marine records (reviewed by McInerney & Wing, 2011). Carbon cycle perturbation, as well as extensive dissolution of deep ocean carbonates due to a sudden rise in the calcite compensation depth (CCD), indicates that the rapid release of (isotopically light) carbon into the ocean-atmospheric system was the cause of the PETM (Dickens et al., 1997, 1995; Pagani et al., 2006; Panchuk et al., 2008; Zachos et al., 2005; Zeebe et al., 2009). In addition to evidence for warming and carbon cycle perturbations, the PETM is associated with changes in the hydrological cycle and associated increases in terrestrial sediment flux, nutrient inputs to the surface ocean and algal productivity (review by Carmichael et al., 2017).

The combination of warming, higher sedimentation rates, and increased nutrient inputs and algal productivity have all been invoked as causes of widespread anoxia during the Oceanic Anoxic Events (OAEs) of the Mesozoic and could have caused the same during the PETM (Sluijs et al., 2014). However, during the PETM, the deep (open) ocean evidently experienced only a minor deoxygenation in the deep Atlantic (e.g. Chun et al., 2010; Plike et al., 2014) and deep Pacific (Colosimo et al., 2006; Palike et al., 2014; Zhou et al., 2014). However, there is evidence of water column suboxic/anoxic conditions in shelfal and marginal marine settings

and restricted basins. These include evidence of water column deoxygenation in the marginal sediments of the North Atlantic, i.e. eastern Gulf of Mexico (Kopp et al., 2009; Lippert and Zachos, 2007; Stassen et al., 2012) and Bay of Biscay (e.g. Palike et al., 2014; Pardo et al., 1997), Arctic Ocean (e.g. Sluijs et al., 2008; Stein et al., 2006), and Southwest Pacific (Kaiho et al., 1996; Nicolo et al., 2010). In addition, there is evidence from the Eurasian shelves (e.g. Boltovskoy et al., 1992; Gradstein et al., 1994; Pak & Miller, 1992; Pardo et al., 1997), including the Tethyan region; i.e. Western- (e.g. Braga et al., 1975; Egger et al., 2005), Eastern- (e.g. Bolle et al., 2000; Dickson et al., 2014a, 2014b; Gavrilov et al., 2003, 1997), and Southern margins (e.g. Ernst et al., 2006; Khozyem et al., 2013; Speijer and Wagner, 2002).

In a few continental shelf and marginal settings, water column anoxia developed to such an extent that photic zone euxinia occurred, indicated by the presence of biomarkers exclusive to green sulfur biomarkers, isorenieratane and other derivatives of isorenieratene (Summons and Powell, 1986). This includes marginal sites or restricted basins in the Arctic Ocean (IODP Site M0004; Sluijs et al., 2006); North Sea (Fur and Store Bælt; Schoon et al., 2013), West Siberian Sea (well 10; Frieling et al., 2014), Gulf Coastal Plain (Harrell Core; Sluijs et al., 2014), and eastern shelf of the South Atlantic (Dahomey Basin; Frieling et al., 2017). In addition Gavrilov et al. (2003) invoked biomarkers derived from Chlorobium bacteria in the Peri-Tethys sediments (Tadjik depression, Kurpai) as evidence of photic zone euxinia although the specific biomarker is not specifically mentioned in that study. Thus, the PETM shares some characteristics with OAEs but appears to lack the magnitude of global marine anoxia (see review by Robinson et al., 2017). Moreover, although organic carbon burial could have been crucial to terminating PETM warming (e.g. John et al., 2008), it does not appear to be as strong as during OAEs that are characterized by a positive $\delta^{13}C$ anomaly (Jenkyns, 2010). Parsing the similarities and differences in these climatic and biogeochemical interactions among the PETM and OAEs, therefore, remains an important component to understanding all of these events, but it also requires a better understanding of the extent and nature of PETM marine anoxia/euxinia. This is especially true for shallow shelf margins, where the extent of water column anoxia remains unclear, and especially in the Peri-Tethys Ocean, where dy-oxygenation appears to have been particularly pronounced (Dickson et al., 2014b; Gavrilov et al., 2003). Here, we have analysed organic geochemical biomarkers, especially those for water column anoxia and photic zone euxinia, in PETM sediments from the northern Peri-Tethys (Guru-Fatima, Kheu River, and Dzhengutay), southern Peri-Tethys (Dababiya) and western Peri-Tethys (North Atlantic; Zumaia), Figure *5.1*.

In addition, we explore the impact of water column anoxia on the marine Nitrogen cycle using $\delta^{15}N_{bulk}$ and the first to date $\delta^{15}N_{por}$ for the PETM. Consequences of marine anoxia today

(e.g. Horak et al., 2016) and during OAEs (e.g. Higgins et al., 2012) are higher rates of denitrification and annamox, both of which lead to the loss of N from the ocean to the atmosphere. $\delta^{15}N_{bulk}$ of sediments from Peri-Tethys region (Junium et al., 2018; Khozyem et al., 2015) and Arctic Ocean (Knies et al., 2008) display a negative excursion during the PETM. Similarly, a negative $\delta^{15}N_{bulk}$ excursion has been reported during the Mesozoic OAEs (Jenkyns et al., 2007; Junium and Arthur, 2007; Kashiyama et al., 2008; Kuypers et al., 2004; Ohkouchi et al., 2006). Classically this negative excursion in $\delta^{15}N_{bulk}$ is interpreted to reflect an increase in N_2-fixing cyanobacteria (Kuypers et al., 2004; Rau et al., 1987). However, Higgins et al., (2012), used the stable nitrogen composition of porphyrins ($\delta^{15}N_{porphyrin}$) and suggested that N_2 fixing eukaryotes dominated during OAE 2, not N_2-fixing cyanobacteria. However, whether a similar mechanism operated during the understanding of the PETM remains largely unclear.

5.2. Samples and method

5.2.1 Sampling of the PETM sections

The occurrence of the PETM has been throughout the Peri-Tethys realm, and along the northern margin is commonly associated with the deposition of organic-rich sediments. Collectively, these sections allow Paleocene—Eocene organic rich shales to be traced across about 2500 km, from Central Asia to the Caucasus (e.g. Gavrilov et al., 2009, 2003), including the Guru-Fatima section located in the eastern (Central Asia) region and the Dzhengutay and Kheu River sections located in the western (Caucasus) regions (Figure *5.1*), all three of which are studied here.

The lithology of the Guru-Fatima section is comprised of grey calcareous mudstone (<1 wt.% TOC), overlain by an organic rich shale horizon (7–20 wt.% TOC), which is covered by a laminated mudstone (~3 wt.% TOC) and an organic lean mudstone (<1 wt.% TOC (Fig. 5.2, Dickson et al., 2014). Elemental sulfur increases from <1 wt.% in the deepest and top horizons to 3 wt.% in the organic rich horizon (Figure *5.2*). A negative bulk $\delta^{13}C_{org}$ excursion of 4 ‰ occurs in the section, with values of –26 ‰ in the deepest horizon (grey calcareous marls), –30 ‰ in the organic rich shale and –28 ‰ the overlying laminated mudstone (Dickson et al., 2014; Figure *5.2*). Guru Fatima sediments were sampled from an archived drill core at the Geological Institute of the Russian Academy of Science.

The Dzhengutay section is composed of calcareous mudstone (<1 wt.% TOC) with an intermediate organic rich shale horizon (~3.5 wt.% TOC) (Dickson et al., 2014b; Figure *5.3*).

The elemental sulfur content also increases from non-detectable values in the calcareous mudstone to ~1 wt.% in the organic rich horizons. A negative bulk $\delta^{13}C_{org}$ excursion of 4‰ is expressed in the section, with values of –25 ‰ in the calcareous mudstone and –29 ‰ in the intermediate organic rich shale (Figure *5.3*; Dickson et al., 2014b). Dzhengutay sediments were sampled from an outcrop exposure that had been cut back significantly to prevent (potentially) degraded and contaminated surface sediments from impacting biomarker analyses.

The Kheu River section is composed of organic lean silty claystones (<1 wt.% TOC) with an intermediate organic rich shale (mean 5 wt.% TOC; Figure *5.4*) (Dickson et al., 2014b). Elemental sulfur values also increase from <1 wt.% in the organic lean sections to ~4 wt.% in the organic rich horizon. A negative bulk $\delta^{13}C_{org}$ excursion of –4.5 ‰ is expressed in the section, with values decreasing from –24 ‰ in the organic lean sediments to –30 ‰ in the organic rich horizon. Kheu River sediments were obtained from an outcrop exposure that had been cut back to avoid exposed materials and are the same as reported in Dickson et al. (2014).

In addition to the northern Peri-Tethys sections, we analysed the Dababiya section located on the southern continental shelf (Khozyem et al., 2015) (Figure *5.1*). The Dababiya section is a Global Stratotype Standard Section and Point (GSSP) (Aubry et al., 2007), and one of the most expanded PETM sections. The lithology of Dababiya is comprised of marl and marly shale overlain by non-calcareous clay, brown and laminated phosphatic shale, grey shale and grey marl to marly limestone. The TOC contents of Dababiya are generally low (<1 wt.% TOC) (Khozyem et al., 2015). The bulk $\delta^{13}C_{org}$ values exhibit a 3‰ negative carbon isotope excursion in $\delta^{13}C_{org}$ with values of –24 ‰ in the deepest and uppermost marly sections and –28 ‰ in the intermediate non-calcareous and shale horizons (Figure *5.5*) (Khozyem et al., 2015). Dababiya sediments were sampled from an outcrop in the NW section, located 50 m northwest of the GSSP exposure, and as with other sections the outcrop was cut back to avoid exposed materials.

The Zumaia section is located in the western Peri-Tethys and deposited in lower to mid bathyal settings, at about 1 km paleowater depth (Rodríguez-Tovar et al., 2011); it is the most complete and representative section of early Paleogene in the Pyrenees and a key reference for the Paleocene–Eocene boundary (Pujalte et al., 1998). The lithology is composed of alternating marl and limestone, interrupted by a 4 m horizon of reddish claystone and silty claystones (the Siliciclastic Unit (SU; Schmitz et al., 2001)). TOC content of Zumaia is low through the entire section (<1 wt.% TOC) (Manners et al., 2013). The bulk $\delta^{13}C_{org}$ values at Zumaia express a negative CIE of 4 ‰, decreasing from –24 ‰ in the marly and carbonate sections to –28 ‰ in the Siliciclastic Unit (Figure *5.6*) (Manners et al., 2013). Zumaia sediments were sampled from an outcrop, cutting back to avoid exposed materials.

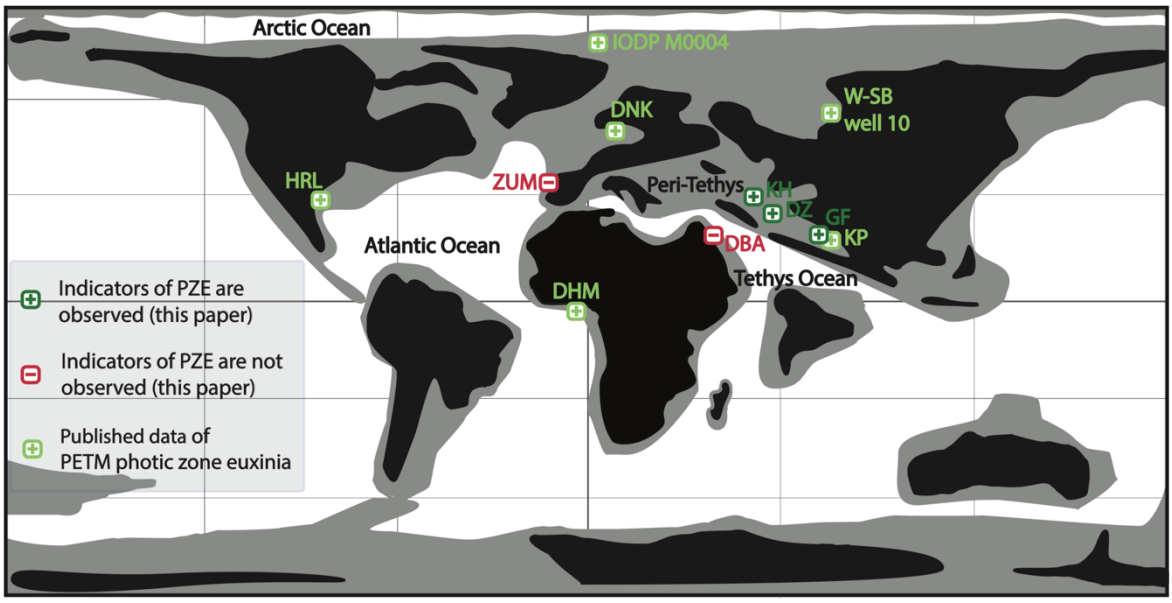

Figure 5.1. Schematic of Paleocene-Eocene world map, highlighting the locations at which PZE during the PETM is observed. Positive-dark green symbols indicate evidence for PZE (this study), light green-positive symbols represent previously published evidence for PZE (Frieling et al., 2017, 2014; Gavrilov et al., 2003; Schoon et al., 2013; Sluijs et al., 2006; Sluijs et al., 2014), and negative-red symbols indicate lack of evidence for PZE (this study).

5.2.2. Analytical methods

Biomarker analyses were conducted on a total of 36 sediments, including 13 sediments from Dzhengutay, 10 sediments from Guru Fatima, 3 sediments from Dababiya and 10 rock samples from Zumaia. Biomarkers in Kheu River sediments have been previously published (Dickson et al., 2014), but here we report new data on isorenieratene and its derivatives. Prior to any treatment, Zumaia rock samples were washed (by methanol and dichloromethane (DCM)), and then the cleaned samples were powdered using ball mill. Sediments from other sites were too porous to allow rigorous washing and instead surface material was physically removed before extraction.

5.2.2.1. Bulk geochemistry

The $\delta^{15}N_{bulk}$ was determined for the Dzhengutay section using a Thermo Scientific Flash IRMS Elemental Analyzer, coupled to a Delta V Advantage IRMS through a Conflo IV universal interface. Dried sediments (not acidified) were transferred into tin capsules (Costech), which were folded and crushed before being analyzed on the IRMS. $\delta^{15}N$ values were calculated using the authentic standards USGS40 and USGS41a (both are glutamic acid, purchased from USGS), along with several in-house laboratory standards (glutamic acid and tyrosine). The standard deviation (σ) for $\delta^{15}N_{bulk}$ is ~0.3. For Dababiya samples, T_{max} (an indicator of thermal maturity) was obtained using a Rock-Eval 6 instrument (with a σ of ±10°C).

5.2.2.2. Biomarker extraction

The methods for Kheu River biomarker extraction, separation and analysis are explained in (Dickson et al., 2014b). To obtain total lipid extracts (TLEs) from the other sites, either about 5 g (Dzhengutay and Guru Fatima) or 1 g (Dababiya) of sediment were extracted with 10 ml of a mixture of dichloromethane (DCM) and methanol (MeOH) (1:1, vol) by micro microwave-assisted method (MILESTONIE Ethos Ex Microwave solvent extraction). The microwave program consisted of a 10 min ramp to 70 °C (max. 1000 W), followed by a 10 min hold at 70 °C (max. 1000 W) and 20 min cooling period. After microwave extraction the samples were centrifuged (1500 rpm, 5 minutes) and the resulting supernatant collected. An additional 10 ml of DCM:MeOH were added to the sediment, centrifuged, and the supernatant again collected. This procedure was repeated four times. To obtain TLEs from the organic lean Zumaia sediments, 35 g of sediment were extracted with 220 ml of DCM:MeOH (1:1, vol) azeotrope using a Soxhlet apparatus for 24 hrs. Solvent-washed activated copper turnings were added to the TLE for 24 hrs to remove elemental sulfur. The TLE was then concentrated using rotatory evaporator.

50% of each TLE from Dzhengutay, Guru Fatima, and Dababiya was used for GC-MS analysis. TLEs from organic rich samples with TOC >1 wt.% (a total of 7 samples from Dzhengutay and Guru Fatima), were separated into three fractions (aliphatic, aromatic and polar) using short (4 cm) silica gel open column chromatography. Aliphatic, aromatic, and polar fractions were eluted using 3 ml of hexane, 4 ml of hexane:DCM (3:1) and 4 ml of DCM:MeOH (1:2), respectively. For the other samples 50 % of the TLE was measured on the GC-MS. TLEs were derivatised (silylated) with BSTFA (N,O-bis(trimethylsilyl)-trifluoroacetamide; 30 µl) and pyridine, and heated (70°C for 1 hr).

The Zumaia TLEs (similar to those from Kheu River (Dickson et al., 2014b)) were separated into two fractions (fatty acid and neutral) using silica gel flash column

chromatography. Fatty acid and neutral fractions were eluted using 7 ml of chloroform and 7 ml of chloroform:acetic acid (100:1), respectively. The neutral fraction was further separated into two fractions (apolar and polar) on an alumina column. Apolar and polar fractions were eluted using 5 ml of *n*-hexane:DCM (9:1) and 4 ml DCM:MeOH (1:2). The apolar fractions were used for GC-MS analysis.

For all samples, prior to GC-MS analysis, a known amount of C_{36} *n*-alkane was added as an internal standard for the (semi-)quantification of the biomarkers of interest (isorenieratane).

For samples from Dzhengutay and Guru Fatima the other 50 % of the TLE was used to obtain porphyrins. Porphyrin pre-purification was conducted using silica gel flash column chromatography. TLEs were separated in to four fractions, i.e. hexane, hexane:DCM (1:1), DCM and MeOH. Porphyrins (mixed porphyrin, i.e. Ni- and VO-chelated porphyrins) were eluted in the middle two fractions.

5.2.2.3. Biomarker analysis

Biomarker distributions were determined using a Thermo Scientific^{TM} ISQ Series Single Quadruple GC-MS system. Separation of compounds was carried out on a Zebron non-polar column (50 m x 0.32 mm, 0.10 µm film thickness), with He a carrier gas and an injection volume of 1 µl. The GC programme was: injection at 70 °C (1 min hold), heating to 130 °C at a rate of 20 °C/min, then to 300 °C at 4 °C/min, followed by a 24 min hold. The mass spectrometer continuously scanned between *m/z* 50 and 650, and identification of biomarkers was carried out based on published retention times and spectra as well as comparison with standard samples.

$\delta^{15}N$ of porphyrins was determined for the Guru Fatima and Dzhengutay sediments to explore the N cycle excursion during the PETM. Following the porphyrin pre-purification (5.2.2), porphyrin fractions were purified by prep. HP-LC (Agilent 1200 series) equipped with a multi-wavelength UV/Vis detector (Higgins et al., 2009). Porphyrin-containing fractions were injected onto two ZORBAX SIL columns (4.6 x 250 mm, 5 µm) and eluted at 1 mL min^{-1}. Porphyrin peaks were detected by absorbance at 393 and 405 nm. After purification $\delta^{15}N_{porphyrin}$ was measured according to the methods in Higgins et al., (2009). Briefly, HPLC-purified porphyrins were placed in quartz tubes and oxidized under UV light in a biosafety cabinet for six hours, then dried and chemically oxidized using re-crystallized 0.05 M $K_2S_2O_8$ dissolved in fresh 0.15 M NaOH. Nitrate concentration was measured using a chemiluminescent NO_x analyser (Teledyne NO/NOx Analyzer 200E). $\delta^{15}N_{porphyrin}$ values were

measured using the denitrifier method (Sigman et al., 2001), on a Delta V Advantage isotope ratio mass spectrometer. Isotopic measurements were calibrated based on the N_2 reference scale using standard reference materials, i.e. IAEA N3 and USGS 34. Purification of porphyrin and $\delta^{15}N_{porphyrin}$ measurements were conducted at Harvard University, USA.

5.3. Results

5.3.1. Bulk geochemistry and thermal maturity

Bulk geochemical data (TOC contents and $\delta^{15}C_{org}$ values) were obtained previously and described in the site descriptions above. New data presented here for the first time are the $\delta^{15}N_{bulk}$ from the Dzhengutay section. These range from 2 ‰ prior to and after the PETM (as defined by the CIE) to –2 ‰ during the PETM, yielding a 4‰ negative excursion (Figure *5.3*). The thermal maturity of Dababiya section as determined by Rock Eval T_{max} values is 470-600 °C.

5.3.2. Aliphatic compounds

The distributions of biomarkers in these sections provide insight into the changes in OM source during the PETM. Although the differences in thermal maturity make it difficult to compare absolute values of various biomarker indices, we focus on relative trends within each section to qualitatively explore changes in inputs. We focus on the aliphatic fraction, which contains a range of algal, higher plant and bacterial biomarkers.

The aliphatic fraction from the Guru Fatima section contains *n*-alkanes (C_{16}-C_{35}), isoprenoids (pristane, phytane and lycopane), steranes (ααα isomers of C_{27}-C_{29} also methyl sterane) and hopanes (C_{27}-$C_{32,}$ dominated by αβ isomers). The ratio of the short to long chain *n*-alkanes [$C_{17}/(C_{17}+C_{31})$] in the organic rich PETM horizons (~1) is slightly higher than pre-PETM (~0.8) and post-PETM (~0.2) sediments (Figure *5.2*). These values are consistent with a moderate thermal maturity and a mixture of algal and higher plant inputs. The odd-over-even carbon number predominance (carbon preference index, CPI; Bray and Evans, 1961) of the long-chain (C_{25}-C_{37}) *n*-alkanes during the PETM (~1) is lower than pre-PETM (~1.4) and post PETM (~2) (Figure *5.2*). The lycopane ratio (lycopane/C_{31} *n*-alkane ratio; Sinninghe Damsté et al., 2003), is applied as a proxy for anoxic conditions. The lycopane/C_{31} *n*-alkane ratio is

<0.8 during the PETM, although it is lower (<0.3) in the pre- and post PETM sediments. The degree of hopane isomerisation 22S/(22S+22R) (Mackenzie et al., 1980) is 0.4.

The aliphatic hydrocarbon fractions from Dzhengutay contain *n*-alkanes (C_{16}-C_{35}), isoprenoids (pristane, phytane and lycopane), steranes (ααα isomers of C_{27}-C_{29} also methyl sterane) and hopanes (C_{27}-$C_{32,}$ dominated by αβ isomers). Unlike at Guru-Fatima, pre- and post-PETM sediments at Dzhengutay are organic lean and do not yield long-chain *n*-alkanes and hopanes (Figure *5.3*). The ratio of the short to long chain *n*-alkanes [$C_{17}/(C_{17}+C_{31})$] has relatively variable values around ~0.8 in the PETM black shale horizon. The CPI in the PETM horizon indicates a slight odd-over-even carbon number predominance (CPI~1.4; Figure *5.3*). The lycopane/C_{31} *n*-alkane ratio is ~0.5 during the PETM (Figure *5.3*), although was not measurable (~0) in the pre- and post PETM samples. The degree of hopane isomerisation 22S/(22S+22R) (Mackenzie et al., 1980) is 0.4, similar to Guru Fatima.

As previously reported (Dickson et al., 2014b), the apolar fraction from Kheu River contains abundant *n*-alkanes (C_{17}-C_{35}), isoprenoids (pristane, phytane, lycopane), and hopanes (C_{27}-C_{31}, ββ, αβ and βα isomers), as well as sterenes (C_{27}-C_{29}) and subordinate abundances of steranes. The ratio of the short to long chain *n*-alkanes [$C_{17}/(C_{17}+C_{31})$] is variable (<0.1–0.5) in the pre-PETM and the organic rich PETM horizon, although at the end of the PETM these values decrease and are not measurable post-PETM (Figure *5.4*). The CPI is variable during the PETM horizon (0.4–2.5), but slightly higher than pre- and post-PETM (<1) sediments. The lycopane/C_{31} *n*-alkane ratio during the PETM organic rich sediments, although variable (0.1–2), is higher than pre- to post-PETM (~0.5) horizons. The degree of hopane isomerisation 22S/(22S+22R) (Mackenzie et al., 1980) is as low as 0.03.

Based on the biomarker distribution (for instance presence of fatty acids and alcohols), the sediments from Zumaia are the least mature amongst the studied sections here, but organic lean. The biomarkers of interest; i.e. *n*-alkanes, isoprenoids, steranes, hopanes, and lycopane are largely absent in these TLEs (Figure *5.5*). The apolar fraction from Zumaia is dominated by fatty acids.

Sediments from Dababiya section are of the highest thermal maturity amongst the studied sections (over mature), and no biomarkers (including biomarkers of interest) were detected in our total lipid extracts (Figure *5.6*).

5.3.3. Aromatic compounds

The aromatic fractions from all three northern Tethys marginal sections (Dzhengutay, Guru Fatima and Kheu River) contain isorenieratene derivatives, including isorenieratane (Figure

5.2, Figure *5.3*, 5.4). The presence of derivatives of isorenieratene (e.g. isorenieratane) (Imhoff, 1995; Koopmans et al., 1996a), a carotenoid that originates from brown coloured strains of photosynthetic green sulfur bacteria (chlorobiacae) (Imhoff, 1995 and references therein), indicates the establishment of photic zone euxinia. Isorenieratane is absent or below detection in all pre- and post-CIE (PETM) sediments at all three sites, and its concentration in the PETM sediments varies among the three sites. Concentrations are highest at Guru Fatima (Figure *5.2*), varying between 50 to 200 μg g^{-1} sediment. Lower concentrations occur at Dzhengutay (~10 μg g^{-1} sediments, Figure *5.3*), which has a similar thermal maturity to Guru Fatima. Among the northern Tethyan sites, isorenieratane concentrations are lowest at Kheu River, commonly being below detection or having low concentrations (0.5 μg g^{-1} sediment) in the PETM interval. The Kheu River section is less thermally mature (discussed in 5.4.1), and it is possible that isorenieratene derivatives remain in the S-bound fraction. In contrast to the northern Tethys sites, the lipid extractions from Zumaia sediments do not contain isorenieratane or it is below the detection level. As Zumaia sediments are low in maturity (discussed in 5.4.1), the isorenieratene derivatives in these samples could be S-bounded (Sinninghe Damste et al., 1990). The sediments of Dababiya are of high maturity (discussed in 5.4.1) and isorenieratene derivatives are absent in these sediments.

5.3.4. Compound specific $\delta^{15}N_{porphyrin}$

$\delta^{15}N_{porphyrin}$ was determined on samples from the Guru Fatima and Dzhengutay sections, mainly from within the PETM black shales. In general, porphyrin concentrations were too low outside of the black shale interval to allow us to measure $\delta^{15}N_{porphyrin}$. In Guru Fatima, $\delta^{15}N_{porphyrin}$ are obtained from pre-PETM and the PETM horizon (Figure *5.2*). The $\delta^{15}N_{porphyrin}$ values in the organic rich horizons are variable (–5 ‰ to 4 ‰), but generally higher than the pre-PETM value (2 ‰), expressing a 2 ‰ positive excursion during the PETM. In Dzhengutay, $\delta^{15}N_{porphyrin}$ was obtained from PETM horizon only. The $\delta^{15}N_{porphyrin}$, although generally lower than Guru Fatima (Figure *5.3*), are positive (~1 ‰–3 ‰).

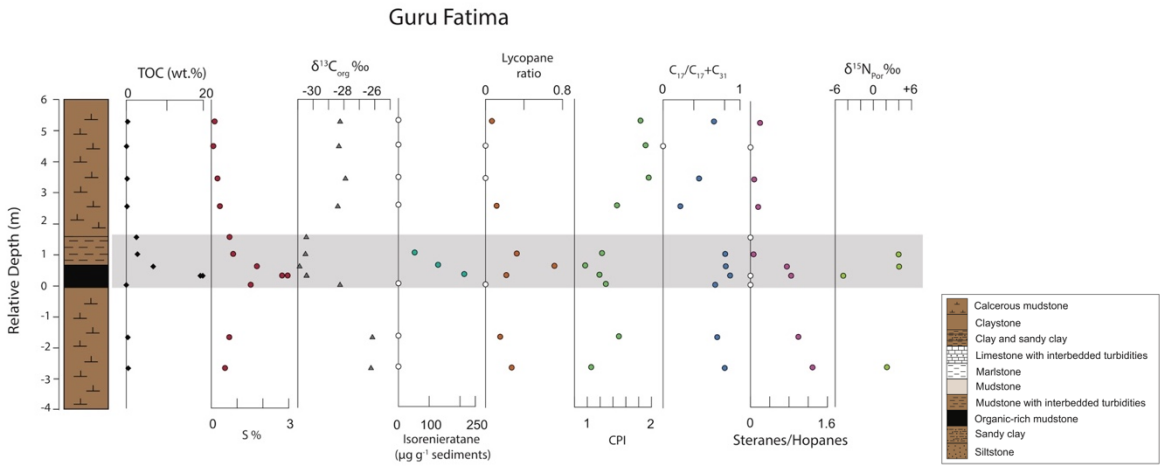

Figure 5.2. Results from the Guru Fatima Section. Lithology, TOC, elemental sulfur, $\delta^{13}C$, isorenieratane, lycopane ratio, CPI, the ratio of short to long chain n-alkanes, the ratio of algal to bacterial derived biomarkers, and $\delta^{15}N_{por}$. The legend of lithology symbols used in this chapter. Bulk geochemical data are from Dickson et al., (2014b). Relative depth is based on the onset of the PETM CIE.

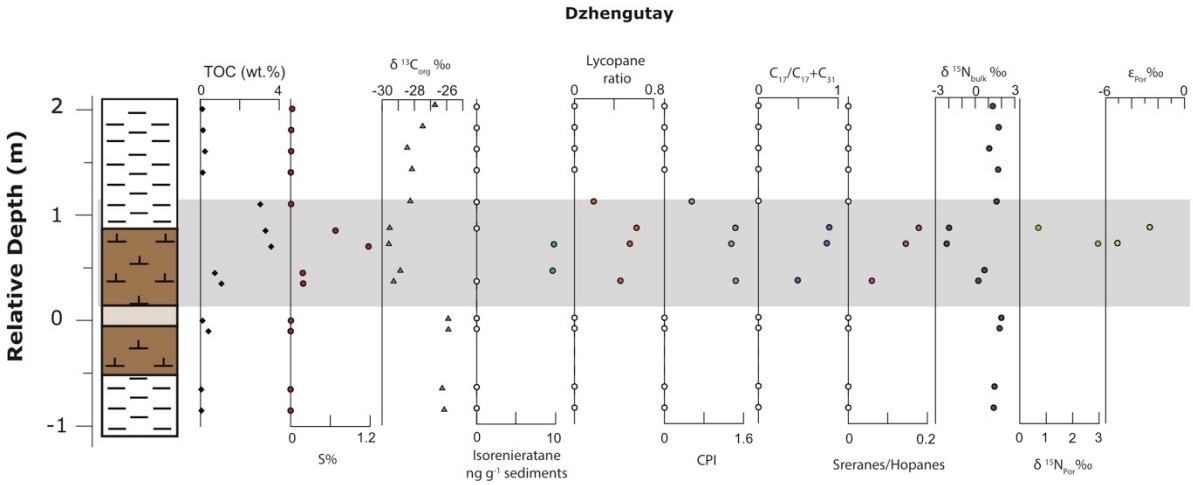

Figure 5.3. Results from the Dzhengutay section. Lithology, TOC, elemental sulfur, $\delta^{13}C$, isorenieratane, lycopane ratio, CPI, the ratio of short to long chain n-alkanes, the ratio of algal to bacterial derived biomarkers, $\delta^{15}N_{bulk}$, $\delta^{15}N_{por}$, ε_{por}. Bulk geochemical data are from Dickson et al., (2014b). Relative depth is based on the onset of the PETM CIE. The key for the lithology symbols is in Figure 5.3.

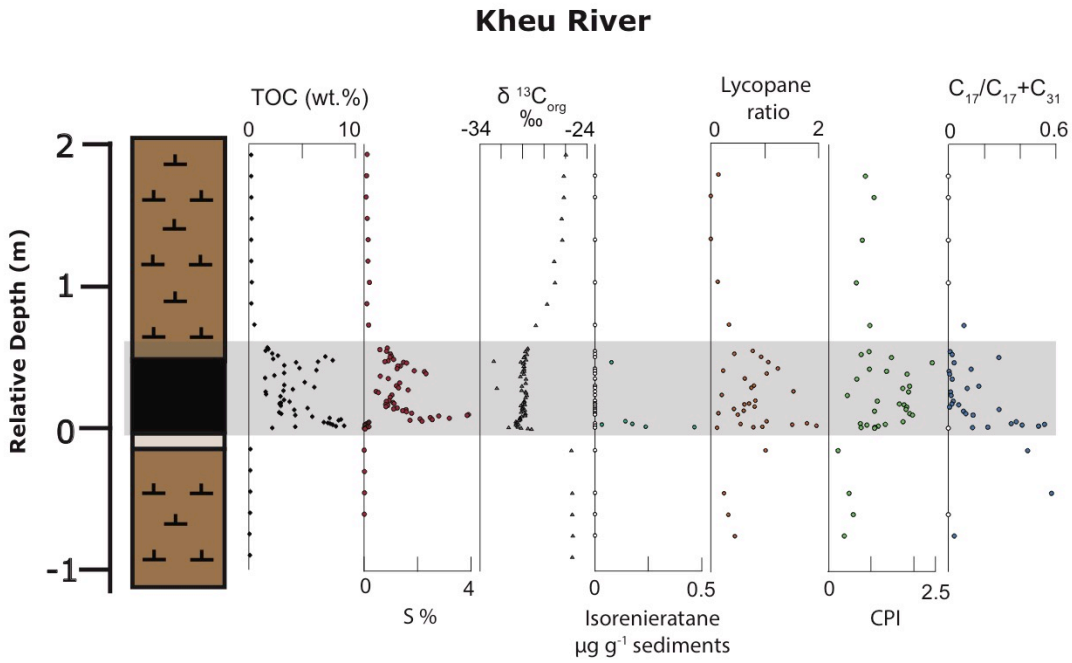

Figure 5.4. Results from the Kheu River section. Lithology, TOC, elemental sulfur, $\delta^{13}C$, isorenieratane, lycopane ratio, CPI, the ratio of short to long chain n-alkanes. Bulk geochemical data are from Dickson et al., (2014b). Relative depth is based on the onset of the PETM CIE. The key for the lithology symbols is in Figure 5.3.

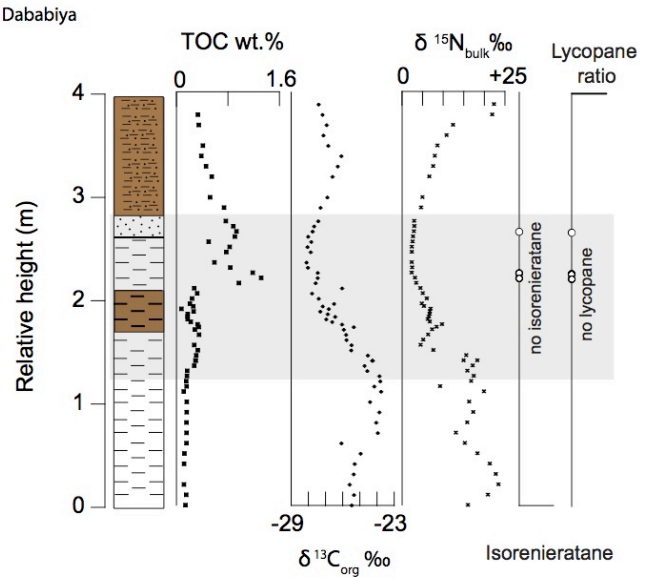

Figure 5.5. Results from Dababiya NW section. Lithology, TOC, $\delta^{13}C$, isorenieratane, lycopane ratio. Bulk geochemical data are from (Khozyem et al., 2015). Relative height (m) is based on the local surface. The key for the lithology symbols is in Figure 5.3.

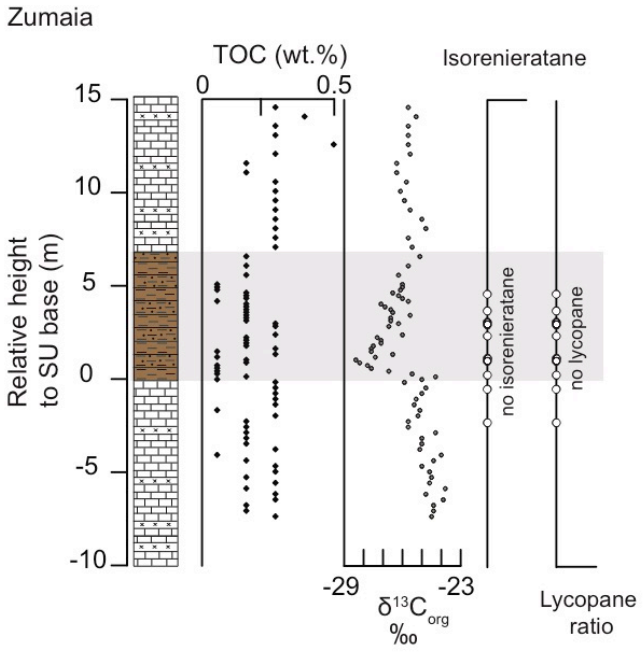

Figure 5.6. Results from Zumaia section, Lithology, TOC, $\delta^{13}C$, isorenieratane, lycopane ratio. Bulk geochemical data are from (Manners et al., 2013). Relative height (m) is based on the start of the Siliciclastic Unit (SU). The key for the lithology symbols is in Figure 5.3.

5.4. Discussion

5.4.1. Thermal maturity of the discussed sections

The thermal maturity of the Dababiya section as determined by Rock Eval T_{max} values of 470-600 °C is high (over mature regarding the OM) and obtaining lipid biomarkers from this host rock was not achieved. Rock Eval was not performed on the other studied sections, therefore to compare the thermal maturity of the other studied sections, their obtained hopane distributions was assessed (explained in 5.3.2). The degree of hopane isomerisation 22S/(22S+22R) (Mackenzie et al., 1980) indicate relatively lower thermal maturity in Kheu River (~0.03), and higher in Dzhengutay (~0.4) and Guru Fatima (~0.4). The biomarker distribution at Zumaia (see 5.3.2) does not contain hopanes to compare with other sections, however these samples contain fatty acids indicating a lower maturity of these samples compared to the other studied sections. Altogether, the maturity of organic matter at Dababiya (over mature) is more than Dzhengutay and Guru Fatima, which are *per se* at higher stage of maturity that Kheu River. Zumaia is the least mature among the studied sections.

5.4.2. Spread of photic zone euxinia in the Peri-Tethys margins during the PETM

Multiple lines of evidence indicate significant redox changes during the PETM (CIE) in the northern margins of Peri-Tethys, i.e. in Guru Fatima, Dzhengutay and Kheu River sections. These include elevated TOC contents as some of the highest observed during the PETM (Dickson et al., 2014b; Gavrilov et al., 2003); high and dynamic abundances of redox sensitive trace metals, such as molybdenum (Mo), rhenium (Re), manganese (Mn) (Dickson et al., 2014); high abundances of Fe, and especially high proportions contained within reactive minerals (Dickson et al., 2014); and high burial rates of reactive phosphorus (P) (Dickson et al., 2014). These proxies suggest that anoxia occurred not only in sediments, but extended into the water column, although the extent remains unclear. Our data provide the first comprehensive evidence that anoxia, and even euxinia, extended into the photic zone of the water column in the northern Peri-Tethys during the PETM.

Building on previous work (Dickson et al., 2014), we show that lycopane, a biomarker predominantly associated with anoxic oxygen minimum zones (Sinninghe Damsté et al., 2003), occurred across the Northern Tethys during the PETM. In Guru-Fatima (the eastern part of the basin), the lycopane ratio reaches ~0.7 during the PETM, although below the detection level in the pre- and post-PETM intervals, indicating an increase in the intensity of water column deoxygenation towards anoxia. The same increase occurs at the Dzhengutay and Kheu River sections, with maxima of ~0.6 and ~1, respectively. This suggests that Kheu River experienced the most pronounced water column anoxia, although this could be a consequence of its lower thermal maturity as isoprenoidal hydrocarbons will crack more readily than straight-chain components (e.g. Summons et al., 1988). In any case, the maximum PETM values at each site are consistent with those observed in recent sediments of the OMZ of the Arabia Sea (0.8, Schulte et al. 1999, Sinninghe Damsté et al. 2003) and across the Peruvian Shelf (2.5, Farrington et al. 1988; Sinninghe Damsté et al. 2003). Although, it is noteworthy that the lycopane ratio is generally interpreted as local relative changes with a sedimentary sequence rather than as absolute values (Sinninghe Damsté et al., 2003).

The presence of isorenieratane in the PETM organic rich sediments of Guru Fatima, and below the detection level in the pre- and post-PETM horizons, indicates the establishment of photic zone euxinia during the PETM. The same holds for the occurrence of isorenieratane within the PETM organic rich horizons of Dzhengutay and Kheu River. The higher abundances of isorenieratane at Guru Fatima than at Dzhengutay and Kheu River suggests that the eastern

part of the basin experienced more pronounced water column anoxia/euxinia during the PETM. Similarly, the persistence of anoxia and photic zone euxinia biomarkers in Guru Fatima suggests persistent PZE, contrasting with the evidently episodic water column anoxia and PZE in the western basin. We note the much lower resolution of the biomarker data at Guru Fatima and Dzhengutay than at Kheu River, but our conclusions are consistent with those inferred from other geochemical proxies (Dickson et al., 2014b). Although, an episodic anoxia during the PETM has been previously attributed to episodic water column ventilation (Dickson et al., 2014b, 2012; Friedrich, 2010; Kenig et al., 2004; Sluijs et al., 2014), the cyclic nature of anoxia in the western part of the basin could be raised from the astronomically controlled variations in the hydrological cycle activities which increase is expressed in the sedimentary cycles; i.e. a regular fluctuation of TOC content and carbonates is expressed in three and four cycles at Kheu River and Dzhengutay, respectively (Gavrilov et al., 2009).

In the southern Peri-Tethys, i.e. Dababiya NE section, redox sensitive proxies (V, nickel (Ni), Mo, Mn and cerium (Ce) anomalies) reveal two intervals of anoxic/euxinic conditions during the early and middle PETM, each associated with high surface water productivity (Khozyem et al., 2015). Establishment of water column euxinic condition during the PETM (Schulte et al., 2011) and a general oxygen depleted sea floor with episodes of fully anoxic (or euxinic) condition (Soliman et al., 2006), based on the geochemical and mineralogical proxies) pyrite framboids, pseudomorphs of hematite spherules, calcite and detrital minerals), have also been inferred in the Dababiya GSSP and Quarry sections, respectively. However, in contrast to the northern Peri-Tethys sites, TOC content remains low (<1 wt.%) throughout the PETM (although they do increase). In fact, the sediments are so organic lean that no organic compounds, including those for anoxia or photic zone euxinia, were detected. Considering the high T_{max} values of 470-600 °C, this could be due to thermal degradation of sedimentary organic content. Given the very low organic carbon contents, it seems unlikely that persistently anoxic conditions prevailed in Dababiya sediments – unlike those of the northern Peri-Tethys.

In the western the Peri-Tethys, i.e. the upper to mid bathyal sequence of Zumaia, the negative CIE is associated with a planktic foraminiferal faunal turnover (Canudo et al., 1995; Molina et al., 1999), which has been invoked as evidence for development of a low oxygen minimum zone (suboxic condition). Specific evidence includes an increase in the abundance of the low oxygen tolerant genera such as Chiloguembelina spp (Canudo et al., 1995). However, neither anoxia nor photic zone euxinia biomarkers (lycopane and isorenieratene derivatives) were detected in the Zumaia sediments (Figure *5.6*). Nor do TOC contents increase, although that could be due to the dramatic increases in sedimentation rate and changes

in lithology that occurred at Zumaia during the PETM (Manners et al., 2013). Given the bathyal location of Zumaia (Alegret et al., 2018) and the poor organic matter preservation, it is plausible that lycopane and isorenieratene derivatives were degraded during transport and burial. However, we have no evidence for that and it seems unlikely that PZE in this region would not be associated with any seafloor deoxygenation (e.g. Yao and Millero, 1995). Instead and consistent with foraminiferal assemblages, it appears that deoxygenation in the Zumaia section only developed to suboxic conditions at best (as indicated by planktic foraminiferal (Canudo et al., 1995; Molina et al., 1999))..

The occurrence of widespread deoxygenation during the PETM is thought to reflect a response to a combination of an increased hydrological cycle (per se as a result of elevated temperature and pCO_2; (Carmichael et al., 2017), warming and increased algal productivity due to increased continental chemical weathering and nutrient input (Bralower, 2002; Sluijs et al., 2014). This is similar to that invoked for the Mesozoic OAEs (Jenkyns, 2010). However, during the PETM deoxygenation was restricted to restricted basins and the open ocean appears to have only suffered from minor changes in oxygenation (Colosimo et al., 2006; Pälike et al., 2014; Zhou et al., 2014). On the shelf, marginal marine settings and restricted basins where the nutrient trap efficiency is amplified, however, the PETM deoxygenation seem to be more intense (compared to deep ocean) and developed into suboxic/anoxic condition (e.g. Sluijs et al., 2008; Nicolo et al., 2010; Egger et al., 2005; Bolle et al., 2000; Dickson et al., 2012; Sluijs et al., 2006; Sluijs et al., 2014; Frieling et al., 2017); or even PZE (Frieling et al., 2014) as in the northern peri-Tethys (this study). The mechanism to explain PETM anoxia in the Peri-Tethys must not only account for (a) the widespread deoxygenation of the water column at the PETM, and (b) apparently stronger and more persistent anoxic conditions along the northern margin (or within northern marginal basins) (e.g. Dickson et al., 2014b; Gavrilov et al., 2003; Junium et al., 2018) but also (c) must explain the apparent increase in anoxia from west to east of the basin and its apparently episodic (or cyclical) character in the west.

An increase in marine productivity during the PETM anoxic horizons, comparing to the pre- and post PETM sediments, is highlighted by the change $C_{17}/ C_{17}+ C_{31}$ ratio in the northern Peri-Tethys, although less obvious at Guru Fatima (Figure *5.2*, Figure *5.3* and Figure *5.4*). The connection of increased marine productivity and intensity of photic zone euxinia is especially manifest in the early stages of PETM at Kheu River where the pronounced increase of marine productivity accompanies PZE (Figure *5.4*). The elevation in marine productivity accompanies an increase of nutrient availability. This appears in the carbon-preference index (CPI), as a proxy for estimating the potential contribution from higher terrestrial plants to sediments. The CPI values in the western part of the basin (Dzhengutay and Kheu River) increase during the

PETM (Figure *5.3* and Figure *5.4*), indicating an increase in the higher terrestrial input during the PETM. Increase of CPI follows the same trend with marine productivity, suggesting that terrestrial input was the dominant source of nutrients into the western section. Although in Guru Fatima the CPI decreased during the PETM (Figure *5.4*), this could result from the pronounced marine production which dilutes terrestrial OM. The influx of terrestrial nutrient input in Tethys releam is correlated with increased weathered lithogenic material, indicated by CIA and Ti/Al proxies (Dickson et al., 2014b).

Altogether our results suggest that terrestrial input stimulated marine productivity, leading to anoxic/euxinic conditions in the northern Peri-Tethys margins. Therefore, the variation in the intensity of anoxia in the western and eastern part of the basin could result from variations in marine productivity, as a consequent of either variations in nutrient input quantity or differences in local properties of the basin (morphology) which influenced towards different responses to the nutrient elevation. The latter, however, seems more likely, when comparing the intensity of anoxia in the Zumaia bathyal section to the epicontinental sections of the northern Peri-Tethys.

Collectively, based on the published and new results, we conclude that development of PZE during the PETM was well established in the restricted and epicontinental basins, i.e. the widen area of the northern Peri-Tethys margins from west to east; Kurpai (Gavrilov et al., 2003), Guru Fatima, Dzhengutay and Kheu River; as well as in the Arctic Ocean (IODP Site M0004; Sluijs et al., 2006); North Sea (Fur and Store Bælt; Schoon et al., 2013), West Siberian Sea (well 10; Frieling et al., 2014). PZE also developed in some marginal and continental shelf area as reported in the eastern Gulf of Mexico (Harrell Core; Sluijs et al., 2014) and eastern shelf of the South Atlantic (Dahomey Basin; Frieling et al., 2017). Development of photic zone euxinia in these basins, is likely driven by the morphology of the restricted basins, acting as nutrient traps that amplified productivity and intensified anoxia. In the open marginal settings (e.g. Zumaia), where the nutrient trap efficiency was not as high as epicontinental or marginal settings, deoxygenation only developed to suboxic condition.

5.4.3. Marine N cycle during the PETM

Nitrogen is a key-nutrient and a biolimiting factor for marine productivity (e.g. Redfield, 1934; Tyrrell, 1999). The marine N-cycle is tightly linked to the degree of oxygenation of the water column as anaerobic microbial activities lead to loss of bio-available nitrogen through denitrification and anammox. The dynamics of the marine N-cycle can be studied using $\delta^{15}N_{bulk}$

of sediments. An increase in loss of bio-available nitrogen is compensated by an increase in marine N_2-fixers, which results in a decrease in $\delta^{15}N_{bulk}$. Depleted $\delta^{15}N_{bulk}$ is reported from sapropels of the Eastern Mediterranean Sea (Möbius et al., 2010), the Cretaceous OAEs (Rau et al., 1987), and during the PETM in the Peri-Tethys (Junium et al., 2018; Khozyem et al., 2015) and Arctic Ocean (Knies et al., 2008). Consistent with these findings is the $\delta^{15}N_{bulk}$ measured at Dzhengutay, yielding a 4‰ negative excursion during the PETM (Fig. 5.3) which is similar to that observed in organic-rich OAE 2 sediments (Higgins et al., 2012) and the PETM section in Arctic ocean (Knies et al., 2008) and Kheu River (Junium et al., 2018) but smaller than those observed in other PETM sections in Tethys margins (Dababiya; Khozyem et al., 2015). Considering the occurrence of anoxic/euxinic condition in Peri-Tethys, intense denitrification in the anoxic water column and consequent nutrient limitation in the photic zone, likely favoured nitrogen fixing organisms. The difference (ε_{por}) between $\delta^{15}N_{porphyrin}$ and $\delta^{15}N_{bulk}$ can provide insights into the relative contribution of eukaryotes and cyanobacteria N_2 fixers. The negative values of ε_{por} (–2.5‰ and –5‰) at Dzhengutay is the common feature of fresh water cyanobacteria (most likely Anabaena Variabills (Higgins et al., 2011)), expressing the dominant control of fresh water export during the PETM. Whereas, marine environment cyanobacteria ($-2<\varepsilon_{por}<+2$) (Higgins et al., 2011) and eukaryotic phytoplanktons ($0<\varepsilon_{por}<10$) (Beaumont et al., 2000; Higgins et al., 2011; Kennicutt et al., 1992; Sachs et al., 1999) have a different range of ε_{por} values. Although $\delta^{15}N_{bulk}$ was not measured at Guru Fatima, the positive $\delta^{15}N_{porphyrin}$ values (~ +4‰ at 0.6 and 1 mbsf, Figure *5.2*) during the PETM, assuming depleted $\delta^{15}N_{bulk}$ values, is in line with Dzhengutay results on the fresh water cyanobacteria as the dominate nitrogen fixing organisms. Domination of fresh water cyanobacteria suggests that nitrogen supply to the photic zone was dominated by enhanced terrestrial run off, forming a lid of reduced salinity at the surface water on the top of the stratified basin and photic zone euxinia. Previous ε_{por} analysis suggest that during the OAE2 the majority of export production was dominated by eukaryotes (Higgins et al., 2012). However, ε_{por} values in Peri-Tethys reveals that nutrient availability during the PETM was dominantly from a riverine source, which was intensified by accelerated hydrological cycle during the PETM. The value of $\delta^{15}N_{porphyrin}$ at the onset of PETM in Guru Fatima is more depleted (~–5‰, Figure *5.2*) than the upper section. The negative values of $\delta^{15}N_{porphyrin}$ corresponds to the pronounced TOC values also the concentration of isorenieratane (Figure *5.2*). These might suggest a slightly different condition and domination of nitrogen fixing organisms by marine environment cyanobacteria ($-2<\varepsilon_{por}<+2$) (Higgins et al., 2011) or eukaryotic phytoplanktons ($0<\varepsilon_{por}<10$) (Beaumont et al., 2000; Higgins et al., 2011; Kennicutt

et al., 1992; Sachs et al., 1999) at the onset of PETM, although calculation of ε_{por} is not possible at Guru Fatima ($\delta^{15}N_{bulk}$ is not measured).

5.5. Conclusion

Our results demonstrate that during the PETM, PZE only developed in the restricted marginal and epicontinental basins, but not in the open marginal settings. This could be influenced by the morphology of the restricted basins acting as nutrient traps that amplifies productivity and intensifies anoxic conditions. The $\delta^{15}N_{bulk}$ and $\delta^{15}N_{porphyrin}$ demonstrate a perturbation in the marine N cycle and suggest that fresh water N_2 fixing cyanobacteria thrived in the water surface, fuelling primary productivity. The ε_{por} values in Peri-Tethys exhibits that nutrient availability was dominantly relied on the terrestrial riverine, which was intensified by accelerated hydrological cycle during the PETM.

Chapter 6

The carbon isotope pattern of marine algal biomarkers, with a new record of PETM sea surface temperature

Preface

This chapter is under preparation and modification for submission as an article to *EPSL*. The lead author of the paper is LB. LB carried out analysis (unless stated), interpreted the organic geochemical data set and wrote the chapter. RP and DN made comments and suggestions on the initial draft made by LB. Total lipid extraction, GC-MS and LC-MS analyses of some of the Kheu River sediments were performed by K. Taylor and R. Rees-Owen (as published in (Dickson et al., 2014b)). Sediment samples were provided by A. Dickson (Royal Holloway University of London).

Abstract

The Paleocene-Eocene thermal maximum (PETM) corresponds to a massive release of ^{13}C-depleted carbon to the ocean-atmosphere system. However, the magnitude of the carbon isotope excursion (CIE) varies widely between different PETM records and is suspected to be biased through various factors, i.e. physiological, regional or local climate factors. Assessing the magnitude of these factors for individual records provide insights towards the calibration of the CIE records, leading to better understanding of the duration and magnitude of the PETM carbon cycle perturbation. Here, we analyse a range of marine biomarkers for compound specific $\delta^{13}C$ in Paleocene-Eocene sediments from the northern Peri-Tethys (Guru-Fatima and Dzhengutay sections). These $\delta^{13}C$ records are combined with TEX_{86}-based sea surface temperature (SST) estimates from the Kheu River section, providing the first record of SST estimates for the PETM from the northern Peri-Tethys. Collectively, these data demonstrate that isotopic fractionation was stimulated by marine algae during the PETM and performed an important role in the response to the perturbated carbon cycle. The magnitude of fluctuation is varied between pristane and phytane, likely due to biological differences. In Guru-Fatima the

$\delta^{13}C_{Pr}$ and $\delta^{13}C_{Ph}$ CIE is likely influenced by enhanced marine productivity and physiological factors, while in Dzhengutay where marine productivity is relatively less, $\delta^{13}C_{Pr}$ and $\delta^{13}C_{Ph}$ demonstrate more ^{13}C depleted values. Distribution of GDGTs at Kheu River indicate relatively high SSTs during the PETM (TEX_{86}^{H}-SST~37°C), with a 6°C cooling at the end of the PETM.

6.1. Introduction

The Paleocene-Eocene Thermal Maximum (PETM) (Kennett and Stott, 1991) is the most pronounced hyperthermal event of the Cenozoic. The PETM occurred ~56 million years ago (Ma) and lasted for ~120–220 ka (reviewed by McInerney & Wing, 2011). The key feature of the PETM is an abrupt increase in global temperature, which is expressed in the negative excursion of foraminiferal $\delta^{18}O$ (Cramer et al., 1999; Fricke et al., 2004; Kennett and Stott, 1991; Kozdon et al., 2011; Thomas et al., 1999; Zachos et al., 2006, 2003, 2001), increase in foraminiferal Mg/Ca ratios (Tripati and Elderfield, 2005; Zachos et al., 2003) and relative increase in TEX_{86}, based on the distribution of sedimentary isoprenoid glycerol dibiphytanyl glycerol tetraethers (isoGDGTs) (Frieling et al., 2014; Sluijs et al., 2006; Sluijs et al., 2014, 2011). Although theses proxies and their attributed paleotemprature calibrations are influenced by local factors and come with their own uncertainties, they all infer an increase of 4 to 8°C in sea surface temperature (SST) during the PETM. A similar change in temperature (5–8°C) is recorded on land (Fricke et al., 2004; Koch et al., 2003; Sluijs et al., 2014; Weijers et al., 2007; Wing et al., 2005). The warming trend is coincident with a negative carbon isotope excursion (CIE), indicating a massive and rapid injection of isotopically light carbon into the ocean-atmospheric system (e.g. Dickens et al., 1997; Pagani et al., 2006; Panchuk et al., 2008; Zachos et al., 2005; Zeebe et al., 2009). Despite a range of hypotheses (Deconto et al., 2012; Dickens et al., 1997, 1995b; Gutjahr et al., 2017; Higgins and Schrag, 2006; Kurtz et al., 2003; Svensen et al., 2004; Westerhold et al., 2009), the source, magnitude and mechanism of this carbon release is an ongoing debate (reviewed by McInerney & Wing, 2011), hindering a holistic understanding of the carbon cycle during the PETM. One of the problems is that the records of the CIE vary widely. The mean magnitude of CIE not only varies in different realms; i.e. –4.7±1.5 ‰ in terrestrial records and –2.8±1.3 ‰ in marine deposits, but also differs within carbon types; i.e. bulk marine carbonate (–2.7±1.1 ‰), soil carbonate (–5.5±1.7 ‰), bulk marine organic carbon (–4.1±2.2 ‰), bulk organic soil matter (–3.5±0.6 ‰), benthic

foraminifers (–2.5±1.0 ‰), and planktic foraminifers (–2.7±1.0 ‰) (reviewed in McInerney and Wing, 2011). These variations are driven by one or a combination of different factors e.g. changes in the isotopic composition of the carbon source, mixed components with different $\delta^{13}C$, changes in isotope fractionation through physiological changes (Sluijs and Dickens, 2012), regional or local climate factors. For instance, $\delta^{13}C_{TOC}$ in marine sediment is influenced by changes in the amount of terrestrial input (Hilting et al., 2008), diagenesis (J. M. Hayes et al., 1989), and/or high organic matter preservation (high TOC) and burial of more depleted organic matter.

Therefore the magnitude of CIE across the PETM remains uncertain (Dickens, 2011). Assessing the magnitude of these biases using individual biomarker records of $\delta^{13}C$ (that are not influenced by biases due to terrestrial input) provide insights into the duration and magnitude of the carbon cycle perturbation (PETM carbon cycle). However, there are only a few marine compound specific $\delta^{13}C_{organic}$ records available for the PETM. Kodina et al., (1995) presents $\delta^{13}C_{isorenieratane}$, $\delta^{13}C_{pristane,}$ $\delta^{13}C_{phytane}$ and $\delta^{13}C_{chroman}$ from black shales of the Kurpai PETM section in the eastern Causcus (central Asia), although pre-PETM measurements and therefore CIE is not recorded. A $\delta^{13}C$ record of 4,24-dimethylcholestan-3-one from the Aktumusk PETM section in the eastern Causcus (central Asia) (Bolle et al., 2000), although data from the pre-PETM data is not sufficient to resolve the magnitude of the CIE. Pagani et al., (2006b) analysed the $\delta^{13}C$ records of marine derived *n*-alkanes ($\delta^{13}C_{17}$) in the central Arctic Ocean (ODP Site 302), although the CIE recorded $\delta^{13}C_{17}$ is suspected to be biased by an increased marine productivity during the PETM. The record of $\delta^{13}C_{crenarchaeol}$ in the North Sea spans the PETM, although suspected to be influenced depth-dependant variations (Schoon et al., 2013). The study of single-species $\delta^{13}C_{dinoflagellate\ cyst}$ (Bass River) reveals variation in the $\delta^{13}C$ values of different species, but is likely biased by ecological factors (Sluijs et al., 2018). Here we provide new insights into the PETM carbon perturbation, by investigation the magnitude of marine CIE records of $\delta^{13}C_{pristane}$ and $\delta^{13}C_{phytane}$ of marine sections from the margins of northern Peri-Tethys. We also present a TEX_{86}-based sea surface record, as the first record of PETM SST in the northern Peri-Tethys.

6.2. Samples and Methods

6.2.1. Sampling of the PETM sections

The occurrence of the PETM throughout the northern Peri-Tethys realm is commonly associated with the deposition of organic-rich sediments. Collectively, Paleocene-Eocene

organic rich shales can be traced across about 2500 km, from Central Asia to the Caucasus (e.g. Gavrilov et al., 2009, 2003), including the Guru-Fatima section located in the eastern (Central Asia) region, and Dzhengutay also Kheu River sections located in the western (Caucasus) regions (Figure *6.1*) which are studied here.

The Kheu River (KR) section is comprised of organic-lean silty claystones (<1 wt.% TOC) with an intermediate organic rich shale (mean 5 wt.% TOC; Figure *6.2*) (Dickson et al., 2014b). Elemental sulfur values also increase from <1 wt.% in the organic lean sections to ~4 wt.% in the organic rich horizon. A bulk $\delta^{13}C_{org}$ excursion of –4.5‰ is expressed in the section, with values decreasing from around –26‰ in the organic lean sediments to ~–30.5 ‰ in the organic rich horizon, representing the PETM (Dickson et al., 2014). Kheu River sediments were obtained from an outcrop exposure that had been cut back to avoid exposed materials and are the same as reported in Dickson et al. (2014).

The Guru-Fatima section is comprised of grey calcareous mudstone (<1 wt.% TOC), overlain by an organic rich shale horizon (7–20 wt.% TOC), which is covered by a laminated mudstone (~3 wt.% TOC) and an organic lean mudstone (<1 wt.% TOC (*Figure 6.3*, Dickson et al., 2014). Elemental sulfur increases from <1 wt.% in the deepest and top horizons to 3 wt.% in the organic rich horizon (*Figure 6.3*). The PETM is characterized by a bulk $\delta^{13}C_{org}$ CIE of –4‰ in the section, with values of –26‰ in the deepest horizon (grey calcareous marls), –30‰ in the organic rich shale and –28‰ in the overlying laminated mudstone (Dickson et al., 2014; *Figure 6.3*). Guru-Fatima sediments were sampled from an archived drill core at the Geological Institute of the Russian Academy of Science.

The Dzhengutay section is comprised of calcareous mudstone (<1 wt.% TOC) with an intermediate organic rich shale horizon (~3.5 wt.% TOC) ((Dickson et al., 2014b), Figure *6.4*). The elemental sulfur content also increases from non-detectable values in the calcareous mudstone to ~1 wt.% in the organic rich horizons. The PETM is reflected in a bulk $\delta^{13}C_{org}$ excursion of –4‰ in the section, with values of –26‰ in the calcareous mudstone and –29‰ in the intermediate organic rich shale (Figure *6.4* (Dickson et al., 2014b)). Dzhengutay sediments were sampled from an outcrop exposure that had been cut back significantly to prevent potentially degraded and contaminated surface sediments from impacting biomarker analyses.

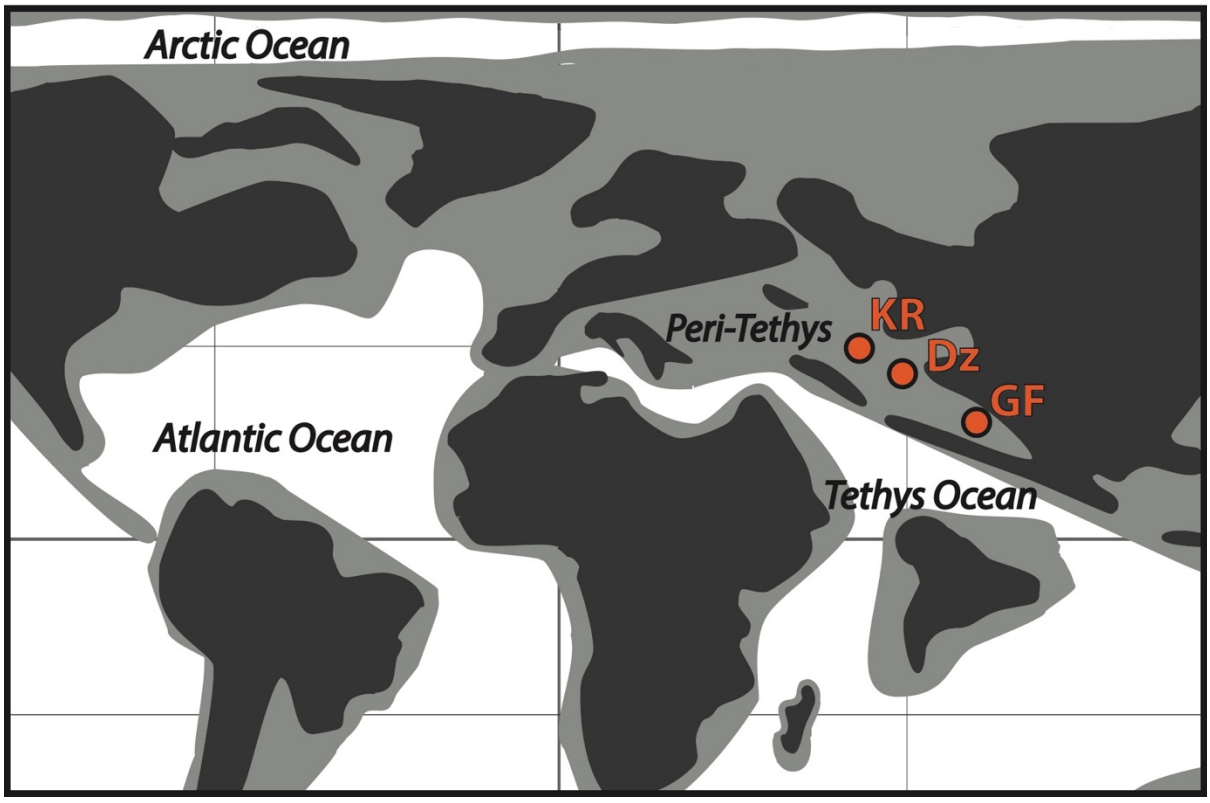

Figure 6.1. Schematic of the Paleocene-Eocene map, highlighting the location of Kheu River (KR), Dzhengutay (Dz) and Guru-Fatima (GF). Based on paleogeographic reconstructions from www.scotese.com

6.2.2. Analytical methods

Biomarker analyses were conducted on a total of 29 samples, including 13 from Dzhengutay, 10 from Guru-Fatima and 6 from Kheu River. Biomarkers in Kheu River sediments have been previously published (Dickson et al., 2014), but here we expanded the sample set and report new data on the distribution of GDGTs and TEX_{86}-based SSTs.

6.2.3. Biomarker extraction and separation

The methods for the Kheu River biomarker extraction, separation and analysis are explained in Dickson et al. (2014b). In addition to these, six organic lean sediments from pre and post PETM sections were analysed. To obtain TLEs from the organic lean sediments, higher volumes (~30g) of sediments were extracted with 220ml of a dichloromethane (DCM): methanol (MeOH) (1:1, vol) azeotrope using a Soxhlet apparatus for 24 hrs.

To obtain total lipid extracts (TLEs) from Guru-Fatima section and Dzhengutay, about 5g of sediments were extracted with 10ml of dichloromethane (DCM): methanol (MeOH) (1:1, vol) by micro microwave-assisted method (MILESTONIE Ethos Ex Microwave solvent extraction). The microwave program consisted of a 10 min ramp to 70°C (max. 1000 W), followed by a 10 min hold at 70°C (max. 1000 W) and 20 min cooling period. After microwave extraction the samples were centrifuged (1500 rpm, 5 minutes) and the resulting supernatant collected. An additional 10 ml of DCM:MeOH were added to the sediment, centrifuged, and the supernatant again collected. Solvent-washed activated copper turnings were added to the TLE for 24 hrs to remove elemental sulfur. The TLE was then concentrated using rotatory evaporator. Samples with a higher TOC content (>1 wt.%) were separated into three fractions (aliphatic, aromatic and polar) using short (4 cm) silica gel open column chromatography. Aliphatic, aromatic, and polar fractions were eluted using 3 ml of hexane, 4 ml of hexane:DCM (3:1) and 4 ml of DCM:MeOH (1:2), respectively. All fractions were then dried under a gentle stream of N_2. Samples with lower TOC content (<1 wt.%) used for GC-MS analysis as TLEs.

To analysis glycerol dialkyl glycerol tetraether (GDGTs) the polar fractions or TLEs were dissolved in hexane:IPA (99:1) and passed through a 0.45 μm PTFE filter by a syringe with a bayonette adaptor.

6.2.4. Biomarker analysis

Biomarker distributions in the aliphatic fraction were determined using a Thermo Scientific^{TM} ISQ Series Single Quadruple GC-MS system. Separation of compounds was carried out on a Zebron non-polar column (50 m x 0.32 mm, 0.10 μm film thickness), with He a carrier gas and an injection volume of 1 μl. The GC programme was: injection at 70 °C (1 min hold), heating to 130°C at a rate of 20°C/min, then to 300°C at 4°C/min, followed by a 24 min hold. The mass spectrometer continuously scanned between *m/z* 50 and 650, and identification of biomarkers was carried out based on published retention times and spectra as well as comparison with standard samples.

Distribution of large organic molecules of GDGTs in the polar fraction was determined using a High Pressure Liquid Chromatography-atmospheric pressure chemical ionisation-Mass Spectrometry (HPLC-APCI-MS) with a ThermoFisher Scientific Accela Quantum Access triple quadrupole MS in selected ion monitoring mode. Normal phase separation achieved with two HPLC BEH HILIC columns (2.1 mm x 150 mm, 1.7 μm i.d) at a flow rate of 0.2 ml/min. The initial solvent hexane:iso-propanol (IPA) (98.2:1.8) eluted isocratically for 25 min,

followed by an increase in solvent polarity to 3.5% IPA in 25 min, and then by a sharp increase to 10% IPA in 30 min (Hopmans et al., 2016). After separation, to analyse isoprenoid and branched GDGTs, Selection Ion Monitoring (SIM) was performed at *m*/*z*: 1302, 1300, 1298, 1296, 1294, 1292, 1050, 1048, 1046, 1036, 1034, 1032, 1022, 1020, 1018, 744, 659 to increase the sensitivity and reproducibility. Distribution of GDGTs was analysed in the respective molecular ion (M^+) chromatograms.

Compound specific $\delta^{13}C$ of the saturated hydrocarbon fraction was determined using an Agilent Industries 7890A gas chromatograph coupled to an IsoPrime 100 GC-combustion-isotope ration MS (GC-C-IRMS) system. Samples were injected onto a capillary column (50 m x 0.32 m, 0.17 μm film thickness) using He for carrier gas. The GC oven temperature programme was the same as for GC-MS analyses. Samples were measured in duplicate and the presented value reflect the mean of duplicates. $\delta^{13}C$ values were converted to Vienna Peedee Belemnite (VPDB) by bracketing with an in-house gas (CO_2) of known $\delta^{13}C$ value. Instrument stability was monitored by regular analysis of an in-house fatty acid methyl ester standard mixture; long-term precision is ± 0.3‰.

6.3. Results

6.3.1. Aliphatic compounds

As previously reported (Dickson et al., 2014b), the apolar fraction of PETM sediments from Kheu River contains abundant *n*-alkanes (C_{17}-–C_{35}), isoprenoids (pristane, phytane, lycopane), and hopanes (C_{27}-C_{31}, ββ, αβ and βα isomers), as well as steranes (C_{27}–C_{29}) and subordinate abundances of steranes. Of interest to this project is the hopane distribution. The average C_{31} hopane maturity index ($C_{31}\ \frac{\beta\beta}{\beta\beta+\beta\alpha+\alpha\beta}$) is 0.7, indicating that the organic matter is relatively thermally immature (Figure *6.2*), also the degree of hopane isomerisation 22S/(22S+22R) (Mackenzie et al., 1980) indicate relatively low thermal maturity in Kheu River (~0.03).

The aliphatic fraction from the Guru-Fatima section contains *n*-alkanes (C_{16}–C_{35}), isoprenoids (pristane, phytane and lycopane), steranes (ααα isomers of C_{27}–C_{29} also methyl sterane) and hopanes (C_{27}–$C_{32,}$ dominated by αβ isomers). The average ratio of the short to long chain *n*-alkanes [C_{17}/(C_{17}+C_{31})] in the organic rich horizon is ~1, being (slightly) higher than pre-PETM (~0.8) and post-PETM (~0.2), *Figure 6.3*. The odd-over-even carbon number predominance (CPI) of the long chain (C_{25}–C_{37}) *n*-alkanes during the PETM is ~1 and is relatively lower than pre-PETM (~1.4) and post PETM (~2). Predominance of long and short

chain odd number n-alkanes are characteristic of terrestrial (Rieley et al., 1991) and marine (Jaffé et al., 2001) source of organic matter, respectively. Therefore, Terrestrial_Aquatic Ratio (TAR), $(C_{27}+C_{29}+C_{31})/(C_{15}+C_{17}+C_{19})$, (Bourbonniere and Meyers, 1996) is established to investigate the changes in the relative contributions of organic matter from terrestrial and marine source; i.e. if the source of organic matter is terrestrial; TAR>1. Generally, TAR values in Guru Fatima remain<1 through the whole interval from pre- to post-PETM, and do not show any changes during the PETM. The hopane maturity index ($\frac{\beta\beta}{\beta\beta+\beta\alpha+\alpha\beta}$) is not measurable, as ββ isomers are not detected, possibly due to relatively high thermal maturity of the host rock. The degree of hopane isomerisation 22S/(22S+22R) (Mackenzie et al., 1980) in Guru Fatima is ~0.4, indicating higher thermal maturity than Kheu River sediments.

The aliphatic hydrocarbon fractions from the Dzhengutay contain *n*-alkanes (C_{16}–C_{35}), isoprenoids (pristane, phytane and lycopane), steranes (ααα isomers of C_{27}–C_{29} also methyl sterane) and hopanes (C_{27}–C_{32}, dominated by αβ isomers). The ratio of the short to long chain *n*-alkanes [$C_{17}/(C_{17}+C_{31})$] is not measurable prior to- and after the PETM, but has relatively higher and variable values of ~0.8 in the black shale horizon. The long-chain *n*-alkanes are not detectable in pre- and post-PETM sediments, but in the organic rich horizon during the PETM have a slight odd-over-even carbon number predominance (CPI~1.4; Figure *6.4*). TAR value is generally <1 where the peaks are strong enough to calculate. Similar to Guru Fatima, the ββ isomers are not detected in the hopane distribution and therefore hopane maturity index ($\frac{\beta\beta}{\beta\beta+\beta\alpha+\alpha\beta}$) is as low as 0, indicating the relatively high maturity of the host rock. The degree of hopane isomerisation 22S/(22S+22R) (Mackenzie et al., 1980) at Dzhengutay is ~0.4, indicating a similar thermal maturity as Guru Fatima sediments, although both sections are thermally more mature than Kheu River.

6.3.2. Distribution of GDGTs

The polar fractions from Kheu River contained isoprenoid GDGTs, but branched GDGTs were not detected. Isoprenoid GDGTs are dominated by crenarchaeol and crenarchaeol regioisomer (Figure *4.2*, in chapter 4). GDGTs were not detected in pre-PETM samples. To reconstruct SST, TEX_{86}^{H} applied (Kim et al., 2010). TEX_{86}^{H} derived SST involves a combination of GDGT-1, GDGT-2, GDGT-3 and Crenarchaeol isomer (Cren.′) (numbers refer to different GDGTs and are shown in the appendix). GDGT index-2 is defined as below:

$$TEX86 = \frac{(GDGT-2)+(GDGT-3)+(Cren.')}{(GDGT-1)+(GDGT-2)+(GDGT-3)+(Cren.')}$$

TEX_{86}^{H}-SST= 68.4 × (log (TEX86)) + 38.6 (calibration error: ± 2.5 °C)

Samples from Guru-Fatima and Dzhengutay did not contain GDGTs (neither isoprenoid nor branched GDGTs), likely arising from the higher thermal maturity of these sediments (Schouten et al., 2004).

6.3.3. Compound specific $\delta^{13}C$

The $\delta^{13}C$ values of pristine (Pr), phytane (Ph) and *n*-Alkane C_{17} were measured in Guru-Fatima and Dzhengutay. The $\delta^{13}C_{Pr}$ and $\delta^{13}C_{Ph}$ in both sections show more depleted values through the PETM, comparing to pre- and post PETM. In Guru-Fatima, $\delta^{13}C_{Pr}$ expresses a ~–4.6 ‰ excursion during the PETM, with values decreasing from ~–29.8 ‰ to ~–34.4 ‰, while $\delta^{13}C_{Ph}$ decrease from ~–30‰ to ~–32.9 ‰ (~–2.9 ‰ excursion), *Figure 6.3*. Due to low abundance of biomarkers in pre- and post-PETM sediments of Dzhengutay, it was not possible to obtain compound specific $\delta^{13}C$ from these intervals. $\delta^{13}C_{Pr}$ and $\delta^{13}C_{Ph}$ are only detected in the organic rich horizon, therefore analysing the CIE is not achievable. The values of $\delta^{13}C_{Pr}$ (~–35 ‰) and $\delta^{13}C_{Ph}$ (~–34 ‰) in Dzhengutay are lighter than those of recorded in the organic rich horizon of Guru-Fatima.

A)

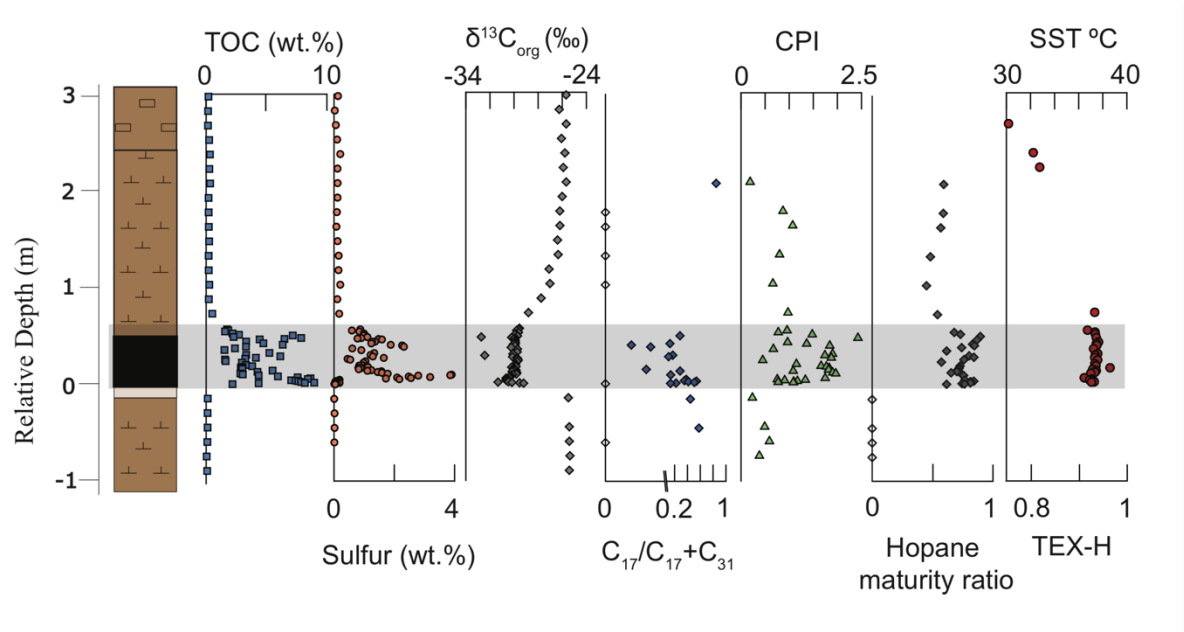

B)

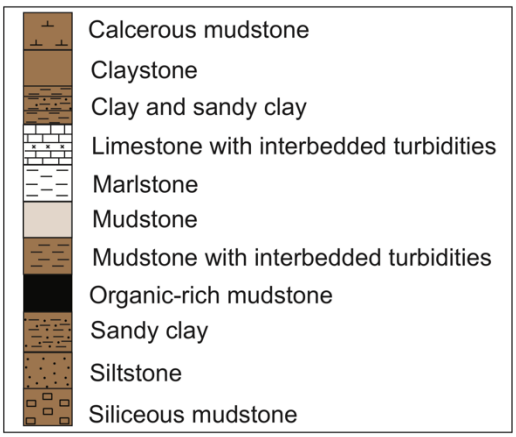

Figure 6.2. A) Kheu River section, relative depth is based on the sample expressing the start of the PETM CIE. Bulk geochemical data are from (Dickson et al., 2014b). Total organic carbon (TOC) content, sulfur content, bulk $\delta^{13}C_{organic}$, the ratio of short and long chain n-alkanes, CPI, hopane ration, SST °C based on TEX-H. Grey box highlights PETM. B) Legend of lithology symbols used in this chapter.

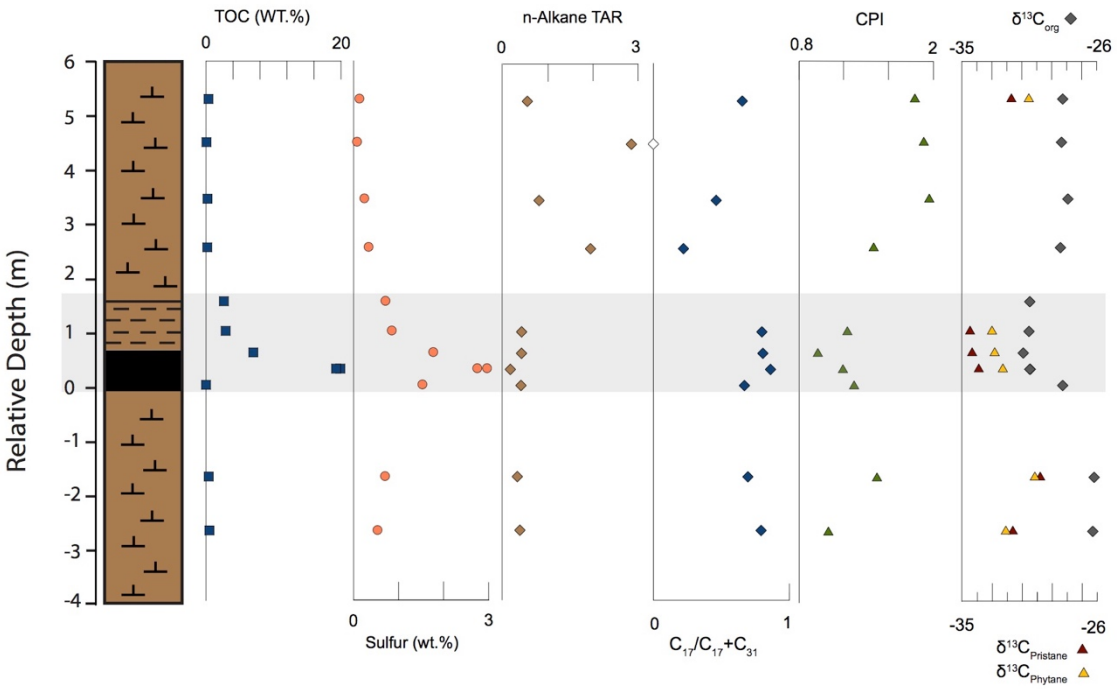

Figure 6.3. Guru-Fatima section, relative depth is based on the sample expressing the start of the PETM CIE. Bulk geochemical data are from (Dickson et al., 2014b). Total organic carbon (TOC) content and sulfur content, TAR, the ratio of short and long chain n-alkanes, CPI, the ratio of steranes/hopanes, bulk $\delta^{13}C_{organic}$ (grey diamond), compound specific $\delta^{13}C_{Pr}$ (red triangle) and $\delta^{13}C_{Ph}$ (yellow triangle). The lithology symbol key is in Figure 6.2 (B).

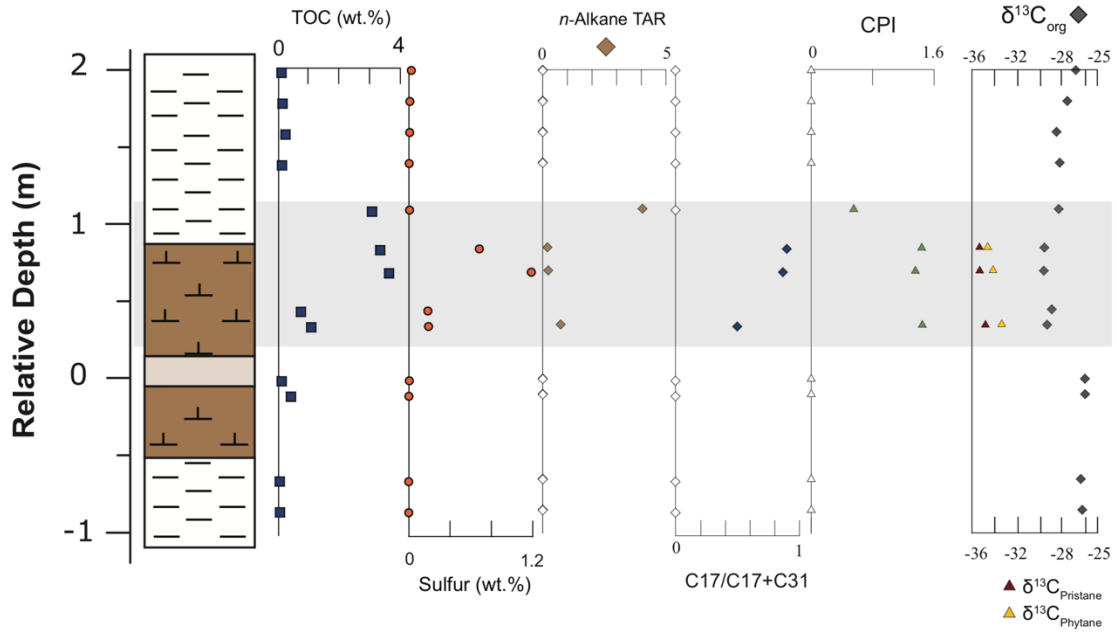

Figure 6.4. Dzhengutay section, relative depth is based on the sample expressing the start of the PETM CIE. Bulk geochemical data are from (Dickson et al., 2014b). Total organic carbon (TOC) content and sulfur content, TAR, the ratio of short and long chain n-alkanes, CPI, the ratio of steranes/hopanes, bulk $\delta^{13}C_{organic}$ (grey diamond), compound specific $\delta^{13}C_{Pr}$ (red triangle), $\delta^{13}C_{Ph}$ (yellow triangle). The lithology symbol key is in Figure 6.2 (B).

6.4. Discussion

6.4.1. How the Peri-Tethys sea surface temperature (SST) changed during and after the PETM?

Isoprenoid glycerol dibiphytanyl glycerol tetraethers (GDGTs), widespread in marine environment, are mainly biosynthesised by a dominant group of marine planktonic archaea (Thaumarchaeota) (See review Schouten et al., 2013). GDGTs are well established as a proxy for reconstruction of sea surface temperature (e.g. Kim et al., 2010; Schouten et al., 2002, 2013; Taylor et al., 2013). However, GDGTs are sensitive to thermal maturation, and degrade when biomarker parameters indicate some levels of thermal maturities, i.e. hopane (ββ/ββ+αβ+βα) ratio <0.5 (Schouten et al., 2004). Therefore, the absence of GDGTs in Guru-Fatima and Dzhengutay is likely caused by high thermal maturity of these sediments which leads to the degradation of GDGTs. In Guru-Fatima and Dzhengutay sediments thermal maturity is quite high (Tmax ~ 435°C in Guru Fatima) and the biological isomers of hopane (ββ) are not detected; i.e. hopane (ββ/ββ+αβ+βα) ratio is 0. However, Kheu River sediments are less mature, hopane (ββ/ββ+αβ+βα) ratio>0.5 (~0.6 and ~0.8 in post-PETM and PETM sediments, respectively; the difference is possibly related to the mineral matrix effects (Peters and Moldowan, 1991)), and GDGTs are detected in the PETM and post-PETM.

The distribution of isoprenoid GDGTs varies between sub-tropical and sub-polar sediments and crenarchaeol regioisomer (Cren.′) seems to be a more important factor in sub-tropical temperature adaption, rather than in sub-polar. Therefore, two different calibrations are recommended; TEX_{86}^{H} for SST estimated to be >15°C and TEX_{86}^{L} for SST estimated to be <15°C (Kim et al., 2010). Considering that global temperature was high during the PETM (e.g. Frieling et al., 2014; Sluijs et al., 2011; Sluijs et al., 2006, 2014), TEX_{86}^{H} is the more appropriate calibration for PETM sediments. Moreover, the SST estimations of $\delta^{18}O$ of planktonic foraminifera from PETM sediments from Wilson lake in New Jersey (Zachos et al.,

2006) shows more agreement with TEX_{86}^{H} -SST, rather than TEX_{86}^{L}-SST (Kim et al., 2010), also TEX_{86}^{H} calibration generates more realistic pre-PETM and PETM SST comparing to TEX_{86}^{L} in Gulf of Mexico (Sluijs et al., 2014). Here we applied TEX_{86}^{H} calibration to convert TEX_{86} values to SST.

The TEX_{86}^{H} -SST indicate PETM SSTs to be consistently warmer than post PETM intervals (*Figure 6.2*). TEX_{86}^{H}-SST values seem to be converged at 37°C during the PETM and decrease to 31°C towards the post PETM (*Figure 6.2*). The organic lean nature of the pre PETM sediments at Kheu River, did not allow an estimate of pre-PETM SST. However, we found evidence for a substantial SST cooling (~6°C) after the PETM, such as argued before in other PETM intervals (e.g. Frieling et al., 2014; Sluijs et al., 2014, 2011; Zachos et al., 2006). SST cooling occurs simultaneously with the recovery $\delta^{13}C_{org}$ towards the pre-PETM values and a significant reduction in carbon burial (TOC); and right after the organic-rich interval (*Figure 6.2*). We contend that the substantial photosynthesis and enhanced marine productivity in the Peri-Tethys during the PETM (Dickson et al., 2014; Chapter 5 of this thesis) played a rule in consuming the excessive atmospheric CO_2. Following the drop of pCO_2, temperature decreased (SST cooling trend, ~6°C), *Figure 6.2*.

In the previously studied PETM sections where SST from both pre- and post-PETM are available, the pre-PETM values are slightly different (warmer) from the post-PETM SST. For instance, the PETM sequence in marine sediments of the Arctic region (Site 302-4A), where SST rose from 18°C to over 23°C and subsequently decrease to 17°C by end of the event (Sluijs et al., 2006) or in the Gulf of Mexico, where SST rose from 29°C to 35°C during the PETM, followed by a cooling to ~26–27°C in the post PETM sequence (Sluijs et al., 2014). Leading to estimate that Peri-Tethys SST warmed up for ~5–6°C during the PETM. Although our record of PETM SST is novel in the Tethyan mid-latitude (Kheu River paleolatitude ~ 40°N; Winguth et al., 2012) and Peri-Tethys region, estimated warming of ~5–6°C is similar or slightly different comparing to the PETM record of the mid-latitude Atlantic; i.e. warming of 6°C in the Harrell Core, Gulf of Mexico ~32°N (Sluijs et al., 2014), or at higher latitudes i.e. 7°C (to ~27°C) in the epicontinental west Siberian sea (paleolatitude ~58°N) (Frieling et al., 2014). Although TEX_{86}^{H} has a calibration error of 2.5°C, SST of 37°C in the Kheu River is higher than the HadCM3L climate model that reconstructs the global mean surface temperature anomaly for the PETM (Donkley Jones et al., 2013).

6.4.2. Stable carbon isotope patterns of marine biomarker lipids (pristane and phytane) during the PETM

To evaluate the response of marine organisms across the PETM in the Peri-Tethys Ocean, we analysed the carbon isotopic composition of TOC and marine derived biomarkers; i.e. pristane (Pr: 2,6,10,14-tetramethylpentadecane) and phytane (Ph: 2,6,10,14-tetramethylhexadecane), as common biomarkers in geological records. Pr and Ph are presumed to predominantly originate from the phytyl side chain of chlorophyll pigments (Li et al., 1995; Volkman and Maxwell, 1986). Chlorophyll and therefore Pr and Ph originate from either marine or terrestrial photosynthesis organisms. However, in the northern Peri-Tethys setting, the biomarker records do not support a predominant contribution of terrestrial organic matter, specifically during the PETM when the marine productivity is highly pronounced. As discussed in chapter 5, an increased marine productivity and domination of marine source organic matter in the pre-Tethys during the PETM is evidenced by a general increase in the ratio of marine to terrestrial organic matter during the PETM as expressed in $C_{17}/(C_{17}+C_{31})$ ratio, although less obvious in Guru Fatima. Similarly, is the Terrestrial_Aquatic Ratio (TAR) which is generally at the marine threshold in the Peri-Tethys sections (*Figure 6.3* and Figure *6.4*). Therefore, we argue that Pr and Ph in Guru-Fatima and Dzhengutay are predominantly originate from marine algae, rather than originating from a terrestrial source.

In Guru-Fatima, $\delta^{13}C_{Pr}$ and $\delta^{13}C_{Ph}$ express a negative CIE at the onset of the PETM, similar to what is reflected in $\delta^{13}C_{TOC}$ (*Figure 6.3*). The negative CIE for $\delta^{13}C_{Pr}$ and $\delta^{13}C_{Ph}$ are ~–4.6‰ and ~–2.9‰, respectively. These negative excursions in $\delta^{13}C_{Pr}$ and $\delta^{13}C_{Ph}$ reflect an enhanced isotopic fractionation by marine algae as primary producers during the PETM.

Although diagenesis factors alter the isotopic composition by 3‰ (Hayes et al., 1989) however the individual biomarkers of the photosynthesis organisms and primary production are expected to be less influenced (Hayes, 1993). Therefore, the difference (1.7‰) between the magnitude of CIE of $^{13}\delta C_{Pr}$ (–2.9‰) and $\delta^{13}C_{Ph}$ (–4.6‰), could be attributed to the biological factors, similar to what is recorded in different dinoflagellate cyst species (Sluijs et al., 2018). The recorded CIEs ($\delta^{13}C_{Pr}$ and $\delta^{13}C$) in Guru Fatima are in the same range as the previously reports of compound specific records during the PETM. The record of $\delta^{13}C_{17}$ in the PETM depositions of Arctic ocean record a CIE of –3.6‰, although a larger CIE is expected and the $\delta^{13}C_{17}$ values during the PETM are suspected to be influenced by physiological factors (Pagani et al., 2006b). The record of glycerol dipiphytanyl glycerol tetraether lipids (GDGTs) in the North Sea record a magnitude of –3.6‰, although these GDGT $\delta^{13}C$ values are suspected to be underestimated as are potentially masked by glacially disturbed intervals (Schoon et al.,

2013). Although the study on the magnitude of CIE based on single-species dinoflagellate cyst, reflect the high influence of biological factors on their response to pCO_2, the values vary between ~–2‰ and ~–4‰ (Sluijs et al., 2018). Unfortunately, the reports of compound specific $\delta^{13}C$ from the PETM horizons of Peri-Tethys; in Kurpai (Kodina et al., 1995) and Aktumusk (Bolle et al., 2000); obtaining the record CIE from marine algae was not plausible (due to the lack of marine compound $\delta^{13}C$ from pre-PETM sediments) to compare.

$\delta^{13}C_{TOC}$ demonstrated the same CIE values (~–4‰) in either Dzhengutay and Guru Fatima. However, the $\delta^{13}C_{Pr}$ (~–35 ‰) and $\delta^{13}C_{Ph}$ (~–34 ‰) obtained from the Dzhengutay organic rich horizon (Figure *6.4*), are more depleted (~1‰) than those of recorded in the organic rich horizon of Guru-Fatima. The relatively heavier $\delta^{13}C_{Pr}$ and $\delta^{13}C_{ph}$ values (more ^{13}C-enriched) in Guru-Fatima comparing to Dzhengutay, could be caused by the physiological factors; i.e. increase in the volume of surface area of cells and algal growth rate (Popp et al., 1998) that overwhelms the influence of the injected light carbon to the environment (as occurred during PETM). This has been also invoked for the $\delta^{13}C_{17}$ in the Arctic PETM section, where the marine sourced $\delta^{13}C_{17}$ values does not show the expected ^{13}C depletion during the PETM (Pagani et al., 2006b). In Guru Fatima (TOC~20 wt.%), where the $\delta^{13}C_{Pr}$ and $\delta^{13}C_{Ph}$ are less depleted than Dzhengutay (TOC~4 wt.%), TOC and therefore marine productivity (Dickson et al., 2014; also discussed in chapter 5) are also more enhanced during the PETM (*Figure 6.3* andFigure *6.4*). Accordingly, we argue that the enhanced algal production and the attributed physiological factors could be the reason for the Guru Fatima record of less algal $\delta^{13}C$ depletion as well. Considering the record of TOC and $\delta^{13}C$ Guru Fatima and Dzhengutay, it seems that enhanced marine productivity plays an important role in the response of carbon cycle to the perturbation in carbon cycle.

6.5. Conclusion

Our results ($\delta^{13}C_{Pr}$ and $\delta^{13}C_{Ph}$) demonstrate that during the PETM, isotopic fractionation was enhanced by marine algae, and plays an important role in the response to the perturbated carbon cycle. However, this was influenced by enhanced marine productivity and physiological factors. The TEX_{86}^{H}-SST values indicate a decrease of SST from 37°C during the PETM to 31°C towards the post PETM in the northern Peri-Tethys. We conclude that the substantial photosynthesis and enhanced marine productivity in the Peri-Tethys during the PETM played

an important role in consuming the excessive atmospheric CO_2. Following the drop of pCO_2, temperature decreased (SST cooling trend, ~6°C).

Chapter 7

Conclusions and future work

Preface

This chapter presents an overall conclusion on development of marine anoxia, based on the collection of data from different time intervals (presented and discussed in Chapters 3–6). The main objective of this thesis was to gain a better insight into the factors involved in development of anoxia during warm climates. For this purpose, a range of biomarkers was used, with emphasises on isorenieratane and lycopane. Given that warm climates amplify anoxia, SST variation was also calculated throughout these sections by applying TEX_{86}. This conclusion provides a context for the future investigations on the triggers and consequences of marine anoxia.

7.1 Answering research questions and presenting a context for the future work

Here is a brief summary of the thesis answers to the specific questions discussed in chapter 1, alongside with a context for future explorations.

7.1.1. To assess the drivers of anoxia and redox variability in the proto-South Atlantic basin during the Aptian

As discussed in chapter 3, the variations in redox conditions in the northern South Atlantic was reconstructed by high-resolution bulk geochemical and biomarker data from DSDP Site 364 (Figure 3.1.). During the Aptian, the South Atlantic was a restricted basin in its early opening phase. However, the high-amplitude fluctuations in redox condition (apparent in TOC, TS and HI) indicate that the restricted morphology of the basin *per se* did not cause anoxic conditions but instead preconditioned the basin for development of anoxia during episodes of enhanced OM production and export. The development of anoxic conditions in the water column,

including photic zone euxinia that sometimes extended to very shallow water depths (<15 m), is evidenced by the presence of the biomarkers such as lycopane, isorenieratane, and chlorobactene. Time series analyses of the high-resolution TOC dataset (Fig. 3.2 and 3.3) indicates that the fluctuating nature of nutrient availability likely resulted from eccentricity-modulated precession changes in weathering and runoff. As the basin morphology changed during the late Aptian–Albian (towards a less restricted basin and/or due to deepening of Site 364), the water column become dominantly oxygenated as evidenced by lack of anoxia biomarkers. Altogether, these results show that anoxia (and photic zone euxinia) only develop when a combination of increased nutrient availability and basin restriction coincide.

7.1.2. To reconstruct sea surface temperature in the proto-South Atlantic basin during the Aptian–late Albian, and the perturbations in the carbon cycle

As discussed in chapter 4, the Aptian–Coniancian sediments of Site 364 (Units 7a to 5), although suffering from numerous coring gaps, allowed a reconstruction of the long-term evolution of the carbon cycle (using $\delta^{13}C_{org}$) and on assessment of the influence of OAEs in the South Atlantic. The record of $\delta^{13}C_{org}$ demonstrates a positive carbon isotope excursion (~2‰) during the Aptian, which I related to the later stages of OAE 1a, dated at ~120 Myr (Fig. 3.4. and 4.1). The characteristic negative excursion is missed in the core gaps. During the late Albian–Early Cenomanian, when the South Atlantic basin was larger and fairly oxygenated, the records of $\delta^{13}C_{org}$ indicate a major negative carbon isotope excursion (~ 3‰) (Fig. 4.1). This excursion (alongside the increase in TOC at Site 364) is potentially the latest Albian "Breistroffer event"; OAE 1d. This indicates that OAE 1d was a strong triggering factor for the development of anoxia in the continental shelf of the South Atlantic when the basin was not restricted (as with OAE 1a).

7.1.3. To reconstruct the spread of photic zone euxinia during the Paleocene-Eocene Thermal Maximum (PETM)

As discussed in chapter 5, a collection of sediments from the margins of north eastern (Guru-Fatima, Kheu River, and Dzhengutay sections), southern (Dababiya section) and western Peri-Tethys (North Atlantic; Zumaia section) made it possible to explore the intensity of anoxia on the Peri-Tethys margin during the PETM. Analysing a range of biomarkers, particularly lycopane and isorenieratane show that photic zone euxinia was widespread in the northern Peri-

Tethys continental shelf (from the east toward west: Guru-Fatima, Dzhengutay, and Kheu River (Figure *5.2*, Figure *5.3*,Figure *5.4*). The lack of anoxia/PZE biomarkers in the southern Peri-Tethys, i.e. Dababiya section, is attributed to the post depositional factors and is not informative of the depositional environment (Figure *5.5*). Similarly, in the western the Peri-Tethys, i.e. upper to mid bathyal sequence of Zumaia, although lack of lycopane and isorenieratane can be caused by degradation during transport and burial, there is no evidence for the development of anoxia/PZE at this basin and it seems that deoxygenation in the Zumaia section only developed to suboxic conditions (as indicated by planktic foraminiferal (Canudo et al., 1995; Molina et al., 1999). Collectively, my results demonstrate that the expansion of anoxia and photic zone euxinia only developed in restricted marginal and epicontinental basins, not in the open marginal settings. This demonstrated the critical importance of basin morphology to amplify nutrient trapping during the PETM. Similar to Site 364 during the Aptian, with the correct basin morphology deoxygenation (anoxia and/or PZE) can developed during climate perturbations (in this case the PETM).

7.1.4. To reconstruct the PETM record of sea surface temperature in the Peri-Tethys

My results (chapter 5) demonstrate that during the PETM, anoxia/euxinia was well developed into the epicontinental basins of NE Peri-Tethys and played an important role in the response to the perturbated carbon cycle. Following that the TEX_{86}^{H}-SST values (chapter 6) indicate a decrease of SST from 37°C during the PETM to 31°C towards the post PETM in the northern Peri-Tethys (Kheu River section, Figure *6.2*). This indicates that the enhanced photosynthetic activity and subsequent increase of marine productivity in the Peri-Tethys (chapter 5) played an important role in consuming the excessive atmospheric CO_2. Following the drop of pCO_2, temperature decreased (SST cooling trend, ~6°C).

7.2. Final Remarks

Considering that the spread of oceanic deoxygenation is expanding exponentially in the modern ocean, more understanding of the factors involved in the spread of anoxia under greenhouse climate is needed. This thesis attempts to make a better understanding of greenhouse climate and hyperthermal events that lead to the spread of marine anoxia. A wide range of biomarkers was used to gain a better insight into the climatic processes and mechanisms that lead to the

spread of marine anoxia during the past warm climates, more specifically the Cretaceous and Paleocene–Eocene. The key interpretations from this study are as follow:

The intensity and persistence of redox variations in the proto South Atlantic during the Aptian–late Aptian was reconstructed, using bulk data and biomarkers. The high preservation of organic matter in the restricted basin and development of anoxia/euxinia, terminated when the basin opening phases continued towards a non-restricted configuration. This confirms the important rule of basin morphology in development of anoxia. However, the high amplitude fluctuations in TOC, HI, TS, lycopane and isorenieratane indicate that basin restriction per se did not cause anoxic conditions to develop but preconditioned the basin. Based on the power spectrum, the fluctuations in marine productivity are resulted from eccentricity-modulated precession changes in the delivery of biolimiting nutrients from weathering and terrestrial runoff. Accompany of enhancement in nutrient availability and basin morphology, not only caused development of anoxia/euxinia it was expanded towards photic zone (photic zone euxinia). Development of anoxia returned to the continental shelves of the basin, triggered by OAE 1d even when the basin was not restricted.

During the PETM, photic zone euxinia was only developed in the restricted marginal and epicontinental basins, and not in the open marginal settings. This is further evidence of high importance of the basin morphology as a nutrient trap for development of anoxia. $\delta^{13}C_{Pr}$ and $\delta^{13}C_{Ph}$ demonstrate that during the PETM, isotopic fractionation was enhanced by marine algae, although the CIE values are different, possibly as a result of biological factors. SST variations during the PETM was calculated for the first time in the Peri-Tethys. TEX_{86}-SST shows a cooling trend from PETM towards the post PETM in the northern Peri-Tethys. The substantial photosynthesis and enhanced marine productivity in the Peri-Tethys during the PETM played an important role in consuming the excessive atmospheric CO_2. Following the drop of pCO_2, temperature decreased (SST cooling trend, ~6°C).

7.2.1. Comparison between OAEs and PETM

Despite many common features that PETM shares with the Mesozoic OAEs, i.e. being associated with warming, changes in the hydrological cycle, terrestrial sediment flux and nutrient inputs to the surface ocean, and algal productivity (Carmichael et al., 2017); the extent of ocean deoxygenation and spread of anoxia/euxinia during the PETM are not as expanded as the Mesozoic OAEs.

For instance during the OAE 2 (93.5 Ma), one the Cretaceous OAEs that is identified globally, seafloor anoxic/suboxic condition was widely established in Southwest Tethys Sea, Atlantic, equatorial Pacific and Indian oceans (Forster et al., 2008; Schlanger et al., 1987; Sepulveda et al., 2009; Sinninghe Damsté and Köster, 1998; Takashima et al., 2010). While during the PETM, the evidence of water column suboxic/anoxic conditions are mainly confined to shelf and marginal marine settings and restricted basins (Bolle et al., 2000; Dickson et al., 2014; Egger et al., 2005; Kopp et al., 2009; Lippert and Zachos, 2007; Nicolo et al., 2010; Pälike et al., 2014; Pardo et al., 1997; Speijer and Wagner, 2002; Stein et al., 2006) and open ocean evidently experienced only a minor deoxygenation, i.e. in the deep Atlantic (Chun et al., 2010; Pälike et al., 2014) and the deep Pacific (Colosimo et al., 2006; Pälike et al., 2014; Zhou et al., 2014). Furthermore, evidence of Photic zone euxinia during the OAE2 are expanded in the South and North Atlantic (Forster et al., 2008; Kuypers et al., 2004; Pancost et al., 2004), Southwest Tethys Sea (Pancost et al., 2004; Sinninghe Damsté and Köster, 1998), the Apennines (Pancost et al., 2004; Sinninghe Damsté and Köster, 1998), Oued Bahloul (Pancost et al., 2004) and Levant Platform (Sepulveda et al., 2009). While evidences of photic zone euxinia during the PETM are few and only confined to restricted and epicontinental basins, i.e. Arctic Ocean (Sluijs et al., 2006); North Sea (Schoon et al., 2013), West Siberian Sea (Frieling et al., 2014), Gulf Coastal Plain (Sluijs et al., 2014), and eastern shelf of the South Atlantic (Frieling et al., 2017), northern Peri-Tethys (Chapter 5 and Gavrilov et al., 2003).

According to the GENIE Earth System model (Ridgwell et al., 2007) observations, oceanic deoxygenation changes associated with OAE2 are mainly influenced by enhanced marine productivity, as a result of increased terrestrial riverine and nutrient availability (Monteiro et al., 2012). As discussed in Chapter 5, development of anoxia and PZE during the PETM is also directed by the enhanced nutrient input and marine productivity in the specific morphologies, i.e. restricted and epicontinental, that acted as nutrient trap (Although a model is not yet available for the PETM marine deoxygenation changes). While the mechanism of marine deoxygenation during the OAE2 and PETM seem to be similar, the reason for different response in terms of expansion of marine anoxia remains unclear. Although contrasting world geography and basin morphologies, as well as different oceanography and water circulations during these two time periods are some of the potential reasons, this question needs to be explored by using earth system data-models that includes detailed ocean biogeochemistry.

7.3. Future Works

- This is the first ever study of Aptian aged anoxic environments in the South Atlantic, focusing on one basin. Reconstructing the extent of the impact of astronomical forcing on driving basins in the proto-South Atlantic anoxic, and providing a global image of Aptian climate, should be the focus of future studies.
- In this thesis, the organic biomarkers in the sediments of Unit 5 – at the DSDP Site 364- are not studied through high resolution. The study of organic biomarkers in high resolution could release new insights into the intensity and persistence of OAE 1d anoxia in the South Atlantic. Therefore, it should be the focus of future studies.
- As discussed in chapter 4, although T_{max} values do not express any sudden change between Unit 7b and younger part of the sequence (Units 7a and 6- at the DSDP 364-), the C_{31} hopane ratio varies and sharply decrease from ~0.6 in Unit 7a to ~0.2 in Unit 7b. This indicates thermal alternation of the biological stereochemistry of the hopane stereoisomers in a significant portion in Unit 7b. The mechanism causing the rapid decline in C_{31} hopane ratio in Unit 7b is currently not known and should be the focus of future study.
- The absence of GDGTs in Unit 7b could be raised from thermal alternation (Schouten et al., 2004). Presuming that distribution of GDGTs is thermally altered, then the domination of GDGT0 is expected (Schouten et al., 2013, 2004), however the absence of GDGT0 in the studied samples of Unit 7b in this thesis or their low abundance in the previous studied by Naafs and Pancost, (2014), does not follow the presumed distribution. Our data suggests that further researches should be focused on the influence of thermal maturity on the distribution of GDGTs.
- Future research directions on the spread of photic zone euxinia during the PETM, as the best analogue for the potential impacts of future climate changing, involve obtaining a global overview, which demands organic geochemistry analysis on sediments from more locations.
- The final question, which remains under debate, is “Why photic zone euxinia during the PETM only developed in restricted basins, while during the Mesozoic OAEs it is much more widespread?”. This is a highly recommended project; a possible method to explore this question is by using earth system models that include detailed ocean biogeochemistry.

Appendix

This appendix provides supplementary information and further studies that has been done during this PhD.

Appendix I

Zumaia PETM Section

In collaboration with:

D. Naafs, A. Ralph, H.R. Manners, S.T. Grimes and R. Pancost

Zumaia PETM section located in the western Peri-Tethys (paleo-location: western Peri-Tethys (North Atlantic; Zumaia) is the most complete and representative section of early Paleogene of the Pyrenees and a key reference for the Paleocene–Eocene boundary (Pujalte et al., 1998). Zumaia sediments are deposited in lower to mid bathyal settings, at about 1 km depth (Rodríguez-Tovar et al., 2011). The $\delta^{13}C_{org}$ values at Zumaia express a negative excursion (–4 ‰), decreasing from –28 ‰ in the marly and carbonate sections to –24 ‰ in the Siliciclastic Unit (SU) (Manners et al., 2013). Organic biomarkers obtained from 26 sediments of Zumaia sections (method explained in chapter 5) were studied from pre to post PETM section. A pilot study of fatty acids, *n*-alkanes and reworked OM (UCM) demonstrated that terrestrial input was increased during the PETM comparing to the pre and post PETM section. Presuming the enhanced hydrological activities (*per se* as a result of elevated temperature and *p*CO2, Carmichael et al., 2017), the enhanced terrestrial input is expected. A pronounced increase in the terrestrial sediments accumulation rate during the PETM, is also observed in the high resolution cyclostratigraphy study in the Zumaia PETM section (Jones et al., 2017). However, the fatty acids and apolar biomarker proxies demonstrate a cyclic variation in the intensity of terrestrial input, for example accumulation of fatty acids varies periodically during the PETM, Fig. A.1. The cyclic variations are likely caused by astronomical derived variations in hydrological cycle activities. The bulk geochemical proxies (Si/Fe) during the PETM demonstrate that the astronomically controlled on the silicate weathering during the PETM (Jones et al., 2017). Further detailed studies will be focused on the distribution and variations of biomarkers in Zumaia section.

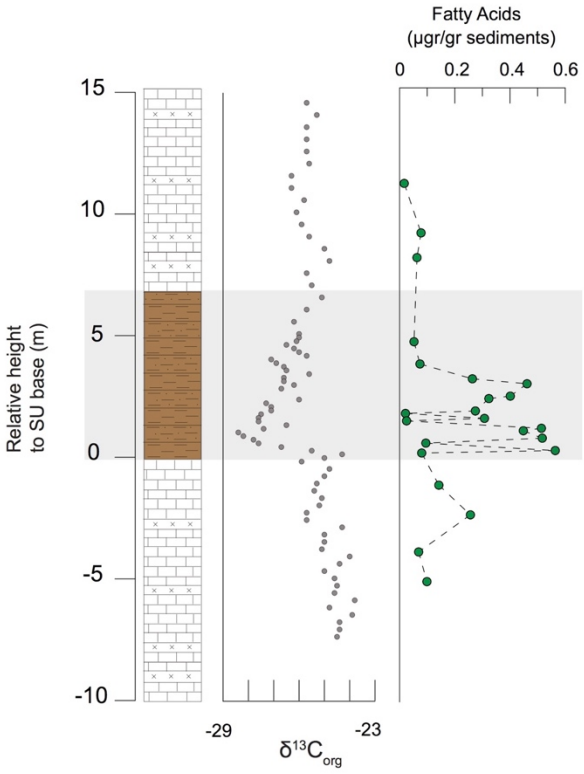

Figure A.1: Lithology and distribution of fatty acids in the Zumaia section. Relative height (m) is based on the start of the Siliciclastic Unit (SU).

References

Alegret, L., Matías, R., Vega Pérez, M., 2018. Environmental instability during the latest Paleocene at Zumaia (Basque- Cantabric Basin): The bellwether of the Paleocene-Eocene Thermal Maximum. Palaeogeogr. Palaeoclimatol. Palaeoecol. 1–0. https://doi.org/10.1016/j.palaeo.2018.02.018

Alsenz, H., Regnery, J., Ashckenazi-Polivoda, S., Meilijson, A., Ron-Yankovich, L., Abramovich, S., Illner, P., Almogi-Labin, A., Feinstein, S., Berner, Z., Püttmann, W., 2013. Sea surface temperature record of a Late Cretaceous tropical Southern Tethys upwelling system. Palaeogeogr. Palaeoclimatol. Palaeoecol. 392, 350–358. https://doi.org/10.1016/j.palaeo.2013.09.013

Amiot, R., Le, C., I, C.B.L., 2004. Latitudinal temperature gradient during the Cretaceous Upper Campanian – Middle Maastrichtian : y 18 O record of continental vertebrates 226, 255–272. https://doi.org/10.1016/j.epsl.2004.07.015

Armstrong, H.A., Wagner, T., Herringshaw, L.G., Farnsworth, A.J., Lunt, D.J., Harland, M., Imber, J., Loptson, C., Atar, E.F.L.L., 2016. Hadley circulation and precipitation changes controling black shale deposition in the Late Jurassic Boreal Seaway. Paleoceanography 31, 1041–1053. https://doi.org/10.1002/2015PA002911

Arthur, M. a, Sageman, B.B., 2004. Sea-level control on source-rock development: Perspectives from the Holocene Black Sea, the Mid-Cretaceous Western Interior Basin of North America, and the Late Devonian Appalachian Basin. SEPM Spec. Publ. 82, 35–59. https://doi.org/10.2110/pec.05.82.0035

Arthur, M., Sageman, B.B., 1994. Marine Shales: Depositional Mechanisms and Environments of Ancient Deposits. Annu. Rev. Earth Planet. Sci. 22, 499–551. https://doi.org/10.1146/annurev.earth.22.1.499

Arthur, M.A., Dean, W.E., Stow, D.A. V, 1984. Models for the deposition of Mesozoic-Cenozoic fine-grained organic-carbon-rich sediment in the deep sea. Geol. Soc. London, Spec. Publ. 15, 527–560. https://doi.org/10.1144/gsl.sp.1984.015.01.34

Aubry, M.-P., Ouda, K., Dupuis, C., Berggren, W. a, Van Couvering, J. a, 2007. The Global Standard Stratotype-section and Point (GSSP) for the base of the Eocene Series in the Dababiya section (Egypt). Episodes 30, 271–286.

Barral, A., Gomez, B., Fourel, F., Daviero-Gomez, V., Lécuyer, C., 2017. CO2and temperature decoupling at the million-year scale during the Cretaceous Greenhouse. Sci. Rep. 7, 1–7. https://doi.org/10.1038/s41598-017-08234-0

Barker, C., 1974. Pyrolysis techniques for source rock evaluation. Am. Assoc. Pet. Geol. Bull. 58, 2349–2361.

Barron, E.J., 1983. A warm, equable Cretaceous: The nature of the problem. Earth Sci. Rev. 19, 305–338. https://doi.org/10.1016/0012-8252(83)90001-6

Beaumont, V.I., Jahnke, L.L., Des Marais, D.J., 2000. Nitrogen isotopic fractionation in the synthesis of photosynthetic pigments in Rhodobacter capsulatus and Anabaena cylindrica. Org. Geochem. 31, 1075–1085. https://doi.org/10.1016/S0146-6380(00)00133-9

Beckmann, B., Flogel, S., Hofmann, P., Schulz, M., Wagner, T., 2005. Orbital forcing of Cretaceous river discharge in tropical Africa and ocean response. Nature 437, 241–244. https://doi.org/doi: 10.1038/nature03976

Beerling, D.J., Lomax, B.H., Royer, D.L., Upchurch, G.R., Kump, L.R., 2002. An atmospheric pCO2 reconstruction across the Cretaceous-Tertiary boundary from leaf megafossils. Proc. Natl. Acad. Sci. U. S. A. 99, 7836–7840. https://doi.org/10.1073/pnas.122573099

Behrooz, L., Naafs, B.D.A., Dickson, A.J., Love, G.D., Batenburg, S.J., Pancost, R.D., 2018. Astronomically driven variations in depositional environments in the South Atlantic during the Early Cretaceous. Paleoceanogr. Paleoclimatology. https://doi.org/10.1029/2018PA003338

Berner, R.A., 1997. The Rise of Plants and Their Effect on Weathering and Atmospheric CO2. Science (80-.). 276, 544–546.

Bice, K.L., Birgel, D., Meyers, P.A., Dahl, K.A., Hinrichs, K.U., Norris, R.D., 2006. A multiple proxy and model study of Cretaceous upper ocean temperatures and atmospheric CO2 concentrations. Paleoceanography 21, 1–17. https://doi.org/10.1029/2005PA001203

Blaga, C.I., Reichart, G.J., Heiri, O., Sinninghe Damsté, J.S., 2009. Tetraether membrane lipid distributions in water-column particulate matter and sediments: A study of 47 European lakes along a north-south transect. J. Paleolimnol. 41, 523–540. https://doi.org/10.1007/s10933-008-9242-2

Bolle, M.-P.P., Pardo, a., Hinrichs, K.-U.U., Adatte, T., Von Salis, K., Burns, S., Keller, G., Muzylev, N., 2000. The Paleocene-Eocene transition in the marginal northeastern Tethys (Kazakhstan and Uzbekistan). Int. J. Earth Sci. 89, 390–414. https://doi.org/10.1007/s005310000092

Boltovskoy, E., Watanabe, S., Totah, V.I., Ocampo, J.V., 1992. Cenozoic benthic bathyal foraminifers of DSDP Site 548 (North Atlantic). Micropaleontology 38, 183–207.

Bornemann, A., Pross, J., Reichelt, K., Herrle, J.O., Hemleben, C., Mutterlose, J., 2005. Reconstruction of short-term palaeoceanographic changes during the formation of the Late Albian "Niveau Breistroffer" black shales (Oceanic Anoxic Event 1d, SE France). J. Geol. Soc. London. 162, 623–639. https://doi.org/10.1144/0016-764903-171

Bottini, C., Erba, E., Tiraboschi, D., Jenkyns, H.C., Schouten, S., Sinninghe Damsté, J.S., 2015. Climate variability and ocean fertility during the Aptian Stage. Clim. Past 11, 383–402. https://doi.org/10.5194/cp-11-383-2015

Bourbonniere, R.A., Meyers, P.A., 1996. Sedimentary geolipid records of historical changes in the watersheds and productivities of Lakes Ontario and Erie. Limnol. Oceanogr. 41, 352–359. https://doi.org/10.4319/lo.1996.41.2.0352

Braga, G., De, B.R., Grunig, A., Proto Decima, F., 1975. Foraminiferi bentonici del Paleocene ed Eocene della Sezione di Possagno. Schweiz Palaontol Abh 97, 85–111.

Bralower, T.J., 2002. Evidence of surface water oligotrophy during the Paleocene-Eocene thermal maximum: Nannofossil assemblage data from Ocean Drilling Program Site 690, Maud Rise, Weddell Sea. Paleoceanography 17, 12–13. https://doi.org/10.1029/2001PA000662

Bralower, T.J., Arthur, M.A., Leckie, R.M., Sliter, W. V., Allard, D.J., Schlanger, S.O., 1994. Timing and paleoceanography of oceanic dysoxia/anoxia in the late Barremian to early Aptian (early Cretaceous). Palaios 9, 335–369. https://doi.org/10.2307/3515055

Brassell, S.C., Lewis, C.A., de Leeuw, J.W., Lange, F., Sinninghe Damsté, J.S., 1986. Isoprenoid thiophenes: novel products of sediments diagenesis? Nature 320, 160–162.

Bray, E.E., Evans, E.D., 1961. Distribution of n-paraffins as a clue to recognition of source beds. Geochim. Cosmochim. Acta 22, 2–15.

Brocks, J.J., Schaeffer, P., 2008. Okenane, a biomarker for purple sulfur bacteria (Chromatiaceae), and other new carotenoid derivatives from the 1640Ma Barney Creek Formation, Geochimica et Cosmochimica Acta. https://doi.org/10.1016/j.gca.2007.12.006

Canfield, D.E., Green, W.J., Nixon, P., 1995. 210Pb and stable lead through the redox transition zone of an Antarctic lake. Geochim. Cosmochim. Acta 59, 2459–2468. https://doi.org/10.1016/0016-7037(95)00140-9

Canfield, D.E., Jorgensen, B.B., Fossing, H., Glud, R., Gundersen, J., Ramsing, N.B., Thamdrup, B., Hansen, J.W., Nielsen, L.P., Hall, P.O., 1993. Pathways of organic

carbon oxidation in three continental margin sediments. Mar. Geol. 113, 27–40. https://doi.org/10.1016/0025-3227(93)90147-N

Canfield, D.E., Thamdrup, B., 2009. Towards a consistent classification scheme for geochemical environments, or, why we wish the term “suboxic” would go away: Editorial. Geobiology 7, 385–392. https://doi.org/10.1111/j.1472-4669.2009.00214.x

Canfield, D.E., Thamdrup, B., Hansen, J.W., 1993. The anaerobic degradation of organic matter in Danish coastal sediments: Iron reduction, manganese reduction, and sulfate reduction. Geochim. Cosmochim. Acta 57, 3867–3883. https://doi.org/10.1016/0016-7037(93)90340-3

Canudo, J.I., Keller, G., Molina, E., Ortiz, N., 1995. Planktic foraminiferal turnover and δ13C isotopes across the Paleocene-Eocene transition at Caravaca and Zumaya, Spain. Palaeogeogr. Palaeoclimatol. Palaeoecol. 114, 75–100. https://doi.org/10.1016/0031-0182(95)00073-U

Cao, C., Love, G.D., Hays, L.E., Wang, W., Shen, S., Summons, R.E., 2009. Biogeochemical evidence for euxinic oceans and ecological disturbance presaging the end-Permian mass extinction event. Earth Planet. Sci. Lett. 281, 188–201. https://doi.org/10.1016/j.epsl.2009.02.012

Carmichael, M.J., Inglis, G.N., Badger, M.P.S., Naafs, B.D.A., Behrooz, L., Remmelzwaal, S., Monteiro, F.M., Rohrssen, M., Farnsworth, A., Buss, H.L., Dickson, A.J., Valdes, P.J., Lunt, D.J., Pancost, R.D., 2017. Hydrological and associated biogeochemical consequences of rapid global warming during the Paleocene-Eocene Thermal Maximum. Glob. Planet. Change 157, 114–138. https://doi.org/10.1016/j.gloplacha.2017.07.014

Chicarelli, M.I., Hayes, J.M., Popp, B.N., Eckardt, C.B., Maxwell, J.R., 1993. Carbon and nitrogen isotopic composi- tions of alkyl porphyrin from the Triassic Serpiano oil shale. Geochim. Cosmochim. Acta 57, 1307–1311.

Christensen, P.B., Nielsen, L.P., Revsbech, N.P., Sørensen, J., 1989. Microzonation of denitrification activity in stream sediments as studied with a combined oxygen and nitrous oxide microsensor. Appl. Environ. Microbiol. 55, 1234–1241. https://doi.org/0099-2240/89/051234-08$02.00/0

Chun, C.O.J., Delaney, M.L., Zachos, J.C., 2010. Paleoredox changes across the Paleocene-Eocene thermal maximum, Walvis Ridge (ODP Sites 1262, 1263, and 1266): Evidence from Mn and U enrichment factors 25. https://doi.org/10.1029/2009PA001861

Clarke, L.J., Jenkyns, H.C., 1999. New oxygen isotope evidence for long-term Cretaceous climatic change in the Southern Hemisphere. Geology 27, 699–702. https://doi.org/10.1130/0091-7613(1999)027<0699:NOIEFL>2.3.CO;2

Cline, J.D., Richards, F.A., 1972. Oxygen Deficient Conditions and Nitrate Reduction in the Eastern Tropical Ocean1. Limnol. Oceanogr. 17, 885–900.

Colosimo, A.B., Bralower, T.J., Zachos, J.C., 2006. Evidence for lysocline shoaling at the Paleocene/Eocene thermal maximum on shatsky rise, northwest Pacific. Proc. Ocean Drill. Program, Sci. Results 198, 1–36.

Conley, D.J., Carstensen, J., Aigars, J., Axe, P., Bonsdorff, E., Eremina, T., Haahti, B.M., Humborg, C., Jonsson, P., Kotta, J., Lännegren, C., Larsson, U., Maximov, A., Medina, M.R., Lysiak-Pastuszak, E., Remeikaitè-Nikienè, N., Walve, J., Wilhelms, S., Zillén, L., 2011. Hypoxia is increasing in the coastal zone of the baltic sea. Environ. Sci. Technol. 45, 6777–6783. https://doi.org/10.1021/es201212r

Cramer, B.S., Aubry, M.P., Miller, K.G., Olsson, R.K., Wright, J.D., Kent, D. V., 1999. An exceptional chronologic, isotopic, and clay mineralogic record of the latest Paleocene thermal maximum, Bass River, NJ, ODP 174AX. Bull. la Soc. Geol. Fr. 170, 883–897.

Cramer, B.S., Toggweiler, J.R., Wright, J.D., Katz, M.E., Miller, K.G., 2009. Ocean overturning since the Late Cretaceous : Inferences from a new benthic foraminiferal isotope compilation 24, 1–14. https://doi.org/10.1029/2008PA001683

Cranwell, P.A., 1973. Chain-length distribution of n-alkanes from lake sediments in relation to post-glacial environmental change. Freshw. Biol. 3, 259–265.

de Leeuw, J.W., Cox, H.C., van Graas, G., van de Meer, F.W., Peakman, T.M., Baas, J.M. a., van de Graaf, B., 1989. Limited double bond isomerisation and selective hydrogenation of sterenes during early diagenesis. Geochim. Cosmochim. Acta 53, 903–909. https://doi.org/10.1016/0016-7037(89)90034-3

de Leeuw, J.W., Sinninghe Damsté, J.S., Leeuw, J.W. De, Sinninghe Damsté, J.S., 1990. Organic Sulfur Compounds and Other Biomarkers as Indicators of Palaesalinity, in: Orr, W.L., White, C.M. (Eds.), Geochemistry of Sulfur in Fossil Fuels. American Chemical Society, Washington, D.C., pp. 417–443.

Dean, W.E., Hay, W.W., Sibuet, J.-C., 1984. Geologic Evolution, Sedimentation and Paleoenvironments of the Angola Basin and Adjacent Walvis Ridge : Synthesis of Results of Deep Sea Drilling Project Legs 75, in: W.W. Hay, J.-C., Sibuet et al. (Eds.), Initial Reports of the Deep Sea Drilling Project, Vol. 75. U.S. Govern- ment: Printing Office, Washington, D.C., pp. 509–542.

Deconto, R.M., Galeotti, S., Pagani, M., Tracy, D., Schaefer, K., Zhang, T., Pollard, D., Beerling, D.J., 2012. Past extreme warming events linked to massive carbon release from thawing permafrost. Nature 484, 87–91. https://doi.org/10.1038/nature10929

Demaison, G.J., Moore, G.T., 1980. Anoxic environment and oil source bed genesis. Org. Geochem. 2, 9–31.

Deroo, G., Herbin, J.P., J. Roucaché, 1983. 37. Organic geochemistry of upper Jurassic-Cretaceous sediments from Site 511, LEG 71, Western South Atlantic, in: Ludwig, W.J., Krasheninnikov, V.A., Al., E. (Eds.), Initial Reports of the Deep Sea Drilling Project 41. U.S. Government Printing Office. Institut Français du Pétrole, Paris, France, pp. 1001–1013. https://doi.org/https://doi.org/10.1594/PANGAEA.815172

Deroo, G., Herbin, J.P.P., Huc, A.Y.Y., 1984. Organic Geochemistry of Cretaceous Black Shales from Deep Sea Drilling Project Site 530, Leg 75, Eastern South Atlantic, in: Hay, W.W., Sibuet, J.C., et al. (Eds.), Initial Reports of the Deep Sea Drilling Project; Part V: Organic Geochemistry. U.S. Government Printing Offic, Washington, pp. 983–999. https://doi.org/10.2973/dsdp.proc.75.130.1984

Devol, A.H., 1981. Vertical distribution of zooplankton respiration in realtion to the intense oxygen minumium zones in two British Columbia fjords. J. Plankton Res. 3, 593–602.

Diaz, R.J., 2001. Overview of Hypoxia around the World. J. Environ. Qual. 30, 275. https://doi.org/10.2134/jeq2001.302275x

Diaz, R.J., Rosenberg, R., 2008. Spreading Consequences Dead Zones and Consequences for Marine Ecosystems. Science (80-.). 321, 926–929.

Dickens, G.R., 2011. Methane release from gas hydrate systems during the Paleocene-Eocene thermal maximum and other past hyperthermal events : setting appropriate parameters for discussion. Clim. Past Discuss. 7, 1139–1174. https://doi.org/10.5194/cpd-7-1139-2011

Dickens, G.R., Castillo, M.M., Walker, J.C.G., 1997. A blast of gas in the latest Paleocene: Simulating first-order effects of massive dissociation of oceanic methane hydrate. Geology 25, 259–262. https://doi.org/10.1130/0091-7613(1997)025<0259:ABOGIT>2.3.CO

Dickens, G.R., Neil, J.R.O., Rea, D.K., Owen, R.M., 1995a. Dissociation of oceanic methan hydrate as a cause of the carbon isotpe excursion at the end of the Paleocen. Paleoceanography 10, 965–971. https://doi.org/10.1029/95PA02087

Dickens, G.R., Neil, J.R.O., Rea, D.K., Owen, R.M., 1995b. That Bottom Water Temperature Increased By More Than During a Brief Time Interval. Paleoceanography 10, 965–971. https://doi.org/10.1029/95PA02087

Dickson, A.J., Cohen, A.S., Coe, A.L., 2014a. Continental margin molybdenum isotope signatures from the early Eocene. Earth Planet. Sci. Lett. 404, 389–395.

https://doi.org/10.1016/j.epsl.2014.08.004
Dickson, A.J., Cohen, A.S., Coe, A.L., 2012. Seawater oxygenation during the Paleocene-Eocene Thermal Maximum. Geology 40, 639–642. https://doi.org/10.1130/G32977.1
Dickson, A.J., Rees-Owen, R.L., März, C., Coe, A.L., Cohen, A.S., Pancost, R.D., Taylor, K., Shcherbinina, E., 2014b. The spread of marine anoxia on the northern Tethys margin during the Paleocene-Eocene Thermal Maximum. Paleoceanography 29, 471–488. https://doi.org/10.1002/2014PA002629
Dickson, A.J., Saker-clark, M., Jenkyns, H.C., Bottini, C., Erba, E., Russo, F., Gorbanenko, O., Naafs, B.D.A., Pancost, R.D., Robinson, S.A., 2017. A Southern Hemisphere record of global trace-metal drawdown and orbital modulation of organic-matter burial across the Cenomanian – Turonian boundary (Ocean Drilling Program Site 1138 , Kerguelen Plateau). Sidementology 64, 186–203. https://doi.org/10.1111/sed.12303
Dugdale, R.C., Goering, J.J., Barber, R.T., Smith, R.L., Packard, T.T., 1977. Denitrification and hydrogen sulfide in the Peru upwelling region during 1976. Deep. Res. 24, 601–608. https://doi.org/10.1016/0146-6291(77)90530-6
Dumitrescu, M., Brassell, S.C., 2006. Compositional and isotopic characteristics of organic matter for the early Aptian Oceanic Anoxic Event at Shatsky Rise, ODP Leg 198. Palaeogeogr. Palaeoclimatol. Palaeoecol. 235, 168–191. https://doi.org/10.1016/j.palaeo.2005.09.028
Dunham, K.W., Meyers, P.A., Ho, E.S, et al., 1988. Organic geochemistry of Cretaceous black shales and adjacent strata from the Galicia Margin, North Atlantic Ocean, in: Boillot, G., Winterer, E.L., Al., E. (Eds.), Proceedings of the Ocean Drilling Program, Scientific Results. Ocean Drilling Program, College Station Texas, pp. 557–565.
Egger, H., Homayoun, M., Huber, H., Rögl, F., Schmitz, B., 2005. Early Eocene climatic, volcanic, and biotic events in the northwestern Tethyan Untersberg section, Austria. Palaeogeogr. Palaeoclimatol. Palaeoecol. 217, 243–264. https://doi.org/10.1016/j.palaeo.2004.12.006
Eldrett, J.S., Ma, C., Bergman, S.C., Ozkan, A., Minisini, D., Lutz, B., Jackett, S.J., Macaulay, C., Kelly, A.E., 2015. Origin of limestone-marlstone cycles: Astronomic forcing of organic-rich sedimentary rocks from the Cenomanian to early Coniacian of the Cretaceous Western Interior Seaway, USA. Earth Planet. Sci. Lett. 423, 98–113. https://doi.org/10.1016/j.epsl.2015.04.026
Ensminger, A., 1977. Evolution de compos~s polycycliques sedimentaires., in: Th6se, Docteur 6s Sciences, l'Univer- Sit6 Louis Pasteur de Strasbourg, France.
Ernst, S.R., Guasti, E., Dupuis, C., Speijer, R.P., 2006. Environmental perturbation in the southern Tethys across the Paleocene/Eocene boundary (Dababiya, Egypt): Foraminiferal and clay mineral records. Mar. Micropaleontol. 60, 89–111. https://doi.org/10.1016/j.marmicro.2006.03.002
Farrimond, P., Talbot, H.M., Watson, D.F., Schulz, L.K., Wilhelms, A., 2004. Methylhopanoids: Molecular indicators of ancient bacteria and a petroleum correlation tool. Geochim. Cosmochim. Acta 68, 3873–3882. https://doi.org/10.1016/j.gca.2004.04.011
Farrington, J.W., Davis, A.C., Sulanowski, J., McCaffrey, M.A., McCarthy, M., Clifford, C.H., Dickinson, P., Volkman, J.K., 1988. Biogeochemistry of lipids in surface sediments of the Peru Upwelling Area at 15??S. Org. Geochem. 13, 607–617. https://doi.org/10.1016/0146-6380(88)90080-0
Fassell, M.L., Bralower, T.J., 1999. Warm, equable mid-Cretaceous: Stable isotope evidence. Geol. Soc. Am. Spec. Pap. 332, 121–142.
Ficken, K.J., Li, B., Swain, D.L., Eglinton, G., 2000. An n-alkane proxy for the sedimentary input of submerged/floating freshwater aquatic macrophytes. Org. Geochem. 31, 745–749. https://doi.org/10.1016/S0146-6380(00)00081-4
Fischer, A.., Arthur, M.A., 1977. Secular variations in the pelagic realm, in: Cook, H., Enos,

P. (Eds.), Deep-Water Carbonate Environments. Tulsa, OK: SEPM, pp. 19–50.
Flögel, S., Beckmann, B., Hofmann, P., Bornemann, A., Westerhold, T., Norris, R.D.D., Dullo, C., Wagner, T., 2008. Evolution of tropical watersheds and continental hydrology during the Late Cretaceous greenhouse; impact on marine carbon burial and possible implications for the future. Earth Planet. Sci. Lett. 274, 1–13. https://doi.org/10.1016/j.epsl.2008.06.011
Flögel, S., Wagner, T., 2006. Insolation-control on the Late Cretaceous hydrological cycle and tropical African climate-global climate modelling linked to marine climate records. Palaeogeogr. Palaeoclimatol. Palaeoecol. 235, 288–304. https://doi.org/https://doi.org/10.1016/j.palaeo.2005.09.034
Foresman, J.B., 1984. Organic Geochemistry DSDP Leg 40, Continental Rise of Southwest Africa, in: Deep Sea Drilling Projects and Publications; Part III: Organic Geochemistry. pp. 557–567. https://doi.org/10.2973/dsdp.proc.40.111.1978
Forster, A., Kuypers, M.M.M., Turgeon, S.C., Brumsack, H.-J., Petrizzo, M.R., Sinninghe Damsté, J.S., 2008. The Cenomanian/Turonian oceanic anoxic event in the South Atlantic: New insights from a geochemical study of DSDP Site 530A. Palaeogeogr. Palaeoclimatol. Palaeoecol. 267, 256–283. https://doi.org/10.1016/j.palaeo.2008.07.006
Forster, A., Schouten, S., Baas, M., Sinninghe Damsté, J.S., 2007a. Mid-Cretaceous (Albian – Santonian) sea surface temperature record of the tropical Atlantic Ocean. Geology 35, 919–922. https://doi.org/10.1130/G23874A.1
Forster, A., Schouten, S., Moriya, K., Wilson, P.A., Damsté, J.S.S.S., Sinninghe Damsté, J.S., Damsté, J.S.S.S., Sinninghe Damsté, J.S., 2007b. Tropical warming and intermittent cooling during the Cenomanian/Turonian oceanic anoxic event 2: Sea surface temperature records from the equatorial Atlantic. Paleoceanography 22, 1–14. https://doi.org/10.1029/2006PA001349
Foster, G.L., Royer, D.L., Lunt, D.J., 2017. Future climate forcing potentially without precedent in the last 420 million years. Nat. Commun. 8. https://doi.org/10.1038/ncomms14845
Fowler, M.G., McAlpine, K.D., 1995. The Egret Member, a Prolific Kimmeridgian Source Rock from Offshore Eastern Canada, in: Katz B.J. (Ed.), Petroleum Source Rocks. Casebooks in Earth Sciences. Springer, Berlin, Heidelberg, pp. 111–130. https://doi.org/https://doi.org/10.1007/978-3-642-78911-3_7
Francis, J.E., Frake, L.A., 1993. Creataceous Climates, in: Wright, V.P. (Ed.), Sedimentology Review/1. Blackwell Publishing Ltd., Oxford, UK., pp. 17–30. https://doi.org/10.1002/9781444304534.ch2
Freeman, K.H., Hayes, J.M., 1992. Fractionation of carbon isotopes by phytoplankton and estimates of ancient CO2 levels. Global Biogeochem. Cycles 6, 185–198. https://doi.org/10.1029/92GB00190
Fricke, H.C., Wing, S.L., Scott, L.W., Wing, S.L., Scott, L.W., 2004. Oxygen isotope and paleobotanical estimates of temperature and d18O - latitude gradients over North America during the Early Eocene. Am. J. Sci. 304, 612–635. https://doi.org/10.2475/ajs.304.7.612
Friedrich, O., 2010. Benthic foraminifera and their role to decipher paleoenvironment during mid-Cretaceous Oceanic Anoxic Events – the “anoxic benthic foraminifera” paradox. Rev. Micropaléontologie 53, 175–192. https://doi.org/10.1016/j.revmic.2009.06.001
Friedrich, O., Erbacher, J., 2006. Benthic foraminiferal assemblages from Demerara Rise (ODP Leg 207, western tropical Atlantic): possible evidence for a progressive opening of the Equatorial Atlantic Gateway. Cretac. Res. 27, 377–397. https://doi.org/10.1016/j.cretres.2005.07.006
Friedrich, O., Norris, R.D., Erbacher, J., 2012. Evolution of middle to Late Cretaceous oceans — A 55 m . y . record of Earth ’ s temperature and carbon cycle ABSTRACT 107–110. https://doi.org/10.1130/G32701.1

Frieling, J., Gebhardt, H., Huber, M., Adekeye, O.A., Akande, S.O., Reichart, G., Middelburg, J.J., Schouten, S., Sluijs, A., 2017. Extreme warmth and heat-stressed plankton in the tropics during the Paleocene-Eocene Thermal Maximum. Sci. Adv. 3, e1600891. https://doi.org/10.1126/sciadv.1600891

Frieling, J., Iakovleva, A.I., Reichart, G.-J., Aleksandrova, G.N., Gnibidenko, Z.N., Schouten, S., Sluijs, A., 2014. Paleocene-Eocene warming and biotic response in the epicontinental West Siberian Sea. Geology 42, 767–770. https://doi.org/10.1130/G35724.1

Galbraith, E.D., Sigman, D.M., Robinson, R.S., Pedersen, T.F., 2008. Nitrogen in the marine environment, 2nd ed. Academic Press.

Gambacorta, A., Gliozzi, A., De Rosa, M., 1995. Archaeal lipids and their biotechnological applications. World J. Microbiol. Biotechnol. 11, 115–131. https://doi.org/10.1007/BF00339140

Gavrilov, Y., Shcherbinina, E., Golovanova, O., Pokrovsky, B., 2009. A variety of PETM record in different setting , northeastern Peri-Tethys. Clim. Botic Events Paleogene 1–4.

Gavrilov, Y.O., Kodina, L.A., Lubchenko, I.Y., Muzylöv, N.G., 1997. The Late Paleocene anoxic event in epicontinental seas of Peri-Tethys and formation of the sapropelite unit: sedimentology and geochemistry. Lithol. Miner. Resour. 32, 427–450.

Gavrilov, Y.O., Shcherbinina, E.A., Oberhansli Hedi, 2003. Paleocene-Eocene boundary events in the northern Peri-Tethys, in: Wing, S.L., Gingerich, P.D., Schmitz, B., Thomas, E. (Eds.), Causes and Consequences of Globally Warm Climates in the Early Palaeogene, GSA Special Paper. Geological Society of America Special Paper 369, Geological Society of America, pp. 25–47.

Gibbison, R., Peakman, T.M., Maxwell, J.R., 1995. Novel porphyrins as molecular fossils for anoxygenic photosynthesis. Tetrahedron Lett. 36, 9057–9060. https://doi.org/10.1016/0040-4039(95)01911-Z

Giorgioni, M., Weissert, H., Bernasconi, S.M., Hochuli, P.A., Keller, C.E., Coccioni, R., Petrizzo, M.R., Lukeneder, A., Garcia, T.I., 2015. Paleoceanographic changes during the Albian-Cenomanian in the Tethys and North Atlantic and the onset of the Cretaceous chalk. Glob. Planet. Change 126, 46–61. https://doi.org/10.1016/j.gloplacha.2015.01.005

Gloe, A., Pfennig, N., Brockmann, H., Trowitzsch, W., 1975. A new bacteriochlorophyll from brown-colored chlorobiaceae. Arch. Microbiol. 102, 103–109. https://doi.org/10.1007/BF00428353

Godwin, H., 1962. Half-life of radiocarbon. Nature 195 https://doi.org/doi:10.1038/195984a0.

Gonzalez-Vila, F.J., 1995. Alkane biomarkers, geochemical significance and application in oil shale geochemistry, in: Snape, C. (Ed.), Composition, Geochemistry and Conversions of Oil Shales. Kluwer Academic Publishes, pp. 51–68. https://doi.org/10.1017/CBO9781107415324.004

González-Vila, F.J., Polvillo, O., Boski, T., Moura, D., De Andrés, J.R., 2003. Biomarker patterns in a time-resolved holocene/terminal Pleistocene sedimentary sequence from the Guadiana river estuarine area (SW Portugal/Spain border). Org. Geochem. 34, 1601–1613. https://doi.org/10.1016/j.orggeochem.2003.08.006

Goodwin, N.S., Mann, A.L., Patience, R.L., 1988. Structure and significance of C30 4-methyl steranes in lacustrine shales and oils. Org. Geochem. 12, 495–506. https://doi.org/10.1016/0146-6380(88)90159-3

Gradstein, F.M., Kaminski, M.A., Berggren, W.A., Kristiansen, I.L., D'lorio, M.A., 1994. Cenozoic biostratigraphy of the North Sea and Labrador Shelf. Micropaleontology 40, 1–152.

Gradstein, F.M., Ogg, J.G., Schmitz, M., Ogg, G., 2012. The Geological Time Scale 2012 2 Valume Set, Volume Set. ed. Elsevier. https://doi.org/https://doi.org/10.1016/C2011-1-08249-8

Grinsted, A., Moore, J.C., Jevrejeva, S., 2004. Application of the cross wavelet transform and wavelet coherence to geophysical time series. Nonlinear Process Geophys 11, 561–566. https://doi.org/10.5194/npg-11-561-2004

Gutjahr, M., Ridgwell, A., Sexton, P.F., Anagnostou, E., Pearson, P.N., Pälike, H., Norris, R.D., Thomas, E., Foster, G.L., 2017. Very large release of mostly volcanic carbon during the Palaeocene-Eocene Thermal Maximum. Nature 548. https://doi.org/10.1038/nature23646

Handoh, I.C., Bigg, G.R., Jones, E.J.W., 2003. Evolution of upwelling in the Atlantic Ocean basin 202, 31–58. https://doi.org/10.1016/S0031-0182(03)00571-6

Hanson, R.S., Hanson, T.E., 1996. Methanotrophic bacteria. Microbiol. Rev. 60, 439–71.

Hartwig, A., di Primio, R., Anka, Z., Horsfield, B., 2012. Source rock characteristics and compositional kinetic models of Cretaceous organic rich black shales offshore southwestern Africa. Org. Geochem. 51, 17–34. https://doi.org/10.1016/j.orggeochem.2012.07.008

Hatch, J.R., Jacobson, S.R., Witzke, B.J., Risatti, J.B., Anders, D.E., Watney, W.L., Newell, K.D., Vuletich, A.K., 1987. Possible Late Middle Ordovician Organic Carbon Isotope Excursion: Evidence from Ordovician Oils and Hydrocarbon Source Rocks, Mid-Continent and East-Central United States. Am. Assoc. Pet. Geol. Bull. 71, 1342–1354.

Hay, W.W., 2008. Evolving ideas about the Cretaceous climate and ocean circulation. Cretac. Res. 29, 725–753. https://doi.org/10.1016/j.cretres.2008.05.025

Hayes, J.M., 1993. Factors controlling 13 C contents of sedimentary organic compounds: Principles and evidence. Mar. Geol. 113, 111–125. https://doi.org/10.1016/0025-3227(93)90153-M

Hayes, J.M., Popp, B.N., Takigiku, R., Johnson, M.W., 1989. An isotopic study of biogeochemical relationships between carbonates and organic carbon in the Greenhorn Formation. Geochim. Cosmochim. Acta 53, 2961–2972. https://doi.org/10.1016/0016-7037(89)90172-5

Hayes, M., Popp, B.N., Takkzklj, R.A.Y., Icm, M.W., 1989. An isotopic study of bi ~ geo ~ hemi ~ al relationships between carbonates and organic carbon in the Greenhorn Formation.

Heine, C., Zoethout, J., Müller, R.D., 2013. Kinematics of the South Atlantic rift. Solid Earth 4, 215–253. https://doi.org/10.5194/se-4-215-2013

Herman, A.B., Spicer, R.A., 1996. Palaeobotanical evidence for a warm Cretaceous Arctic Ocean. Nature 380. Nature 380, 330–333.

Herrle, J.O., 2006. The Response of Marine Biota to OAE 1b, in: EOS Trans AGU, 87 (52), Fall Meet. San Francisco, p. 31D–04.

Hesselbo, S.P., Gröcke, D.R., Jenkyns, H.C., Bjerrum, C.J., Farrimond, P., Morgans Bell, H.S., Green, O.R., 2000. Massive dissociation of gas hydrate during a Jurassic oceanic anoxic\nevent. Nature 406, 392–395. https://doi.org/10.1038/35019044

Higgins, J.A., Schrag, D.P., 2006. Beyond methane: Towards a theory for the Paleocene-Eocene Thermal Maximum. Earth Planet. Sci. Lett. 245, 523–537. https://doi.org/10.1016/j.epsl.2006.03.009

Higgins, M.B., Robinson, R.S., Casciotti, K.L., McIlvin, M.R., Pearson, A., 2009. A Method for Determining the Nitrogen Isotopic Composition of Porphyrins. Anal. Chem. 81, 184–192. https://doi.org/10.1021/ac8017185

Higgins, M.B., Robinson, R.S., Husson, J.M., Carter, S.J., Pearson, A., 2012. Dominant eukaryotic export production during ocean anoxic events reflects the importance of recycled NH4+. Proc. Natl. Acad. Sci. 109, 2269–2274. https://doi.org/10.1073/pnas.1104313109

Higgins, M.B., Wolfe-Simon, F., Robinson, R.S., Qin, Y., Saito, M.A., Pearson, A., 2011. Paleoenvironmental implications of taxonomic variation among d15N values of chloropigments. Geochim. Cosmochim. Acta 75, 7351–7363.

https://doi.org/10.1016/j.gca.2011.04.024
Hilting, A.K., Kump, L.R., Bralower, T.J., 2008. Variations in the oceanic vertical carbon isotope gradient and their implications for the Paleocene-Eocene biological pump. Paleoceanography 23, 1–15. https://doi.org/10.1029/2007PA001458
Ho, S.L., Mollenhauer, G., Fietz, S., Martínez-Garcia, A., Lamy, F., Rueda, G., Schipper, K., Méheust, M., Rosell-Melé, A., Stein, R., Tiedemann, R., 2014. Appraisal of TEX86 and TEX86L thermometries in subpolar and polar regions. Geochim. Cosmochim. Acta.
Hofmann, P., Ricken, W., Schwark, L., Leythaeuser, D., 1999. Coupled oceanic effects of climatic cycles from late Albian deep-sea sections of the North Atlantic, in: Barrera, E., Johnson, C. (Eds.), The Evolution OfCretaceous Ocean/Climate Systems. Geological Society ofAmerica Special Publication, pp. 143–159. https://doi.org/DOI: 10.1130/0-8137-2332-9.143
Hofmann, P., Stüsser, I., Wagner, T., Schouten, S., Sinninghe Damsté, J.S., 2008. Climate-ocean coupling off North-West Africa during the Lower Albian: The Oceanic Anoxic Event 1b. Palaeogeogr. Palaeoclimatol. Palaeoecol. 262, 157–165. https://doi.org/10.1016/j.palaeo.2008.02.014
Hofmann, P., Wagner, T., 2011. ITCZ controls on Late Cretaceous black shale sedimentation in the tropical Atlantic Ocean. Paleoceanography 26, 1–11. https://doi.org/10.1029/2011PA002154
Hofmann, P., Wagner, T., Beckmann, B., 2003. Millennial- to centennial-scale record of African climate variability and organic carbon accumulation in the Coniacian–Santonian eastern tropical Atlantic (Ocean Drilling Program Site 959, off Ivory Coast and Ghana).. Geology 31, 135–138. https://doi.org/10.1130/00917613(2003)031<0135:MTCSRO>2.0.CO;2
Holbourn, A., Kuhnt, W., El Albani, A., Pletsch, T., Luderer, F., Wagner, T., 1999. Upper Cretaceous palaeoenvironments and benthonic foraminiferal assemblages of potential source rocks from the western African margin, Central Atlantic. Geol. Soc. London, Spec. Publ. 153, 195–222. https://doi.org/10.1144/GSL.SP.1999.153.01.13
Hong, S.K., Lee, Y.I., 2012. Evaluation of atmospheric carbon dioxide concentrations during the Cretaceous. Earth Planet. Sci. Lett. 23, 327–328.
Hopmans, E.C., Schouten, S., Sinninghe Damsté, J.S., 2016. The effect of improved chromatography on GDGT-based palaeoproxies. Org. Geochem. 93, 1–6. https://doi.org/10.1016/j.orggeochem.2015.12.006
Horak, R.E.A., Ruef, W., Ward, B.B., Devol, A.H., 2016. Expansion of denitrification and anoxia in the eastern tropical North Pacific from 1972 to 2012. Geophys. Res. Lett. 2014, 1–8. https://doi.org/10.1002/2013GL058740.Received
Hotinski, R.M., Bice, K.L., Kump, L.R., Najjar, R.G., Arthur, M.A., 2001. Ocean stagnation and end-Permian anoxia. Geology 29, 7–10. https://doi.org/10.1130/0091-7613(2001)029<0007:OSAEPA>2.0.CO;2
Hou, D., Li, M., Huang, Q., 2000. Marine transgressional events in the gigantic freshwater lake Songliao: Paleontological and geochemical evidence. Org. Geochem. 31, 763–768. https://doi.org/10.1016/S0146-6380(00)00065-6
Huang, C., Hinnov, L., Fischer, A.G., Grippo, A., Herbert, T., 2010. Astronomical tuning of the Aptian Stage from Italian reference sections. Geology 38, 899–902. https://doi.org/10.1130/G31177.1
Huang, W.Y., Meinschein, W.G., 1979. Sterols as ecological indicators. Geochim. Cosmochim. Acta 43, 739–745. https://doi.org/10.1016/0016-7037(79)90257-6
Huber, B., Hodell, D., HAMILTON, C.P., 1995. Middle-Late Cretaceous climate of the southern high-latitudes - stable isotopic evidence for minimal equator-to-pole thermal-gradients. Geol. Soc. Am. Bull. 107, 1164–1191. https://doi.org/10.1130/0016-7606(1995)107<1164:MLCCOT>2.3.CO;2
Huber, B.T., Norris, R.D., MacLeod, K.G., 2002. Deep-sea paleotemperature record of

extreme warmth during the Cretaceous. Geology 30, 123–126. https://doi.org/10.1130/0091-7613(2002)030<0123:DSPROE>2.0.CO;2
Imhoff, J., 1995. Taxonomy and physiology of phototrophic purple bacteria and green sulfur bacteria, in: Blankenship, R.E., Madigan, C.E., Bauer, M.T. (Eds.), Anoxygenic Photosynthetic Bacteria. Kluwer Academic Publishers. Printed in The Netherlands., pp. 1–15. https://doi.org/10.1007/0-306-47954-0_1
Ingall, E.D., Bustin, R.M., Van Cappellen, P., 1993. Influence of water column anoxia on the burial and preservation of carbon and phosphorus in marine shales. Geochim. Cosmochim. Acta 57, 303–316. https://doi.org/10.1016/0016-7037(93)90433-W
Ivanenkov, B.H., Rozanov, A., 1961. Hydrogen sulphide contamination of the intermediate water layersof the Arabian Sea and the Bay of Bengal. Okeanologica 1(3), 443–449.
Jaffé, R., Mead, R., Hernandez, M.E., Peralba, M.C., DiGuida, O.A., 2001. Origin and transport of sedimentary organic matter in two subtropical estuaries: A comparative, biomarker-based study. Org. Geochem. 32, 507–526. https://doi.org/10.1016/S0146-6380(00)00192-3
Jahren, A.H., Arens, N.C., Sarmiento, G., Guerrero, J., Amundson, R., Jahren, A.H., Sciences, P., 2001. Terrestrial record of methane hydrate dissociation in the Early Cretaceous. https://doi.org/10.1130/0091-7613(2001)029<0159
Jarvis, I., Gale, A.S., Jenkyns, H.C., Pearce, M.A., 2006. Secular variation in Late Cretaceous carbon isotopes: a new delta C-13 carbonate reference curve for the Cenomanian-Campanian (99.6-70.6 Ma). Geol. Mag. 143, 561–608. https://doi.org/10.1017/S0016756806002421
Jarvis, I., Lignum, J.S., Grcke, D.R., Jenkyns, H.C., Pearce, M.A., 2011. Black shale deposition, atmospheric CO2 drawdown, and cooling during the Cenomanian-Turonian Oceanic Anoxic Event. Paleoceanography 26, 1–17. https://doi.org/10.1029/2010PA002081
Jenkyns, H.C., 2018. Transient cooling episodes during Cretaceous Oceanic Anoxic Events with special reference to OAE 1a (Early Aptian). Philos. Trans. R. Soc. A 376, 1–26.
Jenkyns, H.C., 2010. Geochemistry of oceanic anoxic events. Geochemistry, Geophys. Geosystems 11, Q03004. https://doi.org/10.1029/2009GC002788
Jenkyns, H.C., 1980. Cretaceous anoxic events: from continents to oceans. J. Geol. Soc. London. 137, 171–188. https://doi.org/10.1144/gsjgs.137.2.0171
Jenkyns, H.C., 1988. The Early Toarcian (Jurassic) Anoxic Event: Stratigraphic, Sedimentary, And Geochemical Evidence. Am. J. Sci. 288, 101–105.
Jenkyns, H.C., Gale, a. S., Corfield, R.M., 1994. Carbon- and oxygen-isotope stratigraphy of the English Chalk and Italian Scaglia and its palaeoclimatic significance. Geol. Mag. 131, 1. https://doi.org/10.1017/S0016756800010451
Jenkyns, H.C., Matthews, A., Tsikos, H., Erel, Y., 2007. Nitrate reduction, sulfate reduction, and sedimentary iron isotope evolution during the Cenomanian-Turonian oceanic anoxic event. Paleoceanography 22, 1–17. https://doi.org/10.1029/2006PA001355
Jenkyns, H.C., Schouten-Huibers, L., Schouten, S., Sinninghe Damsté, J.S., 2012. Warm Middle Jurassic-Early Cretaceous high-latitude sea-surface temperatures from the Southern Ocean. Clim. Past 8, 215–225. https://doi.org/10.5194/cp-8-215-2012
Jenkyns, H.C., Trans, P., Lond, R.S., 2003. Evidence for rapid climate change in the Mesozoic − Palaeogene greenhouse world Evidence for rapid climate change in the Mesozoic – Palaeogene greenhouse world 1885–1916. https://doi.org/10.1098/rsta.2003.1240
Jiamo, F., Guoying, S., Jiayou, X., Eglinton, G., Gowar, A.P., Rongfen, J., Shanfa, F., Pingan, P., 1990. Application of biological markers in the assessment of paleoenvironments of Chinese non-marine sediments. Org. Geochem. 16, 769–779. https://doi.org/10.1016/0146-6380(90)90116-H
John, M., Bohaty, S.M., Zachos, J.C., Sluijs, A., Gibbs, S., Brinkhuis, H., Bralower, T.J.,

John, C.M., Bohaty, S.M., Zachos, J.C., Sluijs, A., Gibbs, S., Brinkhuis, H., Bralower, T.J., 2008. North American continental margin records of the Paleocene-Eocene thermal maximum: Implications for global carbon and hydrological cycling. Paleoceanography 23, 1–20. https://doi.org/10.1029/2007PA001465

Jones, T.D., Lunt, D.J., Schmidt, D.N., Ridgwell, A., Sluijs, A., Valdes, P.J., Maslin, M., 2013. Climate model and proxy data constraints on ocean warming across the Paleocene–Eocene Thermal Maximum. Earth Sci. Rev. 125, 123–145. https://doi.org/10.1016/j.earscirev.2013.07.004

Jones, T.D., Manners, H.R., Hoggett, M., Turner, S.K., Leng, M.J., Pancost, R.D., Ridgwell, A., Alegret, L., Duller, R., Grimes, S.T., 2017. Orbital forcing of terrestrial hydrology , weathering and carbon sequestration during the Palaeocene-Eocene Thermal Maximum. Clim. Past Discuss. 1–22.

Junium, C.K., Arthur, M.A., 2007. Nitrogen cycling during the Cretaceous, Cenomanian-Turonian Oceanic Anoxic Event II. Geochemistry, Geophys. Geosystems 8, 1–18. https://doi.org/10.1029/2006GC001328

Junium, C.K., Dickson, A.J., Uveges, B.T., 2018. Perturbation to the nitrogen cycle during rapid Early Eocene global warming. Nat. Commun. 9, 3186. https://doi.org/10.1038/s41467-018-05486-w

Kaiho, K., Arinobu, T., Ishiwatari, R., Morgans, H.E.G., Okada, H., Takeda, N., Tazaki, K., Zhou, G., Kajiwara, Y., Matsumoto, R., Hirai, A., Niitsuma, N., Wada, H., 1996. Latest Paleocene benthic foraminiferal extinction and environmental changes at Tawanui, New Zealand. Paleoceanography 11, 447–465.

Karner, M.B., DeLong, E.F., Karl, D.M., 2001. Archaeal dominance in the mesopelagic zone of the Pacific Ocean. Nature 409, 507–510. https://doi.org/10.1038/35054051

Kashiyama, Y., Ogawa, N.O., Kuroda, J., Shiro, M., Nomoto, S., Tada, R., Kitazato, H., Ohkouchi, N., 2008. Diazotrophic cyanobacteria as the major photoautotrophs during mid-Cretaceous oceanic anoxic events: Nitrogen and carbon isotopic evidence from sedimentary porphyrin. Org. Geochem. 39, 532–549. https://doi.org/10.1016/j.orggeochem.2007.11.010

Katz, B.J., 1984. Organic Geochemical Character of Selected Cores, Deep Sea Drilling Project Hole 530A, in: Deep Sea Drilling Projects and Publications; Part V: Organic Geochemistry. pp. 1031–1034. https://doi.org/10.2973/dsdp.proc.75.134.1984

Kemper, E., 1987. Das Klima der KreideZeit. Geol. Jahrb. A 96, 5–185.

Kenig, F., Hudson, J.D., Damsté, J.S.S., Popp, B.N., 2004. Intermittent euxinia: Reconciliation of a Jurassic black shale with its biofacies. Geology 32, 421–424. https://doi.org/10.1130/G20356.1

Kennedy, W.J., Cooper, M., 1975. Cretaceous ammonite distributions and the opening of the South Atlantic. J. Geol. Soc. London. 131, 283–288. https://doi.org/10.1144/gsjgs.131.3.0283

Kennett, J.P., Stott, L.D., 1991. Abrupt deep-sea warming, palaeoceanographic changes and benthic extinctions at the end of the Palaeocene. Nature 353, 225–229. https://doi.org/10.1038/353225a0

Kennicutt, M.C., Bidigare, R.R., Macko, S.A., Keeney-kennicutt, W.L., 1992. The stable isotopic composition of photosynthetic pigments and related biochernicals. Chem. Geol. 101, 235–245.

Khozyem, H., Adatte, T., Spangenberg, J.E., Keller, G., Tantawy, A.A., Ulianov, A., 2015. New geochemical constraints on the Paleocene–Eocene thermal maximum: Dababiya GSSP, Egypt. Palaeogeogr. Palaeoclimatol. Palaeoecol. 429, 117–135. https://doi.org/10.1016/j.palaeo.2015.04.003

Khozyem, H., Adatte, T., Spangenberg, J.E., Tantawy, A.A., Keller, G., 2013. Palaeoenvironmental and climatic changes during the Palaeocene–Eocene Thermal Maximum (PETM) at the Wadi Nukhul Section, Sinai, Egypt. J. Geol. Soc. London.

170, 341–352. https://doi.org/10.1144/jgs2012-046
Kim, J.-H., van der Meer, J., Schouten, S., Helmke, P., Willmott, V., Sangiorgi, F., Koç, N., Hopmans, E.C., Damsté, J.S.S., 2010. New indices and calibrations derived from the distribution of crenarchaeal isoprenoid tetraether lipids: Implications for past sea surface temperature reconstructions. Geochim. Cosmochim. Acta 74, 4639–4654. https://doi.org/10.1016/j.gca.2010.05.027
Knies, J., Mann, U., Popp, B.N., Stein, R., Brumsack, H.J.J.J., 2008. Surface water productivity and paleoceanographic implications in the Cenozoic Arctic Ocean. Paleoceanography 23, 1–12. https://doi.org/10.1029/2007PA001455
Koch, P.L., Clyde, W.C., Hepple, R.P., Fogel, M.L., Wing, S.L., Zachos, J.C., Anonymous, 2003. Carbon and oxygen isotope records from Paleosols spanning the Paleocene-Eocene boundary, Bighorn Basin, Wyoming; Causes and consequences of globally warm climates in the early Paleogene. Causes Consequences Glob. Warm Clim. Early Paleogene 369, 49–64.
Kochhann, K.G.D., Koutsoukos, E.A.M., Fauth, G., 2014a. Aptian-Albian benthic foraminifera from DSDP Site 364 (offshore Angola): A paleoenvironmental and paleobiogeographic appraisal. Cretac. Res. 48, 1–11. https://doi.org/10.1016/j.cretres.2013.11.009
Kochhann, K.G.D., Koutsoukos, E.A.M., Fauth, G., Sial, A.N., 2013. Aptian-Albian planktic foraminifera from DSDP Site 364 (offshore Angola): Biostratigraphy, paleoecology, and paleoceanographic significance. J. Foraminifer. Res. 43, 443–463. https://doi.org/10.2113/gsjfr.43.4.443
Kodina, L.A., Huang, Y., Gavrilov, Y. o., Jones, M., Eglinton, G., 1995. Environment of Upper Paleocene black shale deposition in Sothern Russia and adjacent regions as revealed by isotope and biomarker study, in: Grimalt, J.O., Carmen, D. (Eds.), Organic Geochemistry, Developments and Applications to Energy, Climate, Environment and Human History: Selelcted Papers from the 17th International Meeting on Organic Geochemistry. Selected papers from the 17th international meeting on organic geochemistry, Donostia-San Sebastian, The Basque Country, Spain, pp. 192–194.
Kodner, R.B., Pearson, A., Summons, R.E., Knoll, A.H., 2008. Sterols in red and green algae: quantification, phylogeny, and relevance for the interpretation of geologic steranes. Geobiology 6, 411–420. https://doi.org/10.1111/j.1472-4669.2008.00167.x
Koga, Y., Nishihara, M., Morii, H., Akagawa-Matsushita, M., 1993. Ether polar lipids of methanogenic bacteria: structures, comparative aspects, and biosyntheses. Microbiol. Rev. 57, 164–182.
Koopmans, M.P., Köster, J., Van Kaam-Peters, H.M.E.E., Kenig, F., Schouten, S., Hartgers, W.A., De Leeuw, J.W., Sinninghe Damsté, J.S., 1996a. Diagenetic and catagenetic products of isorenieratene: Molecular indicators for photic zone anoxia. Geochim. Cosmochim. Acta 60, 4467–4496. https://doi.org/10.1016/S0016-7037(96)00238-4
Koopmans, M.P., Schouten, S., Kohnen, M.E.L., Sinninghe Damsté, J.S., 1996b. Restricted utility of aryl isoprenoids as indicators for photic zone anoxia. Geochim. Cosmochim. Acta 60, 4873–4876. https://doi.org/10.1016/S0016-7037(96)00303-1
Kopp, R.E., Schumann, D., Raub, T.D., Powars, D.S., Godfrey, L. V., Swanson-Hysell, N.L., Maloof, A.C., Vali, H., 2009. An Appalachian Amazon? Magnetofossil evidence for the development of a tropical river-like system in the mid-Atlantic United States during the Paleocene-Eocene thermal maximum. Paleoceanography 24, n/a-n/a. https://doi.org/10.1029/2009PA001783
Kozdon, R., Kelly, D.C., Kita, N.T., Fournelle, J.H., Valley, J.W., 2011. Planktonic foraminiferal oxygen isotope analysis by ion microprobe technique suggests warm tropical sea surface temperatures during the Early Paleogene. Paleoceanography 26, 1–17. https://doi.org/10.1029/2010PA002056
Kuhnt, W., Holbourn, A., Moullade, M., 2011. Transient global cooling at the onset of early

Aptian oceanic anoxic event (OAE) 1a 323–326. https://doi.org/10.1130/G31554.1
Kurtz, A.C., Kump, L.R., Arthur, M.A., Zachos, J.C., Paytan, A., 2003. Early Cenozoic decoupling of the global carbon and sulfur cycles. Paleoceanography 18. https://doi.org/10.1029/2003PA000908
Kuypers, M.M.M., Blokker, P., Hopmans, E.C., Kinkel, H., Pancost, R.D., Schouten, S., Sinninghe Damsté, J.S., 2002. Archaeal remains dominate marine organic matter from the early Albian oceanic anoxic event 1b. Palaeogeogr. Palaeoclimatol. Palaeoecol. 185, 211–234. https://doi.org/10.1016/S0031-0182(02)00301-2
Kuypers, M.M.M., Lourens, L.J., Rijpstra, W.I.C., Pancost, R.D., Nijenhuis, I.A., Sinninghe Damsté, J.S., 2004. Orbital forcing of organic carbon burial in the proto-North Atlantic during oceanic anoxic event 2. Earth Planet. Sci. Lett. 228, 465–482. https://doi.org/10.1016/j.epsl.2004.09.037
Kuypers, M.M.M., Pancost, R.D., Nijenhuis, I.A., Sinninghe Damsté, J.S., 2002. Enhanced productivity led to increased organic carbon burial in the exinic North Atlantic basin during the late Cenomanian oceanic anoxic event. Paleoceanography 17, 1051. https://doi.org/10.1029/2000PA000569
Kuypers, M.M.M.M., van Breugel, Y., Schouten, S., Erba, E., Sinninghe Damsté, J.S., Damsté, J.S.S., 2004. N2-fixing cyanobacteria supplied nutrient N for Cretaceous oceanic anoxic events. Geology 32, 853. https://doi.org/10.1130/G20458.1
Landais, P., Michels, R., Kister, J., Derepge, J.-M., Benkheddat, Z., 1991. Behavior of oxidized Type II kerogen during artificial maturation. Energy & Fuels 5, 860–866. https://doi.org/10.1021/ef00030a014
Leckie, R.M., 1984. Mid-Cretaceous panktonic foraminiferal biostratigraphy off Central Morocco, Deep Sea Drilling Project Leg 79, Sites 545 and 547, in: Hinz, K., Winterer, E.L. (Eds.), Initial Reports of the Deep Sea Drilling Project, Vol. 79. US Government Printing Office, Washington, pp. 579–620.
Leg 40 Shipboard Scientific Party, 1978. Angola Continental Margin_Sites 364 and 365, in: Bolli, H.M., Ryan, W.B.F., McKnight, B.K., Kagami, H., Melguen, M., Siesser, W.G., Longoria, J.F., Decima, F.P., Foresman, J.B., Hottman, W.E., J.H., N. (Eds.), Initial Reports of the Deep Sea Drilling Project. US Government Printing Office, Washington, pp. 357–455. https://doi.org/10.2973/dsdp.proc.40.104.1978
Li, L., Keller, G., 1998. Maastrichtian climate , productivity and fauna1 turnovers in planktic foraminifera in South Atlantic DSDP sites 525A and 21. Mar. Geochemistry 33, 55–86.
Li, M., Larter, S.R., Taylor, P., Jones, D.M., Bowler, B., Bjorøy, M., 1995. Biomarkers or not biomarkers? A new hypothesis for the origin of pristane involving derivation from methyltrimethyltridecylchromans (MTTCs) formed during diagenesis from chlorophyll and alkylphenols. Org. Geochem. 23, 159–167. https://doi.org/10.1016/0146-6380(94)00112-E
Lippert, P.C., Zachos, J.C., 2007. A biogenic origin for anomalous fine-grained magnetic material at the Paleocone-Eocene boundary at Wilson Lake, New Jersey. Paleoceanography 22, 1–8. https://doi.org/10.1029/2007PA001471
Littler, K., Robinson, S.A., Bown, P.R., 2014. An offset in TEX86 values between interbedded lithologies: Implications for sea-surface temperature reconstructions. Palaeogeogr. Palaeoclimatol. Palaeoecol. 399. https://doi.org/10.1016/j.palaeo.2014.02.009
Littler, K., Robinson, S.A., Bown, P.R., Nederbragt, A.J., Pancost, R.D., 2011. High sea-surface temperatures during the Early Cretaceous Epoch. Nat. Geosci. 4, 169–172. https://doi.org/10.1038/ngeo1081
Lunt, D.J., Farnsworth, A., Loptson, C., L Foster, G., Markwick, P., O'Brien, C.L., Pancost, R.D., Robinson, S.A., Wrobel, N., 2016. Palaeogeographic controls on climate and proxy interpretation. Clim. Past 12, 1181–1198. https://doi.org/10.5194/cp-12-1181-2016

Martin, J.E., Amiot, R., Lécuyer, C., Benton, M.J., 2014. Sea surface temperature contributes to marine crocodylomorph evolution. Nat. Commun. 5, 1–7. https://doi.org/10.1038/ncomms5658

Mackenzie, A.S., Brassell, S.C., Eglinton, G., Maxwell, J.R., 1982. Chemical fossils: The geological fate of steroids. Science (80-.). 217, 491–504. https://doi.org/10.1126/science.217.4559.491

Mackenzie, A.S., Patience, R.L., Maxwell, J.R., Vandenbroucke, M., Durand, B., 1980. Molecular parameters of maturation in the Toarcian shales, Paris Basin, France—I. Changes in the configurations of acyclic isoprenoid alkanes, steranes and triterpanes. Geochim. Cosmochim. Acta 44, 1709–1721. https://doi.org/10.1016/0016-7037(80)90222-7

MacLeod, K.G., Huber, B.T., Berrocoso, A.J., Wendler, I., Berrocoso, Á.J.Á.J., Wendler, I., 2013. A stable and hot Turonian without glacial δ18O excursions is indicated by exquisitely preserved Tanzanian foraminifera. Geology 41, 1083–1086. https://doi.org/10.1130/G34510.1

Macleod, K.G., Londoño, C.I., Martin, E.E., Berrocoso, Á.J., Basak, C., Isaza Londoño, C., Martin, E.E., Jiménez Berrocoso, Á., Basak, C., Londoño, C.I., Martin, E.E., Berrocoso, Á.J., Basak, C., Isaza Londoño, C., Martin, E.E., Jiménez Berrocoso, Á., Basak, C., 2011. Changes in North Atlantic circulation at the end of the Cretaceous greenhouse interval. Nat. Geosci. 4, 779–782. https://doi.org/10.1038/ngeo1284

Malinverno, A., Erba, E., Herbert, T.D., 2010. Orbital tuning as an inverse problem: Chronology of the early Aptian oceanic anoxic event 1a (Selli Level) in the Cismon APTICORE. Paleoceanography 25, 1–16. https://doi.org/10.1029/2009PA001769

Manners, H.R., Grimes, S.T., Sutton, P.A., Domingo, L., Leng, M.J., Twitchett, R.J., Hart, M.B., Dunkley Jones, T., Pancost, R.D., Duller, R., Lopez-Martinez, N., 2013. Magnitude and profile of organic carbon isotope records from the Paleocene-Eocene Thermal Maximum: Evidence from northern Spain. Earth Planet. Sci. Lett. 376, 220–230. https://doi.org/10.1016/j.epsl.2013.06.016

Matsumoto, R., Utada, M., Kagami, H., 1978. Sedimentary Petrology of DSDP Cores From Sites 362 and 353, The Walvis Ridge, and Site 364, The Angola Basin, Drilled on LEG 40, in: Deep Sea Drilling Projects and Publications; Part II: Studies In Sedimentology. pp. 469–483. https://doi.org/10.2973/dsdp.proc.40.106.1978

Matsumoto, T., 1978. Notes on Inoceramus, Mesozoic bivalves from the Southeastern Atlantic, DSDP Sites 361 and 364 , LEG 40, in: Deep Sea Drilling Projects and Publications; to Volumes XXXVIII, XXXIX, XL, and XLI. pp. 703–707. https://doi.org/10.2973/dsdp.proc.38394041s.311.1978

McAnena, A., Flögel, S., Hofmann, P., Herrle, J.O., Griesand, A., Pross, J., Talbot, H.M., Rethemeyer, J., Wallmann, K., Wagner, T., 2013. Atlantic cooling associated with a marine biotic crisis during the mid-Cretaceous period. Nat. Geosci. 6, 558–561. https://doi.org/10.1038/NGEO1850

Mcinerney, F.A., Wing, S.L., 2011. The Paleocene-Eocene Thermal Maximum: A Perturbation of Carbon Cycle, Climate, and Biosphere with Implications for the Future. Annu. Rev. Earth Planet. Sci. 39, 489–516. https://doi.org/10.1146/annurev-earth-040610-133431

Menegatti, A.P., Weissert, H., Brown, R.S., Tyson, R. V., Farrimond, P., Strasser, A., Caron, M., 1998. High-resolution 13C stratigraphy through the early Aptian “Livello Selli” of the Alpine Tethys Alessio. Paleoceanography 13, 530–545. https://doi.org/10.1029/98PA01793

Menzel, D., Van Bergen, P.F., Schouten, S., Sinninghe Damsté, J.S., 2003. Reconstruction of changes in export productivity during Pliocene sapropel deposition: A biomarker approach. Palaeogeogr. Palaeoclimatol. Palaeoecol. 190, 273–287. https://doi.org/10.1016/S0031-0182(02)00610-7

Meyer, K.M., Kump, L.R., 2008. Oceanic Euxinia in Earth History: Causes and Consequences. Annu. Rev. Earth Planet. Sci. 36, 251–288. https://doi.org/10.1146/annurev.earth.36.031207.124256

Meyers, P., 2003. Application of organic geochemistry to paleolimnological reconstruction: a summary of examples from the Laurention Great Lakes. Org. Geochem. 34, 261–289. https://doi.org/10.1016/S0146-6380(02)00168-7

Meyers, P.A., 2006. Paleoceanographic and paleoclimatic similarities between Mediterranean sapropels and Cretaceous black shales. Palaeogeogr. Palaeoclimatol. Palaeoecol. 235, 305–320. https://doi.org/10.1016/j.palaeo.2005.10.025

Meyers, P.A., Bernasconi, S.M., Forster, A., 2006. Origins and accumulation of organic matter in expanded Albian to Santonian black shale sequences on the Demerara Rise, South American margin. Org. Geochem. 37, 1816–1830. https://doi.org/10.1016/j.orggeochem.2006.08.009

Meyers, P.A., Trull, T.W., Kawka, O.E., 1984. Organic Geochemical Comparison of Cretaceous Green and Black Claystones from Hole 530A in the Angola Basin, in: Deep Sea Drilling Projects and Publications; Part V: Organic Geochemistry. pp. 1009–1018.

Miller, K.G., Wright, J.D., Browning, J. V, 2005. Visions of ice sheets in a greenhouse world. Mar. Geol. 217, 215–231. https://doi.org/10.1016/j.margeo.2005.02.007

Möbius, J., Lahajnar, N., Emeis, K.C., 2010. Diagenetic control of nitrogen isotope ratios in Holocene sapropels and recent sediments from the Eastern Mediterranean Sea. Biogeosciences 7, 3901–3914. https://doi.org/10.5194/bg-7-3901-2010

Moldowan, J.., Seifert, W.K., gallegos, E.J., 1985. Relationship Between Petroleum Composition and Depositional Environment of Petroleum Source Rocks. Am. Assoc. Pet. Geol. Bull. 69, 1255–1268.

Molina, E., Appenillas, I., Pardo, A., 1999. High resolution planktic foraminiferal biostratigraphy and correlation across the Paleocene/Eocene boundary in the Tethys. Bull. la Socie´te´ Ge´ologique Fr. 170, 521–530.

Monteiro, F.M., Pancost, R.D., Ridgwell, A., Donnadieu, Y., 2012. Nutrients as the dominant control on the spread of anoxia and euxinia across the Cenomanian-Turonian oceanic anoxic event (OAE2): Model-data comparison. Paleoceanography 27, 1–17. https://doi.org/10.1029/2012PA002351

Murray, J.W., İzdar, E., 1989. The 1988 Black Sea Oceanographic Expedition: Overview and New Discoveries. Oceanography 2, 15–21. https://doi.org/10.5670/oceanog.1989.25

Mutterlose, J., Bornemann, A., Herrle, J., 2009. The Aptian – Albian cold snap: Evidence for "mid" Cretaceous icehouse interludes. Neues Jahrb. für Geol. und Paläontologie - Abhandlungen 252, 217–225. https://doi.org/10.1127/0077-7749/2009/0252-0217

Naafs, B.D., Monteiro, F.M., Froehner, S., Lowson, C., Quijano, M., Castro, J., Donnadieu, Y., Schmidt, D.N., Ridgwell, A.J., Pancost, R.D., 2013. Anoxia and the nitrogen cycle during Cretaceous oceanic anoxic event 1A (≈120 Ma); a data-model comparison. AGU 2013 fall Meet. 2013, 2017.

Naafs, B.D.A., Castro, J.M., De Gea, G.A., Quijano, M.L., Schmidt, D.N., Pancost, R.D., 2016. Gradual and sustained carbon dioxide release during Aptian Oceanic Anoxic Event 1a. Nat. Geosci. 9. https://doi.org/10.1038/ngeo2627

Naafs, B.D.A., Pancost, R.D., 2014. Environmental conditions in the South Atlantic (Angola Basin) during the Early Cretaceous. Org. Geochem. 76, 184–193. https://doi.org/10.1016/j.orggeochem.2014.08.005

Naafs, B.D.A.D.A., Pancost, R.D.D., 2016. Sea-surface temperature evolution across Aptian Oceanic Anoxic Event 1a. Geology 44, G38575.1. https://doi.org/10.1130/G38575.1

Nicolo, M.J., Dickens, G.R., Hollis, C.J., 2010. South Pacific intermediate water oxygen depletion at the onset of the Paleocene-Eocene thermal maximum as depicted in New Zealand margin sections. Paleoceanography 25, 1–12. https://doi.org/10.1029/2009PA001904

Nielsen, J.K., Shen, Y., 2004. Evidence for sulfidic deep water during the Late Permian in the East Greenland Basin. Geology 32, 1037–1040. https://doi.org/10.1130/G20987.1

O'Brien, C.L., Robinson, S.A., Pancost, R.D., Sinninghe Damsté, J.S., Schouten, S., Lunt, D.J., Alsenz, H., Bornemann, A., Bottini, C., Brassell, S.C., Farnsworth, A., Forster, A., Huber, B.T., Inglis, G.N., Jenkyns, H.C., Linnert, C., Littler, K., Markwick, P., McAnena, A., Mutterlose, J., Naafs, B.D.A., Püttmann, W., Sluijs, A., van Helmond, N.A.G.M., Vellekoop, J., Wagner, T., Wrobel, N.E., 2017a. Cretaceous sea-surface temperature evolution: Constraints from TEX86 and planktonic foraminiferal oxygen isotopes. Earth-Science Rev. 172, 224–247. https://doi.org/10.1016/j.earscirev.2017.07.012

Ohba, M., UEDA, H., 2010. A GCM Study on Effects of Continental Drift on Tropical Climate at the Early and Late Cretaceous. J. Meteorol. Soc. Japan 88, 869–881. https://doi.org/10.2151/jmsj.2010-601

Ohkouchi, N., Kashiyama, Y., Kuroda, J., Ogawa, N.O., Kitazato, H., 2006. The importance of diazotrophic cyanobacteria as primary producers during Cretaceous Oceanic Anoxic Event 2. Biogeosciences 3, 467–478. https://doi.org/10.5194/bg-3-467-2006

Orphan, V.J., House, C.H., Hinrichs, K.-U., McKeegan, K.D., DeLong, E.F., 2002. Multiple archaeal groups mediate methane oxidation in anoxic cold seep sediments. Proc. Natl. Acad. Sci. 99, 7663–7668. https://doi.org/10.1073/pnas.072210299

Ourisson, G., Albrecht, P., 1992. Hopanoids. 1. Geohopanoids: the most abundant natural products on Earth? Acc. Chem. Res. 25, 398–402. https://doi.org/DOI: 10.1021/ar00021a003

Owens, J.D., Lyons, T.W., Li, X., Macleod, K.G., Gordon, G., Kuypers, M.M.M., Anbar, A., Kuhnt, W., 2012. Iron isotope and trace metal records of iron cycling in the proto-North Atlantic during the Cenomanian-Turonian oceanic anoxic event (OAE-2) 27, 1–13. https://doi.org/10.1029/2012PA002328

Pagani, M., Caldeira, K., Archer, D., Zachos, J.C., 2006a. An ancient carbon mystery. Science (80-.). 314, 1556–1557. https://doi.org/10.1126/science.1136110

Pagani, M., Pedentchouk, N., Huber, M., Sluijs, A., Schouten, S., Brinkhuis, H., Damsté, J.S.S., Dickens, G.R., Backman, J., Clemens, S., Cronin, T., Eynaud, F., Gattacceca, J., Jakobsson, M., Jordan, R., Kaminski, M., King, J., Koc, N., Martinez, N.C., McInroy, D., Moore, T.C., O'Regan, M., Onodera, J., Pälike, H., Rea, B., Rio, D., Sakamoto, T., Smith, D.C., St John, K.E.K., Suto, I., Suzuki, N., Takahashi, K., Watanabe, M., Yamamoto, M., 2006b. Arctic hydrology during global warming at the Palaeocene/Eocene thermal maximum. Nature 442, 671–675. https://doi.org/10.1038/nature05043

Pagani, M., Pedentchouk, N., Huber, M., Sluijs, A., Schouten, S., Brinkhuis, H., Dickens, G.R., Scientists, E., 2006c. Arctic hydrology during global warming at the Palaeocene / Eocene thermal maximum. Nature 442, 671–675. https://doi.org/10.1038/nature05043

Paillard, D., Labeyrie, L., Yiou, P., 1996. Macintosh Program performs time-series analysis. Eos Trans. Am. Geophys. Union 77, 379. https://doi.org/10.1029/96EO00259

Pak, D.K., Miller, K.G., 1992. Paleocene to Eocene benthic foraminiferal isotopes and assemblages: Implications for deepwater circulation. Paleoceanography 7, 405–422. https://doi.org/10.1029/92PA01234

Pälike, C., Delaney, M.L., Zachos, J.C., 2014. Deep-sea redox across the Paleocene-Eocene thermal maximum. Geochemistry Geophys. Geosystems 15, 1038–1053. https://doi.org/10.1002/2013GC005074.Received

Pälike, C., Delaney, M.L., Zachos, J.C., Plike, C., Delaney, M.L., Zachos, J.C., Pälike, C., Delaney, M.L., Zachos, J.C., Palike, C., Delaney, M.L., Zachos, J.C., 2014. Deep-sea redox across the Paleocene-Eocene thermal maximum. Geochemistry Geophys. Geosystems, AGU Publ. 15, 1038–1053. https://doi.org/10.1002/2013GC005074.Received

Panchuk, K., Ridgwell, A., Kump, L.R., 2008. Sedimentary response to Paleocene-Eocene thermal maximum carbon release: A model-data comparison. Geology 36, 315–318. https://doi.org/10.1130/G24474A.1

Pancost, R.D., Bouloubassi, I., Aloisi, G., Sinninghe Damsté, J.S., 2001. Three series of non-isoprenoidal dialkyl glycerol diethers in cold-seep carbonate crusts. Org. Geochem. 32, 695–707. https://doi.org/10.1016/S0146-6380(01)00015-8

Pancost, R.D., Crawford, N., Magness, S., Turner, A., Jenkyns, H.C., Maxwell, J.R., 2004. Further evidence for the development of photic-zone euxinic conditions during Mesozoic oceanic anoxic events. J. Geol. Soc. London. 161, 353–364. https://doi.org/10.1144/0016764903-059

Pancost, R.D., Sinninghe Damsté, J.S., de Lint, S. De, Van Der Maarel, M.J.E.C., Gottschal, J.C., The Medinaut Shipboard Scientific Party, 2000. Biomarker Evidence for Widespread Anaerobic Methane Oxidation in Mediterranean Sediments by a Consortium of Methaogenic Archaea and Bacteria. Appl. Environ. Microbiol. 66, 1126–1132. https://doi.org/10.1128/AEM.66.3.1126-1132.2000

Pardo, A., Keller, G., Molina, E., Canudo, J.I., 1997. Planktic foraminiferal turnover across the Paleocene-Eocene transition at DSDP Site 401, Bay of Biscay, North Atlantic. Mar. Micropaleontol. 29, 129–158. https://doi.org/10.1016/S0377-8398(96)00035-7

Pérez-Diaz, L., Eagles, G., 2014. Constraining South Atlantic growth with seafloor spreading data. Tectonics 33, 1848–1873. https://doi.org/10.1002/2014TC003644

Pérez-Díaz, L., Eagles, G., 2017. South Atlantic paleobathymetry since early Cretaceous. Sci. Rep. 7, 1–16. https://doi.org/10.1038/s41598-017-11959-7

Pearson, A., Higgins, M.B., Robinson, R.S., Carter, S.J., 2010. A High-Resolution Porphyrin Nitrogen Isotope Record of an Oceanic Anoxic Event, in: American Geophysical Union, Fall Meeting. pp. 3–4.

Pearson, P.N., Palmer, M.R., 2000. Atmospheric carbon dioxide concentrations over the past 60 million years. Nature 406, 695.

Peters, K.E., Moldowan, J.M., 1991. Effects of source, thermal maturity, and biodegradation on the distribution and isomerization of homohopanes in petroleum. Org. Geochem. 17, 47–61. https://doi.org/10.1016/0146-6380(91)90039-M

Pirrie, D., Marshall, J.D., Doyle, P., Riccardi, A.C., 2004. Cool early Albian climates; new data from Argentina. Cretac. Res. 25, 27–33. https://doi.org/10.1016/j.cretres.2003.10.002

Popp, B.N., Laws, E.A., Bridigare, R.R., Dore, J.E., Hanson, K.L., Wakeham, S.G., 1998. Effect of phytplankton cell geometry on carbon isotopis fractionation. Geochim. Cosmochim. Acta 62, 69–77.

Poulsen, C.J., Barron, E.J., Johnson, C.C., Fawcett, P., 1999. Links between climatic factors and regional oceanic circulation in the mid-Cretaceous, in: Barrera, E., Johnson, C. (Eds.), The Evolution of Cretaceous Ocean/Climate Systems. Geological Society of America Volume 332, pp. 73–89. https://doi.org/https://doi.org/10.1130/0-8137-2332-9.73

Pucéat, E., Lécuyer, C., Sheppard, S.M.F., Dromart, G., Stéphane, R., Grandjean, P., 2003. Thermal evolution of Cretaceous Tethyan marine waters inferred from oxygen isotope composition of fish tooth enamels. Paleoceanography 18, 1–12. https://doi.org/10.1029/2002PA000823

Pujalte, V., Baceta, J.I., Orue-Etxebarria, X., Payros, A., 1998. Paleocene Strata Of The Basque Country, Western Pyrenees, Northern Spain: Facies And Sequence Development In A Deep-Water Starved Basin. Mesozoic Cenozoic Seq. Stratigr. Eur. Basins 60, 311–325. https://doi.org/10.2110/pec.98.02.0303

Quirk, M.M., Wardroper, A.M.K., Wheatley, R.E., Maxwell, J.R., 1984. Extended hopanoids in peat environments. Chem. Geol. 42, 25–43. https://doi.org/10.1016/0009-2541(84)90003-2

Ratnayake, N.P., Suzuki, N., Okada, M., Takagi, M., 2006. The variations of stable carbon isotope ratio of land plant-derived n-alkanes in deep-sea sediments from the Bering Sea and the North Pacific Ocean during the last 250,000 years. Chem. Geol. 228, 197–208. https://doi.org/10.1016/j.chemgeo.2005.10.005

Rau, G.H., Arthur, M.A., Dean, W.., 1987. 15N/ 14 N variations in Cretaceous Atlantic sedimentary sequences: Implication for past changes in marine nitrogen biogeochemistry. Earth Planet. Sci. Lett. 82, 269–279.

Raynaud, J.F.F., Robert, P., 1978. Microscopical survey of organic matter from DSDP Sites 361, 362, and 364, in: Deep Sea Drilling Projects and Publications; Supplement to Volumes XXXVIII, XXXIX, XL, and XLI. pp. 663–669. https://doi.org/doi:10.2973/dsdp.proc.38394041s.306.1978

Redfield, A., 1934. On the proportions of organic derivatives in seawater and their relation to the composition of plankton, in: Johnstone, J. (Ed.), James Johnstone Memorial Volume. Liverpool, UK, pp. 176–192.

Repeta, D.J., Simpson, D.J., Jørgensen, B.B., Jannasch, H.W., 1989. Evidence for anoxygenic photosynthesis from the distribution of bacteriochlorophylls in the Black Sea. Nature 342, 69–72. https://doi.org/10.1038/342069a0

Reyment, R.A., Tait, E.A., 1972. Atlantic, Biostratigraphical dating of the early history of the South. Philos. Trans. R. Soc. B 264, 55–95. https://doi.org/10.1098/rsta.1892.0001

Ridgwell, A., Hargreaves, J.C., Edwards, N.R., Annan, J.D., Lenton, T.M., Marsh, R., Yool, A., Watson, A., 2007. Marine geochemical data assimilation in an efficient Earth System Model of global biogeochemical cycling. Biogeosciences Discuss. 4, 87–104.

Rieley, G., Collier, R.J., Jones, D.M., Eglinton, G., 1991. The biogeochemistry of Ellesmere Lake, U.K.-I: source correlation of leaf wax inputs to the sedimentary lipid record. Org. Geochem. 17, 901–912. https://doi.org/10.1016/0146-6380(91)90031-E

Robinson, S.A., Clarke, L.J., Nederbragt, A., Wood, I.G., 2008. Mid-Cretaceous oceanic anoxic events in the Pacific Ocean revealed by carbon-isotope stratigraphy of the Calera Limestone, California, USA. Bull. Geol. Soc. Am. 120, 1416–1426. https://doi.org/10.1130/B26350.1

Robinson, S.A., Heimhofer, U., Hesselbo, S.P., Petrizzo, M.R., 2017. Mesozoic climates and oceans – a tribute to Hugh Jenkyns and Helmut Weissert. Sedimentology 64, 1–15. https://doi.org/10.1111/sed.12349

Robinson, R.S., Sigman, D.M., DiFiore, P.J., Rohde, M.M., Mashiotta, T.A., Lea, D.W., 2005. Diatom-bound 15N/14N: New support for enhanced nutrient consumption in the ice age subantarctic. Paleoceanography 20, 1–14. https://doi.org/10.1029/2004PA001114

Rodríguez-Tovar, J., F., Uchman, A., Alegret, L., Molina, E., 2011. Impact of the Paleocene–Eocene Thermal Maximum on the macrobenthic community: Ichnological record from the Zumaia section, northern Spain. Mar. Geol. 282, 178–187. https://doi.org/10.1016/j.margeo.2011.02.009

Rohling, E.J., 1994. Review and new aspects concerning the formation of eastern Mediterranean sapropels. Marine Geol. 122, 1–28. https://doi.org/10.1016/0025-3227(94)90202-X

Ruble, T.E., Bakel, A.J., Paul Philp, R., 1994. Compound specific isotopic variability in Uinta Basin native bitumens: paleoenvironmental implications. Org. Geochem. 21, 661–671. https://doi.org/10.1016/0146-6380(94)90011-6

Rullkötter, J., Mukhopadhyay, P.K., Welte, D.H., 1984. Geochemistry and Petrography of Organic Matter in Sediments from Hole 530A, Angola Basin, and Hole 532, Walvis Ridge, Deep Sea Drilling Project. Cover. Leg 75 cruises Drill. Vessel Glomar Chall. Walvis Bay, South Africa, to Recife, Brazil 75, 1069–1087. https://doi.org/10.2973/dsdp.proc.79.132.1984

Sachs, J.P., Repeta, D.J., Goericke, R., 1999. Nitrogen and carbon isotopic ratios of

chlorophyll from marine phytoplankton. Geochim. Cosmochim. Acta 63, 1431–1441. https://doi.org/10.1016/s0016-7037(99)00097-6

Schlanger, S.O., Jenkyns, H.C., 1976. Cretaceous Oceanic Anoxic Events: Causes and Concequences. Geol. En Minbouw 55, 179–184.

Schmidt, K., 1978. Biosynthesis of cartenoids, in: Clayton, R.K., Sistrom, W.R., Eds (Eds.), Photosynthesis Bacteria. Plenum Press, New York, pp. 729–50.

Schmitz, B., Pujalte, V., Núñez-Betelu, K., 2001. Climate and sea-level perturbations during the Initial Eocene Thermal Maximum: Evidence from siliciclastic units in the Basque basin (Ermua, Zumaia and Trabakua Pass), northern Spain. Palaeogeogr. Palaeoclimatol. Palaeoecol. 165, 299–320. https://doi.org/10.1016/S0031-0182(00)00167-X

Schoon, P.L., Heilmann-Clausen, C., Schultz, B.P., Sluijs, A., Sinninghe Damsté, J.S., Schouten, S., Pagh Schultz, B., Sluijs, A., Sinninghe Damsté, J.S., Schouten, S., 2013. Recognition of Early Eocene global carbon isotope excursions using lipids of marine Thaumarchaeota. Earth Planet. Sci. Lett. 373, 160–168. https://doi.org/10.1016/j.epsl.2013.04.037

Schouten, S., Hopmans, E.C., Forster, A., van Breugel, Y., Kuypers, M.M.M., Sinninghe Damsté, J.S., Darnsté, J.S.S., 2003. Extremely high sea-surface temperatures at low latitudes during the middle Cretaceous as revealed by archeal membrane lipds. Geology 31, 1069–1072. https://doi.org/10.1130/G19876.1

Schouten, S., Hopmans, E.C., M, E.S., 2002. Distributional variations in marine crenarchaeotal membrane lipids : a new tool for reconstructing ancient sea water temperatures. Earth Planet. Sci. Lett. 204, 265–274. https://doi.org/10.1016/S0012-821X(02)00979-2

Schouten, S., Hopmans, E.C., Sinninghe Damsté, J.S., 2013. The organic geochemistry of glycerol dialkyl glycerol tetraether lipids: A review. Org. Geochem. 54, 19–61. https://doi.org/10.1016/j.orggeochem.2012.09.006

Schouten, S., Hopmans, E.C., Sinninghe Damsté, J.S., 2004. The effect of maturity and depositional redox conditions on archaeal tetraether lipid palaeothermometry. Org. Geochem. 35, 567–571. https://doi.org/10.1016/j.orggeochem.2004.01.012

Schouten, S., Rampen, S.W., Geenevasen, J.A.J., Sinninghe Damsté, J.S., 2005. Structural identification of steryl alkyl ethers in marine sediments. Org. Geochem. 36, 1323–1333. https://doi.org/10.1016/j.orggeochem.2005.04.002

Schouten, S., Van Der Maarel, M.J.E.C., Huber, R., Damsté, J.S.S., 1997. 2,6,10,15,19-Pentamethylicosenes in Methanolobus bombayensis, a marine methanogenic archaeon, and in Methanosarcina mazei. Org. Geochem. 26, 409–414. https://doi.org/10.1016/S0146-6380(97)00011-9

Schubert, C.J., Calvert, S.E., 2001. Nitrogen and carbon isotopic composition of marine and terrestrial organic matter in Arctic Ocean sediments: Deep Sea Res. Part I Oceanogr. Res. Pap. 48, 789–810. https://doi.org/10.1016/S0967-0637(00)00069-8

Schulte, P., Scheibner, C., Speijer, R.P., 2011. Fluvial discharge and sea-level changes controlling black shale deposition during the Paleocene-Eocene Thermal Maximum in the Dababiya Quarry section, Egypt. Chem. Geol. 285, 167–183. https://doi.org/10.1016/j.chemgeo.2011.04.004

Schulte, S., Rostek, F., Bard, E., Rullkötter, J., Marchal, O., 1999. Variations of oxygen-minimum and primary productivity recorded in sediments of the Arabian Sea. Earth Planet. Sci. Lett. 173, 205–221. https://doi.org/10.1016/S0012-821X(99)00232-0

Schulz, M., Mudelsee, M., 2002. REDFIT: Estimating red-noise spectra directly from unevenly spaced paleoclimatic time series. Comput. Geosci. 28, 421–426. https://doi.org/10.1016/S0098-3004(01)00044-9

Scott, R.W., Formolo, M., Rush, N., Owens, J.D., Oboh-Ikuenobe, F., 2013. Upper Albian OAE 1d event in the Chihuahua Trough, New Mexico, U.S.A. Cretac. Res. 46, 136–150. https://doi.org/10.1016/j.cretres.2013.08.011

Seifert, W.K., Moldowan, J.M., 1980. The effect of thermal stress on source-rock quality as measured by hopane stereochemistry. Phys. Chem. Earth 12, 229–237. https://doi.org/10.1016/0079-1946(79)90107-1

Sepulveda, J., Wendler, J.E., Summons, R.E., Hinrichs, K.-U., 2009. Rapid Resurgence of Marine Productivity After the Cretaceous-Paleogene Mass Extinction. Science (80-.). 326, 129–132. https://doi.org/10.1126/science.1176233

Shen, Y., Canfield, D.E., Knoll, A.H., 2002. Middle Proterozoic ocean chemistry: Evidence from the McArthur Basin, northern Australia. Am. J. Sci. 302, 81–109. https://doi.org/10.1126/science.3.53.32

Shipboard Scientific Party, 1984. 1. INTRODUCTION AND EXPLANATORY NOTES, DEEP SEA DRILLING PROJECT LEG 75 1 Shipboard Scientific Party 2, in: Deep Sea Drilling Project Leg 75; Introduction and Explanatory Notes, Deep Sea Drilling Project Leg 75. pp. 3–25. https://doi.org/doi:10.2973/dsdp.proc.75.101.1984

Sibuet, J., Hay, W.W., Prunier, A., Montadert, L., Hinz, K., Fritsch, J., 1984. Early evolution of the South Atlantic Ocean: Role of the rifting episode. Sites J. 20Th Century /Contemporary French Stud. 75, 469–481.

Sigman, D.M., Casciotti, K.L., Andreani, M., Barford, C., Galanter, M., Böhlke, J.K., 2001. A bacterial method for the nitrogen isotopic analysis of nitrate in seawater and freshwater. Anal. Chem. 73, 4145–4153. https://doi.org/10.1021/ac010088e

Simoneit, B.R.T., 1978. Lipid analyses of sediments from Site 364 in the Angola Basin, DSDP LEG 40, in: White, S.M., Supko, P.R., Natland, J., Gardner, J., Herring, J. (Eds.), Initial Reports of the Deep Sea Drilling Project; Supplement to Volumes XXXVIII, XXXIX, XL, and XLI. Texas A & M University, Ocean Drilling Program, College Station, TX, United States, pp. 659–662. https://doi.org/10.2973/dsdp.proc.38394041s.305.1978

Sinninghe Damsté, J.S., de Leeuw, J.W., 1990. Analysis, structure and geochemical significance of organically- bound sulphur in the geosphere: state of the art and future research. Org. Geochem. 16, 1077–1103. https://doi.org/10.1016/0146-6380(90)90145-P

Sinninghe Damsté, J.S., Kock-Van Dalen, A.C., De Leeuw, J.W., Schenck, P.A., 1988. Identification of homologous series of alkylated thiophenes, thiolanes,thianes and Benzothiophenes present in pyrolysates of sulphur-rich kerogens. J. Chromatogr. 435, 435–452. https://doi.org/doi:10.1016/S0021-9673(01)82208-1

Sinninghe Damsté, J.S., Kuypers, M.M.M., Pancost, R.D., Schouten, S., 2008. Organic Geochemistry The carbon isotopic response of algae , (cyano) bacteria , archaea and higher plants to the late Cenomanian perturbation of the global carbon cycle : Insights from biomarkers in black shales from the Cape Verde Basin (DSDP Site 367. Org. Geochem. 39, 1703–1718. https://doi.org/10.1016/j.orggeochem.2008.01.012

Sinninghe Damsté, J.S., Kuypers, M.M.M., Schouten, S., Schulte, S., Rullkötter, J., 2003. The lycopane/C31 n-alkane ratio as a proxy to assess palaeoxicity during sediment deposition. Earth Planet. Sci. Lett. 209, 215–226. https://doi.org/10.1016/S0012-821X(03)00066-9

Sinninghe Damsté, J.S., Ossebaar, J., Schouten, S., Verschuren, D., 2012. Distribution of tetraether lipids in the 25-ka sedimentary record of Lake Challa: Extracting reliable TEX 86 and MBT/CBT palaeotemperatures from an equatorial African lake. Quat. Sci. Rev. 50, 43–54. https://doi.org/10.1016/j.quascirev.2012.07.001

Sinninghe Damsté, J.S., Rijpstra, W.I.C., de Leeuw, J.W., Schenck, P.A., 1989. The occurrence and identification of series of organic sulphur compounds in oils and sediment extracts: II. Their presence in samples from hypersaline and non-hypersaline palaeoenvironments and possible application as source, palaeoenvironmental and matur. Geochim. Cosmochim. Acta 53, 1323–1341. https://doi.org/10.1016/0016-7037(89)90066-5

Sinninghe Damsté, J.S., van Bentum, E.C., Reichart, G.J., Pross, J., Schouten, S., 2010. A

CO2 decrease-driven cooling and increased latitudinal temperature gradient during the mid-Cretaceous Oceanic Anoxic Event 2. Earth Planet. Sci. Lett. 293, 97–103. https://doi.org/10.1016/j.epsl.2010.02.027

Sinninghe Damsté, J.S., Van Duin, A.C.T., Hollander, D., Kohnen, M.E.L., De Leeuw, J.W., 1995. Early diagenesis of bacteriohopanepolyol derivatives: Formation of fossil homohopanoids. Geochim. Cosmochim. Acta 59, 5141–5157. https://doi.org/10.1016/0016-7037(95)00338-X

Slomp, C.P., 2009. Reconstructing the history of euxinia in a coastal sea. Rev. la Asoc. Geol. Argentina 65, 603–611. https://doi.org/10.1126/science

Słowakiewicz, M., Tucker, M.E., Perri, E., Pancost, R.D., 2015. Nearshore euxinia in the photic zone of an ancient sea. Palaeogeogr. Palaeoclimatol. Palaeoecol. 426, 242–259. https://doi.org/http://dx.doi.org/10.1016/j.palaeo.2015.03.022

Sluijs, A., Bijl, P.K., Schouten, S., Röhl, U., Reichart, G.J., Brinkhuis, H., 2011. Southern ocean warming, sea level and hydrological change during the Paleocene-Eocene thermal maximum. Clim. Past 7, 47–61. https://doi.org/10.5194/cp-7-47-2011

Sluijs, A., Dickens, G.R., 2012. Assessing offsets between the δ13C of sedimentary components and the global exogenic carbon pool across early Paleogene carbon cycle perturbations. Global Biogeochem. Cycles 26, 1–14. https://doi.org/10.1029/2011GB004224

Sluijs, A., Röhl, U., Schouten, S., Brumsack, H.-J.J., Sangiorgi, F., Sinninghe Damsté, J.S., Brinkhuis, H., 2008. Arctic late Paleocene-early Eocene paleoenvironments with special emphasis on the Paleocene-Eocene thermal maximum (Lomonosov Ridge, Integrated Ocean Drilling Program Expedition 302). Paleoceanography 23, n/a-n/a. https://doi.org/10.1029/2007PA001495

Sluijs, A., Roij, L. Van, Frieling, J., Laks, J., Reichart, G., 2018. Single-species dinoflagellate cyst carbon isotope ecology across the Paleocene-Eocene Thermal Maximum 1–4. https://doi.org/10.1130/G39598.1

Sluijs, A., Schouten, S., Pagani, M., Woltering, M., Brinkhuis, H., Damsté, J.S.S., Dickens, G.R., Huber, M., Reichart, G.-J., Stein, R., Matthiessen, J., Lourens, L.J., Pedentchouk, N., Backman, J., Moran, K., the Expedition 302 Scientists, 2006. Subtropical Arctic Ocean temperatures during the Palaeocene/Eocene thermal maximum. Nature. https://doi.org/10.1038/nature04668

Sluijs, A., van Roij, L., Harrington, G.J., Schouten, S., Sessa, J.A., LeVay, L.J., Reichart, G.-J., Slomp, C.P., 2014. Warming, euxinia and sea level rise during the Paleocene–Eocene Thermal Maximum on t5he Gulf Coastal Plain: implications for ocean oxygenation and nutrient cycling. Clim. Past 10, 1421–1439. https://doi.org/10.5194/cp-10-1421-2014

Soliman, M.F., Ahmed, E.A., Kurzweil, H., 2006. Geochemistry and mineralogy of the Paleocene/Eocene boundary at Gabal Dababiya (GSSP) and Gabal Owaina sections, Nile Valley, Egypt | MicroAccess. Stratigraphy 3.

Sousa Júnior, G.R., Santos, A.L.S., de Lima, S.G., Lopes, J.A.D., Reis, F.A.M., Santos Neto, E. V., Chang, H.K., 2013. Evidence for euphotic zone anoxia during the deposition of Aptian source rocks based on aryl isoprenoids in petroleum, Sergipe–Alagoas Basin, northeastern Brazil. Org. Geochem. 63, 94–104. https://doi.org/10.1016/j.orggeochem.2013.07.009

Speijer, R.P., Wagner, T., 2002. Sea-level changes and black shales associated with the late Paleocene thermal maximum (LPTM): organic geochemical and micropaleontologic evidence from the southern Tethyam margin (Egypt-Israel). Catastrophic events mass extinctions impacts beyond. Geol. Soc. Am. Spec. Pap. 356, 533–549.

Stanley, D.J., 1978. Ionian Sea sapropel distribution and late Quaternary paleoceanography in the eastern Mediterranean. Nature 274, 149–152.

Stassen, P., Thomas, E., Speijer, R.P., 2012. Integrated stratigraphy of the Paleocene-Eocene thermal maximum in the New Jersey Coastal Plain: Toward understanding the effects of

global warming in a shelf environment. Paleoceanography 27, 1–17. https://doi.org/10.1029/2012PA002323
Stein, R., 1991. Lecture Notes in Earth Sciences Ruediger Stein Accumulation of Organic Carbon in Marine Sediments Springer-Verlag.
Stein, R., Boucsein, B., Meyer, H., 2006. Anoxia and high primary production in the Paleogene central Arctic Ocean: First detailed records from Lomonosov Ridge. Geophys. Res. Lett 33. https://doi.org/10.1029/2006GL026776
Stein, R., Rullkotter, J., Welte, D.H., 1986. Accumulation of organic-carbon-rich sediments in the Late Jurassic and Cretaceous Atlantic Ocean - A synthesis. Chem. Geol. 56, 1–32. https://doi.org/10.1016/0009-2541(86)90107-5
Stow, D.A. V, Dean, W.E., 1984. Middle Cretaceous Black Shales at Site 530 in the Southeastern Angola Basin, in: Deep Sea Drilling Projects and Publications; Part IV: Sedimentology and Inorganic Geochemistry. pp. 809–817. https://doi.org/10.2973/dsdp.proc.75.120.1984
Summons, R.E., Bradley, A.S., Jahnke, L.L., Waldbauer, J.R., 2006. Steroids, triterpenoids and molecular oxygen. Philos. Trans. R. Soc. B 361, 951–968. https://doi.org/10.1098/rstb.2006.1837
Summons, R.E., Powell, T.G., 1986. Chlorobiaceae in Palaeozoic seas revealed by biological markers, isotopes and geology. Nature 319, 763–765. https://doi.org/10.1038/319763a0
Summons, R.E., Powell, T.G., Boreham, C.J., 1988. Petroleum geology and geochemistry of the Middle Proterozoic McArthur Basin, Northern Australia: III. Composition of extractable hydrocarbons. Geochim. Cosmochim. Acta 52, 1747–1763. https://doi.org/10.1016/0016-7037(88)90001-4
Summons, R.E., Thomas, J., Maxwell, J.R., Boreham, J., 1992. Secular and environmental constraints on the occurrence of dinosterane in sediments. Geochimica Cosmochim. Acta 56, 2437–2444. https://doi.org/10.1016/0016-7037(92)90200-3
Summons, R.E., Volkman, J.K., Boreham, C.J., 1987. Dinosterane and other steroidal hydrocarbons of dinoflagellate origin in sediments and petroleum. Geochim. Cosmochim. Acta 51, 3075–3082. https://doi.org/10.1016/0016-7037(87)90381-4
Svensen, H.H., Planke, S., Malthe-sorenssen, A., Jantveit, B., Myklebust, R., Eidem, T.R., Rey, S.S., 2004. Eocene global warming Hydrothermal vents prompt methane release. Nature 429, 3–6. https://doi.org/10.1038/nature02575.1.
Tabor, C.R., Poulsen, C.J., Lunt, D.J., Rosenbloom, N.A., Otto-Bliesner, B.L., Markwick, P.J., Brady, E.C., Farnsworth, A., Feng, R., 2016. The cause of Late Cretaceous cooling: A multimodel-proxy comparison. Geology 44. https://doi.org/10.1130/G38363.1
Takashima, R., Nishi, H., Yamanaka, T., Hayashi, K., Waseda, A., Obuse, A., 2010. High-resolution terrestrial carbon isotope and planktic foraminiferal records of the Upper Cenomanian to the Lower Campanian in the Northwest Pacific. Earth Planet. Sci. Lett. 289, 570–582. https://doi.org/10.1016/j.epsl.2009.11.058.
Taylor, K.W.R.R., Huber, M., Hollis, C.J., Hernandez-Sanchez, M.T., Pancost, R.D., 2013. Re-evaluating modern and Palaeogene GDGT distributions: Implications for SST reconstructions. Glob. Planet. Change. https://doi.org/10.1016/j.gloplacha.2013.06.011
Tedeschi, L.R., Jenkyns, H.C., Robinson, S.A., Sanjinés, A.E.S., Viviers, M.C., Quintaes, C.M.S.P., Vazquez, J.C., 2017. New age constraints on Aptian evaporites and carbonates from the South Atlantic: Implications for Oceanic Anoxic Event 1a. Geology 45, 543–546. https://doi.org/10.1130/G38886.1
Thibault, N., Gardin, S., 2006. Maastrichtian calcareous nannofossil biostratigraphy and paleoecology in the Equatorial Atlantic (Demerara Rise , ODP Leg 207 Hole 1258A) Biostratigraphie et Paléoécologie des nannofossiles calcaires du Maastrichtien dans l ' Atlantique équatorial (Pla. Rev. Micropaléontologie 49, 199–214. https://doi.org/10.1016/j.revmic.2006.08.002
Thomas, D.J., Bralowe, T.J., Zachos, J.C., 1999. New evidence for subtropical warming

during the Late Paleocene thermal maximum: stable isotopes from the Deep Sea Drilling Project Site 527, Wavis Ridge. Paleoceanography 14, 561–570. https://doi.org/10.1029/1999PA900031

Tierney, J.E., Tingley, M.P., 2015. A TEX86 surface sediment database and extended Bayesian calibration. Sci Data 2. https://doi.org/10.1038/sdata.2015.29

Tierney, J.E., Tingley, M.P., 2014. A Bayesian, spatially-varying calibration model for the TEX86proxy. Geochim. Cosmochim. Acta 127, 83–106. https://doi.org/10.1016/j.gca.2013.11.026

Tripati, A., Elderfield, H., 2005. Paleoclimate: Deep-sea temperature and circulation changes at the Paleocene-Eocene Thermal Maximum. Science (80-.). https://doi.org/10.1126/science.1109202

Trommer, G., Siccha, M., van der Meer, M.T.J., Schouten, S., Sinninghe Damsté, J.S., Schulz, H., Hemleben, C., Kucera, M., 2009. Distribution of Crenarchaeota tetraether membrane lipids in surface sediments from the Red Sea. Org. Geochem. 40, 724–731. https://doi.org/10.1016/j.orggeochem.2009.03.001

Tsikos, H., Karakitsios, V., van Breugel, Y., Walsworth-Bell, B., Bombardiere, L., Petrizzo, M.R., Sinninghe Damsté, J.S., Schouten, S., Erba, E., Premoli Silva, I., Farrimond, P., Tyson, R. V., Jenkyns, H.C., 2004. Organic-carbon deposition in the Cretaceous of the Ionian Basin, NW Greece: The Paquier Event (OAE 1b) revisited. Geol. Mag. 141, 401–416. https://doi.org/10.1017/S0016756804009409

Tyrrell, T., 1999. The relative influences of nitrogen and phosohorus on oceanic primary production. Nature 400, 525–531. https://doi.org/10.1038/22941

Uda, I., Sugai, A., Itoh, Y.H., Itoh, T., 2001. Variation in molecular species of polar lipids from thermoplasma acidophilum depends on growth temperature. Lipids 36, 103–105. https://doi.org/10.1007/s11745-001-0914-2

van Breugel, Y., Schouten, S., Tsikos, H., Erba, E., Price, G.D., Damsté, J.S.S., 2007. Synchronous negative carbon isotope shifts in marine and terrestrial biomarkers at the onset of the early Aptian oceanic anoxic event 1a: Evidence for the release of 13C-depleted carbon into the atmosphere. Paleoceanography 22, 1–13. https://doi.org/10.1029/2006PA001341

Van Gemerden, H., Mas, J., 1995. Ecology of Phototrophic Sulfur Bacteria, in: Lankenship, R.E., Madigan, M.T., Bauer, C.E. (Eds.), Anoxygenic Photosynthetic Bacteria. Springer, Dordrecht, pp. 49–85. https://doi.org/10.1007/0-306-47954-0_4

Voigt, S., Jung, C., Friedrich, O., Frank, M., Teschner, C., Hoffmann, J., 2013. Tectonically restricted deep-ocean circulation at the end of the Cretaceous greenhouse. Earth Planet. Sci. Lett. 369–370, 169–177. https://doi.org/10.1016/j.epsl.2013.03.019

Volkman, J.K., Barrett, S.M., Dunstan, G.A., Jeffrey, S.W., 1994. Sterol biomarkers for microalgae from the green algal class Prasinophyceae. Org. Geochem. 21, 1211–1218. https://doi.org/10.1016/0146-6380(94)90164-3

Volkman, J.K., Barrett, S.M., Dunstan, G.A., Jeffrey, S.W., 1993. Geochemical significance of the occurrence of dinosterol and other 4-methyl sterols in a marine diatom. Org. Geochem. 20, 7–15. https://doi.org/10.1016/0146-6380(93)90076-N

Volkman, J.K., Kearney, P., Jeffrey, S.W., 1990. A new source of 4-methyl sterols and 5α(H)-stanols in sediments: prymnesiophyte microalgae of the genus Pavlova. Org. Geochem. 15, 489–497. https://doi.org/10.1016/0146-6380(90)90094-G

Volkman, J.K., Maxwell, J.R., 1986. Acyclic isoprenoids as biological markers, in: Biological Markers in the Sedimentary Record. Elsevier, New York, pp. 1–42.

Wagner, T., Herrle, J.O., Damsté, J.S.S., Schouten, S., Stüsser, I., Hofmann, P., 2008. Rapid warming and salinity changes of Cretaceous surface waters in the subtropical north Atlantic. Geology 36, 203–206. https://doi.org/10.1130/G24523A.1

Wagner, T., Hofmann, P., Flögel, S., 2013. Marine black shale deposition and Hadley Cell dynamics: A conceptual framework for the Cretaceous Atlantic Ocean. Mar. Pet. Geol.

43, 222–238. https://doi.org/10.1016/j.marpetgeo.2013.02.005
Wagner, T., Pletsch, T., 1999. Tectono-sedimentary controls on Cretaceous black shale deposition along the opening Equatorial Atlantic Gateway (ODP Leg 159). Geol. Soc. London, Spec. Publ. 153, 241–265. https://doi.org/10.1144/GSL.SP.1999.153.01.15
Wagner, T., Sinninghe Damsté, J.S., Hofmann, P., Beckmann, B., 2004. Euxinia and primary production in Late Cretaceous eastern equatorial Atlantic surface waters fostered orbitally driven formation of marine black shales. Paleoceanography 19, 1–13. https://doi.org/10.1029/2003PA000898
Wagreich, M., 2012. "OAE 3" - Regional Atlantic organic carbon burial during the Coniacian-Santonian. Clim. Past 8, 1447–1455. https://doi.org/10.5194/cp-8-1447-2012
Wakeham, S.G., Lewis, C.M., Hopmans, E.C., Schouten, S., Sinninghe Damsté, J.S., 2003. Archaea mediate anaerobic oxidation of methane in deep euxinic waters of the Black Sea. Geochim. Cosmochim. Acta 67, 1359–1374. https://doi.org/10.1016/S0016-7037(02)01220-6
Wang, J., Chen, L., Li, L., He, J., Chen, J., Jiang, C., Wang, W., Li, S., Li, Y., Zhang, R., 2014. Preliminary identification of palaeofloods with the alkane ratio C31/C17 and their potential link to global climate changes. Sci. Rep. 4, 6502. https://doi.org/10.1038/srep06502
Wang, Y., Huang, C., Sun, B., Quan, C., Wu, J., Lin, Z., 2014. Paleo-CO2 variation trends and the Cretaceous greenhouse climate. Earth-Science Rev. 129, 136–147. https://doi.org/10.1016/j.earscirev.2013.11.001
Weijers, J.W.H., Schouten, S., Sluijs, A., Brinkhuis, H., Sinninghe Damsté, J.S., 2007. Warm arctic continents during the Palaeocene-Eocene thermal maximum. Earth Planet. Sci. Lett. 261, 230–238. https://doi.org/10.1016/j.epsl.2007.06.033
Weijers, J.W.H., Schouten, S., Spaargaren, O.C., Sinninghe Damsté, J.S., 2006. Occurrence and distribution of tetraether membrane lipids in soils: Implications for the use of the TEX86 proxy and the BIT index. Org. Geochem. 37, 1680–1693. https://doi.org/10.1016/j.orggeochem.2006.07.018
Weissert, H., 2000. Deciphering methane ' s fingerprint. Nature 406, 356.
Wenchuan, Q., Dickman, M., Sumin, W., Ruijin, W., Pingzhong, Z., Jianfa, C., 1999. Evidence for an aquatic plant origin of ketones found in Taihu Lake sediments. Hydrobiologia 397, 149–154.
Westerhold, T., Röhl, U., McCarren, H.K., Zachos, J.C., 2009. Latest on the absolute age of the Paleocene-Eocene Thermal Maximum (PETM): New insights from exact stratigraphic position of key ash layers + 19 and - 17. Earth Planet. Sci. Lett. 287, 412–419. https://doi.org/10.1016/j.epsl.2009.08.027
Wilson, P. a, Norris, R.D., 2001. Warm tropical ocean surface and global anoxia during the mid-Cretaceous period. Nature 412, 425–429. https://doi.org/10.1038/35086553
Wilson, P.A., Oceanography, S., Science, E., Way, E., 2002. Testing the Cretaceous greenhouse hypothesis using glassy foraminiferal calcite from the core of the Turonian tropics on Demerara Rise 607–610.
Wing, S.L., Harrington, G.J., Smith, F. a, Bloch, J.I., Boyer, D.M., Freeman, K.H., 2005. Transient Floral Change and. Science (80-.). 310, 993–996. https://doi.org/10.1126/science.1116913
Winguth, A.M.E., Thomas, E., Winguth, C., 2012. Global decline in ocean ventilation, oxygenation, and productivity during the Paleocene-Eocene Thermal Maximum: Implications for the benthic extinction. Geology 40, 263–266. https://doi.org/10.1130/G32529.1
Wishner, K.F., Gowing, M.M., Celia, G., 2000. Living in suboxia: Ecology of an Arabian Sea oxygen minimum zone copepod. Limnol. Oceanogr. 45, 1576–1593. https://doi.org/10.4319/lo.2000.45.7.1576
Woese, C.R., Kandler, O., Wheelis, M.L., 1990. Towards a natural system of organisms:

proposal for the domains Archaea, Bacteria, and Eucarya. Proc. Natl. Acad. Sci. 87, 4576–4579. https://doi.org/10.1073/pnas.87.12.4576

Xu, W., Ruhl, M., Jenkyns, H.C., Hesselbo, S.P., Riding, J.B., Selby, D., Naafs, B.D.A., Weijers, J.W.H., Pancost, R.D., Tegelaar, E.W., Idiz, E.F., 2017. Carbon sequestration in an expanded lake system during the Toarcian oceanic anoxic event. Nat. Geosci. 10. https://doi.org/10.1038/ngeo2871

Yao, W., Millero, F.J., 1995. The chemistry of the anoxic waters in the Framvaren Fjord, Norway. Aquat. Geochemistry 1, 53–88. https://doi.org/10.1007/BF01025231

Zachos, J.C., Pagani, M., Sloan, L., Thomas, E., Billups, K., 2001. Trends, Global Rhythms, Aberrations in Global Climate 65Ma to Present. Science (80-.). 292, 686–693. https://doi.org/10.1126/science.1059412

Zachos, J.C., Röhl, U., Schellenberg, S.A., Sluijs, A., Hodell, D.A., Kelly, D.C., Thomas, E., Nicolo, M., Raffi, I., Lourens, L.J., McCarren, H., Kroon, D., 2005. Rapid acidification of the ocean during the Paleocean-Eocene Thermal Maximum. Science (80-.). 308, 1611–1615. https://doi.org/10.1126/science.1109004

Zachos, J.C., Schouten, S., Bohaty, S., Quattlebaum, T., Sluijs, A., Brinkhuis, H., Gibbs, S.J., Bralower, T.J., 2006. Extreme warming of mid-latitude coastal ocean during the Paleocene-Eocene Thermal Maximum: Inferences from TEX86 and isotope data. Geology 34, 737–740. https://doi.org/10.1130/G22522.1

Zachos, J.C., Wara, M.W., Bohaty, S., Delaney, M.L., Rose, M., Brill, A., Bralower, T.J., Premoli-Silva, I., Bralower, T.J., Premoli-Silva, I., Petrizzo, M.R., Brill, A., Bralower, T.J., Premoli-Silva, I., 2003. A Transient Rise in Tropical Sea Surface Temperature During the Paleocene-Eocene Thermal Maximum. Science 302, 2001–2004. https://doi.org/10.1126/science.1090110

Zeebe, R.E., Zachos, J.C., Dickens, G.R., 2009. Carbon dioxide forcing alone insufficient to explain Palaeocene–Eocene Thermal Maximum warming. Nat. Geosci. 2, 576–580. https://doi.org/10.1038/ngeo578

Zhang, Y.G., Zhang, C.L., Liu, X.L., Li, L., Hinrichs, K.U., Noakes, J.E., 2011. Methane Index: A tetraether archaeal lipid biomarker indicator for detecting the instability of marine gas hydrates. Earth Planet. Sci. Lett. 307, 525–534. https://doi.org/10.1016/j.epsl.2011.05.031

Zhou, X., Thomas, E., Rickaby, R.E.M., Winguth, A.M.E., Lu, Z., 2014. I/Ca evidence for upper ocean deoxygenation during the PETM. Paleoceanography 29, 964–975. https://doi.org/10.1002/2014PA002702

Zhou, X., Jenkyns, H.C., Owens, J.D., Junium, C.K., Zheng, X.Y., Sageman, B.B., Hardisty, D.S., Lyons, T.W., Ridgwell, A., Lu, Z., 2015. Upper ocean oxygenation dynamics from I/Ca ratios during the Cenomanian-Turonian OAE 2. Paleoceanography 30. https://doi.org/10.1002/2014PA002741

Zimmerman, H.B., Boersma, A., McCoy, F.W., 1987. Carbonaceous sediments and palaeoenvironment of the Cretaceous South Atlantic Ocean. Geol. Soc. London, Spec. Publ. 26, 271–286. https://doi.org/10.1144/GSL.SP.1987.026.01.19